

The consolidated European synthesis of CO₂ emissions and removals for EU27 and UK: 1990-2020

Matthew J. McGrath¹, Ana Maria Roxana Petrescu², Philippe Peylin¹, Robbie M. Andrew³, Bradley Matthews⁴, Frank Dentener⁵, Juraj Balkovič⁶, Vladislav Bastrikov⁷, Meike Becker^{8,9}, Gregoire Broquet¹, Philippe Ciais¹, Audrey Fortems-Cheiney¹, Raphael Ganzenmüller¹⁰, Giacomo Grassi⁵, Ian Harris¹¹, Matthew Jones¹², Juergen Knauer¹³, Matthias Kuhnert¹⁴, Guillaume Monteil¹⁵, Saqr Munassar¹⁶, Paul I. Palmer¹⁷, Glen P. Peters³, Chunjing Qiu¹, Mart-Jan Schelhaas¹⁸, Oksana Tarasova¹⁹, Matteo Vizzarri^{5,20}, Karina Winkler^{18,21}, Gianpaolo Balsamo²², Antoine Berchet¹, Peter Briggs¹³, Patrick Brockmann¹, Frédéric Chevallier¹, Giulia Conchedda²³, Monica Crippa²⁴, Stijn Dellaert²⁵, Hugo A. C. Denier van der Gon²⁵, Sara Filipek¹⁸, Pierre Friedlingstein²⁶, Richard Fuchs²⁰, Michael Gauss²⁷, Christoph Gerbig¹⁶, Diego Guizzardi⁵, Dirk Günther²⁸, Richard A. Houghton²⁹, Greet Janssens-Maenhout⁵, Ronny Laurerwald³⁰, Bas Lerink¹⁸, Ingrid T. Lujckx¹⁸, Géraud Moulas³¹, Marilena Muntean⁵, Gert-Jan Nabuurs¹⁸, Aurélie Paquirrissamy¹, Lucia Perugini³², Wouter Peters¹⁸, Roberto Pilli³³, Julia Pongratz^{10,34}, Pierre Regnier³⁵, Marko Scholze¹⁵, Yusuf Serençil³⁶, Pete Smith¹⁴, Efisio Solazzo²⁴, Rona L. Thompson³⁷, Francesco N. Tubiello²², Timo Vesala^{38,39}, Sophia Walther¹⁶

¹Laboratoire des Sciences du Climat et de l'Environnement, CEA CNRS UVSQ UPSACLAY Orme des Merisiers, Gif-sur-Yvette, France
²Department of Earth Sciences, Vrije Universiteit Amsterdam, 1081HV, Amsterdam, the Netherlands
³CICERO Center for International Climate Research, Oslo, Norway
⁴Environment Agency Austria, Spittelauer Lände 5 1090, Vienna, Austria
⁵European Commission, Joint Research Centre, Via E. Fermi, 2749, TP 26/A, 21027, Ispra, Italy
⁶International Institute for Applied Systems Analysis (IIASA), 2361 Laxenburg, Austria
⁷Science Partners, 75010 Paris, France
⁸Geophysical Institute, University of Bergen, Bergen, Norway
⁹Bjerknes Centre for Climate Research, Bergen, Norway
¹⁰Department of Geography, Ludwig-Maximilians-Universität München, Luisenstraße 37, 80333 München, Germany
¹¹National Centre for Atmospheric Science (NCAS), University of East Anglia, Norwich, United Kingdom; and Climatic Research Unit, School of Environmental Sciences, University of East Anglia, Norwich, United Kingdom
¹²Tyndall Centre for Climate Change Research, School of Environmental Sciences, University of East Anglia, Norwich Research Park, Norwich NR4 7TJ, United Kingdom
¹³Hawkesbury Institute for the Environment, Western Sydney University, Locked Bag 1797, Penrith, NSW 2751, Australia
¹⁴Institute of Biological and Environmental Sciences, University of Aberdeen, 23 St Machar Drive, Aberdeen, AB24 3UU, United Kingdom
¹⁵Dept. of Physical Geography and Ecosystem Science, Lund University, Sweden
¹⁶Max Planck Institute for Biogeochemistry, Hans-Knöll-Strasse 10, 07745 Jena, Germany
¹⁷School of GeoSciences, University of Edinburgh, Edinburgh, United Kingdom
¹⁸Wageningen Environmental Research, Wageningen University and Research (WUR), Wageningen, 6708PB, the Netherlands
¹⁹Science and Innovation Department, World Meteorological Organization (WMO), Geneva, Switzerland
²⁰Università degli Studi di Milano, Milano, Italy
²¹Land Use Change & Climate Research Group, IMK-IFU, Karlsruhe Institute of Technology (KIT), Karlsruhe, Germany
²²European Centre for Medium-Range Weather Forecasts (ECMWF), Reading, RG2 9AX, United Kingdom
²³FAO, Statistics Division, Via Terme di Caracalla, Rome 00153, Italy
²⁴UniSystems Company, Milan, Italy
²⁵Department of Climate, Air and Sustainability, TNO, Princetonlaan 6, 3584 CB Utrecht, the Netherlands
²⁶College of Engineering, Mathematics and Physical Sciences, University of Exeter, Exeter EX4 4QF, United Kingdom
²⁷Norwegian Meteorological Institute, Oslo, Norway
²⁸Umweltbundesamt (UBA), 14193 Berlin, Germany
²⁹Woodwell Climate Research Center, Falmouth, Massachusetts, United States of America
³⁰Université Paris-Saclay, INRAE, AgroParisTech, UMR ECOSYS, Thiverval-Grignon, France
³¹ARTIC, 39 rue des Mathurins, 75008 Paris, France
³²Centro Euro-Mediterraneo sui Cambiamenti Climatici (CMCC), Viterbo, Italy
³³Scientific consultant, Padua, Italy
³⁴Max Planck Institute for Meteorology, Bundesstrasse 53, 20146 Hamburg, Germany
³⁵Biogeochemistry and Modeling of the Earth System, Université Libre de Bruxelles, 1050 Bruxelles, Belgium
³⁶Istanbul University, Faculty of Forestry, Department of Watershed Management, 34473 Sariyer, Istanbul, Turkey
³⁷Norwegian Institute for Air Research (NILU), Kjeller, Norway
³⁸University of Helsinki, Institute for Atmospheric and Earth System Research/Physics, Faculty of Science, 00560 Helsinki, Finland

Style Definition: Heading 2: Font: Bold, Font colour: Text 1

Deleted: 0... Gianpaolo Balsamo²²... Antoine Berchet¹, Peter Briggs¹³, Patrick Brockmann¹, Frédéric Chevallier¹, Giulia Conchedda²³... Monica Crippa²⁴, Stijn Dellaert²⁵...ellaert²⁵, Hugo A. C. Denier van der Gon²⁵...on²⁵, Sara Filipek¹⁸, Pierre Friedlingstein²⁴...riedlingstein²⁶, Richard Fuchs²⁰, Michael Gauss²⁵...auss²⁷, Christoph Gerbig¹⁶, Diego Guizzardi⁵, Dirk Günther²⁶...ünther²⁸, Richard A. Houghton²⁷...oughton²⁹... [1]

Deleted: Vesala³⁶

Deleted: 37

Formatted ... [2]

Formatted: French

Formatted: French

Formatted: Font colour: Text 1

Deleted: France

Formatted: Left

Formatted: Left

Formatted: Left

Deleted: UK

Deleted: UK

Formatted: Left

Formatted: Left

Formatted ... [3]

Deleted: 0

Deleted: 1...uropean Centre for Medium-Range Weath... [4]

Formatted: Left

Deleted: 2

Deleted: 23Department

Deleted: 24College ...6College of Engineering, Mathem... [5]

Deleted: 25Norwegian

Deleted: 26Umweltbundesamt

Deleted: 27Woodwell ...9Woodwell Climate Research C... [6]

Deleted: 28Université

Formatted: Left

Deleted: 29ARTTIC

Deleted: 30Centro

Deleted: 31Scientific

Deleted: 32Max

Deleted: 33Biogeochemistry

Deleted: 34Istanbul

Deleted: 35Norwegian

Formatted: Left

Deleted: 36University

156 ³⁹Institute for Atmospheric and Earth System Research/Forest Sciences, Faculty of Agriculture and Forestry, University of
157 Helsinki, Helsinki, Finland

Deleted: ³⁷Institute

158
159
160 Correspondence to: M.J. McGrath (matthew.mcgrath@lscce.ipsl.fr)
161

162 Abstract

Formatted: Heading 1, Space After: 0 pt, Line spacing: single

163 Quantification of land surface-atmosphere fluxes of carbon dioxide (CO₂) fluxes and their trends and
164 uncertainties is essential for monitoring progress of the EU27+UK bloc as it strives to meet ambitious targets
165 determined by both international agreements and internal regulation. This study provides a consolidated synthesis of
166 fossil sources (CO₂ fossil) and natural (including formally managed ecosystems) sources and sinks over land (CO₂
167 land) using bottom-up (BU) and top-down (TD) approaches for the European Union and United Kingdom
168 (EU27+UK), updating earlier syntheses (Petrescu et al., 2020, 2021b). Given the wide scope of the work and the
169 variety of approaches involved, this study aims to answer essential questions identified in the previous syntheses and
170 understand the differences between datasets, particularly for poorly characterized fluxes from managed and
171 unmanaged ecosystems. The work integrates updated emission inventory data, process-based model results, data-
172 driven categorical model results, and inverse modeling estimates, extending the previous period 1990-2018 to the year
173 2020 to the extent possible. BU and TD products are compared with the European National Greenhouse Gas Inventory
174 (NGHGI) reported by Parties including the year 2019 under the United Nations Framework Convention on Climate
175 Change (UNFCCC). The uncertainties of the EU27+UK NGHGI were evaluated using the standard deviation reported
176 by the EU Member States following the guidelines of the Intergovernmental Panel on Climate Change (IPCC) and
177 harmonized by gap-filling procedures. Variation in estimates produced with other methods, such as atmospheric
178 inversion models (TD) or spatially disaggregated inventory datasets (BU), originate from within-model uncertainty
179 related to parameterization as well as structural differences between models. By comparing the NGHGI with other
180 approaches, key sources of differences between estimates arise primarily in activities. System boundaries and
181 emission categories create differences in CO₂ fossil datasets, while different land use definitions for reporting
182 emissions from Land Use, Land Use Change and Forestry (LULUCF) activities result in differences for CO₂ land.
183 The latter has important consequences for atmospheric inversions, leading to inversions reporting stronger sinks in
184 vegetation and soils than are reported by the NGHGI.

Deleted: sectoral

Deleted: ies

Deleted: s

Deleted: s

185 **For CO₂ fossil emissions**, after harmonizing estimates based on common activities and selecting the most recent
186 year available for all datasets, the UNFCCC NGHGI for the EU27+UK accounts for $926 \pm 13 \text{ Tg C yr}^{-1}$ while eight
187 other BU sources report a mean value of $948 [937,961] [25^{\text{th}},75^{\text{th}} \text{ percentile}] \text{ Tg C yr}^{-1}$. The sole top-down inversion
188 of fossil emissions currently available accounts for $875 \text{ Tg C in this same year, a value outside the uncertainty of both}$
189 **the NGHGI and bottom-up ensemble estimates and for which uncertainty estimates are not currently available. For**
190 **the net CO₂ land fluxes**, during the most recent five-year period including the NGHGI estimates, the NGHGI
191 accounted for $-91 \pm 32 \text{ Tg C yr}^{-1}$ while six other BU approaches reported a mean sink of $-62 [-117,-49] \text{ Tg C yr}^{-1}$ and
192 a 15-member ensemble of dynamic global vegetation models (DGVMs) reported $-69 [-152,-5] \text{ Tg C yr}^{-1}$. The five-

Formatted: Normal paragraph, Left, Indent: First line: 0 cm, Line spacing: single, Border: Top: (No border), Bottom: (No border), Left: (No border), Right: (No border), Between : (No border)

Deleted: $3392 \pm 49 \text{ Tg CO}_2 \text{ yr}^{-1}$ (

Deleted:)

Deleted: $3340 [3238,3401] [25^{\text{th}},75^{\text{th}} \text{ percentile}] \text{ Tg CO}_2 \text{ yr}^{-1}$ (...

Deleted:)

Deleted: $3800 \text{ Tg CO}_2 \text{ yr}^{-1}$ (

Deleted: $1038 \text{ Tg C yr}^{-1}$), a value close to that of the NGHGI, but for which uncertainty estimates are not yet available

206 year mean of three TD regional ensembles combined with one non-ensemble inversion of -73 Tg C yr^{-1} has a slightly
 207 smaller spread (0th-100th percentile of $[-135, +45] \text{ Tg C yr}^{-1}$), and was calculated after removing net land-atmosphere
 208 CO₂ fluxes caused by lateral transport of carbon (crop trade, wood trade, river transport, and net uptake from inland
 209 water bodies) resulting in increased agreement with the NGHGI and bottom-up approaches. Results at the category
 210 level (Forestland, Cropland, Grassland) show generally good agreement between the NGHGI and category-specific
 211 models, but results for DGVMs are mixed. Overall, for both CO₂ fossil and net CO₂ land fluxes, we find current
 212 independent approaches are consistent with the NGHGI at the scale of the EU27+UK. We conclude that CO₂
 213 emissions from fossil sources have decreased over the past 30 years in the EU27+UK, while land fluxes are relatively
 214 stable: positive or negative trends larger (smaller) than $0.07 (-0.61) \text{ Tg C yr}^{-2}$ can be ruled out for the NGHGI. In
 215 addition, a gap on the order of $1000 \text{ Tg C yr}^{-1}$ between CO₂ fossil emissions and net CO₂ uptake by the land exists
 216 regardless of the type of approach (NGHGI, TD, BU), falling well outside all available estimates of uncertainties.
 217 However, uncertainties in top-down approaches to estimate CO₂ fossil emissions remain uncharacterized and are likely
 218 substantial, in addition to known uncertainties in top-down estimates of the land fluxes. The data used to plot the
 219 figures are available at <https://doi.org/10.5281/zenodo.8148461> (McGrath et al., 2023).

- Deleted: crops, wood trade and inland waters
- Deleted: the
- Deleted: sub-sector
- Deleted: sub-sector
- Deleted: a
- Formatted: Subscript
- Formatted: Subscript
- Deleted: large uncertainties on net uptake of CO₂ by the land surface prevent trend identification

Deleted: ¶

220 1. Introduction

221 Atmospheric mole fractions of greenhouse gasses (GHGs) reflect a balance between emissions from both
 222 human activities and natural sources, and removals by the terrestrial biosphere, oceans, and atmospheric oxidation.
 223 Increasing levels of GHG in the atmosphere due to human activities have been the major driver of climate change
 224 since the pre-industrial period (IPCC, 2021). In 2020, GHG mole fractions reached record highs, with globally
 225 averaged mole fractions of 413.2 parts per million (ppm) for carbon dioxide (CO₂), representing 149% of the pre-
 226 industrial level (WMO, 2021). The rise in CO₂ mole fractions in recent decades is caused primarily by CO₂ emissions
 227 from fossil sources. Globally, fossil emissions in 2020 (excluding the cement carbonation sink) totalled $9500 \pm 500 \text{ Tg}$
 228 C yr⁻¹, with expectations to rise in 2021 as the world recovered from the first year of the Covid-19 pandemic
 229 (Friedlingstein et al., 2022). In contrast, global net CO₂ emissions from land use and land use change (LULUC,
 230 primarily deforestation; see glossary at Table A1 for more details) estimated from bookkeeping models and dynamic
 231 global vegetation models (DGVMs) were estimated to have a small decreasing trend over the past two decades, albeit
 232 with low confidence, and a value in the year 2020 of $900 \pm 700 \text{ Tg C yr}^{-1}$ (Friedlingstein et al., 2022). This decrease,
 233 however, is almost an order of magnitude less than the growth in fossil emissions over the same period, and therefore
 234 the total fossil and net LULUC flux has still increased.

- Deleted: ¶
- Formatted: Heading 1, Space After: 0 pt, Line spacing: single, No bullets or numbering
- Deleted: concentration

- Deleted: concentration
- Deleted: totalled
- Deleted: .
- Deleted: 0.
- Deleted: Gt
- Deleted: ($34.8 \pm 1.8 \text{ Gt CO}_2 \text{ yr}^{-1}$)
- Deleted:

235 As all countries in the EU27+UK are Annex I Parties¹ to the United Nations Framework Convention on
 236 Climate Change (UNFCCC), they prepare and report national GHG emission inventories (NGHGIs) on an annual

¹ Annex I Parties include the industrialized countries that were members of the OECD (Organization for Economic Co-operation and Development) in 1992 plus countries with economies in transition (the EIT Parties), including the Russian Federation, the Baltic States, and several central and eastern European states (UNFCCC, <https://unfccc.int/parties-observers>, last access: February 2022).

Formatted: Footer Char, Font: (Default) Calibri, 11 pt

254 basis. These inventories contain annual timeseries of each country’s GHG emissions from the 1990 base year² until
255 two years before the year of reporting and were originally set to track progress towards their reduction targets under
256 the Kyoto Protocol (UNFCCC, 1997). Annex I NGHGs are reported according to the Decision 24/CP.19 of the
257 UNFCCC Conference of the Parties (COP) which states that the national inventories *shall* be compiled using the
258 methodologies provided in the *IPCC Guidelines for National Greenhouse Gas Inventories* (IPCC, 2006). The 2006
259 IPCC Guidelines provide methodological guidance for estimating emissions for well-defined sectors using national
260 activity and available emission factors. Decision trees indicate the appropriate level of methodological sophistication
261 (*Tiered methods*) based on the absolute contribution of the sector to the national GHG balance and the country’s
262 national circumstances (availability and resolution of national activity data and emission factors). Generally, Tier 1
263 methods are based on global or regional default emission factors that can be used with aggregated activity data, while
264 Tier 2 methods rely on country-specific factors and/or activity data at a higher category resolution. Tier 3 methods are
265 based on more detailed process-level modeling or in some cases facility-level emission observations. Annex I Parties
266 are furthermore required to estimate and report uncertainties in emissions (95 % confidence interval) following the
267 2006 IPCC guidelines using, as a minimum requirement, the Gaussian error propagation method (approach 1). Annex
268 I Parties are furthermore encouraged to use Monte-Carlo methods (approach 2) or a hybrid approach. Additional
269 information on the NGHGs can be found in Appendix A₂.

Deleted: 1

270 In addition to the NGHGs, other research groups and international institutions produce independent
271 estimates of national GHG emissions with two approaches: atmospheric inversions (top-down, TD) and GHG
272 inventories based on the same principle as NGHGs but using slightly different methods (tiers), activity data, and/or
273 emissions factors (bottom-up, BU). The current work has a strong focus on the EU27, and therefore sits within the
274 context of recent legislation passed by the European Parliament concerning commitments for the LULUCF sector to
275 achieve the objectives of the Paris Agreement and the reduction target for the Union (EU, 2018a and the proposed
276 amendments, EU, 2021a). This legislation requires that, “Member States shall ensure that their accounts and other
277 data provided under this Regulation are accurate, complete, consistent, comparable and transparent”. The TD and BU
278 methods discussed below include the most up-to-date publicly available spatially explicit information, which can help
279 provide a quality check and increase public confidence in NGHGs.

280 The work presented in this paper covers dozens of distinct datasets and models, in addition to the individual
281 country submissions to the UNFCCC of the EU Member States and the UK. As Annex I Parties, the NGHGs of the
282 EU Member States and the UK are consistent with the general guidance laid out in IPCC (2006) yet still differ in
283 specific approaches, models, and parameters, in addition to definitional differences in the underlying system
284 boundaries and activity datasets. For the land-based sector, Member States are only required to report terrestrial
285 biospheric fluxes from managed lands, instead of distinguishing between direct and indirect human-induced and
286 natural effects on carbon fluxes for all ecosystems (Grassi et al., 2018a, 2021). This “managed land proxy” avoids

Formatted: Footer Char, Font: (Default) Calibri, 11 pt

² For most Annex I Parties, the historical base year is 1990. However, parties included in Annex I with an economy in transition during the early 1990s (EIT Parties) were allowed to choose one year up to a few years before 1990 as reference because of a non-representative collapse during the breakup of the Soviet Union. For the EU27+UK, this includes Bulgaria (1988), Hungary (1985–1987), Poland (1988), Romania (1989), and Slovenia (1986).

288 [having to quantify, for example, increased carbon uptake in remote Forest land due to reactive nitrogen emissions](#)
289 [from both natural soils and human-applied synthetic fertilizers](#). A comprehensive investigation of detailed differences
290 between all datasets is beyond the scope of this paper, though systematic analyses have been previously made for
291 specific sectors (e.g. AFOLU³ - Petrescu et al., 2020; previous synthesis to this work - Petrescu et al., 2021b;
292 FAOSTAT versus UNFCCC NGHGs - Tubiello et al., 2021, Grassi et al., 2022a; UNFCCC versus bookkeeping
293 models - Grassi et al., 2023; and UNFCCC versus inversions - Deng et al., 2021) and by the Global Carbon Project
294 CO₂ syntheses (e.g., Friedlingstein et al., 2022).

Deleted: 2022b

295 Every year (time “t”) the Global Carbon Project (GCP) in its Global Carbon Budget (GCB) quantifies large-
296 scale CO₂ budgets up to the previous year (“t-1”), bringing in information from global to large latitude bands, including
297 various observation-based flux estimates from BU and TD approaches (Friedlingstein et al., 2022). The current
298 manuscript, given the focus on a single region (“Europe”) with extensive data coverage, dives into more detail than
299 the GCB, including [category-specific models related to LULUCF](#) (e.g., Forest land, Grassland, Cropland) and making
300 heavy use of the EU27+UK NGHGI in an effort to [advance a trust-building process by mutual understanding](#)
301 [developed through comparison of both approaches](#). Compared to Petrescu et al. (2021b), the current work updates
302 datasets, methods, and uncertainties.

Deleted: sector

Deleted: build mutual trust in the various approaches

303 BU observation-based approaches used in the GCB rely heavily on statistical data combined with Tier 1 and
304 Tier 2 approaches. In the current work, focusing on a region that is well-covered with data and models (EU27+UK),
305 BU also refers to Tier 3 process-based models (see Sect. 2). At regional and country scales, systematic and regular
306 comparison of these observation-based CO₂ flux estimates with reported fluxes under the UNFCCC is more difficult.
307 Continuing our previous efforts within the European project VERIFY (VERIFY, 2022), the current study compares
308 observation-based flux estimates of BU versus TD approaches and compares them with NGHGI for the EU27+UK
309 bloc and five sub-regions. VERIFY also provides, as a first attempt, similar comparisons for all European countries
310 (VERIFY Synthesis Plots, 2022). The methodological and scientific challenges to compare these different estimates
311 have been partly investigated before (Pongratz et al., 2021, Grassi et al., 2018a, for LULUCF; Andrew, 2020, for
312 fossil sectors) but such comparisons were not done in a systematic and comprehensive way, including both fossil and
313 land-based CO₂ fluxes, before Petrescu et al. (2021b).

Deleted: -

314 As Petrescu et al. (2021b) is the most comprehensive comparison of the NGHGI and research datasets
315 (including both TD and BU approaches) for the EU27+UK to date, the focus of the current paper is on improvement
316 of estimates in the most recent version in comparison with the previous one, including changes in the uncertainty
317 estimates and identification of the knowledge gaps and added value for policy making. Official NGHGI emissions are
318 compared with research datasets, including necessary harmonization of the latter on total emissions to ensure
319 consistency. Differences and inconsistencies between emission estimates were analyzed, and recommendations were
320 made towards future evaluation of NGHGI data. It is important to remember that, while NGHGIs include uncertainty
321 estimates, the “uncertainty analysis should be seen, first and foremost, as a means to help prioritize national efforts to
322 reduce the uncertainty of inventories in the future, and guide decisions on methodological choice” (Volume 1, Chapter

Formatted: Footer Char, Font: 11 pt, Font colour: Auto

³ We refer here to AFOLU as defined by the IPCC AR5: Agriculture, Forestry and Other Land Use. [For further details on the differences between AFOLU, LULUCF, and LULUC, please see the glossary at Table A1.](#)

327 3, IPCC, 2006) and were therefore not developed to enable comparisons between countries or other datasets. In
328 addition, individual spatially disaggregated research emission datasets often lack quantification of uncertainty. Here,
329 we focus on the mean value and various percentiles (0th, 25th, 75th, 100th) of different research products of the same
330 type to get a first estimate of uncertainty (see Sect. 2). Not all models/inventories provided an update for v2021, and,
331 therefore, for the non-updated datasets the previously published timeseries are shown.

332 The dataset assembled in this paper (McGrath et al., 2023) provides annual values of carbon dioxide
333 emissions and sinks in fossil and LULUCF sectors for the EU27+UK across a range of data products based on different
334 methodologies. This enables, for example, researchers producing datasets based on new methods a source of
335 evaluation in the form of a best-estimate range of values. Decision makers may also find the results useful for targeting
336 mitigation efforts in the EU27+UK by providing a more complete subsectorial breakdown. While NGHGs already
337 provide detailed data-based disaggregation based on activities, the dataset here adds additional constraints from
338 independent data and models used outside of the inventory community. In addition, this paper outlines a methodology
339 by which users of country-level CO₂ emission data can compare datasets against NGHGs and identify where
340 agreement occurs for the right (and wrong) reasons. Section 3.1 highlights the extreme difference between current
341 fossil emissions and uptake by the land surface. Section 3.2 looks at an ensemble of bottom-up estimates of fossil
342 CO₂ emissions, in addition to a preliminary inversion using atmospheric NO₂ observations as a constraint. Sections
343 3.3.2 and 3.3.3 show that better agreement between the NGHGI and other models occurs when the models are driven
344 strongly by category-specific data in forestry, grasslands, and croplands, as opposed to more generalized models
345 created to couple to atmospheric models in global climate projections. Section 3.3.4 highlights the challenges
346 currently facing comparison of atmospheric inversion models with NGHGs, while simultaneously showing
347 improvement by accounting for net emissions for lateral transfer of carbon between countries. Section 3.4 provides
348 more discussion around uncertainties in both top-down and bottom-up estimates.

349 A list of acronyms and terminology is provided in Table A1 for easy reference.
350

351 **2. CO₂ data sources and estimation approaches**

352 The CO₂ emissions and removals in the EU27+UK estimated by inversions and anthropogenic emission
353 inventories resolved at the source category level were analyzed. At the time of this work, data of CO₂ fossil emissions
354 and CO₂ land⁴ emissions and removals (Tables 1 and 2) covered the period from 1990 to 2020, with some of the data
355 only available for shorter time periods. Since then, some datasets have been updated to include 2021, but not all, and

⁴The IPCC Good Practice Guidance (GPG) for Land Use, Land Use Change and Forestry (IPCC, 2003) describes a uniform structure for reporting emissions and removals of greenhouse gases. This format for reporting can be seen as “land based”, all land in the country must be identified as having remained in one of six categories since a previous survey, or as having changed to a different (identified) category in that period. According to IPCC Special Report on Climate Change and Land: Land covers the terrestrial portion of the biosphere that comprises the natural resources (soil, near surface air, vegetation and other biota, and water) the ecological processes, topography, and human settlements and infrastructure that operate within that system”. Some communities prefer “biogenic” to describe these fluxes, while others find this confusing as fluxes from unmanaged forests, for example, are “biogenic” but not included in inventories reported to the UNFCCC. As this comparison is central to our work, we decided that “land” as defined by the IPCC was a good compromise. However, we avoid the word “natural” as much as possible, under the assumption that almost all terrestrial ecosystems are significantly impacted by humans in the current era.

Formatted: Subscript

Formatted: Subscript

Formatted: Subscript

Formatted: Heading 1, Space After: 0 pt, Line spacing: single, No bullets or numbering, Tab stops: Not at 0,48 cm

Formatted: Footer Char, Font: (Default) Calibri, 11 pt, Font colour: Auto

Formatted: Footer Char, Font: (Default) Calibri, 11 pt

Formatted: Footer Char, Font: (Default) Calibri, 11 pt, Font colour: Auto

Formatted: Footer Char, Font: (Default) Calibri, 11 pt

Formatted: Footer Char, Font: (Default) Calibri, 11 pt, Font colour: Auto

Deleted: classes

Deleted: class

Deleted: SRCCCL

Formatted: Footer Char, Font: (Default) Calibri, 11 pt

Deleted: However, we avoid the word “natural” as much as possible, since terrestrial ecosystems outside of human influence are rare in the current era

356 we made the decision to stay with the original time window for simplicity. The estimates are available both from
357 peer-reviewed literature and from new research results from the VERIFY project. BU results are compared to NGHGI
358 reported in 2021 (which contain the timeseries for 1990-2019). Data sources are summarized in Tables 1 and 2 with
359 the detailed description of all products provided in Appendices A2-A4. In Appendix A2, the harmonized methodology
360 for calculation of uncertainties submitted by Member States to the UNFCCC in their National Inventory Reports
361 (NIRs) is explained. This includes the same 95 % confidence interval as is typically reported, but involved an
362 extensive gap-filling to cover more categories and more years than available in Petrescu et al. (2021b), which limited
363 uncertainty estimation to a single year.

364 BU anthropogenic CO₂ fossil estimates include global inventory datasets such as the Emissions Database for
365 Global Atmospheric Research (EDGAR v6.0.), Statistical Review of World Energy by BP, the Carbon Dioxide
366 Information Analysis Center (CDIAC), the Global Carbon Project (GCP), the Energy Information Administration's
367 (EIA) "International" dataset, and the International Energy Agency (IEA) (see Table 1). These datasets are all
368 described in detail by Andrew (2020). CO₂ land emission estimates are derived from BU biogeochemical models (e.g.,
369 DGVMs, bookkeeping models, see Table 2). TD approaches include both high spatial resolution regional inversions
370 (CarboScopeReg, EUROCOM (Monteil et al., 2020), inversions based on the CIF-CHIMERE system (Berchet et al.,
371 2021) and LUMIA) and coarser spatial resolution global inversions (GCP 2021: Friedlingstein et al., 2022). Most of
372 the inversions were carried out for CO₂ land emissions, with only a single inversion for CO₂ fossil emissions (CIF-
373 CHIMERE). Note that CIF-CHIMERE provides estimates for both CO₂ land and CO₂ fossil from separate simulations.
374 These estimates are described in Sect. 2.3.

375 The sign of the fluxes is defined from an atmospheric perspective: positive values represent a net source to
376 the atmosphere and negative values a net removal from the atmosphere. As an overview of potential uncertainty
377 sources, Table C1 presents the use of emission factor data (EF), activity data (AD), and, whenever available,
378 uncertainty methods used for all CO₂ land data sources in this study, in addition to more details on each model in
379 Appendices A. The referenced data used for the figures' replicability purposes are available for download (McGrath
380 et. al, 2023). Upon request, the codes necessary to plot the figures in the same style and layout can be provided. The
381 focus is on EU27+UK emissions. In the VERIFY project, an additional web tool was developed which allows for the
382 selection and display of all plots shown in this paper, not only for the EU Member States and UK but for a total of 79
383 countries and groups of countries in Europe (Table A2, Appendix A). The data is free and can be accessed upon
384 registration (VERIFY Synthesis Plots, 2022). An overview of the datasets, including contact information, is provided
385 in Table C1.

386 For the sake of harmonization, we report the mean values of all ensembles. For small sample sizes (e.g., the
387 regional inversions of CSR with four members), the literature does not give a clear indication on whether the mean or
388 the median is preferred; a preference for one or the other depends on what one wishes to demonstrate. While the mean
389 and median converge in the case of independent randomly-distributed data, the median downplays data skewness. We
390 display the mean for all ensembles. As the number of datasets in some ensembles is small (less than five), we display
391 the minimum and maximum annual values for every year (i.e., the 0th/100th percentiles) to give an idea of the spread.
392 For ensembles with more than ten members (i.e., TRENDY), we show the mean and the 0th/100th percentiles along

Deleted: 1

Deleted: 2

Deleted: e.g.

Deleted: B

Deleted: 2

Deleted: 1

Formatted: Font: (Default) Times New Roman, 10 pt

Deleted: In particular, the median downplays the skewness of the data (outliers). We have taken efforts to exclude outliers from the datasets used to construct ensembles, and consequently the datasets which remain should be randomly distributed. For this reason, w

404 with the 25th/75th percentiles in the figures. This combination demonstrates "more likely" and "possible" behavior;
405 as only one ensemble has both bars, displaying them does not overwhelm the reader much more than the standard
406 graphs, and we find the added information to be worth the trade-off. In the text, we report the mean and 0/100th
407 percentiles for small ensembles and mean along with the 25th/75th for larger ensembles. We make every effort to
408 limit the number of significant figures as a function of the error bars. In some cases (e.g., asymmetric error bars which
409 overlap zero), we retain an extra significant figure to improve readability.

410 The current work extends Petrescu et al. (2021b) by updating the included datasets (both increasing the
411 number of years covered and in some cases updating the model versions), adding datasets, and highlighting changes
412 in terms of mean annual emissions and trends. For clarity, the data from Petrescu et al. (2021b) is labeled as v2019,
413 while the latest results are labeled v2021.

414

415 2.1. CO₂ anthropogenic emissions from NGHGI

416 The UNFCCC NGHGI (2021) estimates for the period 1990 to year $t-2$ (2019), collected for the EU27 and UK,
417 are the basis for this dataset. For historical reasons, a few EU countries provide data for a different base year than
418 1990⁵, yet it should be noted that regardless of the base year all countries of the EU27+UK bloc are obliged to report
419 estimates for the period 1990 to year $t-2$. The Annex I Parties to the UNFCCC are required to report annual GHG
420 inventories that include a NIR, with qualitative information on data and methods and a Common Reporting Format
421 (CRF) set of tables that provide quantitative information on GHG emission by category. This annually updated dataset
422 includes anthropogenic emissions and removals. For the land-based sector, the managed land proxy is used as a way
423 to report only anthropogenic fluxes (Grassi et al., 2018a, 2021). This proxy allows Member States to report all fluxes
424 coming from land designed as "managed" without trying to disentangle their natural and anthropogenic origins.
425 Spatially-explicit maps of managed lands are not currently available, even for the relatively data-rich region of the
426 European Union and United Kingdom. However, most of the European Union is classified by the Member States as
427 managed land; current estimates from available country-aggregated data indicates only 5 % of land in the EU is
428 unmanaged, including some Forest land, Grassland, and Wetlands. Figure B1 shows the annual NGHGI (2021)
429 anthropogenic CO₂ timeseries disaggregated by sector in order to provide context.

430

431 2.2. CO₂ fossil emissions

432 CO₂ fossil emissions occur when fossil carbon compounds are broken down via combustion or other non-
433 combusive industrial processes. Most of these fossil compounds are in the form of fossil fuels, such as coal, oil, and
434 natural gas. Another source category of fossil CO₂ emissions is fossil carbonates, such as calcium carbonate and
435 magnesium carbonate, which are used in industrial processes. Because CO₂ fossil emissions are largely connected
436 with energy, which is a closely tracked commodity group of high economic importance, there is a wealth of underlying

Formatted: Heading 2, Space After: 0 pt, Line spacing: single

Deleted: land management

Formatted: Heading 2, Space After: 0 pt, Line spacing: single

⁵ For most Annex I Parties, the historical base year is 1990. However, parties included in Annex I with an economy in transition during the early 1990s (EIT Parties) were allowed to choose one year up to a few years before 1990 as reference because of a non-representative collapse during the breakup of the Soviet Union (e.g., Bulgaria, 1988, Hungary, 1985–1987, Poland, 1988, Romania, 1989, and Slovenia, 1986).

Formatted: Footer Char, Font: (Default) Calibri, 11 pt

438 data that can be used for estimating emissions. However, differences in collection, treatment, interpretation and
439 inclusion of various factors – such as carbon contents and fractions of the fuel’s carbon that is oxidized – lead to
440 methodological differences (Appendix A3) resulting in differences of emissions between datasets (Andrew, 2020).
441 The datasets are also not fully independent, as discussed in Sec. 2.4. Atmospheric inversions for emissions of fossil
442 CO₂ are not as established as their bottom-up counterparts (Brophy et al., 2019). The main reason is that the types of
443 atmospheric measurements suitable for fossil CO₂ atmospheric inversions have not yet been widely deployed (Ciais
444 et al., 2015). One of the rare inversions is presented below.

Deleted: monitoring instruments

445 In this analysis, the inventory-based bottom-up CO₂ fossil emissions estimates are separated and presented
446 per fuel type and reported for the last year when all data products are available (2017). This updates Andrew (2020)
447 and Petrescu et al. (2021b) which both report the year 2014. In order to provide a quasi-independent estimate of fossil
448 emissions assimilating satellite observations of the atmosphere subject to current capabilities of atmospheric
449 inversions, the CIF-CHIMERE model was used to produce a fossil fuel CO₂ emission estimate for the year 2017. CIF-
450 CHIMERE is a coupling between the variational mode of the Community Inversion Framework (CIF) platform
451 developed in the VERIFY project (Berchet et al., 2021), the CHIMERE chemistry transport model (Menut et al., 2013)
452 and the adjoint of this model (Fortems-Cheiney et al., 2021a). To overcome the lack of CO₂ observation networks
453 suitable for the monitoring of fossil CO₂ emissions at national scale, this inversion is based on the assimilation of
454 satellite NO₂ data, which are representative of NO_x emissions, as NO_x is co-emitted with CO₂ during fossil fuel
455 combustion. The uncertainties in the anthropogenic activities underlying the fossil fuel combustion are shared by both
456 CO₂ and co-emitted species. Therefore, in principle, information from co-emitted species such as NO_x and CO can
457 be used to decrease the uncertainties in fossil fuel CO₂ emissions. Recent top-down inversions of anthropogenic CO₂
458 emissions from Europe indicate that uncertainties using satellite measurements of NO₂ are much lower than for co-
459 emitted CO when deriving fossil CO₂ emissions (Konovalov et al., 2016). Therefore, results shown below only
460 incorporate NO₂ and not CO observations. The CHIMERE model includes a full chemistry scheme to enable linkage
461 of observations of atmospheric NO_x mole fractions to surface NO_x emissions. While the spatial and temporal coverage
462 of the NO₂ observations is large, there are many factors contribute to uncertainty in fossil fuel emission activity data,
463 including the uncertainties in NO_x emission factors and thus the ratio of NO_x to CO₂ emissions. Therefore, the
464 influence of using NO₂ observations in determining fossil CO₂ emissions is subject to uncertainties which have not
465 been characterized appropriately yet in the framework of VERIFY. Here, this conversion relies heavily on the
466 emission ratios per country, month and large sector of activity from the TNO-GHGco-v3 inventory (Dellaert et al.,
467 2021), which has been partly developed in VERIFY, and which is based on the most recent UNECE-CLRTAP⁶ and
468 UNFCCC official country reporting respectively for air pollutants and greenhouse gasses. The detailed descriptions
469 of each of the data products are found in Appendix A3.

Deleted: fuel

Deleted: 2

Formatted: Subscript

Formatted: Subscript

Deleted: co-emitted

Formatted: Subscript

Formatted: Subscript

Deleted: that determine

Deleted: 2

Formatted: Subscript

Deleted: 1

471 *Table 1: Data sources for the anthropogenic CO₂ fossil emissions included in this study, all updated from Petrescu*
472 *et al. (2021b):*

Formatted: Caption - VERIFY, Left, Line spacing: single

Formatted: Footer Char, Font: (Default) Calibri, 11 pt

Formatted: Footer Char, Font: (Default) Calibri, 11 pt, Font colour: Auto

Formatted: Footer Char

⁶ UNECE Convention on Long-Range Transboundary Air Pollution, <https://unece.org/environment-policy/air>

Anthropogenic CO ₂ fossil			
Data/model name	Contact / lab	Species / Period	Reference/Metadata
UNFCCC NGHGI (2021)	Member State inventory agencies Annual gap-filled uncertainties provided by the EU GHG inventory team	Anthropogenic fossil CO ₂ 1990-2019	IPCC (2006) UNFCCC NIRs/CRFs https://unfccc.int/ghg-inventories-annex-i-parties/2021 (UNFCCC, 2021a, 2021b)
Compilation of multiple CO ₂ fossil emission data sources (Andrew 2020) EDGAR v6.0, BP, EIA, CDIAC, IEA, GCP, CEDS, PRIMAP	CICERO	CO ₂ fossil country totals and split by fuel type 1990-2018 (or last available year)	EDGAR v6.0 https://edgar.jrc.ec.europa.eu/ BP 2021 report (BP, 2021) EIA https://www.eia.gov/beta/international/data/browser/views/partials/sources.html CDIAC https://energy.appstate.edu/CDIAC (Gilfillan and Marland, 2021) IEA : www.iea.org CEDS https://github.com/JGCRI/CEDS (O'Rourke et al., 2021) GCP (Friedlingstein et al., 2022) PRIMAP-hist (Gütschow et al., 2021) https://doi.org/10.5281/zenodo.4479171
Fossil fuel CO ₂ inversions	LSCE	Inverse fossil fuel CO ₂ emissions 2005-2020	Fortems-Cheiney et al. (2021) Fortems-Cheiney and Broquet (2021)

Deleted: UNFCCC

Field Code Changed

Field Code Changed

Field Code Changed

480

481 **2.3. CO₂ land fluxes**

482 Data products from BU and TD CO₂ land fluxes including CO₂ emissions and removals from land use, land
483 use change, and forestry (LULUCF) activities are summarized in Table 2. All models and approaches produce an

Deleted: ¶

Formatted: Heading 2, Left, Indent: First line: 0 cm, Line spacing: single

537 The two updated inverse model ensembles presented are the GCP2021 for the period 2010-2020 (Friedlingstein
538 et al., 2022) and EUROCOM for the period 2009-2018 (Monteil et al., 2020; Thompson et al., 2020). The GCP
539 inversions are global and include CarbonTracker Europe (CTE: van der Laan-Luijkx et al., 2017), CAMS (Chevallier
540 et al., 2005), the Jena CarboScope (Rödenbeck, 2005), NIESMON-CO₂ (Niwa et al., 2017), CMS-Flux (Liu et al.,
541 2021) and UoE (Feng et al., 2016). The EUROCOM inversions are regional, with a domain limited to Europe and
542 higher spatial resolution atmospheric transport models, with four inversions covering the entire period 2009-2018 as
543 analyzed in Thompson et al. (2020). All inversions provide Net Ecosystem Exchange (NEE) fluxes. These inversions
544 make use of more than 30 atmospheric observing stations within Europe, including flask data and continuous
545 observations and work at typically higher spatial resolution than the global inversion models (Table 2). The prior
546 anthropogenic emissions provided for all regional inversions reported here (i.e., EUROCOM, EUROCOM drought
547 2018, VERIFY CSR, VERIFY CIF-CHIMERE, and VERIFY LUMIA) are all based on EDGAR v4.3, BP statistics,
548 and TNO datasets by generating spatial and temporal distributions through the COFFEE approach (Steinbach et al.,
549 2011). Small differences exist between exact versions used by the different groups. The prior anthropogenic
550 emissions for the GCP global inversions, GridFEDv2021 and v2022, are also based on EDGARv4.3.2 (Janssens-
551 Maenhout et al., 2019). ~~Differences in fossil fuel emissions for the regional inversions only exist for the years 2019~~
552 ~~and 2020, and they only concern the temporal variation within the year, not the annual totals per pixel (or~~
553 ~~country). Therefore, differences~~ in the prior anthropogenic emissions are not expected to explain the large differences
554 seen between the different regional biogenic inversions nor between the regional and global biogenic inversions, but
555 efforts should be continued to harmonize them to the greatest extent possible in future intercomparisons.

Formatted: Normal paragraph, Left, Indent: First line: 0 cm,
Line spacing: single

556 Additional inversions for Europe from three regional scale inversion systems are analyzed. Two of these
557 systems are part of the EUROCOM ensemble, but new runs were carried out for the VERIFY project. The
558 CarboScopeRegional (CSR) inversion system has performed additional runs for VERIFY for the years 2006-2020
559 with multiple ensemble members differing by biogenic prior fluxes and assimilated observations. The results are
560 plotted separately to illustrate two points: 1) that the CSR simulations for VERIFY are not identical to those submitted
561 to EUROCOM (VERIFY runs from CSR included several sites that started shortly before the end of the EURCOM
562 inversion period), and 2) the CSR model was used in four distinct runs in VERIFY. Note that the ensemble members
563 differ from previous years (the spatial correlation length is kept constant this year, while more prior fluxes are used).
564 By presenting CSR separate from the EUROCOM results, one can get an idea of the uncertainty due to various model
565 parameters in one inversion system with one single transport model. The LUMIA inversion system submitted four
566 simulation results to the VERIFY project, based on the ~~set-up developed for the 2018 Drought Task Force project~~
567 ~~(labeled here as EUROCOM, Thompson et al., 2020), but with a refined definition of both prior and observation~~
568 ~~uncertainties. Also, for the years 2019-2020, the transport models (FLEXPART and TMS) were driven by ERA5~~
569 ~~meteorological data, whereas for previous years, ERA-Interim data were used.~~ The four different variants include one
570 reference simulation and three simulations which change spatial correlation lengths, the number of observation sites,
571 and the magnitude of uncertainties in the boundary conditions. As one of the variants is only available for 2019-2020
572 (changing the uncertainties in the boundary conditions), this variant was dropped from the results and only the
573 remaining three simulations are presented, covering the period 2006-2020.

Deleted: Overall, differences

Deleted: .

Deleted: The primary difference is that the years 2019-2020
were added based on boundary conditions using TMS and
ERA5 meteorological data.

579 An inversion of the NEE over 2005-2020 from the CIF-CHIMERE variational inversion system is also
 580 analyzed. The configuration of this inversion is close to that of the PYVAR-CHIMERE NEE inversions in the
 581 EUROCOM ensembles and follows the general principles of Broquet et al. (2013). However, it uses distinct inputs,
 582 which play a critical role in the inversion, such as a more recent ORCHIDEE simulation as prior estimate of the NEE
 583 and a more recent CAMS global inversion to impose the regional CO₂ boundary conditions.

585 *Table 2: Data sources for the land CO₂ emissions included in this study. Details are found in Appendix A4. The*
 586 *timesteps 1Y, 1M, 1W, and 3H refer to the availability of the data: “one year”, “one month”, “one week”, and*
 587 *“three hours”, respectively. An overview of the datasets, including contact information, is provided in Table C1.*

Deleted: 2
Formatted: Caption - VERIFY, Left, Line spacing: single

NGHGI net CO ₂ land flux				
Data source	Contact / lab	Variables Period (timestep) Resolution	References	Status compared to Petrescu et al. (2021b)
UNFCCC NGHGI (2021)	Member State inventory agencies <u>Annual, gap-filled uncertainties provided by the EU GHG inventory team</u>	LULUCF Net CO ₂ emissions/removals ^a . 1990-2019 (1Y) Country-level	IPCC (2006) UNFCCC CRFs <u>https://unfccc.int/process-and-meetings/transparency-and-reporting/reporting-and-review-under-the-convention/greenhouse-gas-inventories-annex-i-parties/national-inventory-submissions-2021</u>	Updated
Inventory and model estimates of net CO₂ land flux				
ORCHIDEE	LSCE	CO ₂ fluxes from all ecosystems reported as Net Biome Productivity (NBP) ^b . 1990-2020 (3H) 0.125° x 0.125°	Ducoudré et al. (1993) Viovy et al. (1996) Polcher et al. (1998) Krinner et al. (2005)	Updated = <u>significant model revisions</u>
CABLE-POP	Western Sydney University	CO ₂ fluxes (NBP). Model includes N cycling. 1990-2020 (1M) 0.125° x 0.125°	Haverd et al. (2018)	New
TRENDY v10	MetOffice UK	CO ₂ fluxes (NBP) 15 models (all except ISAM) 1990-2020 (3H-1M) 0.125° x 0.125°	Friedlingstein et al. (2022; Table 4)	Updated = <u>significant differences in ensemble members</u>

Deleted: <https://unfccc.int/process-and-meetings/transparency-and-reporting/reporting-and-review-under-the-convention/greenhouse-gas-inventories-annex-i-parties/national-inventory-submissions-2019>
Formatted: Font: (Default) Times New Roman, 10 pt
Formatted: No underline
Deleted: Annual uncertainty gap-filling for total LULUCF by Environment Agency Austria (EAA).

CO₂ emissions from inland waters	ULB	Average C fluxes from rivers, lakes and reservoirs, with lateral C transfer from soils. 1990-2018 (-) 0.1° x 0.1°	Lauerwald et al. (2015) Hastie et al. (2019) Raymond et al. (2013)	Not updated
CBM	EC-JRC	CO ₂ fluxes (NBP) as historical 2000-2015 and extrapolation for 2017-2020 (1Y) Country-level	Kurz et al. (2009) Pilli et al. (2022)	Updated
ECOSSE	UNIABDN	CO ₂ fluxes (NBP) from croplands and grassland ecosystems. Crops: 1990-2020 (1Y) Grass: 1990-2018 (1Y) 0.125° x 0.125°	Bradbury et al. (1993) Coleman (1996) Jenkinson (1977, 1987) Smith et al. (1996, 2010a,b)	Updates only for croplands = significant differences
EFISCEN-Space	WUR	CO ₂ fluxes (NBP): single average value for 5 year periods, replicated on a yearly time axis. 0.125° x 0.125°	Verkerk et al. (2016) Schelhaas et al. (2017, 2020) Nabuurs et al. (2018)	Updates for 15 countries
EPIC-IIASA	IIASA	CO ₂ fluxes (NBP) from cropland 1991-2020 (1M) 0.125° x 0.125°	Balkovič et al. (2013, 2018, 2020) Izaurrealde et al. (2006) Williams et al. (1990)	Updated for croplands, new estimates for grasslands
BLUE (VERIFY) and BLUE (GCP)	LMU Munich	CO ₂ fluxes from land use change. VERIFY: 1990-2019 (1Y) GCP: 1990-2020 (1Y) 0.25° x 0.25°	Hansis et al. (2015) Ganzenmüller et al. (2022) - VERIFY Friedlingstein et al. (2022) - GCP2021	Updated
H&N	Woodwell Climate Research Center	CO ₂ fluxes from land use change. 1990-2020 (1Y) Country-level	Houghton and Nassikas (2017)	Updated
FAO	FAOSTAT	CO ₂ emissions / removal from LULUCF processes. 1990-2020 (1Y) Country-level	FAO (2021) Federici et al. (2015) Tubiello et al. (2021)	Updated = significant differences for FL
CO₂ atmospheric inversion estimates				

CSR inversions for VERIFY	MPI -Jena	Total CO ₂ inverse flux (NBP) [Ⓐ] 2006-2020 (3H) 0.5° x 0.5°	Kountouris et al. (2018 a,b)	Updated – <u>significant differences</u>
LUMIA	Lund University (INES)	Total CO ₂ inverse flux (NBP) [Ⓐ] 2006-2020 (1W) 0.25° x 0.25°	Monteil and Scholze (2021)	New
CIF-CHIMERE	LSCE	Total CO ₂ inverse flux (NBP) [Ⓐ] 2005-2020 (3H) 0.5° x 0.5°	Berchet et al. (2021) Broquet et al. (2013)	New
GCP 2021 global inversions (CTE, CAMS, CarboScope, NISMON-CO₂, UoE, CMS-Flux)	GCP	Total CO ₂ inverse flux (NBP) Six inversions 2010-2020 (various)	Friedlingstein et al. (2022) Van der Laan-Luijk et al. (2017) Chevallier et al. (2005) Rödenbeck et al. (2005) Niwa et al. (2017) Feng et al. (2016) Liu et al. (2021)	Updated – <u>significant differences in ensemble members</u>
EUROCOM regional inversions (CSR, LUMIA, PYVAR)	LSCE, ULUND, MPI-Jena, NILU	Total CO ₂ inverse flux (NBP) [Ⓐ] Three inversions 2009-2018 (3H-1M)	Monteil et al. (2020) Thompson et al. (2020)	Updated (also replaced CSR with the mean of the four runs submitted to VERIFY). FLEXINVERT and NAME are not included (Fig. A5)

595 ^a Member States use a mix of gain-loss and stock-change reporting methods (Table 6.12 in EU NIR, 2021). The net flux from a given country
596 can thus be based on either stock changes or flux changes.

597 ^b The definition of NBP varies from model to model. Most models include harvest, but not necessarily other disturbances. Please refer to Table
598 C2 for more details.

599 ^c The net carbon flux from regional inversions over land is the residual after fixing fossil CO₂ emissions and CO₂ fluxes from biomass burning.
600 In other words, any flux not included in those two categories is reflected in the net flux from the inversions. Biomass burning is prescribed in two
601 of the EUROCOM models (LUMIA and FLEXINVERT+; see Monteil et al., 2020, and Thompson et al., 2020) and ignored (i.e., assumed
602 negligible in Europe) for the others.

603 All of the bottom-up models in this work require external forcing datasets. In the context of the VERIFY
604 project (VERIFY, 2022), an effort was made to provide a single, harmonized version of several kinds of data
605 (meteorological, land use/land cover, and nitrogen deposition) on a high-resolution grid over Europe. These datasets
606 were then made available to all of the modeling groups to use in their simulations. Such a practice is common in
607 model intercomparison projects. However, as the models in Table 2 are not all the same type, data harmonization

- Formatted: Footer Char, Font: (Default) Calibri, 11 pt
- Formatted: Footer Char, Font: (Default) Calibri, 11 pt
- Formatted: Footer Char, Font: (Default) Calibri, 11 pt
- Formatted: Footer Char, Font: (Default) Calibri, 11 pt
- Formatted: Footer Char, Font: (Default) Calibri, 11 pt, Subscript
- Formatted: Footer Char, Font: (Default) Calibri, 11 pt
- Formatted: Footer Char, Font: (Default) Calibri, 11 pt, Subscript
- Formatted: Footer Char, Font: (Default) Calibri, 11 pt

608 presented more of a challenge in this work as not all models use the same inputs. All of the datasets described in
609 Appendix A₅ were used by at least one modeling group in this work.

Deleted: 2

610

611 **2.4. Independence of estimates**

Formatted: Heading 2

612 As pointed out by Andrew (2020), bottom-up fossil CO₂ emission datasets are not entirely independent, since
613 they largely rely on activity data reported by national agencies. However, there is some variation here, particularly in
614 traded energy products where, for example, activity data may be sourced from either the exporter or the importer
615 according to some determination of reporting reliability. However, beyond the underlying activity data, other choices
616 do vary between datasets: emission factors, which specific products lead to emissions, and how the activity data are
617 used to estimate the amount of energy product that is consumed, among others. Some examples of differences include:
618 CDIAC avoids using reported energy consumption and relies on estimating apparent consumption from the major
619 energy flows; CEDS initially used a very different estimate for emissions from international shipping; EDGAR and
620 IEA use a Tier 1 approach with default emission factors, while PRIMAP-Hist and GCP use officially reported
621 emissions based on higher Tier methods and country-specific emission factors for selected countries. Further, the
622 emission sources covered can vary widely between datasets, with the IEA usually limited to emissions from energy
623 products, while EDGAR, for example, attempts to include all fossil CO₂ sources. With this lack of full independence
624 between datasets' sources and methods, the uncertainty ranges should be interpreted with caution.

625 In addition to fossil bottom-up methods, the question of dataset independence can be applied to bottom-up
626 inventories of the land fluxes, as well as both bottom-up and top-down models. The issue is perhaps less relevant for
627 model results which, despite sharing input data (as done here to facilitate intercomparison) and 'genetics' (i.e., model
628 development history), create independence through choices of model structure, parameterization, and statistical
629 solvers. This question has been addressed elsewhere for land surface models (e.g., Prentice et al., 2015). For
630 inventories, the NGHGI and FAOSTAT share some data (e.g., Tubiello et al., 2021, for the case of Forestland, and
631 Conchedda and Tubiello, 2020, for drained organic soils in Grassland and Cropland). However, the model approaches
632 can be quite different, with FAOSTAT limited to Tier 1 (applicable to every country in the world based on available
633 statistics) and the NGHGIs, in particular in Europe, using more Tier 2 (regional and country-specific emission factors)
634 and Tier 3 (process-based models) approaches, depending on the country and the specific pool. For example, 21
635 Member States in the European Union report changes of organic carbon stored in mineral soils on Forest land using a
636 Tier 1 method, while only two (Malta and Cyprus) use a Tier 1 method for estimates of carbon stored in living biomass
637 on Forest land (EU NIR, 2021).

638 In this work, the uncertainties for the NGHGI were calculated with assumptions of correlation based on the exact
639 method applied by the country. As detailed in the Appendix A2 (NGHGI uncertainties), subsector values across
640 countries are assumed to be correlated for all countries applying a Tier.1 approach as they share default emission
641 factors. The uncertainties calculated for the NGHGI fossil and LULUCF fluxes, therefore, reflect more accurately
642 spatial dependence between the inventories of each Member State.

643

Formatted: Normal paragraph, Left, Indent: First line: 0 cm, Line spacing: single

3. Results and discussion

3.1. Overall NGHGI reported anthropogenic CO₂ fluxes

In 2019, the UNFCCC NGHGI (2021) net CO₂ flux estimates for EU27+UK accounted for 820 Tg C from all sectors (including LULUCF) and 900 ± 10 Tg C excluding LULUCF (Fig. B1), corresponding to a net sink of LULUCF of -74 ± 30 Tg C, where the uncertainties are 95 % CI calculated in accordance with the gap-filling methods of Appendix A2 and propagated to the sector level through Gaussian quadrature. In 2019, few large economies accounted for the majority of EU27+UK emissions, with Germany, UK, Italy and France representing 53 % of the total CO₂ emissions (excluding LULUCF). For the LULUCF sector, the countries reporting the largest CO₂ sinks in 2019 were Italy, Spain, Sweden, and France accounting for 56 % of the overall EU27+UK sink. Only a few countries (Czech Republic, The Netherlands, Ireland and Denmark) reported a net LULUCF source in 2019. Some countries, like Portugal, report sources in some years due to wildfires, with sinks in other years. The NGHGI shows minimal interannual variability in the LULUCF sector (Fig. B2), largely due to methodology. For example, emissions and removals from Forest land are typically based on forest statistics and surveys that are only completed every 5-10 years (see, for example, the national inventory reports and references cited therein of France, Germany, and Sweden). The largest contributors to IAV in the EU NGHGI forestry fluxes are fires and windstorms (EU NIR, 2021). Consequently, the 2019 values are indicative of longer-term averages.

CO₂ fossil emissions reported by Member States are dominated by the energy sector (energy combustion and fugitives) representing 92 % of the total EU27+UK CO₂ emissions (excluding LULUCF) or 895 Tg C in 2019. The Industrial Process and Product Use (IPPU) sector contributes 7.6 % or 68 Tg C (21 Tg C of which is cement production). CO₂ emissions reported as part of the agriculture sector cover only liming and urea application, UNFCCC categories 3G and 3H⁹ respectively. Together with waste, in 2019 the emissions from agriculture represent 0.4 % of the total UNFCCC CO₂ emissions in the EU27+UK.

An overview of all CO₂ fossil and land datasets in this work (Fig. 1) leads to a series of conclusions: 1) Regardless of the method used (NGHGI, bottom-up models, top-down models), the timeseries of annual fluxes from fossil CO₂ emissions rest almost one order of magnitude higher than removals from CO₂ uptake/removal by the land surface and well outside uncertainty estimates (Figs. 1a-c); 2) Uncertainties are much larger in the LULUCF estimates than in the fossil CO₂ estimates, regardless if one represents uncertainty by internal random error (i.e., the NGHGI totals in Fig. 1a, and the sub-sector LULUCF fluxes in Fig. 1d) or ensemble spread (i.e., bottom-up models in Fig. 1b, and the sub-sector LULUCF fluxes in Fig. 1e); 3) Interannual variability (IAV) is much more present in non-NGHGI LULUCF datasets (colored lines in Figs. 1b,c,e) than in NGHGI LULUCF datasets (Figs. 1a,d) or any of the fossil datasets (black lines in all subplots). As datasets are not fully independent, the uncertainties in Fig. 1 need to be interpreted with caution.

The overall message that fossil CO₂ emissions exceed the land sink (Figs. 1a-c) is the same as found in the Global Carbon Budget (Friedlingstein et al., 2022), although the difference is larger in the EU27+UK. Contrary to

⁹ 3G and 3H refer to UNFCCC category activities, as reported by the standardized common reporting format (CRF) tables, which contain CO₂ emissions from agricultural activities: liming and urea applications.

Formatted: Heading 1, Space After: 0 pt, Line spacing: single, Tab stops: Not at 0,48 cm

Formatted: Heading 2, Line spacing: single

Deleted: In 2019, the UNFCCC NGHGI (2021) net CO₂ flux estimates for EU27+UK, accounted for 3.01 Gt CO₂ from all sectors (including LULUCF) and 3.28 Gt CO₂ excluding LULUCF (Fig. B1), corresponding to a net sink of LULUCF of -0.27 ± 0.11 Gt CO₂

Deleted: The NGHGI shows minimal inter-annual variability (largely due to methodology), and consequently the 2019 values are indicative of longer-term averages, showing a constant trend between 2017-2019.

Deleted: +

Deleted:

Deleted: 3.02 Gt CO₂

Deleted: yr⁻¹

Deleted: 0.2 Gt CO₂ yr⁻¹

Formatted: Normal paragraph, Left, Indent: First line: 0 cm, Line spacing: single

Deleted: Uncertainties are much larger in the LULUCF estimates than in the fossil CO₂ estimates (both for total LULUCF and for individual components of FL, CL, and GL);

Formatted: Footer Char, Font: (Default) Calibri, 11 pt, Font colour: Auto

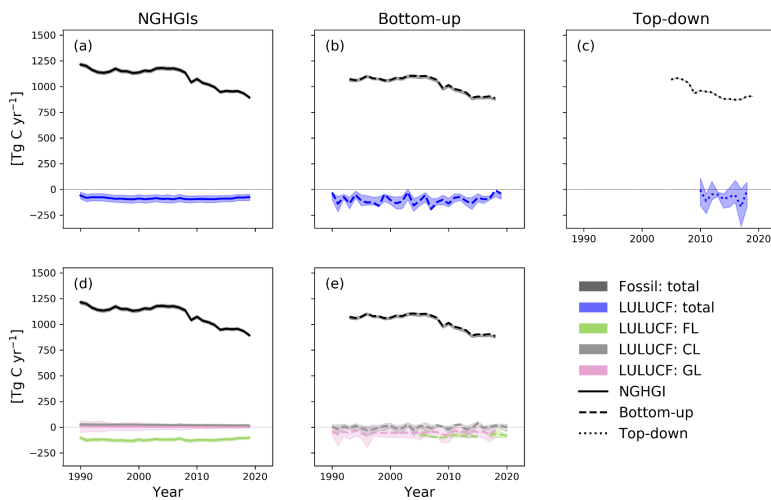
Formatted: Footer Char, Font: (Default) Calibri, 11 pt

Formatted: Footer Char, Font: (Default) Calibri, 11 pt, Font colour: Auto

696 the GCB, however, fossil CO₂ emissions in the EU27+UK have decreased over the past three decades. Again, this
 697 finding is supported by the NGHGI, bottom-up models, and a single atmospheric inversion. By applying a Monte
 698 Carlo analysis and taking each point to be normally distributed around the mean with a width 2σ equal to the given
 699 95 % CI, we realized 1000 linear regressions of the NGHGI across the 1990-2019 period. From this, we fit a normal
 700 distribution to the slopes, and can rule out trends greater than 0.07 or less than -0.61 Tg C yr⁻² with 95 % confidence.
 701 Therefore, any trend over these 30 years is likely less than 1 % of the net carbon uptake, with the vast majority of that
 702 occurring in forests. While the latter conclusion is clear in the NGHGI (Fig. 1d), very large spreads among bottom-
 703 up categorical models lead to more uncertainty (bottom-center).

704 The difference in uncertainty between the estimates of fossil CO₂ emissions and CO₂ uptake/removal by the land
 705 surface is also striking. Eight bottom-up models produce a mean 25-75th percentile spread of 24 Tg C yr⁻¹ across the
 706 overlapping timeseries (center-top, gray shading). On the other hand, four models estimating Grassland
 707 emissions/removals produce an error bar that covers the bottom part of the graph and masks any apparent trend
 708 (bottom-center, light green shading). A similar conclusion can be drawn from top-down estimates of LULUCF fluxes
 709 (top-right, blue shading). Additional work on reducing the uncertainty of LULUCF fluxes in the EU27+UK is highly
 710 welcome.

711



712

713 *Figure 1: A synthesis of all the CO₂ net fluxes shown in the work for the EU27+UK. The estimates are divided by*
 714 *approach: NGHGI estimates (panels a, d); bottom-up methods (b, e); and top-down methods (c). Panels (d) and (e)*
 715 *include a breakdown of the [bottom-up] LULUCF flux into three of the dominant components: FL, GL, and CL.*
 716 *Such a breakdown is not provided for NGHGI CO₂ fossil as partitioning of bottom-up CO₂ fossil datasets*
 717 *corresponding to UNFCCC NGHGI categories is not currently available. The NGHGI UNFCCC uncertainty is*
 718 *calculated for submission year 2021 as the relative error of the NGHGI value, computed with the 95 % confidence*

Deleted: Similarly, carbon uptake by the land surface has remained more or less stable over the past three decades

Deleted: sectorial

Deleted: Eight bottom-up models produce a 25-75 % percentile which is almost invisible on the scale of the graph (center-top, gray shading).

Formatted: Caption - VERIFY, Left, Line spacing: single

Formatted: Font: Subscript

725 interval method gap-filled and provided for every year of the timeseries, except for FL, GL, and CL which are taken
726 directly from the EU NIR (2021). Shaded areas for the other estimates represent the 0th-100th percentiles for
727 groups with fewer than seven members, and the 25th-75th percentile for groups with seven or more members.
728 Ensembles (e.g., TRENDY v10) are included in the above only their mean values, to avoid more heavily weighting
729 the ensembles compared to the other datasets.

730

731 Several caveats remain with this overall synthesis. First, the timeseries were combined rather naively in Fig. 1
732 by taking the mean of annual timeseries for each dataset discussed below. This leads to, for example, the 15-member
733 TRENDY ensemble being given identical weight as the ORCHIDEE high-resolution simulation over Europe. This
734 was done to weigh more heavily the regional approaches under the assumption that higher resolution simulations and
735 more region-specific input data will lead to more accurate results. While the latter assumption appears reasonable,
736 the first assumption can be disputed. Finer resolution leads to models being exposed to values of input variables (e.g.,
737 temperature, rainfall) outside the parameterization range, which may result in unexpected behavior. Process
738 representation can also change with spatial scale. Constant tree mortality, for example, is often used in models at
739 coarse resolution, while abrupt tree mortality (stand-replacing disturbances) may better describe stand-level dynamics.
740 Second, only a single top-down result for fossil CO₂ emissions is currently available, preventing an estimate of the
741 uncertainty for this approach. Third, categorical models were combined disregarding distinctions between those
742 models estimating “Remain” and “Total” fluxes, where Total indicates all land of a particular type (e.g., Forest land)
743 regardless of the length of time it has been this type, i.e., Total is the sum of all Remain and Convert. These points
744 are discussed in more detail in the following sections. However, addressing these points is highly unlikely to alter the
745 overall conclusions in this section.

746

747 3.2. CO₂ fossil emissions

748 The inventory-based fossil CO₂ estimates from nine data sources (and some subsets) are presented as timeseries
749 (1990-last available year) based on Andrew (2020) with the objective to explore differences between datasets and
750 visualize trends (Fig. 2). Because the emissions source coverage (also called the “system boundary”) of datasets
751 varies, comparing total emissions from these datasets is not a like-for-like comparison. Therefore, some harmonization
752 of system boundaries prior to comparison is needed. This harmonization relies on specifying the system boundary of
753 each dataset and, where possible, removing emission sources to produce a near-common system boundary. For
754 example, IEA doesn’t include any carbonates, and thus carbonates were removed from all emissions datasets that
755 include them. UNFCCC (CRFs) Energy+IPPU, CDIAC, CEDS, PRIMAP, and GCP include Energy sector plus all
756 fossil fuels in IPPU; EIA, EDGAR and BP include some fossil fuels in IPPU, while EIA and BP include bunker fuels
757 as well. UNFCCC CRFs include Energy total and Energy combustion. Further details on how data sets are harmonized
758 are provided by Andrew (2020). Because of differing levels of detail provided by datasets, it isn’t possible to do this
759 perfectly, but the approximate harmonization gives something closer to a like-for-like comparison, with the legend in
760 Fig. 2 indicating the most significant remaining differences. The pre-harmonization curves are shown in Appendix
761 A3 (Fig. A1) for reference.

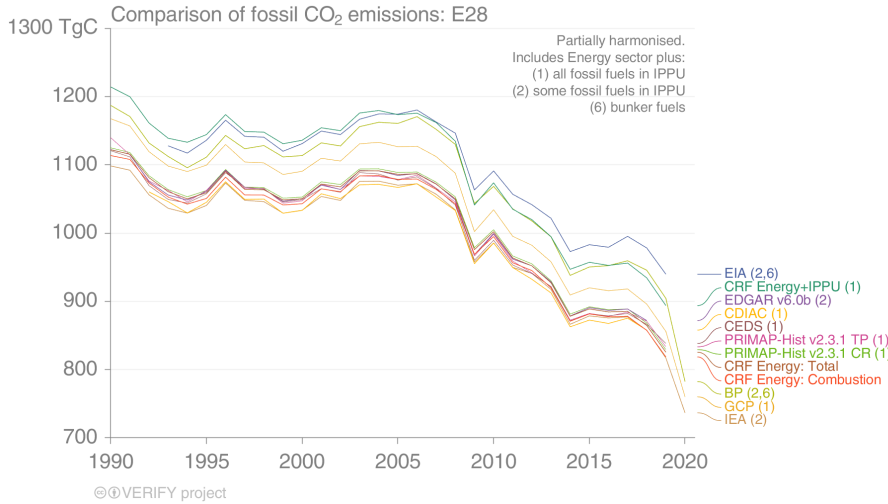
762

Deleted: sector

Deleted: between those models estimating “Remain” and
“Total” fluxes...

Formatted: Heading 2, Space After: 0 pt, Line spacing:
single

Deleted: For example, if IEA doesn't include any carbonates,
then carbonates are removed from all emissions datasets that
report these separately



770

771 *Figure 2: Comparison of EU27+UK fossil CO₂ emissions from multiple inventory datasets with system boundaries*
 772 *harmonized as much as possible. Harmonization is limited by the disaggregated information presented by each*
 773 *dataset. CDIAC does not report emissions prior to 1992 for former-Soviet Union countries. CRF: UNFCCC NGHGI*
 774 *from the Common Reporting Format tables. The pre-harmonization figure is shown in Fig. A1.*

775 Given the remaining differences in system boundaries after harmonization, most datasets agree well
 776 (Andrew, 2020). In response to inconsistencies identified in this work, the EIA recently corrected some double-
 777 counting of emissions from liquid fuels and has revised its estimates of total emissions down about 10 % for the
 778 EU27+UK (pers. comm., US Energy Information Agency, February 2022). For comparison, applying a similar
 779 harmonization procedure to the UNFCCC NGHGI and retaining only Fuel combustion (1A), Fugitive emissions (1B),
 780 Chemical industry (2B), Metal industry (2C), Non-energy products from fuels and solvent use (2D), and Other (2H)
 781 results in emissions of $930 \pm 10 \text{ Tg C yr}^{-1}$ for the year 2017, where the uncertainty was propagated through quadrature
 782 using the gap-filled uncertainties described in this work and taking the total sector uncertainty if the category
 783 uncertainty was not available. This mean value falls within the 25th-75th percentiles of the eight other harmonized
 784 BU sources ($[884, 928] \text{ Tg C yr}^{-1}$). Across the overlapping timeseries, the mean value of the 25th-75th percentile is 24
 785 Tg C yr^{-1} , with a 0th-100th percentile of 100 Tg C yr^{-1} .

786 The sole available inversion for CO₂ fossil fluxes is produced by the CIF-CHIMERE model, shown in Fig. 1c
 787 and Fig. B3 (for a single year). The inversion yields plausible fossil emission estimates, although it is below NGHGI
 788 estimates including both Energy and IPPU (Figs. 1a,c,B3) as well as the ensemble of nine bottom-up inventories.
 789 Uncertainties of CIF-CHIMERE inversion estimate have not yet been quantified, however they are likely largely
 790 driven by large uncertainties in the input data. The satellite observations of NO₂ have large uncertainties, which partly
 791 explains the small departure from the prior fluxes during the optimization. Emission ratios between NO_x and CO₂ are

- Commented [MOU]: Figure has been changed.
- Formatted: Font: Font colour: Auto
- Formatted: Default Paragraph Font, Font: (Default) Times New Roman, 10 pt, Italic
- Formatted: Font:
- Formatted: Font: Font colour: Auto
- Formatted: Left, Space Before: 0 pt, After: 8 pt, Line spacing: Multiple 1,08 li, Border: Top: (No border), Bottom: (No border), Left: (No border), Right: (No border), Between: (No border)
- Formatted: Font:
- Formatted: Font: Font colour: Auto
- Formatted: Font:
- Formatted: Font: Font colour: Auto
- Formatted: Font:
- Formatted: Font: Font colour: Auto
- Formatted: Font:
- Formatted: Font: Font colour: Auto
- Formatted: Font:
- Formatted: Font: Font colour: Auto
- Formatted: Font:
- Formatted: Font: Font colour: Auto
- Formatted: Font:
- Formatted: Font: Font colour: Auto
- Formatted: Font:
- Deleted: 3392 ± 49 Tg CO₂ yr⁻¹ (
- Deleted: 26
- Deleted: 3
- Deleted:)
- Deleted: 3238
- Deleted: 3401
- Deleted: O₂
- Formatted: Superscript
- Formatted: Superscript
- Formatted: Superscript
- Formatted: Superscript
- Formatted: Superscript
- Formatted: Superscript
- Formatted: Superscript
- Formatted: Superscript
- Deleted: The inversion yields plausible and consistent fossil emission estimates compared to nine bottom-up estimates from BU datasets with global coverage (Fig. 1b,c,B3)
- Deleted: 2

803 also uncertain (those from the prior are currently used). The atmospheric ~~chemistry surrounding both production and~~
 804 ~~destruction~~ of NO₂ is another major source of uncertainty. The inversion reports total fossil CO₂ emissions calculated
 805 from NO_x ~~fossil fuel~~ combustion emissions. However, in principle, the derivation of CO₂ emissions from the NO_x
 806 inversions should be restricted to ~~derivation of~~ fossil fuel CO₂ emissions based on the fossil fuel CO₂/NO_x ratio from
 807 the TNO ~~inventory, since there is no process linking the other fossil CO₂ emissions to the NO_x fossil fuel emissions,~~
 808 Future inversions co-assimilating CO₂ data will ~~have to~~ make a clearer distinction in the processing of fossil-fuel and
 809 other anthropogenic emissions ~~in order to exploit the joint fossil fuel signals in CO₂ and NO_x observations.~~ Finally, it
 810 ~~is~~ important to note that the inversion results are not fully independent of the bottom-up methods, as the prior estimates
 811 ~~and CO₂/NO_x emission ratios~~ are based on TNO gridded products. However, part of the lack of departure from the
 812 prior can also be attributed to the general consistency between the prior and the observations, which raise optimistic
 813 perspectives for the co-assimilation of co-emitted species with the data from future CO₂ networks dedicated to
 814 anthropogenic emissions.

815 **3.3. CO₂ land fluxes**

816 This section updates the benchmark data collection of CO₂ emissions and removals from the LULUCF sector in
 817 EU27+UK previously published in Petrescu et al. (2020) and Petrescu et al. (2021b), expanding on the scope of those
 818 works by adding additional datasets and years. ~~The following graphs occasionally show large differences compared~~
 819 ~~to previously-reported values. This may happen when the model has undergone substantial changes since the work~~
 820 ~~of Petrescu et al. (2021b), such as the case with ORCHIDEE and the addition of a dynamic nitrogen cycle coupled to~~
 821 ~~the carbon cycle. Such cases are both identified in the text as appropriate and as well as in Table 2.~~ The countries
 822 analyzed in this study use country-specific activity data and emissions factors for the most important land use
 823 categories and pools (EU NIR 2022, UK NIR 2022). However, several gaps still exist, mainly in non-forest lands and
 824 non-biomass pools (e.g., soil carbon in Forest land mineral soils, dead organic matter on Cropland and Grassland; for
 825 more details, see Table 6.6 in EU NIR, 2021). In addition, since NGHGs largely rely on periodic forest inventories
 826 (carried out every five to ten years) for the most important land use (Forest land), the net CO₂ LULUCF flux often
 827 does not capture the most recent changes, nor the full interannual variability.

828 While the net LULUCF CO₂ flux was relatively stable from 1990 to 2016, staying mostly between ~~-80 to -95 Tg~~
 829 ~~C yr⁻¹~~ in the past three years the sink has weakened to around ~~-70 Tg C yr⁻¹~~ in 2020 (black dotted line in Fig. B2,
 830 Appendix B1; Abad-Viñas, pers. comm, 2022). This weakening occurred mostly in Forest land, due to a combination
 831 of increased natural disturbances, forest aging and increased wood demand (Nabuurs et al., 2013; EU NIR, 2022).
 832 Natural disturbances, including fires (especially in the southern Mediterranean), windthrows, droughts and insect
 833 infestations (especially in central and northern European countries), have increased in recent years (e.g., Seidl et al.,
 834 2014) which explains most of the interannual variability of ~~the~~ NGHGI. Forest aging affects the net sink both through
 835 the forest growth (net increment) - which tends to level off or decline after a certain age ~~and~~ the harvest, because a
 836 greater area of forest reaches forest maturity (Grassi et al., 2018b). Although the exact increase in total harvest in
 837 Europe in recent years is still subject to debate (Ceccherini et al., 2020; Palahi et al. et al., 2021), demand for fuelwood

- Deleted: residence
- Deleted: time
- Formatted: Subscript
- Formatted: Subscript
- Formatted: Subscript
- Deleted: as there is a better-established relationship between CO₂ and NO_x from combustion of fossil fuels
- Formatted: Subscript
- Formatted: Subscript
- Formatted: Subscript
- Formatted: Subscript
- Deleted: '
- Formatted: Subscript
- Formatted: Subscript
- Deleted: ¶
- Formatted: Normal, Line spacing: single, No bullets or numbering, Tab stops: Not at 0,63 cm
- Deleted: (e.g., EU NIR, 2022).
- Deleted: 300
- Deleted: -350
- Formatted: Normal paragraph, Left, Indent: First line: 0 cm, Line spacing: single, Border: Top: (No border), Bottom: (No border), Left: (No border), Right: (No border), Between : (No border)
- Deleted: Mt CO₂/yr
- Deleted: 250 Mt CO₂/yr
- Formatted: Superscript
- Formatted: Superscript
- Deleted: s
- Deleted: - and

854 at least has increased (Camia et al., 2021). The impacts of aging on mortality, another process which affects the net
 855 sink through reduced production and increased respiration, are less clear (e.g., Gray et al., 2016; Senf et al., 2018).
 856 Net carbon uptake as seen by the atmosphere may occur on either managed or unmanaged land, and results from
 857 the balance of processes such as photosynthesis, respiration, and disturbances (e.g., fire, pests, harvest). As discussed
 858 by Petrescu et al. (2020), the fluxes reported in NGHGs relate to emissions and removals from direct LULUCF
 859 activities (clearing of vegetation for agricultural purposes, regrowth after agricultural abandonment, wood harvesting
 860 and recovery after harvest and management) but also indirect CO₂ fluxes due to processes such as responses to
 861 environmental drivers on managed land (e.g., long-term changes in CO₂, air temperature, and water availability).
 862 Additional CO₂ fluxes occur on unmanaged land, but the fraction of unmanaged land in the European Union is only
 863 around 5 % and divided between Forest land, Grassland, and Wetlands. According to Table 4.1 in the EU27 and UK
 864 NGHGs (2021) CRF, almost all land (~95 %) in the EU27+UK is considered managed. France and Greece report
 865 some unmanaged Forest land (1.1 % and 16.6 %, respectively). Hungary and Malta report unmanaged Grassland of
 866 33 % and 100 %, respectively, and Nordic and Baltic countries plus Ireland, Slovakia and Romania report sometimes
 867 quite large (up to 100 %) unmanaged Wetlands.

868 The indirect CO₂ fluxes on managed and unmanaged land due to changing climate, increasing atmospheric
 869 carbon dioxide mole fractions, and nitrogen deposition, are part of the (natural) land sink in the definition used in
 870 IPCC Assessment Reports and the Global Carbon Project's annual global carbon budget (Friedlingstein et al., 2022),
 871 while the direct LULUCF fluxes are termed “net land-use change flux”, as discussed by Grassi et al. (2018a, 2021,
 872 2022a), Petrescu et al. (2020, 2021b) and Pongratz et al. (2021). Results should thus be interpreted with caution due
 873 to these definitional differences, but as most of the land in Europe is managed and the indirect effects are small, the
 874 definitional differences should be modest compared to other sources of uncertainty (Petrescu et al., 2020). Other
 875 relatively recent studies have already analyzed the European land carbon budget using GHG budgets from fluxes,
 876 inventories and inversions (Luyssaert et al., 2012) and from forest inventories (Pilli et al., 2017; Nabuurs et al., 2018).

878 3.3.1. Estimates of CO₂ land fluxes from bottom-up approaches

879
 880 In this section we present annual total net CO₂ land emissions between 1990-2020 i.e., induced by both
 881 LULUCF and natural processes (e.g., environmental changes) from category-specific models as well as from models
 882 that simulate multiple land cover/land use categories. The definitions of the categories may differ from the IPCC
 883 definitions of LULUCF (e.g., FL, CL, GL) where, according to IPCC 2006 guidelines, to become accountable in the
 884 NGHGI under “remaining” categories, a land-use type must be in that category for at least N years (where N is the
 885 length of the transition period; 20 years by default). In an effort to create the most accurate comparison possible in
 886 terms of categories and processes included, total Forest land (FL) has been divided up into Forest land remaining
 887 forest land (FL-FL) and Land converted to forest land (X-FL), while only total Grassland (GL) and Cropland (CL) are
 888 reported. This is largely due to the non-forest categorical models explored here only considering net land use change,
 889 which prevents separating out the “converted” component.

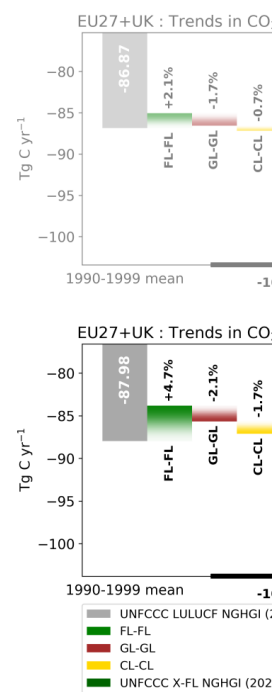
890

Deleted: Carbon

Formatted: Subscript

Deleted: but these fluxes are very small in Europe...
 According to Table 4.1 in the EU27 and UK NGHGs (2021) CRF, almost all land (~95 %) in the EU27+UK is considered managed. France and Greece report some unmanaged forest areas...orest land (1.1 % and 16.6 %, respectively). Hungary and Malta report unmanaged Grassland areas ...f 33 % [13]

Deleted: concentration



Moved down [4]:

Deleted: 3.3.2. LULUCF CO₂ fluxes from NGHGI and decadal changes

Figure 3 shows the decadal change in CO₂ LULUCF flux from the UNFCCC NGHGI (2019) (upper plot) comp... [14]

Deleted: 3

Formatted: Normal, Line spacing: single

Deleted: e.g., environmental changes) from class...category-specific models as well as from models that simulate multiple land cover/land use classes...ategories. The definitions of the classes...ategories may differ from the IPCC definitions of LULUCF (e.g., FL, CL, GL) where, according to IPCC 2006 guidelines, to become account... [15]

1111 **3.3.2. Bottom-up estimates of CO₂ from Forest land**

1112
1113 Fluxes from Forest land which remain in this category (FL-FL) are shown in Fig. 3 (top). These fluxes were
1114 simulated with ecosystem models (CBM and EFISCEN-Space, described in more detail in the Appendices) and
1115 countries' official inventory statistics reported to UNFCCC. The results show that the differences between models are
1116 systematic, with CBM having slightly weaker sinks than EFISCEN-Space. CBM updated its historical data (1990-
1117 2015) and presents new NBP estimates based on extrapolation of historical timeseries (see Appendix A4) for 2017-
1118 2020 (CBMsim). Both CBM and EFISCEN-Space use national forest inventory (NFI) data as the main source of input
1119 to describe the current structure and composition of European forests. NFIs are also the main source of input data for
1120 most countries in the EU27+UK for NGHGIs (EU NIR, 2021), including data for carbon stock changes in various
1121 pools as well as the estimation of forest areas. Given that EFISCEN-Space does not cover all countries in the
1122 EU27+UK (Austria, Bulgaria, Denmark, Hungary, Lithuania, Portugal and Slovenia are missing), the results were
1123 scaled by 1/0.74 to account for the fact that the available countries comprise around 74 % of the forest NBP for the
1124 EU27+UK, according to previous EFISCEN results (Petrescu et al., 2021b). As noted above, EU regulations are
1125 driving Member States to report spatially explicit NGHGIs. Unlike the original EFISCEN, EFISCEN-Space is a
1126 spatially explicit model, in addition to being able to simulate a wider variety of stand structures, species mixtures and
1127 management options. Note that EFISCEN-Space reports only a single mean value for forest fluxes from 2005-2020;
1128 the annually varying value shown in Fig. 3 (top) arises from scaling by annually varying forest areas.

1129 The bottom panel in Fig. 3 presents CO₂ land estimates for total Forest land (FL, including both remain and
1130 convert classes). For the total Forest land, the results were simulated with an ecosystem model (ORCHIDEE) and a
1131 global dataset (FAOSTAT) as it is not possible for these two approaches to separate out the “remain” and “convert”
1132 land use category. This obstacle arises due to the use of net land use/land cover information which does not include
1133 detailed information on the nature of the conversions. Consequently, Fig. 3 (bottom) compares flux estimates to those
1134 on all Forest land from the countries' official inventory statistics (UNFCCC NGHGI, 2021).

1135 The top and bottom panels in Fig. 3 are not directly comparable due to different quantities being displayed (FL-
1136 FL vs. FL). For the NGHGI, the value in the bottom panel is simply the value from the top panel with the addition of
1137 emissions/removals on land converted to Forest land within the past 20 years. The sink gets stronger by around 20
1138 Tg C yr⁻¹ when considering FL, which is to be expected as abandonment of Cropland or Grassland and subsequent
1139 regrowth of forest results in a net uptake of carbon due to storage in woody biomass. The UNFCCC NGHGI
1140 uncertainty of CO₂ estimates from Forest land across the EU27+UK, computed with the error propagation method (95
1141 % confidence interval, see IPCC, 2006), is 13.5 % for the year 2019 (EU NIR, 2021). This percentage is applied
1142 across all years for both FL and FL-FL, and in year 2019 it translates into an uncertainty of 12 Tg C for FL-FL.

1143 Differences within the top panel of Fig. 3 are small, perhaps because all three approaches (NGHGI, CBM,
1144 EFISCEN-Space) rely heavily on forest inventory statistics. The same can be said for FAOSTAT FL fluxes in the
1145 bottom panel of Fig. 3. Among all the data plotted on the two graphs, ORCHIDEE stands out. Despite site-level
1146 evaluation (e.g., Vuichard et al., 2019), the vegetation classes in ORCHIDEE are fairly broad (e.g., temperate
1147 needleleaf evergreen) and parametrized to reproduce global fluxes, which means ORCHIDEE may be less suitable for

Formatted: Font: (Default) Calibri, 12 pt, Not Italic, Font colour: Text 1, Subscript

Formatted: Left, Space After: 8 pt, Line spacing: Multiple 1,08 li

Deleted: class

Deleted: 4

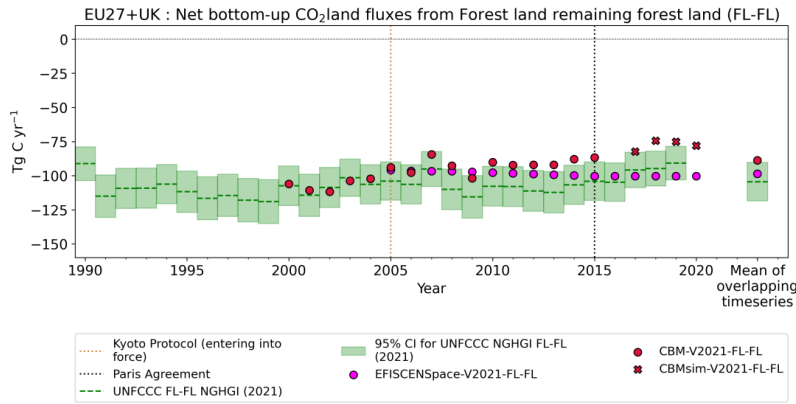
Formatted: Font: Not Bold

Deleted: 2

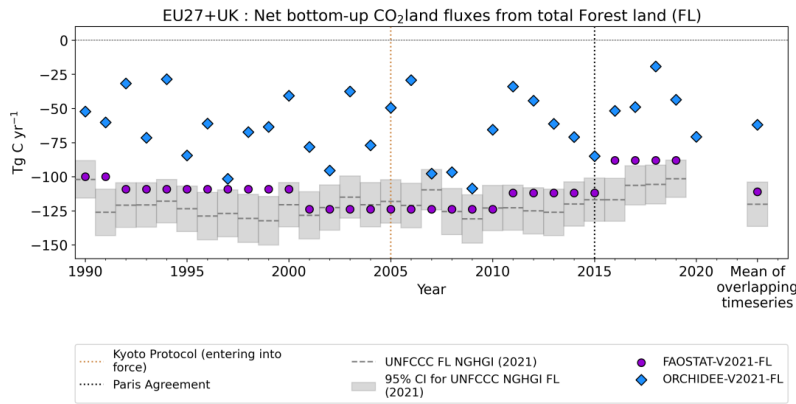
Deleted: 4

1152 regional simulations without further adjustments. As trends in forest carbon strongly result from management, the
 1153 lack of explicit management in this version of ORCHIDEE also likely contributes, given the importance of
 1154 management across Europe.

1155
 1156

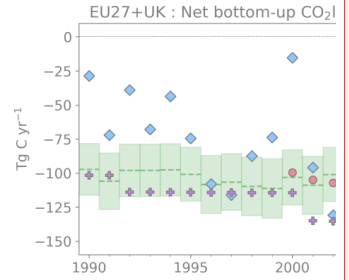


VERIFY Project

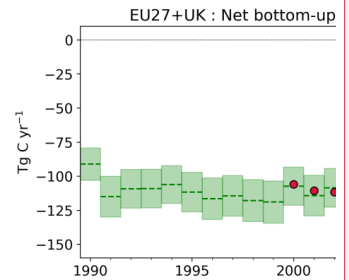


VERIFY Project

1157
 1158 **Figure 3:** Net CO₂ land flux from Forest land remaining forest land (FL-FL, top panel) and total Forest land (FL,
 1159 bottom) for EU27+UK. Means are given for 2005-2019 (top) and 1990-2019 (bottom) on the right side of both
 1160 plots. CBM FL-FL historical estimates include 25 EU and UK countries (excl. Cyprus and Malta), in addition to
 1161 new estimates for 2017-2020 (red crosses). EFISCEN-Space results have been scaled up from available countries as



VERIFY Project



VERIFY Project

Deleted:

Deleted: 4

Deleted: estimates

Formatted: Caption - VERIFY, Left, Line spacing: single

Deleted: K CO₂ from the Petrescu et al. (2021b) synthesis paper (top) and a comparable graph using the updated data this year (bottom).

Deleted: 2006-2015 (top) and

Deleted: bottom

Deleted: and include

Moved (insertion) [2]

Deleted: Net CO₂ land flux from total Forest land estimates (FL) for EU27+UK CO₂ from the UNFCCC NGHGI (2021) submissions, the FAOSTAT data-driven inventory, and the ORCHIDEE DGVM.

1175 *described in the text. FAOSTAT data does not include Romanian inventory estimates. The relative error on the*
1176 *UNFCCC value represents the UNFCCC NGHGI (2021) MS-reported uncertainty with no gap-filling (EU NIR,*
1177 *2021). The fluxes follow the atmospheric convention, where negative values represent a sink while positive values*
1178 *represent a source.*

1179 *Romanian estimates for FL in FAOSTAT (Fig. 3, bottom) have been removed due to a reporting inconsistency,*
1180 *which had not yet been corrected at the time of this analysis. In general, FAOSTAT results match well the NGHGI*
1181 *results, despite differences in models and even occasionally underlying data reported by countries to both*
1182 *organizations (Tubiello et al., 2021). ORCHIDEE was updated to include a dynamic nitrogen cycle coupled to the*
1183 *carbon cycle in this work. As shown in Appendix A4, the coupled nitrogen cycle results in a stronger sink, even if*
1184 *identical forcing is used. ORCHIDEE shows a higher inter-annual variability in carbon fluxes for forests than the*
1185 *NGHGI in Fig. 3 (bottom), because it incorporates meteorological data at sub-monthly timescales, while methods*
1186 *based on forest inventories are generally updated only every few years (e.g. five years for FRA), which results in a*
1187 *more climatological perspective. ORCHIDEE results indicate that climatic perturbations and extreme events (multi-*
1188 *month droughts, in particular) can have significant impacts on the net carbon fluxes depending on their timing in*
1189 *relation to the growing season. Flux tower measurements show that carbon sink strength in a European forest may*
1190 *weaken by 50 % during a summer drought, or a loss of 15 % of net carbon uptake over the course of the year (Ciais*
1191 *et al., 2005). This is also to some extent supported by dendrometer data although such data varies greatly among sites*
1192 *and tree species which obscures a significant net effect (Scharmweber et al., 2020). It should also be noted that*
1193 *dendrometer data measures carbon stored in individual trees, while the NBP reported in figures in this paper include*
1194 *respiratory fluxes from litter and soil. The variability of the weather affects the carbon dynamics of all components of*
1195 *the ecosystems (hence NBP), which, for instance, impacts on carbon assimilation rates, length of the growing season,*
1196 *dynamics of respiration rates and allocation of the carbon in the plant (cf. Fig. 1 and 2 in Reichstein et al. (2013) and*
1197 *Bastos et al. (2020b)).*

1199 3.3.3. Bottom-up estimates of CO₂ from Cropland and Grassland

1201 *Cropland (CL, UNFCCC subsector 4B) and Grassland (GL, UNFCCC sector 4C) include net CO₂ emissions*
1202 *from or removals by soil organic carbon (SOC) under "remaining" and "conversion" categories, and are shown in the*
1203 *top and bottom panels of Fig. 4, respectively, for the EU27+UK along with four other approaches: one bottom-up*
1204 *inventory (FAOSTAT), two category-specific models (EPIC-IIASA, ECOSSE), and one DGVM (ORCHIDEE). The*
1205 *previous synthesis of Petrescu et al. (2021b) compared models against NGHGI results for CL-CL and GL-GL. For*
1206 *the current work, we compare against the total Cropland (CL) and Grassland (GL) values. The reason for this is that*
1207 *FAOSTAT, ECOSSE, EPIC-IIASA, and ORCHIDEE all use land use/land cover maps generated by Approach 1 in*
1208 *IPCC (2006), which only records the total amount of land in a category for each year; information on transitions*
1209 *between categories is unknown. Therefore, it is not possible to separate out "remain" and "convert" categories.*

1210 *For CL during common period (1990-2019), ORCHIDEE simulates a mean sink of -26 Tg C yr⁻¹, while*
1211 *ECOSSE, EPIC-IIASA, and FAOSTAT all simulate mean sources of 21 Tg C yr⁻¹, 10 Tg C yr⁻¹ and 16 Tg C yr⁻¹,*
1212 *respectively. With the exception of ORCHIDEE, all models are in line with the NGHGI results (22 ± 14 Tg C yr⁻¹).*

Deleted: The relative error on the UNFCCC value represents the UNFCCC NGHGI (2021) MS-reported uncertainty with no gap-filling (EU NIR, 2021).

Deleted: Notice that some timeseries have been removed and placed in Fig. 5 as some datasets more accurately depict fluxes from total Forest land (FL).

Deleted: The UNFCCC NGHGI uncertainty of CO₂ estimates for FL-FL across the EU27+UK, computed with the error propagation method (95 % confidence interval) (IPCC, 2006), ranges between 34 % - 55 % when analyzed at the country level for all years, as it varies as a function of the component fluxes (EU NIR, 2019). Despite contrasting methodologies and input data for emission calculation and uncertainties in each method (Appendix A), there is reasonable agreement on the trend in FL-FL fluxes from CBMsim and the UNFCCC NGHGI (2021) (Fig. 4). The magnitude of the values between EFISCEN-Space and the NGHGI (2021) also agree well, though as noted above the EFISCEN-Space results only vary with the amount of forest area which makes the trend much flatter. Given that all three methods (NGHGI, CBM, and EFISCEN-Space) are heavily based on national forest inventory data, the general agreement between the three is not surprising.

Figure 5 presents CO₂ land estimates for total Forest land (both remain and convert classes, "FL"). For the total Forest land, the results were simulated with an ecosystem model (ORCHIDEE) and a global dataset (FAOSTAT) as it is not possible for these two approaches to separate out the "remain" and "convert" land use category. This obstacle arises due to the use of net land use/land cover information which does not include detailed information on the nature of the conversions. Consequently, Fig. 5 compares them [... [16]

Moved up [2]: Net CO₂ land flux from total Forest land estimates (FL) for EU27+UK CO₂ from the UNFCCC

Deleted: ¶ [... [17]

Deleted: 2

Deleted: 5

Deleted: This is in line with flux tower measurements that show significant year to year variability (Ciais et al. 2005).

Deleted: respiration

Deleted: data

Deleted: C

Deleted: A few reasons for differences between estimates seen in Fig. 4 and 5 can be readily identified. For this [... [18]

Formatted: Font: 12 pt, Font colour: Text 1, Subscript

Formatted: Left, Space After: 8 pt, Line spacing: Multiple 1,08 li

Formatted: Subscript

Deleted: Cropland (CL, represented in the UNFCCC NGHGI 2021 as UNFCCC category 4B) includes net CO₂ emi [... [19]

Deleted: the

Deleted: mean over the same period of

1373 The sink in ORCHIDEE arises from the soil, as no simulated biomass in croplands remains from year to year; carbon
1374 is assimilated into biomass growth during the growing season, after which the biomass dies, is partitioned between
1375 litter and harvest (50 % to each), and either decays or vaporizes, respectively. In other words, no woody or perennial
1376 crops are simulated. Given more favorable growing conditions due to climatic changes and CO₂ fertilization,
1377 increased litter leads to more carbon entering the soil in ORCHIDEE in recent decades, which is driving the calculated
1378 CL sink observed in the model.

1379 In the NGHGI, the reported source for the EU27+UK is mostly attributed to emissions from Cropland on
1380 organic soils¹⁶ in the northern part of Europe where CO₂ is emitted due to carbon oxidation from tillage activities and
1381 drainage of peat. In general, annual crops are assumed to be in carbon balance: any carbon assimilated during the year
1382 is respired in the same location. Woody crops (e.g., apple or olive orchards), however, are an exception, and Cropland
1383 on mineral soils uptake carbon in both France and Spain. Romania reports a strong sink on Cropland due to the
1384 inclusion of some forest plantations. Overall, emissions from organic soils on Land converted to cropland dominate,
1385 however, despite accounting for only 9 % of total Cropland area in the EU27+UK, they are responsible for 73 % of
1386 Cropland emissions (EU NIR, 2021). The fact that FAOSTAT values are similar to the UNFCCC values points to the
1387 primary role of drained organic soils, as this is the only flux included for the FAOSTAT dataset in Fig. 4. Finland
1388 and Sweden are of particular importance, as they together account for more than half of the total area of organic soil
1389 in Europe. Organic soils are an important source of emissions when they are under management practices that disturb
1390 the organic matter stored in the soil. In general, the NGHGI emissions from these soils are reported using country-
1391 specific values when they represent an important source within the total budget of GHG emissions.

1392 ORCHIDEE also shows a much larger year-to-year variation than EPIC-IIASA and ECOSSE. This is unlikely
1393 to be caused by model timesteps (EPIC-IIASA and ECOSSE at daily, ORCHIDEE at half-hourly) as both EPIC-
1394 IIASA and ECOSSE use minimum and maximum temperatures during the course of the day as input, not simply the
1395 mean daily temperature. Therefore, all three models should see similar extremes, and crop vegetation may simply be
1396 more sensitive to meteorological forcing in ORCHIDEE. FAOSTAT and NGHGIS are mostly insensitive to inter-
1397 annual variability as the estimations are mainly based on statistical data for surfaces/activities and emission factors
1398 that do not vary with changing environmental conditions.

1399 Both ECOSSE and EPIC show a striking improvement in agreement with the NGHGI between V2019 (Fig.
1400 B5, top) and the current work (Fig. B5, bottom). For ECOSSE, this is the result of improved data, in particular around
1401 residue management using the external tool MIAMI and more realistic fertilizer data (Mueller et al., 2012). For EPIC,
1402 the shifts in net CO₂ fluxes in the current EPIC results stem from the updated soil organic carbon and nitrogen module
1403 (Balkovič et al., 2020) and updates in meteorological forcing. Firstly, the updated soil module resulted in higher
1404 heterotrophic respiration across many EU regions. Besides attributing more carbon to the soil surface emissions,
1405 enhanced respiration leads to higher NPP and yields in regions with low fertilization rates as more nitrogen is released

Deleted: In Petrescu et al. (2021b) (Fig. 6, top) the NGHGI reported a very small but constant source over the whole period (mean of $5.6 \pm 3.5 \text{ Tg C yr}^{-1}$) with almost no inter-annual variability by construction, while all three process-based models simulated a sink. ¶

Deleted: must

Deleted: NGHGIS assume that all aboveground biomass of non-woody crops re-enters the atmosphere at harvest.

Deleted: this

Deleted: c

Deleted: C

Deleted: 6

Formatted: Normal paragraph, Left, Indent: First line: 0 cm, Line spacing: single

Deleted: ORCHIDEE also shows a much larger year-to-year variation due to the response of vegetation and respiration fluxes to sub-daily meteorology. EPIC-IIASA and ECOSSE both operate on daily timescales (ECOSSE was updated to daily for this work, though the previous version was monthly). As both photosynthesis (e.g., Kumarathunge et al., 2019) and respiration (e.g., Yvon-Durocher et al., 2012) show non-linear dependence on temperature, the more extreme temperatures experienced by plants in ORCHIDEE will lead to a higher variation in vegetation response given the same photosynthetic model. High IAV can be seen clearly for drought impacts in ORCHIDEE where regions change from sources to sink in a single year (e.g., for 2003 and 2018 (Ciais et al., 2005; Bastos et al., 2020a)). The other two ecosystem models follow ORCHIDEE's patterns but with smaller magnitudes.

Deleted: 6

Deleted: 6

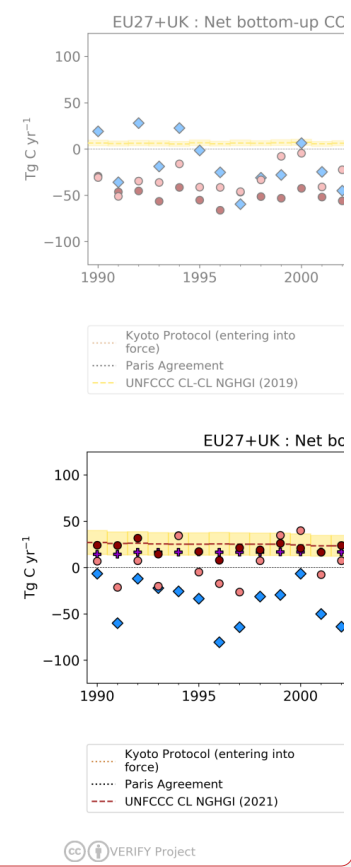
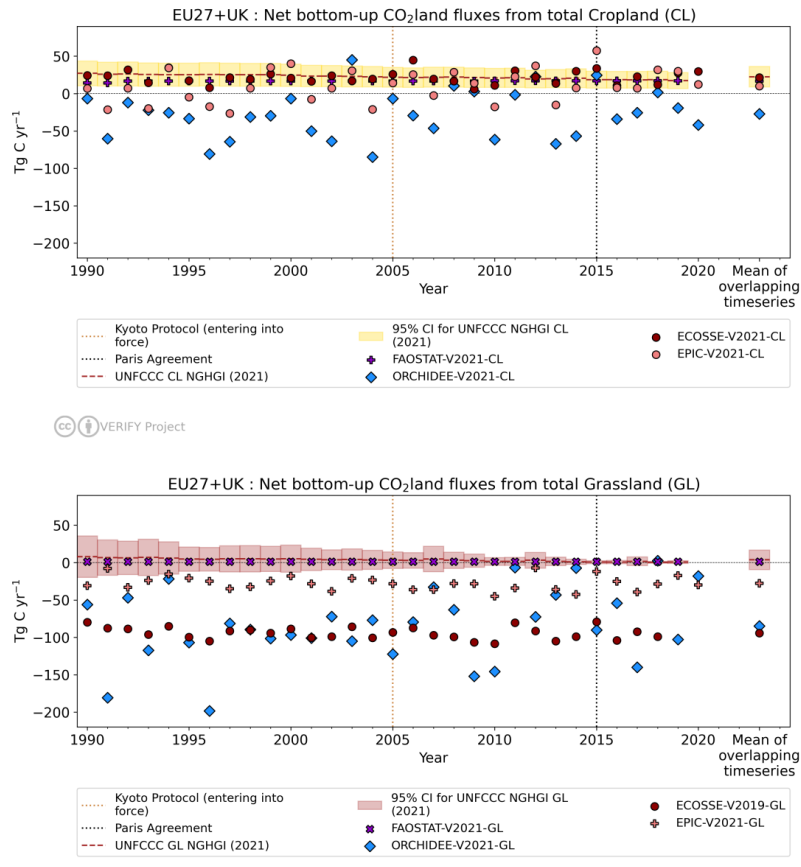
Deleted: . The aboveground biomass is divided into harvest (which is accounted as direct emissions) and residues (biomass that is partly removed and partly left on the field). The external tool MIAMI serves as the central model for the NPP and follows the allocation distribution of Neumann and Smith (2018). The removed residues are set to 50 % as a compromise between the wide range of residue removal rates given by Scarlat et al. (2010). Residue and yield biomass from MIAMI are provided as input into the ECOSSE simulations. Additionally, more realistic fertilizer data (Mueller et al., 2012) were used

Formatted: Footer Char, Font: (Default) Calibri, 11 pt

¹⁶The 2006 IPCC Guidelines largely follow the definition of Histosols by the Food and Agriculture Organization (FAO), but have omitted the thickness criterion from the FAO definition to allow for often historically determined, country-specific definitions of organic soils (see Annex 3A.5, Chapter 3, Volume 4 of IPCC (2006) and Chapter 1, Section 1.2 (Note 3) of IPCC (2014)).

1447 from the SOM pool. Secondly, altered solar radiation and air temperature data affected the full range of carbon
 1448 variables in EPIC, including NPP, harvested biomass, heterotrophic respiration, and leached carbon.
 1449 ORCHIDEE, EPIC-IIASA, and ECOSSE have previously been compared to measurements of net carbon fluxes
 1450 and soil organic carbon changes at the site level (e.g., Balkovič et al., 2020; Chen et al., 2019; Zhang et al., 2018;
 1451 Vuichard et al., 2019). Further comparison is outside the scope of this work, given site heterogeneities and the
 1452 challenges in upscaling such data to a regional level as presented here. We note that this version of ORCHIDEE only
 1453 includes management implicitly, which makes direct comparison to specific sites less informative.
 1454

Formatted: Normal paragraph, Left, Indent: First line: 0 cm, Line spacing: single



Deleted:
 Deleted: 6
 Formatted: Caption - VERIFY, Left, Line spacing: single
 Deleted: from: previous data from Petrescu et al., (2021b) showing only the "remaining" fluxes (CL-CL) (top plot
 Deleted:), and data from
 Deleted: and models showing net carbon fluxes for the total Cropland (CL), with their 1990-2019 mean given on the right (bottom plot). CL net carbon fluxes are estimated with three ecosystem models: ...

1455 **Figure 4:** Net CO₂ land flux from total Cropland (top plot) and total Grassland (bottom panel) estimates for the
 1456 EU27+UK. Total Cropland (CL) data comes from the UNFCCC NGHGI (2021) submissions; ORCHIDEE,
 1457

1467 ECOSSE and EPIC-IIASA process-based models; and the FAOSTAT inventory. Total Grassland (GL) data comes
1468 from the same sources, with the caveat that ECOSSE has not been updated and is therefore identical to Petrescu et
1469 al. (2021b). Values on the far right in both plots indicate the mean of 1990-2019. The relative error on the
1470 UNFCCC value represents the UNFCCC NGHGI (2021) MS-reported uncertainty with no gap-filling (EU NIR,
1471 2021). The fluxes follow the atmospheric convention, where negative values represent a sink while positive values
1472 represent a source.

1473
1474 Differences between mean values may also arise from definitions for each Land type, which vary between
1475 Member States (see Tables 6.18 and 6.22 for Cropland and Grassland, respectively, in EU NIR, 2021). Woody and
1476 annual crops are included in NGHGI Cropland, although annual crops are generally assumed to be in carbon balance
1477 and thus to not contribute to the net flux. This also means that no spatial displacement of emissions ("lateral fluxes")
1478 due to crop trade are taken into account. Grassland includes rangeland and pastureland which is not classified as
1479 Cropland. Urban green spaces, on the other hand, are often included in the Settlements category (EU NIR, 2021),
1480 which is not explicitly simulated by any bottom-up model reported here.

1481 For Grassland, the NGHGI reports a slightly positive net flux over 1990-2019, although with a much larger
1482 uncertainty than for either Forest land or Cropland ($4 \pm 1.3 \text{ Tg C yr}^{-1}$). While increased uncertainty compared to Forest
1483 land emissions is understandable given the emphasis on collecting accurate forestry statistics due to their economic
1484 importance, the increased uncertainty in Grassland compared to Cropland is more puzzling. Uncertainty estimates for
1485 the EU27+UK come from a synthesis of estimates for each of the 28 Member States, and are applied to each year
1486 individually based on the data provided for a single year (2019). The apparent drastic change in uncertainty from
1487 1990 to 2019 is due to the emissions getting much closer to zero (i.e., 7.8 Tg in 1990 compared to 0.5 Tg in 2019),
1488 which itself is due primarily to changes in the way Grassland is treated in the United Kingdom, Bulgaria, and Sweden
1489 (EU NIR, 2021). Additional analysis will be needed to elucidate this issue.

1490 In addition to the NGHGI, updated results for GL are available for ORCHIDEE (using a coupled C-N cycle)
1491 and FAOSTAT. For the first time, EPIC-IIASA contributed estimates for Grassland fluxes using five different
1492 grassland types and simulating carbon export due to herbivores (see Appendix A4 for more details). Both of these
1493 models exhibit a strong sink in Grassland. For ORCHIDEE, this is likely due to the same reasons as the sink in
1494 croplands: more suitable growing conditions due to climate change, CO₂ fertilization, and nitrogen deposition leading
1495 to increased inputs into the soil which are not lost during tillage due to the lack of explicit management in the version
1496 reported here. For EPIC-IIASA, this results from manure left on site and incorporated into the soil. A Tier 1 IPCC
1497 approach, used in both the FAOSTAT inventory and many NGHGIs in the EU27+UK, assumes no changes in either
1498 living or dead biomass pools on Grassland. In addition, it only considers organic soils which have been drained for
1499 grazing, and it only considers mineral soils which have undergone a change in management. This greatly reduces or
1500 eliminates mechanisms which promote sinks in ORCHIDEE and EPIC-IIASA. On the other hand, FAOSTAT reports
1501 a slight source in Grasslands, in line with the NGHGI. This is because, as is the case for Cropland, FAOSTAT data
1502 only considers emissions from drained organic soils. As incorporation of manure in EPIC-IIASA changes grasslands
1503 from a net source to a net sink, consideration of CO₂ from manure input in other inventories may have a similar effect.

1504
1505 3.3.4. Total bottom-up and top-down LULUCF CO₂ estimates

Deleted: , in addition to

Deleted: Note that the FAOSTAT value only includes the carbon flux from organic soils drained for agriculture.

Deleted: Finally, differences in the results between the models and the NGHGIs may arise from definitions. The cropland definition in the IPCC includes cropping systems and agroforestry systems where vegetation falls below the threshold used for the definition of Forest land category, consistent with the selection of national definitions (IPCC glossary). Given that every country is allowed to select their definition of Forest land, which therefore influences the area of Cropland and the total emissions, it is beyond the scope of this study to summarize here the criteria for the 28 countries under consideration and compare those to the methods used in determining the land use/land cover data for the other models. However, the interested reader is referred to Tables 6.10 (forests), 6.18 (croplands), and 6.22 (grassland) in the 2022 NIR of the European Union (EEA/PUBL/2022/023).

Grassland

Grassland (GL, UNFCCC category 4C) includes net CO₂ emissions and removals from soil organic carbon (SOC) under "remaining" and "conversion" categories. The grassland definition in the IPCC includes rangelands and pasture land that is not considered as Cropland, as well as systems with vegetation that fall below the threshold used in the Forest land category (same explanation as for Cropland). This category also includes all grassland from wild lands to recreational areas as well as agricultural and silvo-pastoral systems, subdivided into managed and unmanaged, consistent with national definitions (Petrescu et al., 2021b). For similar reasons to those expressed in the section Cropland above, the current work (Fig. 7, bottom) compares modeled CO₂ flux against NGHGI results for total Grassland (GL). The NGHGIs of countries in the EU27+UK report emissions from managed pastures and grasslands, although the details of what is included varies between countries (Table 6.21).

Formatted

Deleted: 28

Deleted: forest

Deleted: Three possible explanations include: 1) absolute Grassland emissions/removals are lower than for Cropland, which may lead to higher relative uncertainty given th

Deleted:

Deleted:

Deleted: 2

Deleted: g

Deleted: s

Deleted: ;

Deleted: ; and

Deleted: B

Deleted: from all LULUCF categories

Formatted: Normal

1631
 1632 This section analyzes CO₂ emissions and sinks for the LULUCF sector, including NGHGI categories (from Fig.
 1633 B4) and a suite of different bottom-up and top-down approaches. This comparison is challenging due to differences
 1634 in terms of activities covered in the different estimates, as well as differences in terminology (see, for example,
 1635 Petrescu et al., 2020, Fig. 12, and Petrescu et al., 2021b, Sec 3.3.4). Given the differences noted in those references,
 1636 the comparison in this section should be considered as a rough overview that highlights both important aspects of the
 1637 carbon cycle and questions that need to be addressed in the future. Going towards a more specific comparison of only
 1638 net land-use change (LUC) fluxes would require additional considerations. In GCP’s annual global carbon budget, the
 1639 net LUC term is estimated by global DGVMs as the difference between a run with and a run without land-use change
 1640 (i.e., the S3 and S2 simulations from TRENDY, respectively) and by bookkeeping models (Friedlingstein et al., 2022).
 1641 Such an estimate is given in Fig. 13 in Petrescu et al. (2020) for Forest land. However, even taking S3-S2 does not
 1642 permit an apples-to-apples comparison between DGVMs, bottom-up inventories, and bookkeeping models. In
 1643 particular, questions remain about net vs. gross land use change, managed vs. unmanaged land, and emissions from
 1644 wood harvest. In addition, UNFCCC “convert” emissions (i.e., emissions resulting from land that has been converted
 1645 from one type to another) are reported within 20 years following conversion in the “convert” category (biomass losses
 1646 are typically reported in the year of conversion, while net changes in soil organic carbon are reported during the entire
 1647 conversion period). FAOSTAT, DGVMs, and bookkeeping models usually only include “convert” fluxes from the
 1648 year following conversion, although bookkeeping models and DGVMs which deal with gross transitions may be able
 1649 to include this transition period more easily.

Formatted: Normal paragraph, Left, Indent: First line: 0 cm, Line spacing: single, Border: Top: (No border), Bottom: (No border), Left: (No border), Right: (No border), Between : (No border)

Deleted: 3

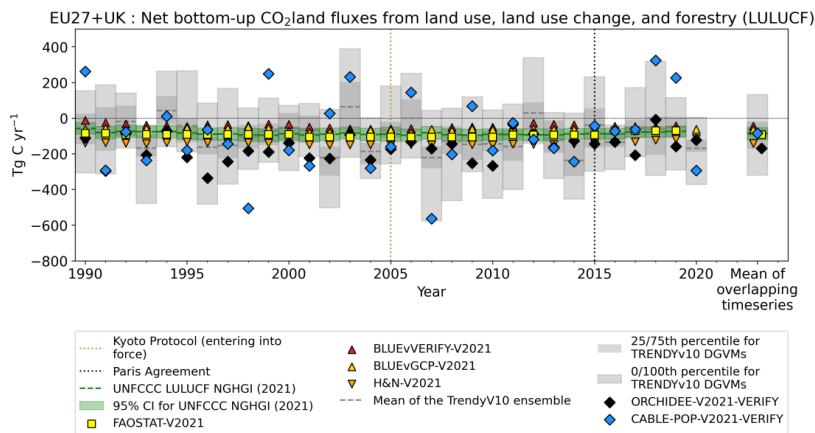
Deleted: To summarize:
 FAOSTAT differs from NGHGIs for reasons recently summarized by Tubiello et al. (2021), Petrescu et al. (2021b), and Grassi et al. (2022a), including numerically different data provided by Member States to FAOSTAT and UNFCCC; different methods (FAOSTAT applies a Tier 1 approach globally, while Member States reports to the UNFCCC vary from Tier 1 to Tier 3); differences between net and gross land use change (FAOSTAT is based on net transitions, following Approach 1 as detailed by the 2006 IPCC guidelines (Chapter 3 of Volume 4, Sect. 3.3.1)); and differences in biomass pools. For the latter, FAOSTAT only considers living biomass pools instead of the five IPCC pools¹⁸ reported to the UNFCCC. A preliminary examination shows that changes in dead wood, litter, and mineral soil carbon stock are generally less than 0.1 t C/ha, which is relatively small compared to reported changes around 1.0 t C/ha in living biomass pools (Tables 6.13, 6.14, 6.15, EU NIR, 2021). On the other hand, changes in organic soil carbon stock are approximately the same magnitude as living biomass, which may lead to significant discrepancies between the NGHGI and FAOSTAT for the EU27.
 DGVMs (represented here by the TRENDY v10 ensemble, as well as the high-resolution ORCHIDEE and CABLE-POP simulations) include the impact of CO₂ fertilization, climate change and land use change for Forest land, Grassland and Cropland categories; they do not explicitly treat the Wetlands, Settlement and Other land categories as in the NGHGIs. They account for the evolution of living biomass, dead biomass, and soil organic carbon for all categories while for NGHGIs reporting is not mandatory for all subcategories depending on the method Tier employed (e.g., dead organic matter in a Tier 1 method is assumed to be constant). There is significant uncertainty associated with the DGVMs’ fluxes both from i) the forcing data, including datasets of land-use changes and the coverage of different land use change practices, ii) model parameters, and iii) model structural uncertainty (i.e., processes not included) (Arnth et al., 2017). Similar to FAOSTAT, DGVMs typically deal with net land use change emissions at the spatial resolution of the model simulations (e.g., 0.5° or 1° for the TRENDY ensemble and 0.125° for the ORCHIDEE and CABLE-POP simulations) instead of gross land use change as reported in NGHGIs. CABLE-POP is an exception to most DGVMs and actually incorporates gross land use transitions (Haverd et al., 2018). The use of gross land use transitions may induce significant differences with coarse resolution model simulations (e.g., the TRENDY ensemble). In addition, DGVMs often do not distinguish [24]

Deleted: all these

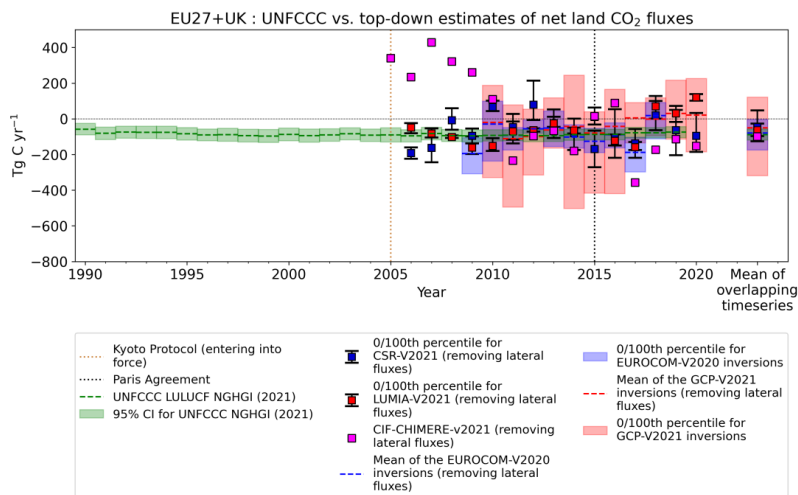
Deleted: in terms of activities

Deleted: C

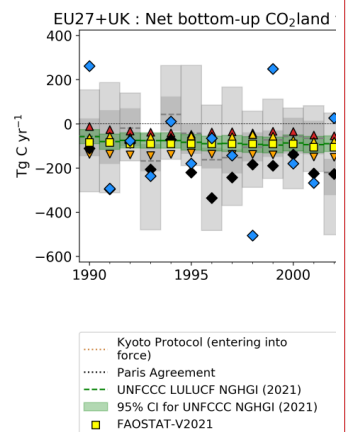
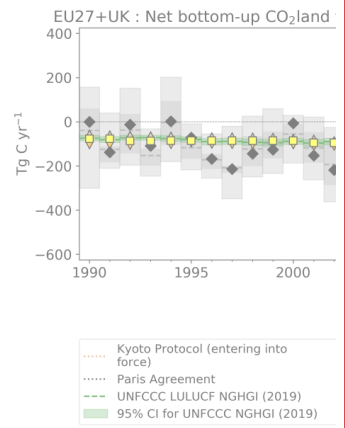
Deleted: However, this approach does not fully resolve the differences mentioned above.



VERIFY Project



VERIFY Project



VERIFY Project

Deleted:

Deleted: 8

Deleted: EU27 + UK

Deleted: previous

Formatted: Caption - VERIFY, Left, Line spacing: single

Deleted: data from Petrescu et al. (2012b) (top plot) and data from seven new or updated sources (bottom plot) including:...

Deleted: ,

1769

1770 Figure 5: Net CO₂ fluxes from total LULUCF activities in the EU27+UK from bottom-up (top) and top-down
 1771 (bottom) methods compared to UNFCCC NGHGI (2021). The bottom-up methods include: BLUE (vVERIFY),
 1772 BLUE (vGCP2021), H&N (GCP2021), DGVMs (TRENDY v10), FAOSTAT (2021), as well as ORCHIDEE and
 1773 CABLE-POP with high-spatial-resolution (0.125°) meteorological forcing (both models are also part of the
 1774 TRENDY ensemble at 0.5°). The spread of the gray bars represents the individual model data for the DGVMs. Top-

1783 *down inversion results are the global GCB2021 ensemble, as well as several regional inversions: the EUROCOM*
1784 *ensemble, the CarboScopeReg model with multiple variants, the LUMIA model with multiple variants, and CIF-*
1785 *CHIMERE. The colored area represents the min/max of top-down model ensemble estimates. Emissions due to*
1786 *lateral fluxes of carbon through rivers, crop trade, and wood trade are removed from the top-down estimates. The*
1787 *mean values of the timeseries for the overlapping periods of 1990-2019 (top) and 2010-2018 (bottom) are shown on*
1788 *the right. The UNFCCC estimate includes all categories (remain and convert), as well as HWP. The relative error*
1789 *of the UNFCCC values represent the UNFCCC NGHGI (2021) Member States reported uncertainty computed with*
1790 *the error propagation method (95 % confidence interval), gap-filled and provided for each year of the timeseries.*
1791 *The fluxes follow the atmospheric convention, where negative values represent a sink while positive values represent*
1792 *a source.*

1793 Figure 5 (top) shows CO₂ fluxes from the NGHGI LULUCF sector compared to all other comparable bottom-
1794 up (BU) estimates in this work: high-resolution S3 simulations for both ORCHIDEE and CABLE-POP; the median
1795 of 15 S3 simulations from the TRENDYv10 DGVM ensemble; three bookkeeping models; and FAOSTAT. As
1796 mentioned above, taking the difference of the TRENDY S2 and S3 simulations does not permit a fully-consistent
1797 comparison between DGVMs, bottom-up inventories, and bookkeeping models for LULUCF fluxes, and for
1798 simplicity we simply report S3 NBP from DGVMs in Fig. 5. Further research is needed in order to establish which
1799 approach (S3-S2, or simply S3) leads to the most consistent comparison. For the overlapping period 1990-2019, the
1800 means of two out of the three bookkeeping models (BLUE vGCP (-61 Tg C yr⁻¹) and BLUE vVERIFY (-43 Tg C yr⁻¹,
1801 using the Hilda+ land use forcing) along with the mean of FAOSTAT (without Romanian forestry fluxes) (-93 Tg C
1802 yr⁻¹) fall within the 95 % confidence interval of the UNFCCC NGHGI estimate of -86 ± 33 Tg C yr⁻¹. Only H&N rests
1803 apart with a stronger sink (-142 Tg C yr⁻¹), although it's difficult to say how different it is from the NGHGI without
1804 uncertainty estimates.

1805 Bookkeeping models like BLUE and H&N always regrow biomass at the same rate. In the bookkeeping
1806 approaches used here, regrowth curves are representative for present-day conditions and kept the same throughout
1807 history, which is the same approach used in the Global Carbon Budget. NGHGIs, on the other hand, include legacy
1808 effects from changing environmental conditions, in particular in soil pools. Recent work by Grassi et al. (2023)
1809 demonstrates that including the sink associated with varying human-induced indirect effects (as estimated by the S2
1810 simulations from the TRENDY DGVM ensemble) into results by bookkeeping models can largely reconcile estimates
1811 of net global LULUCF fluxes between the NGHGIs and bookkeeping models. At the level of the EU27+UK, the
1812 inclusion of this sink results in an overcompensation; the BMs estimate a net sink of -56 Tg C yr⁻¹ compared to the
1813 NGHGI estimate of -88 Tg C yr⁻¹, while the BMs+DGVMs results in -112 Tg C yr⁻¹. However, both of these estimates
1814 fall inside the NGHGI uncertainty range in Fig. 5.

1815 The primary difference between the NGHGI and DGVMs is the interannual variability, with only a small
1816 difference in the means even if there is a substantial amount of spread with the DGVMs: -86 ± 33 Tg C yr⁻¹ and -81 [-
1817 172, -20] Tg C yr⁻¹ for the NGHGI and DGVMs, respectively, where the range for the DGVMs indicates the 25th-75th
1818 percentile of the models in the ensemble. The UNFCCC LULUCF estimates contain CO₂ emissions from all land use
1819 categories and HWP, where a simple analysis shows that for the EU27+UK almost 90 % of the gross flux arises from
1820 only six categories (Table A4). DGVMs currently explicitly include more of these categories than the other methods
1821 (Table C2), which may help explain the closeness between the mean values. ORCHIDEE and CABLE-POP provide
1822 a nice test case of the impact of high spatial resolution forcing on net carbon fluxes in the EU27+UK, as they are

Deleted: classes

Deleted: Biomass burning emissions are included in the C stock estimates. The FAOSTAT estimate includes both Forest land remaining forest land in addition to incorporating afforestation and deforestation as conversion of Forest land to other land types. The means are calculated for the 1990-2019 overlapping period.

Deleted: 8

Formatted: Normal paragraph, Left, Indent: First line: 0 cm, Line spacing: single

Deleted: taking the difference of the TRENDY S2 and S3 simulations provides an estimate of the net flux from land use change, but inconsistencies are introduced either way, and therefore f

Deleted: -

Formatted: Superscript

Deleted: do not include indirect effects on biomass growth due to factors such as CO₂ fertilization, nitrogen deposition, and climate change, while NGHGIs implicitly include these impacts on managed land through updated statistics.

Deleted: 2022b

Deleted:

Deleted: .5

Deleted: 7.9

Deleted: all

Deleted: 8

Deleted: This suggests that indirect effects are small in the EU27+UK.

Formatted: Normal paragraph, Left, Indent: First line: 0 cm, Line spacing: single

Formatted: Not Highlight

Formatted: Subscript

1848 present in both the TRENDY ensemble (0.5 °) as well as the VERIFY results (0.125 °). Using one standard deviation
1849 of the mean annual net CO₂ flux as a measure of the IAV, CABLE-POP indeed shows a much higher IAV at high
1850 resolution (-40 ± 142 Tg C yr⁻¹ and -92 ± 214 Tg C yr⁻¹ for TRENDY and this work across 1990-2019), while the
1851 results for ORCHIDEE are almost identical between the two resolutions. More analysis is therefore required to
1852 confirm the relationship between spatial resolution and interannual variability in DGVMs for the EU27+UK.

1853 The differences between bookkeeping models and UNFCCC and FAOSTAT are discussed in detail
1854 elsewhere, and focus on the inclusion of unmanaged land in bookkeeping models but not FAOSTAT and UNFCCC
1855 methodologies (Petrescu et al., 2020; Grassi et al., 2018a, 2021). ORCHIDEE, CABLE-POP and the TRENDY v10
1856 ensemble means show much higher inter-annual variability as they simulate sub-annual responses of carbon fluxes to
1857 climate, while the climate responses of inventories and bookkeeping models are averaged over multiple years. A
1858 comparison including categorical-specific models (e.g., ECOSSE, EFISCEN-Space, EPIC-IIASA, CBM) where
1859 multiple model results are harmonized and aggregated to produce a “total” LULUCF flux comparable to DGVMs and
1860 bookkeeping models would be insightful; however, such a comparison requires extensive analysis which is beyond
1861 the scope of the current work.

1862 The bottom panel in Figure 5 highlights the range of estimates from global and regional atmospheric inversions
1863 (GCP2021, EUROCOM, CSR, LUMIA, and CIF-CHIMERE; see Table 2 and Appendix A4 for more details) against
1864 bottom-up total annual EU27+UK CO₂ land emissions/removals from the UNFCCC NGHGI (2021). Notice that
1865 unlike other works (e.g., Deng et al., 2022), we have not applied a managed-land mask to the inversions or bottom-up
1866 models in order to be compatible with the managed land proxy in the NGHGIs. The reasons for this are two-fold.
1867 One, most of the land in the European Union is managed, as noted above. Second, no such mask currently exists,
1868 even for the relatively data-rich EU. A managed land mask created solely based on non-intact forests (e.g., Deng et
1869 al., 2022) neglects that Grassland and Wetlands contribute significantly to unmanaged areas in the EU. Including
1870 fluxes from the 5 % of unmanaged land in the EU is unlikely to change any conclusions in this work given the
1871 uncertainties in the LULUCF methods presented here. As soon as a reasonably accurate managed land mask is
1872 available, however, it should be used.

1873 One significant change between this work and Petrescu et al. (2021b) is the removal of emissions and sinks from
1874 inversion results due to lateral transport of carbon from crop trade, wood trade, and inland waters. Bottom-up methods
1875 (including all the NGHGIs for European countries) do not consider emissions and removal of atmospheric CO₂ due
1876 to lateral transport of biomass carbon, while inversions calculate geographically resolved net land-atmosphere CO₂
1877 fluxes without regard to the original location of photosynthetic assimilation. Some lateral transport of soil organic
1878 carbon may be taken into account by measuring stock changes, but given the mix of stock-change and gain-loss
1879 methods used in NGHGIs in the EU, and the presence of methods ranging from Tier 1 to Tier 3, exactly how much is
1880 far from trivial to determine.

1881 Net emissions from lateral transport of carbon (“lateral fluxes”) were prepared generally following the approach
1882 described by Ciais et al. (2021), where crop and wood product fluxes are derived from country-level trade statistics
1883 compiled by the FAO. Inland water emissions and riverine export of terrestrial carbon use spatially explicit
1884 climatological data and a statistical model combined with estimates of gas transfer velocities. A more complete

Deleted: The UNFCCC LULUCF estimates contain CO₂ emissions from all six land use categories and HWP, including remaining categories and conversion to and from a category to another. The DGVMs show high interannual variability, as demonstrated clearly by the high-resolution CABLE-POP simulation in Fig. 8. The mean values for DGVMs across the overlapping period, on the other hand, agree fairly well with the NGHGI: -170 Tg C yr⁻¹, -84 Tg C yr⁻¹, and -81 (min -285, max 118) Tg C yr⁻¹ for ORCHIDEE, CABLE-POP, and TRENDY v10, respectively, compared to the NGHGI mean of -86 ± 33 Tg C yr⁻¹. Note again that ORCHIDEE and CABLE-POP are also part of the TRENDYv10 ensemble, but the simulations included in TRENDY used a coarser meteorological forcing than the one used within the VERIFY project (around 0.125° resolution). CABLE-POP also used a higher resolution land use land cover change (LULCC) dataset for the results submitted to VERIFY (0.25° as opposed to 1.0°). The increased IAV from the high-resolution CABLE-POP compared to ORCHIDEE is suspected to have been introduced through the construction of the LULCC dataset as described in Appendix A2. Gross fluxes are, by definition, larger than net fluxes, and consequently a method which incorporates gross fluxes (like CABLE-POP) can be expected to undergo larger changes than a method incorporating net fluxes (like ORCHIDEE).¶

Deleted: due to the sensitivity of the model fluxes to highly variable meteorological forcing at sub-daily time steps which allow for much more rapid responses to changing conditions, as already discussed in the previous sections. The incorporation of variable climate data and the fact that DGVM models simulate explicitly climate impacts on CO₂ fluxes, which inventories and bookkeeping models do not, explain these differences.

Deleted: sector

Deleted: ¶

Deleted: ¶
3.3.5. Comparison of atmospheric inversions with NGHGI CO₂ estimates¶

Deleted: Figure 9

Deleted: 2

Deleted: The top panel in the figure shows the previous results from Petrescu et al. (2021b). In these inversions, all components of the carbon cycle that contribute to the observed atmospheric CO₂ gradients between stations are implicitly included as the inversions incorporate observed atmospheric concentrations of CO₂. This includes processes where carbon is uptaken by vegetation in one area and emitted in a different area, i.e. emissions due to the respiration of laterally transported carbon.

Deleted: observations assimilated into top-down inversions record all CO₂ fluxes without separating their components

Deleted: We followed Eq. (1) of Deng et al. (2021) without prior masking for managed land.

Deleted: E

1939 description is given in Appendix A4. This adjustment accounts for a combined mean of -140 Tg C yr⁻¹ over the 2010-
1940 2018 common period of the inversions, and has been applied using Eq. 1 in Deng et al. (2021) (without a managed
1941 land mask) to all top-down fluxes reported here unless indicated otherwise.

1942 Uncertainties for net emissions of CO₂ due to lateral transport of carbon are not yet available. However, FAO
1943 and IEA statistics form the basis of calculated fluxes due to wood and crop trade. FAO estimates an uncertainty of 50
1944 % on carbon emissions and removals from forested land (Tubiello et al., 2021). Even if uncertainties in trade fluxes
1945 are not available, 50 % therefore works as a first order approximation given the similarities between the two fluxes
1946 (i.e., a well-tracked value multiplied by an uncertain emission factor). Uncertainties in net carbon uptake by rivers
1947 and lakes are estimated to also be on the order of 50 % due to the fact that these fluxes can only be calculated based
1948 on budget closure including estimates of river exports to the coast, emissions of carbon from the water surface to the
1949 atmosphere, and burial of carbon in aquatic sediments (Battin et al., 2023). Combined, this results in an uncertainty
1950 of around 70 Tg C yr⁻¹ for the lateral fluxes, which is on the same order as the ensemble spread for the regional
1951 inversions as shown in Fig 5, though still lower than that of the global inversions.

1952 Flux estimates from inversion methods for CO₂ land show much more variability than the NGHGI, both on
1953 the interannual scale as well as for any given year (Fig. 5, bottom). The mean values from 2010-2018 show good
1954 agreement but with an order of magnitude more variability in the inversions: -88 ± 60 Tg C yr⁻¹ for EUROCOM and
1955 -80 ± 6 Tg C yr⁻¹ for the NGHGI, where the uncertainty here is the standard deviation of the annual mean values for
1956 each. For any given year, the spread between the inversions is also much greater (170 ± 70 Tg C yr⁻¹ for EUROCOM,
1957 versus 63 ± 3 Tg C yr⁻¹ for the NGHGI, which represents the mean and standard deviation of the 0-100th percentiles
1958 for the inversions and the 95% CI for the NGHGI). This large spread per year can be linked to uncertainty in
1959 atmospheric transport modeling, inversion methods and assumptions, and to limitations of the observation system.
1960 Furthermore, the EUROCOM inversions were designed for the European geographical domain (which is larger than
1961 the EU27+UK) and are still being developed in particular to better constrain the latitudinal and longitudinal boundary
1962 conditions.

1963 The annual mean (overlapping period 2010-2018) of the EUROCOM v2021 inversions (-80 [-175,-4] Tg C yr⁻¹
1964 ¹) is the closest inversion estimate to the timeseries mean of the NGHGI estimates (-88 ± 31 Tg C yr⁻¹), where the
1965 error bars for the inversion indicate the [0th, 100th] percentiles due to the small size of the ensembles. The ensemble of
1966 all regional inversions is consistent with the NGHGI estimates, assuming the spread of the inverse model results is an
1967 accurate proxy of the structural uncertainties. The impact of the net emissions of lateral fluxes due to wood trade,
1968 crop trade, and rivers is clear: without factoring in their contribution of the approximately -140 Tg C yr⁻¹, the sink
1969 from regional inversions, in particular, would be much stronger than even the strongest estimate of the NGHGI (i.e.,
1970 the lower boundary on the green bar in Fig. 5). The mean of the global GCP2021 inversions (-50 [-320,+122] Tg C
1971 yr⁻¹) and regional inversions, CSR (-46 [-126,+47] Tg C yr⁻¹) and LUMIA (-65 [-97,-27] Tg C yr⁻¹) show a lower
1972 absolute value, but report larger interannual variability (min/max). The new CIF-CIMERE product has a mean of -99
1973 Tg C yr⁻¹, showing a trend towards more negative fluxes since 2010, which is not seen in other models and is still
1974 under investigation.

Deleted: 2

Deleted: The C fluxes from inland waters (rivers and lakes) reported in Petrescu et al. (2021b), were replaced in this study by maps of sinks/sources of rivers/lakes, wood and crops, accounting for a combined mean of -136 Tg C yr⁻¹ (ov... [25])

Formatted: Font: (Default) Times New Roman, 10 pt

Deleted: 9

Formatted

... [26]

Deleted: The mean of the EUROCOM ensemble of European inversions shows good agreement with UNFCCC NGHGI data, but with a huge spread of annual model results that extends from significant sources into large sinks. ...hi... [27]

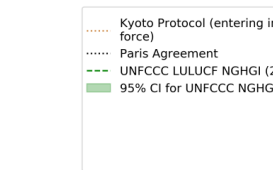
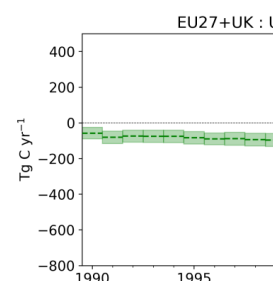
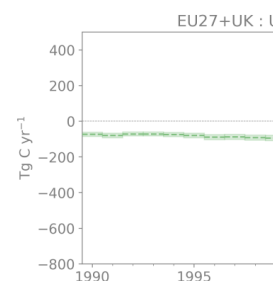
Formatted: Font: Italic

Formatted: Normal paragraph, Left, Line spacing: single

Deleted: d

Formatted

... [28]



Moved down [3]:

Deleted: ¶

Deleted: ¶

2106 The comparison of past and current versions of the inversions shows changes in specific top-down models
2107 (Fig. B5). A reduction in the spread of the estimates is noted over the two past versions of CSR, resulting in a small
2108 source in the most recent estimates. The CSRv2021 (bottom-plot) predicts in 2018 (last common year of both versions)
2109 a small source of 19 [-64, +100] Tg C yr⁻¹ compared to the previous CSRv2019 which simulated a very strong sink of
2110 -253 [-280, -194] Tg C yr⁻¹. This smaller source appears more in line with more positive fluxes expected in years of
2111 extreme drought (e.g., 2018 in Northern Europe, even if this did not impact the whole EU27+UK (Toreti et al., 2019)).

2112 As can be seen in Fig. 5 (bottom), there is also improved agreement between the EUROCOM ensemble and
2113 the NGHGI, including a greatly reduced IAV compared to the previous version. The small EUROCOM ensemble
2114 mean sink for the 2009-2015 period of -1.9 [-335,+322] Tg C yr⁻¹ (top panel) strengthened to -93 [-187,-15] Tg C yr⁻¹
2115 in the v2021 version (bottom panel). The UNFCCC total LULUCF mean is -92 ± 33 Tg C yr⁻¹ for the same time
2116 period. The IAV of EUROCOM was dramatically reduced by removing the FLEXINVERT model from the v2021
2117 ensemble as a clear outlier of annual means due to a slightly shifted seasonal cycle (Appendix A4).

2118 Despite an apparent trend in the mean of the new GCP2021 inversions towards a source near 2017, the spread
2119 of the models precludes significance; following 1000 realizations of a Monte Carlo analysis assuming the min-max
2120 ensemble spread represents 3σ in a normal distribution, the only period of at least four consecutive years for which
2121 the 95% confidence interval comes close to excluding zero is 2015-2018 (26 ± 28 Tg C yr⁻²). The large variability
2122 and high sink observed in the upper plot of Fig. 5 (bottom) shifted to a source in 2019 (21 [-185, +226] Tg C yr⁻¹) due
2123 to the extreme climatic response of the TD models to the drought year, which can also be observed in the BU
2124 simulations (e.g., TRENDY v10, ORCHIDEE, and CABLE-POP in the top panel of Fig. 5). Out of the GCP2021
2125 models, CAMS was the model responsible for the strongest sink in the ensemble during most years (data not shown),
2126 which may be due partly to changes in the stations assimilated.

2128 3.4. Uncertainties in top-down and bottom-up estimates

2129
2130 Uncertainties are essential for complete comparisons between models and approaches. This section
2131 summarizes the main sources of uncertainty estimates interwoven throughout the above text. We also provide a
2132 comparison of available uncertainties between the previous synthesis (V2019) and the current synthesis (V2021) for
2133 both bottom-up and top-down methods. Finally, we give an overview of two important advances in uncertainty
2134 estimation included in this work (one for the NGHGI, and one for top-down approaches), referring the interested
2135 reader to the Appendix A4 for more information.

2136 Several sources of uncertainty arise from the synthesis of bottom-up (BU) inventories and models of carbon
2137 fluxes, which can be summarized as: (a) differences due to input data and structural/parametric uncertainty of models
2138 (Houghton et al., 2012) and (b) differences in definitions (Pongratz et al., 2014; Grassi et al., 2018b, 2021; Petrescu
2139 et al., 2020, 2021b). Posterior uncertainties in top-down (TD) estimates mostly come from: 1) errors in the modeled
2140 atmospheric transport; 2) aggregation errors, i.e., errors arising from the way the flux variables are discretized in space
2141 and time and error correlations in time; 3) errors in the background mole fractions, in particular for regional inversions;
2142 and 4) incomplete information from the observations and hence the dependence on the prior fluxes. The multi-model

Deleted: although

Deleted: 9

Deleted: 2

Deleted: The new GCP2021 inversions show a clear trend towards decreasing the CO₂ sink strength of the land surface after 2017, contrary to the NGHGI estimates which are relatively stable (Fig. 9, bottom).

Deleted: 9

Deleted: 8

Deleted: lower

Deleted: sinks

Formatted: Normal paragraph, Left, Indent: First line: 0 cm, Line spacing: single

Deleted: Table B2 summarizes the processes included in the CO₂ land models presented in this work, as these processes are seen for the moment as the main cause of discrepancies between estimates shown in all the previous figures. → According to Table B2, no bottom-up model or dataset used here contains all of the 13 LULUCF categories reported in the NGHGIS. A simple analysis of the mean 1990-2020 LULUCF fluxes from the EU27+UK NGHGI (Table A3 in Appendix A2) shows that six categories account for almost 90 % of the gross flux: Forest land remaining forest land (56 %), Land converted to cropland (7 %), Land converted to forest land (7 %), Grassland remaining grassland (6 %), Harvested wood products (6 %), and Land converted to settlements (6 %). DGVMs currently include more of these categories than other methods. As shown in Fig. 8, the mean 1990-2019 value of the mean of the 15 TRENDY DGVM simulations is -81.9 Tg C yr⁻¹ (with a range of [-285,118] Tg C yr⁻¹), while those of the ORCHIDEE and CABLE-POP simulations using the high-resolution forcing provided in the VERIFY project are -171 Tg C yr⁻¹ and -84.8 Tg C yr⁻¹, respectively. The means agree quite well for TRENDYv10 and CABLE-POP, but the spread of all the DGVMs is quite large. In addition, the number of categories included may not be a good proxy for quality of comparison. While an ideal model would include all categories in the NGHGI, it must also represent these categories well. Figures 4-7 suggest that sector-specific models currently show better agreement with the NGHGI than DGVMs, although a more detailed analysis including the entire suite of TRENDY models would be insightful. Note that these categories are used as input to top-down approaches, and therefore cannot be disaggregated into results after the simulation.¶

Deleted: 3.6

Formatted: Normal

2187 ensemble approach is being used as a proxy for estimation of systematic error. Calculation of random error is generally
2188 difficult when using the most common inverse model flux optimization approaches.

2189 Figure 6 summarizes the quantifiable uncertainties in this work, compared to previous results from Petrescu
2190 et al. (2021b). With the exception of the NGHGI, all the other uncertainties are calculated from ensembles of
2191 simulations using either: 1) multiple models of the same general type, either using model-specific inputs or attempting
2192 to harmonize inputs as much as possible (e.g., TRENDY), or 2) multiple simulations with the same model, varying
2193 input parameters and/or forcing data (e.g., CarboScopeRegional, LUMIA). As a complete characterization of model
2194 uncertainty involves exploring the full parameter, input data, and model structure space, none of the uncertainties
2195 reported here can be considered “complete”, but they represent best estimates given realistic constraints of resources
2196 and knowledge. The uncertainties represent the mean of overlapping periods for the previous V2019 (overlapping
2197 period: 2006-2015) versus the current V2021 (2010-2018). In general, the differences in mean behaviors between the
2198 two versions falls within uncertainty estimates. Note, however, that this graph can hide certain behaviors. For
2199 example, the similarity in the means for ORCHIDEE-VERIFY for both periods (-129 and -131 Tg C yr⁻¹ for V2019
2200 and V2021, respectively) is likely a coincidence, given the wide fluctuation of annual values and the differences in
2201 the multi-decennial means seen in Fig. 5.

2202 Figure 6 shows notable reductions in the spread of two ensembles: EUROCOM and CSR. Both of these are
2203 regional ensembles. In addition, the CSR results show a weaker sink in the current V2021 version compared to the
2204 previous V2019 version. As noted in Appendix A4, the change for CSR is explained by the inclusion of a corrected
2205 observation dataset for an isolated station in southeastern Europe which heavily influenced the regional results. The
2206 reduction in the spread of the EUROCOM ensemble results from the exclusion of a single member which produces
2207 annual flux results that are clear outliers compared to the remaining three members. More details of this analysis can
2208 be found in Appendix A4. The remaining ensembles retain similar model spread compared to the previous versions.

Deleted:

Deleted: 10

Deleted: 8.5

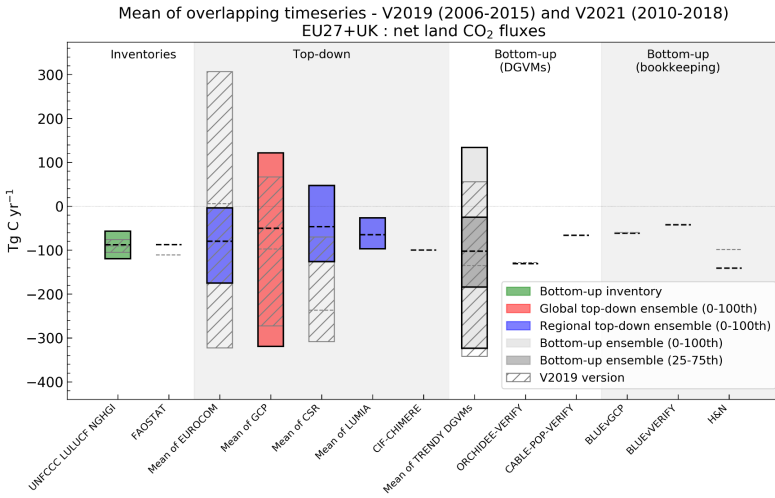
Deleted: .0

Deleted: 8

Deleted: 10

Deleted: 2

Deleted: 2



VERIFY Project

2217

2218 *Figure 6: Mean annual values of overlapping time periods (2006-2015) from Petrescu et al. (2021b) (transparent*
 2219 *boxes and light gray lines) and new means for the 2010-2018 period from the current study (Fig. 5, Sect. 3.3.4). The*
 2220 *hashed boxes and colored boxes depict the “old” and “new” values for ensembles of multiple models, with the top*
 2221 *and bottom of the boxes corresponding to minimum and maximum mean values of the overlapping period. For non-*
 2222 *ensemble models (e.g., CIF-CHIMERE, FAOSTAT) the mean of the old and new overlapping periods are given by*
 2223 *gray dotted and black dashed lines, respectively. The NGHGI UNFCCC uncertainty is calculated for submission*
 2224 *year 2021 as the relative error of the NGHGI value, computed with the 95 % confidence interval method gap-filled*
 2225 *and provided for every year of the timeseries. Inversions for both V2019 and V2021 have been corrected for net*
 2226 *emissions of CO₂ from lateral transport of carbon using identical datasets to enable a fair comparison. The fluxes*
 2227 *follow the atmospheric convention, where negative values represent a sink while positive values represent a source.*

2228

2229 Three advances in uncertainty estimation were made in this study, involving all three classes of models:
 2230 NGHGI, bottom-up, and top-down. In Petrescu et al. (2021b), percentage uncertainties for the NGHGI (2019)
 2231 LULUCF sector and land use categories were taken from reported uncertainties of the EU Member States and UK that
 2232 are used for compiling the National Inventory Reports (NIR) of the EU27+UK bloc, as well as the aggregate
 2233 uncertainties for the block reported in the EU NIR. Uncertainty estimates were only given for a single year and were
 2234 also partially incomplete due to missing uncertainty estimates for some sectors/subsectors of some countries. For the
 2235 current work, we use values compiled by the EU inventory team involving a recently developed procedure to
 2236 harmonize and gap-fill uncertainties reported by the Member States at the sector level (see EU NIR, 2021). Error
 2237 correlations are accounted for, in addition to year-to-year variations in sub-sectoral contributions to the overall
 2238 uncertainty. Extensive details are found in Appendix A2, and permit estimates of uncertainty on an annual basis, as
 2239 opposed to the single value used in the previous synthesis. Note, however, that this procedure was not applied to sub-
 2240 sectoral categories (FL, CL, and GL), for which values were taken directly from EU NIR (2021) and applied across

Deleted: 10
 Formatted: Caption - VERIFY, Left, Line spacing: single
 Deleted: 8 and 9
 Deleted: and 3.3.5

Deleted: 1

2245 the whole timeseries. Synthesis plots created for individual countries and reported on the VERIFY website (VERIFY
2246 Synthesis Plots, 2022) take percentages directly from the respective country's NIR.

2247 The second advance relates to the impact of forcing data on bottom-up models, in particular DGVMs. Figure
2248 A3 (Appendix A4) shows how the ORCHIDEE model responds to both changes in meteorological forcing (for
2249 ORCHIDEE) and nitrogen forcing (for ORCHIDEE-N) over the past several decades. The impact of both is relatively
2250 small compared to interannual variability. This is likely due to at least two reasons. The first reason is that
2251 meteorological forcing used in this work has been re-aligned to the CRU observational dataset at 0.5 degrees and
2252 monthly resolution, thus removing large-scale and long-term differences between the original meteorological datasets.
2253 In addition, extensive spin-up and transient simulations are run for ORCHIDEE before reaching the point at which
2254 the forcing changes (1981 for the meteorological forcing, and 1995 for the nitrogen forcing). Such lengthy simulations
2255 enable woody biomass and soil carbon pools to develop a significant amount of inertia in response to additional
2256 changes. Greater differences may be seen for models where modified forcing data covers the entire length of the pre-
2257 production simulation steps.

2258 The final advance relates to uncertainty characterization in the regional inversion model CSR following the
2259 methodology of Chevallier et al. (2007). Spatially explicit estimates of the uncertainty reduction achieved from the
2260 flux optimization were prepared through a Monte Carlo approach using an ensemble of 40 members. The uncertainty
2261 reduction is then calculated based on the ratio of the prior errors and the posterior spread of the ensemble members,
2262 using a formula such that 0 indicates no reduction and 1 indicates a complete elimination of uncertainty. A preliminary
2263 analysis showed that a considerable reduction may be achieved through the inclusion of more observation stations,
2264 although additional work is needed. For the moment, these maps only reflect random uncertainties, and systematic
2265 uncertainties remain poorly characterized. More information can be found in Appendix A4.

2267 4. Data availability

2268 Annual timeseries for the EU27+UK used in creation of the figures in this work for V2019 and V2021 are
2269 available for public download at <https://doi.org/10.5281/zenodo.8148461> (McGrath et al., 2023). This excludes CO₂
2270 fossil data for the IEA, which is subject to license restrictions. **Most sector-level data from IEA are available for a
2271 fee, although some high-level emissions data can be accessed free-of-charge.** The data are reachable with one click
2272 (without the need for entering login and password), and downloadable with a second click, consistent with the two
2273 click access principle for data published in ESSD (Carlson and Oda, 2018). The data and the DOI number are subject
2274 to future updates and only refers to this version of the paper. In addition, figures and annual timeseries for EU27+UK
2275 as well as other countries and regions are available from VERIFY Synthesis Plots (2022) **as well as a number of
2276 gridded data files submitted to the VERIFY project listed in Table C1. Access to the data files requires free registration
2277 to obtain a username and password. Alternatively, interested users are invited to contact the persons listed in Table
2278 C1 to request gridded datafiles directly from them. We do not provide access to data already made freely available**

Deleted:

Deleted: bottom up

Deleted: 2

Deleted: Figure 11 presents an idea of the spatial uncertainties associated with these datasets. Total CO₂ land fluxes from EU27+UK and five main regions in Europe are presented, divided into top-down (top panel) and bottom-up (bottom panel) approaches for clarity. The regions (North, West, Central, East and South) consist of Annex I Parties to UNFCCC both inside and outside of the EU27+UK bloc, and are listed in Table A1. Figure 11 shows the total CO₂ land fluxes from the NGHGs for base year 1990, as well as five-year mean values for the 2011-2015 and 2015-2019 periods. The five-year periods are used as an exercise for what could be achieved in the first GST and also because they provided the most overlap with the datasets reported here. As the BU models in VERIFY include and simulate CO₂ fluxes for at most three out of the six classes reported to the UNFCCC (FL, CL and GL), for comparison and consistency purposes both UNFCCC total LULUCF (including all six classes and HWP), as well as the UNFCCC FL+CL+GL estimates are shown. Figure 11 presents CO₂ fluxes that include both direct and indirect LULUCF effects on managed land. The total UNFCCC estimates include the total LULUCF emissions and sinks (by the UNFCCC definition) belonging to all six IPCC land classes and the HWP class (see Sect. 2.3 and Appendix B for more details). The NGHGI estimates are plotted and compared against fluxes simulated with statistical global and regional datasets: bookkeeping models, biosphere and sector-specific models, and inversion model ensembles. The error bar represents the variability in model estimates as the min and max values in the ensemble.

... [29]

Formatted: Heading 1, Line spacing: single, No bullets or numbering

Deleted: <https://doi.org/10.5281/zenodo.7365863>

Deleted: 2

2314 elsewhere, as we prefer users use mechanisms put in place by the original providers so that they are able to ensure
2315 their continued funding for their work.

Deleted: .

2317 5. Summary and concluding remarks

Formatted: Heading 1, Space After: 0 pt, Line spacing: single, Tab stops: Not at 0,48 cm

2318 This work represents an update of the Petrescu et al. (2021b) European CO₂ synthesis paper presenting and
2319 investigating differences between the UNFCCC NGHGI, BU data-based inventories, both coarse and high resolution
2320 process-based BU models, and TD approaches represented by both global and regional inversions. Datasets used in
2321 the previous work have been updated by extending the temporal coverage and updating the models and data behind
2322 the calculations. In addition, several new models to expand the number of independent approaches compared have
2323 been added. Additional efforts have been made to improve uncertainty characterization in two approaches, along with
2324 a first attempt to present as many datasets as possible in a clear single figure to draw overarching conclusions.

2325 CO₂ fossil emissions dominate the anthropogenic CO₂ flux in the EU27+UK, regardless of the approach
2326 employed and irrespective of uncertainties, although the datasets are not fully independent, which complicates
2327 uncertainty estimation. Fossil CO₂ emissions are more straightforward to estimate than ecosystem fluxes due to
2328 extensive data collection around fuel production and trade, assuming that fuel statistics and accurate emission factors
2329 are available. A suite of eight BU methods for fossil CO₂ emissions are within the uncertainty of the NGHGI when
2330 methods are harmonized to include similar categories. The remaining differences can often be attributed to definitions,
2331 assumptions about activity data or emission factors, and the allocation of fuel types to different sectors (see Sect. 3.2
2332 and Fig. B3). The one available TD method, a regional European inversion system (CIF-CHIMERE) using an NO_x
2333 proxy to determine CO₂ fossil emissions, shows broad agreement with the BU estimates. However, this initial TD
2334 inversion is not yet capable of distinguishing the minor differences between the various BU estimates and does not
2335 yet quantify uncertainties, unlike, for example, Basu et al. (2020), which presents fossil fuel combustion and cement
2336 production emission including uncertainty estimates for the United States. However, a substantial decrease in the level
2337 of uncertainty of the inverse modeling system is expected in the near-term with the large-scale deployment of
2338 observation networks dedicated to detecting fossil fuel emissions (e.g., with launch of the CO₂M¹⁹ satellite mission in
2339 2025). In the short-term, the CoCO₂ project (CoCO₂, 2022) aims to advance methodology around co-assimilation of
2340 existing CO₂ satellite data (from the OCO-2/3 instruments) and to provide new analysis of the CO/FFCO₂ and
2341 NO_x/FFCO₂ ratios in order to significantly decrease uncertainty in the fossil CO₂ estimates.

Deleted: Fossil CO₂ emissions are more straightforward to estimate than ecosystem fluxes due to combustion being easier to model and parameterize at large scales

Formatted: Subscript

2342 The CO₂ land fluxes belong to the LULUCF sector, which is one of the most uncertain sectors in UNFCCC
2343 reporting. The IPCC guidelines prescribe methodologies that are used to estimate the CO₂ fluxes in the NGHGI, but
2344 grant countries significant freedom to adopt methods appropriate to their national circumstances. Even in the European
2345 Union, Member States use a wide variety of stock-change and gain-loss methods ranging from Tier 1 to Tier 3
2346 depending on the specific LULUCF flux being estimated (EU NIR, 2021). When analyzing the different estimates

Deleted: ²⁰

¹⁹ CO₂M : Copernicus Anthropogenic Carbon Dioxide Monitoring.
https://esamultimedia.esa.int/docs/EarthObservation/CO2M_MRD_v3.0_2021001_Issued.pdf

Formatted: Subscript

2352 from multiple BU sources (inventories and models) similar sources of uncertainties are observed such as: (a)
2353 differences due to input data and structural/parametric uncertainty of models (Houghton et al., 2012; Pongratz et al.,
2354 2021) and (b) differences in definitions (Pongratz et al., 2014; Grassi et al., 2018b; Petrescu et al., 2020, 2021b; Grassi
2355 et al., 2021). Reducing uncertainties in LULUCF estimates is needed given the increasing importance of the sector to
2356 EU climate policy over the next decades. In contrast to the previous 2020 climate and energy package, the LULUCF
2357 sector will now formally contribute to the binding emission reduction targets of the Unions 2030 climate and energy
2358 framework (EU, 2018a; 2018b). Furthermore, the European Climate Law explicitly states that LULUCF, together
2359 with all sectors of the economy, should contribute to achieving climate neutrality within the Union by 2050 (EU,
2360 2021b).

Deleted: C

2361 The LULUCF sector in NGHGs is composed of six land use categories. Of these, Forest land provides the
2362 most important contribution to the net CO₂ land flux in the EU27+UK, followed by Cropland and Grassland. HWP
2363 and “Land converted to settlements” also have non-negligible contributions, and changes in HWP strongly influence
2364 variations in decennial mean net LULUCF fluxes for the region. Of these, all except “Land converted to settlements”
2365 are represented in general ecosystem models, while Forestland, Cropland, and Grassland are simulated by category-
2366 specific process-based and data-driven models. Top-down inversions are capable of simulating net CO₂ fluxes to the
2367 atmosphere, but cannot yet attribute them between different categories.

Deleted: sector

2368 Differences in the detailed category-specific and inversion model results (Fig. 3-5) often come from choices in
2369 the simulation setup and the type of model used: bookkeeping models, process-based DGVMs, inventory-based
2370 statistical methods, or atmospheric inversions. Results also differ based on whether fluxes are attributed to LULUCF
2371 emissions due to the cause or location of occurrence. For example, indirect fluxes resulting from long-term changes
2372 in growing conditions, such as CO₂, air temperature, and water availability on managed land are included in NGHGI
2373 and FAOSTAT. Additional sink capacity compared to pre-industrial conditions (also called the “amplification effect”,
2374 e.g., Gasser and Ciais, 2013) occurs on Forest land in process-based models (e.g., ORCHIDEE or TRENDY DGVMs)
2375 due to improved growing conditions resulting from CO₂ fertilization, climate change, and anthropogenic nitrogen
2376 deposition, while this is not included in bookkeeping models which use the same regrowth curves for pre-industrial
2377 and modern times. The use of gross land use changes fluxes (e.g., in the NGHGI, bookkeeping models, and CABLE-
2378 POP) as opposed to net fluxes also likely plays an important role. We found that adjusting top-down models by
2379 emissions/removals resulting from later transport of carbon through trade and the inland water network improves the
2380 agreement with the NGHGI of the EU27+UK (Fig. 5, compared to Petrescu et al., 2021b).

Deleted: sector

Deleted: 4-9

Formatted: Subscript

Deleted: , while additional sink capacity (e.g., Petrescu et al., 2021b) is included in estimates from process-based models (e.g., ORCHIDEE or TRENDY DGVMs).

Deleted: 9

Deleted: 4-7

2381 Observation-based BU estimates of LULUCF provide large year-to-year flux variability (Figs. 3-4, in particular
2382 for DGVMs like ORCHIDEE, CABLE-POP and the TRENDY ensemble), contrary to the NGHGI, primarily due to
2383 the effect of varying meteorology. In particular, the duration and intensity of the summer growing season can vary
2384 significantly between years (e.g., Bastos et al., 2020a; Thompson et al., 2020). In the framework of periodic NGHGI
2385 assessments, the choice of a reference period (such as 2015-2019, as used here) or the use of a moving window to
2386 calculate the means may be critical to smooth out high inter-annual variability and facilitate comparisons. One can
2387 also imagine incorporating IAV into NGHGs through the use of annual anomalies of emission factors calculated from
2388 Tier 3 observation-based approaches (either BU or TD). TD estimates also show very large inter-annual variability

Deleted: the

2399 and uncertainty (Fig. 5). Uncertainties in the inversion results are primarily due to uncertainties in atmospheric
2400 transport modeling, boundary conditions, technical simplifications and uncertainty inherent to the limitation of the
2401 observation network. Currently, regional inversions (LUMIA, CSR and EUROCOM) are still under development and
2402 face different challenges from the coarser resolution global systems used here to represent regional results (GCP). As
2403 seen in Fig. 6, the mean of the regional inversions appears to agree better with the NGHGI than that of the global
2404 inversions, after the net carbon fluxes from lateral transfers are taken into account. In addition, the inter-model spread
2405 of the regional inversions is smaller. Based on this work, it is difficult to claim that one or the other provides a more
2406 accurate result for the net CO₂ land fluxes across the EU27+UK, although two regional inversion ensembles
2407 (EUROCOM and CSR) dramatically reduced their uncertainties between the previous and current versions of this
2408 synthesis, with CSR showing much more overlap now with the NGHGI (Fig. 6).

Deleted: 9

2409 Uncertainties can be reflected in space as well as in time. Reconciling differences across aggregated EU
2410 regions may be challenging due to diverse methodologies and drivers in each country. On the other hand, the analysis
2411 of smaller regions or individual countries may represent a productive first step towards monitoring the current state
2412 of emissions as national data and experts can be used to help clarify differences across models. Country-level case
2413 studies may help inform the design of future monitoring and verification systems (MVS) for CO₂ which aim to supply
2414 additional evidence for the emissions levels and trends, coupling anthropogenic activities and associated emissions
2415 with the atmospheric patterns of greenhouse gas mole fractions, and perform data assimilation and modeling over a
2416 wide variety of environmental conditions (Pinty et al., 2017).

Deleted: 10

Deleted: Fig. 11 separates mean BU and TD values for all methods into five different regions in Europe. From this figure, it's clear that some regions suffer from higher uncertainties than others. Part of this is likely linked to the sparseness of atmospheric observation data for the TD estimates (e.g., Eastern Europe).

2417 As seen in figures throughout this work, reducing uncertainties of both individual models and classes of
2418 models remains a priority. Some categories (Forestland, Cropland) produce results for multiple category-specific
2419 models which lie within the uncertainty of the NGHGI. This likely reflects the use of data-driven models and the
2420 relatively high quality of data that is available due to the economic importance of these categories. On the other hand,
2421 generalized ecosystem models (the DGVMs, like ORCHIDEE and CABLE-POP) may create mean estimates which
2422 fall within uncertainties, but fall outside of NGHGI uncertainties for any given year due to the sensitivity of processes
2423 in these models to rapidly changing meteorology and the necessity for these models to operate globally, including in
2424 data-poor regions for which parameterization may be impossible. Two advances in characterizing uncertainty were
2425 presented here: one for the case of the NGHGI, and one for the case of the TD model CSR. Additional characterization
2426 of uncertainty both within and across models will enable more fair comparisons between methods.

Deleted: concentration

2427 A more detailed analysis of LULUCF fluxes at the regional/country level is foreseen as part of projects linked
2428 to VERIFY including the RECCAP2 initiative (RECCAP2, 2022) and current and future Horizon Europe funded
2429 projects (e.g., CoCO₂, EYE-CLIMA, AVENGERS, PARIS) which will highlight examples of good practice in
2430 LULUCF flux monitoring amongst European countries. Sect. 3.4 presents a summary of uncertainties to provide
2431 insight into ground observation systems assimilated by inversions. This lays the basis of future improvements for
2432 establishing best practices on how to configure atmospheric inversions and systematically quantify uncertainties. For
2433 the overall estimation of emissions from LULUCF activities on all land types (Fig. 5, top), the comparison is made
2434 more challenging as results from both land use and land use changes are presented. Comparing only the “effect of

Deleted: relatively

Deleted: 3.6

Deleted: 8

2447 land use change” (conversion) is non-trivial. A methodology for reconciling LULUCF country estimates from the
2448 FAOSTAT datasets with the NGHGs is presented in Grassi et al. (2022a) for the global scale.

Deleted: and Grassi et al. (in prep)

2449 The next steps needed to improve and facilitate the reconciliation between BU and TD estimates are the same
2450 as those discussed in Petrescu et al. (2021b): 1) BU process-based models incorporating unified protocols and
2451 guidelines for uniform definitions should be able to disaggregate their estimates to facilitate comparison to NGHGI
2452 and 2006 IPCC practices (e.g., managed vs. unmanaged land, 20-year legacy for ~~categories~~ remaining in the same
2453 ~~category~~, distinction of fluxes arising solely from land use change, Grassi et al. (2022a)); 2) for ~~category~~-specific
2454 models, in particular for cropland and grassland, improving treatment of the contribution of soil organic carbon
2455 dynamics to the budget; 3) for TD estimates, using the recently developed Community Inversion Framework (Berchet
2456 et al., 2021) to better assess the different sources of uncertainties from the inversion set-ups (model transport, prior
2457 fluxes, observation networks), 4) standardize methods to compare datasets with and without interannual variability,
2458 and 5) develop a clear way to report key system boundary, data, or definitional issues, as it often necessary to have
2459 deep understanding of each estimate to know how to do a like-for-like comparison.

Deleted: classes

Deleted: class

Deleted: sector

2460 Similar to Petrescu et al. (2021b), this updated study concludes that a complete, ready-for-purpose monitoring
2461 system providing annual carbon fluxes across Europe is still under development, but data sources are beginning to
2462 show improved agreement compared to previous estimates. Significant effort must still be undertaken to robustly
2463 quantify and then reduce uncertainties (both in the models themselves as well as in their input data) used in such a
2464 system so that differences in the central values can be identified and understood (e.g., Maenhout et al., 2020). Future
2465 activities in the CoCO₂ project (CoCO₂, 2022) will investigate the one and five-year carbon budgets across the data-
2466 rich area of the EU27+UK and deepen the analysis for both global and regional/local (city level) estimates.

Deleted: Therefore, significant effort must still be undertaken to reduce the uncertainty across all potential methods (i.e., structural uncertainty in the models as well as the input data supplied to the models or inventory approaches) used in such a system (e.g. Maenhout et al., 2020)

2467 Achieving the well-below 2°C temperature goal of the Paris Agreement requires consideration of, among
2468 other things, low-carbon energy technologies, forest-based mitigation approaches, and engineered carbon dioxide
2469 removal (Grassi et al., 2018a; Nabuurs et al. 2017). Currently, the EU27+UK reports a sink for LULUCF and forest
2470 management will continue to be the main driver affecting the productivity of European forests for the next decades
2471 (Koehl et al., 2010), shown as well by the domination of Forestland CO₂ fluxes to the LULUCF sector in the NGHGI
2472 for the bloc. Forest management changes forest composition and structure, which affects the exchange of energy with
2473 the atmosphere (Naudts et al., 2016), and therefore the potential of mitigating climate change (Luyssaert et al., 2018;
2474 Grassi et al., 2019). Meteorological extremes can also affect the efficiency of the sink (Thompson et al., 2020). The
2475 EU forest sink is projected to decrease in the near future (Vizzarri et al., 2021). Consequently, for the EU to meet its
2476 ambitious climate targets, it is necessary to maintain and even strengthen the LULUCF sink (EU, 2020).
2477 Understanding the evolution of the CO₂ land fluxes is critical to enable the EU27+UK to meet its ambitious climate
2478 goals.

2479

2480 6. Appendices

Formatted: Heading 1

2481

2491 Appendix A. Data sources, methodology and 2492 uncertainty descriptions

2493 Plots for all countries in Europe as well as dozens of country groups and some countries outside of Europe are available
2494 following a simple registration (VERIFY Synthesis Plots, 2022).

2495

2496 A1. VERIFY project

2497

2498 VERIFY's primary aim is to develop scientifically robust methods to assess the accuracy and potential biases in
2499 national inventories reported by the parties through an independent pre-operational framework. "Pre-operational"
2500 seeks to bridge the gap between pure research efforts and those aiming to provide regular (e.g., annual) updates of a
2501 product. The main concept is to provide observation-based estimates of anthropogenic and terrestrial biospheric GHG
2502 emissions and sinks as well as associated uncertainties. The proposed approach is based on the integration of
2503 atmospheric measurements, improved emission inventories, ecosystem data, and satellite observations, and on an
2504 understanding of processes controlling GHG fluxes (ecosystem models, GHG emission models).

2505 Two complementary approaches relying on observational data-streams were combined in VERIFY to
2506 quantify GHG fluxes:

- 2507 1) atmospheric GHG mole fractions from satellites and ground-based networks (top-down atmospheric inversion
2508 models), and,
2509 2) bottom-up activity data (e.g., fuel use and emission factors, as represented in inventories) and ecosystem
2510 measurements (e.g., aboveground biomass and net ecosystem fluxes, as assimilated into bottom-up and top-down
2511 models).

2512 For CO₂, a specific effort was made to separate fossil fuel emissions from ecosystem fluxes.

2513

2514 The objectives of VERIFY were:

2515 **Objective 1.** Integrate the efforts between the research community, national inventory compilers, operational centers
2516 in Europe, and international organizations towards the definition of future international standards for the verification
2517 of GHG emissions and sinks based on independent observation.

2518 **Objective 2.** Enhance the current observation and modeling ability to accurately and transparently quantify the sinks
2519 and sources of GHGs in the land-use sector for the tracking of land-based mitigation activities.

2520 **Objective 3.** Develop new research approaches to monitor anthropogenic GHG emissions in support of the EU
2521 commitment to reduce its GHG emissions by 40 % by 2030 compared to the year 1990.

2522 **Objective 4.** Produce periodic scientific syntheses of observation-based GHG balance of EU countries and practical
2523 policy-oriented assessments of GHG emission trends, and apply these methodologies to other countries.

2524

2525 For more information on the project team and products/results please visit the VERIFY website (VERIFY, 2022).

Deleted: :

Formatted: Heading 1, Space After: 0 pt, Line spacing: single

Formatted: Left, Space After: 8 pt, Line spacing: Multiple 1,08 li, Border: Top: (No border), Bottom: (No border), Left: (No border), Right: (No border), Between : (No border), Pattern: Clear

Deleted: natural

Deleted: concentration

Formatted: Normal paragraph, Left, Line spacing: single, Pattern: Clear

Deleted: ¶

Deleted: bottom-up activity data (e.g., fuel use and emission factors) and ecosystem measurements (bottom-up models).

2532
2534
2535

Table A1: A short glossary of terminology and acronyms used in this work. Note that nuances may be lost due to space limitations, and therefore these definitions should be considered as a guide.

Terminology/Acronym	Brief description
additional sink capacity	A term referring to a general increased capacity of forests to uptake carbon due to improved growing conditions compared to pre-industrial times, in particular after the year 1950.
AFOLU	Agriculture, forestry, and land use. Includes all LULUCF fluxes (Sector 4) and also fluxes from Agriculture (Sector 3, e.g., CO ₂ emissions from applications of urea to fields).
Annex I Parties	A designation of countries under the UNFCCC. Includes most industrialized countries and economies in transition as determined in 1992. Required to submit more regular and complete inventories to the UNFCCC.
bottom-up (BU)	A model which estimates fluxes by through physical processes and/or data without explicit consideration of atmospheric gas mole fractions. Often subdivided into "data-driven" and "process-based", and include "inventories".
category	Land-use category: Forest land, Cropland. Be careful to avoid confusion with categories. For example, "net emissions from Forest land" (subsector 4A) and the classification of land into Forest land (a category).
CL	Total Cropland (including both "remain" and "convert")
CL-CL	Cropland which remains Cropland from year to year
class	In some IPCC documents, appears to be used in the same manner as "category". We avoid its use here in the same context. However, "class" is used in general to indicate several types of an object ("classes of models", for example).
convert	Land which has been converted to this category in the previous N years (by default, N is equal to 20)
decay	Gradual breakdown and respiration of organic matter
DGVM	Dynamical global vegetation model, a form of bottom-up model.
FL	Total Forest land (including both "remain" and "convert")
FL-FL	Forest land which remains Forest land from year to year
GCB	Global Carbon Budget
GHG	Greenhouse gas (generally CO ₂ in this work)
GL	Total Grassland (including both "remain" and "convert")
GL-GL	Grassland which remains Grassland from year to year
HWP	Harvested wood products. Carbon in timber removed from Forest land is counted here and allowed to slowly decompose (i.e., release CO ₂ to the atmosphere).
IPPU	Industrial processes and product use
LUC	Land use change
LULCC	Land use and land cover change. Includes changes from one land cover type to another without necessarily a change in use (e.g., a change from C3 to C4 species during natural succession of a grassland).
LULUC	Land use and land use change. Does not include fluxes from activities on Forest land remaining Forest land (e.g., thinning).
LULUCF	Land use, land use change, and forestry. "Sector 4" in NGHGI terminology, representing fluxes from Forest land, Grassland, Cropland, Wetlands, Settlements, and Other land, though not all of these Land types are present in other bottom-up models. Note the use of capital letters for Land types to indicate the definitions changes from country to country.
managed land proxy	An assumption used in the NGHGIs which permits Member States to only report fluxes on lands deemed to be "managed" by the MS
mole fraction	The number of molecules of a substance per unit of total molecules. A measure of concentration that is independent of temperature and pressure.

Deleted: Table XXXGLOSSARY: A short glossary of terminology and acronyms used in this work. Note that nuances may be lost due to space limitations, and therefore these definitions should be considered as a guide. ¶ Terminology/Acronym ... [30]

Formatted: Caption - VERIFY

Formatted: Font: (Default) Times New Roman, 10 pt

Formatted: Font: (Default) Times New Roman, 10 pt

Formatted: Font: (Default) Times New Roman, 10 pt

Formatted: Font: (Default) Times New Roman, 10 pt

Formatted: Font: (Default) Times New Roman, 10 pt

Formatted: Font: (Default) Times New Roman, 10 pt

Formatted: Font: (Default) Times New Roman, 10 pt

Formatted: Font: (Default) Times New Roman, 10 pt

Formatted: Font: (Default) Times New Roman, 10 pt

Formatted: Font: (Default) Times New Roman, 10 pt

Formatted: Font: (Default) Times New Roman, 10 pt

Formatted: Font: (Default) Times New Roman, 10 pt

Formatted: Font: (Default) Times New Roman, 10 pt

Formatted: Font: (Default) Times New Roman, 10 pt

Formatted: Font: (Default) Times New Roman, 10 pt

Formatted: Font: (Default) Times New Roman, 10 pt

Formatted: Font: (Default) Times New Roman, 10 pt

Formatted: Font: (Default) Times New Roman, 10 pt

Formatted: Font: (Default) Times New Roman, 10 pt

Formatted: Font: (Default) Times New Roman, 10 pt

Formatted: Font: (Default) Times New Roman, 10 pt

Formatted: Font: (Default) Times New Roman, 10 pt

Formatted: Font: (Default) Times New Roman, 10 pt

Formatted: Font: (Default) Times New Roman, 10 pt

Formatted: Font: (Default) Times New Roman, 10 pt

Formatted: Font: (Default) Times New Roman, 10 pt

Formatted: Font: (Default) Times New Roman, 10 pt

<u>MS</u>	Member State (generally a sovereign country)
<u>net flux (NBP, NEE)</u>	The definition of the net carbon flux varies from approach to approach. In general, in this work, use of “net biome production” includes harvest but perhaps no other disturbances. Regional inversions generally fix fossil emissions and biomass burning (or assume the latter to be negligible). NGHGI are calculated through both stock-change and gain-loss methods, and therefore what is explicit/implicitly included varies from country to country. Table C2 has more details.
<u>NGHGI</u>	National greenhouse gas inventory
<u>remain</u>	Land which has remained in the same category for the past N years (by default, N is equal to 20)
<u>subsector</u>	Divisions of sectors (e.g., Sector 1A is Fuel combustion in the Energy sector). In the case of LULUCF, subsectors may be confused with categories.
<u>sector</u>	The most highly-aggregated level of emission reporting in the NGHGI: Energy (Sector 1), IPPU (Sector 2), Agriculture (Sector 3), LULUCF (Sector 4), and Waste (Sector 5). The word is occasional used in the more generalized sense of a sector of the economy, e.g., the forest sector.
<u>tier</u>	Refers to the level of specificity used to calculate emissions. Tier 1 is the default, for which the IPCC provides generic emission factors and equations. Tier 2 uses the same equations, but region- or country-specific emission factors. Tier 3 uses more complex equations, possibly including process-based modeling.
<u>top-down (TD)</u>	A model which solves for fluxes by optimizing a prior guess based on observed atmospheric mole fractions. Also called an “atmospheric inversion”.
<u>UNFCCC</u>	United Nations Framework Convention on Climate Change
<u>VERIFY</u>	A project funded by the European Commission to build a pre-operational greenhouse gas monitoring system (see Appendix A1)
<u>volatilize</u>	Immediate release of carbon to the atmosphere, similar to instantaneous and complete combustion

Formatted: Font: (Default) Times New Roman, 10 pt

Formatted: Font: (Default) Times New Roman, 10 pt

Formatted: Font: (Default) Times New Roman, 10 pt

Formatted: Font: (Default) Times New Roman, 10 pt

Formatted: Font: (Default) Times New Roman, 10 pt

Formatted: Font: (Default) Times New Roman, 10 pt

Formatted: Font: (Default) Times New Roman, 10 pt

Formatted: Font: (Default) Times New Roman, 10 pt

Formatted: Font: (Default) Times New Roman, 10 pt

Formatted: Font: (Default) Times New Roman, 10 pt

Formatted: Font: (Default) Times New Roman, 10 pt

2541

2542 Table A2: Country grouping used for comparison purposes between BU and TD emissions as reported for the
2543 country- and regional-level synthesis plots available through the VERIFY web portal.

Deleted: /

Formatted: Caption - VERIFY

Country name – geographical Europe	BU-ISO3	Aggregation from TD-ISO3
Luxembourg	LUX	
Belgium	BEL	BENELUX
Netherlands	NLD	BNL
Bulgaria	BGR	BGR
Switzerland	CHE	
Lichtenstein	LIE	CHL
Czech Republic	CZE	Former Czechoslovakia
Slovakia	SVK	CSK
Austria	AUT	AUT
Slovenia	SVN	North Adriatic countries
Croatia	HRV	NAC

Romania	ROU	ROU
Hungary	HUN	HUN
Estonia	EST	
Lithuania	LTU	Baltic countries
Latvia	LVA	BLT
Norway	NOR	NOR
Denmark	DNK	
Sweden	SWE	
Finland	FIN	DSF
Iceland	ISL	ISL
Malta	MLT	MLT
Cyprus	CYP	CYP
France (Corsica incl.)	FRA	FRA
<i>Monaco</i>	<i>MCO</i>	
<i>Andorra</i>	<i>AND</i>	
Italy (Sardinia, Vatican incl.)	ITA	ITA
<i>San Marino</i>	<i>SMR</i>	
United Kingdom (Great Britain + N Ireland)	GBR	UK
<i>Isle of Man</i>	<i>IMN</i>	
Iceland		
Ireland	IRL	IRL
Germany	DEU	DEU
Spain	ESP	IBERIA
Portugal	PRT	IBE
Greece	GRC	GRC
<i>Russia (European part)</i>	<i>RUS European</i>	
<i>Georgia</i>	<i>GEO</i>	<i>RUS European+GEO</i>
<i>Russian Federation</i>	<i>RUS</i>	<i>RUS</i>
Poland	POL	POL
<i>Turkey</i>	<i>TUR</i>	<i>TUR</i>

EU27+UK (Austria, Belgium, Bulgaria, Cyprus, Czech Republic, Germany, Denmark, Spain, Estonia, Finland, France, Greece, Croatia, Hungary, Ireland, Italy, Lithuania, Latvia, Luxembourg, Malta, Netherlands, Poland, Portugal, Romania, Slovakia, Slovenia, Sweden, United Kingdom)	AUT, BEL, BGR, CYP, CZE, DEU, DNK, ESP, EST, FIN, FRA, GRC, HRV, HUN, IRL, ITA, LTU, LVA, LUX, MLT, NDL, POL, PRT, ROU, SVN, SVK, SWE, GBR	E28
Western Europe (Belgium, France, United Kingdom, Ireland, Luxembourg, Netherlands)	BEL, FRA, UK, IRL, LUX, NDL	WEE
Central Europe (Austria, Switzerland, Czech Republic, Germany, Hungary, Poland, Slovakia)	AUT, CHE, CZE, DEU, HUN, POL, SVK	CEE
Northern Europe (Denmark, Estonia, Finland, Lithuania, Latvia, Norway, Sweden)	DNK, EST, FIN, LTU, LVA, NOR, SWE	NOE
South-Western Europe (Spain, Italy, Malta, Portugal)	ESP, ITA, MLT, PRT	SWN
South-Eastern Europe (all) (Albania, Bulgaria, Bosnia and Herzegovina, Cyprus, Georgia, Greece, Croatia, Macedonia, the former Yugoslav, Montenegro, Romania, Serbia, Slovenia, Turkey)	ALB, BGR, BIH, CYP, GEO, GRC, HRV, MKD, MNE, ROU, SRB, SVN, TUR	SEE
South-Eastern Europe (Albania, Bosnia and Herzegovina, Macedonia, the former Yugoslav, Georgia, Turkey, Montenegro, Serbia)	ALB, BIH, MKD, MNE, SRB, GEO, TUR	SEA
South-Eastern Europe (EU) (Bulgaria, Cyprus, Greece, Croatia, Romania, Slovenia)	BGR, CYP, GRC, HRV, ROU, SVN	SEZ
Southern Europe (all) (SOE) (Albania, Bulgaria, Bosnia and Herzegovina, Cyprus, Georgia, Greece, Croatia, Macedonia, the former Yugoslav, Montenegro, Romania, Serbia, Slovenia, Turkey, Italy, Malta, Portugal, Spain)	ALB, BGR, BIH, CYP, GEO, GRC, HRV, MKD, MNE, ROU, SRB, SVN, TUR, ITA, MLT, PRT, ESP	SOE
Southern Europe (SOY) (Albania, Bosnia and Herzegovina, Georgia, Macedonia, the former Yugoslav, Montenegro, Serbia, Turkey)	ALB, BIH, GEO, MKD, MNE, SRB, TUR	SOY
Southern Europe (EU) (SOZ) (Bulgaria, Cyprus, Greece, Croatia, Romania, Slovenia, Italy, Malta, Portugal, Spain)	BGR, CYP, GRC, HRV, ROU, SVN, ITA, MLT, PRT, ESP	SOZ
Eastern Europe (Belarus, Moldova, Republic of, Russian Federation, Ukraine)	BLR, MDA, RUS, UKR	EAE
EU-15 (Austria, Belgium, Germany, Denmark, Spain, Finland, France, United Kingdom, Greece, Ireland, Italy, Luxembourg, Netherlands, Portugal, Sweden)	AUT, BEL, DEU, DNK, ESP, FIN, FRA, GBR, GRC, IRL, ITA, LUX, NDL, PRT, SWE	E15

<p><i>EU-27 (Austria, Belgium, Bulgaria, Cyprus, Czech Republic, Germany, Denmark, Spain, Estonia, Finland, France, Greece, Croatia, Hungary, Ireland, Italy, Lithuania, Latvia, Luxembourg, Malta, Netherlands, Poland, Portugal, Romania, Slovakia, Slovenia, Sweden)</i></p>	<p><i>AUT, BEL, BGR, CYP, CZE, DEU, DNK, ESP, EST, FIN, FRA, GRC, HRV, HUN, IRL, ITA, LTU, LVA, LUX, MLT, NDL, POL, PRT, ROU, SVN, SVK, SWE</i></p>	<p><i>E27</i></p>
<p><i>All Europe (Aaland Islands, Albania, Andorra, Austria, Belgium, Bulgaria, Bosnia and Herzegovina, Belarus, Switzerland, Cyprus, Czech Republic, Germany, Denmark, Spain, Estonia, Finland, France, Faroe Islands, United Kingdom, Guernsey, Greece, Croatia, Hungary, Isle of Man, Ireland, Iceland, Italy, Jersey, Liechtenstein, Lithuania, Luxembourg, Latvia, Moldova, Republic of, Macedonia, the former Yugoslav, Malta, Montenegro, Netherlands, Norway, Poland, Portugal, Romania, Russian Federation, Svalbard and Jan Mayen, San Marino, Serbia, Slovakia, Slovenia, Sweden, Turkey, Ukraine)</i></p>	<p><i>ALA, ALB, AND, AUT, BEL, BGR, BIH, BLR, CHE, CYP, CZE, DEU, DNK, ESP, EST, FIN, FRA, FRO, GBR, GGY, GRC, HRV, HUN, IMN, IRL, ISL, ITA, JET, LIE, LTU, LUX, LVA, MDA, MKD, MLT, MNE, NDL, NOR, POL, PRT, ROU, RUS, SJM, SMR, SRB, SVK, SVN, SWE, TUR, UKR</i></p>	<p><i>EUR</i></p>

2545 *countries highlighted in *italic* are not discussed in the current 2021 synthesis mostly because unavailability of UNFCCC NGHGI reports (non-
2546 Annex I countries²¹) but are present on the web-portal (VERIFY Synthesis Plots, 2022). ▼

2547 ▼

Deleted: Results for Annex I countries (NOR, CHE, ISL) and Eastern European countries (EAE) are represented in Fig. 11.
Deleted:Section Break (Next Page).....

²¹Non-Annex I countries are mostly developing countries. The reporting to UNFCCC is implemented through national communications (NCs) and biennial update reports (BURs): <https://unfccc.int/national-reports-from-non-annex-i-parties>

2551
2552
2553
2554

*Table A3: An overview of major changes of the current study with respect to the original (Petrescu et al., 2020) and most recent (Petrescu et al., 2021b) studies of this series; n/a means a dataset was not used or available. **Bold text indicates changes in this study with respect to the most recent version.***

Dataset	Petrescu et al. (2020)	Petrescu et al. (2021b)	This study
NGHGI Fossil CO₂			
Emissions	n/a	Common reporting framework (CRF), submitted in 2019 1990-2017	Common reporting framework (CRF), submitted in 2021 1990-2019
Uncertainties	n/a	Uncertainty exists for 2016 (error propagation, 95 % confidence interval)	Uncertainty exists for 1990-2019 (error propagation, 95 % confidence interval, gap-filling)
Bottom-up fossil CO₂			
BP	n/a	n/a	Version 2021 1971-2020
CDIAC	n/a	2005-2018	Version 2021v2 1992-2018
CEDS	n/a	2005-2014	Version 2021_04_21 1750-2019
EDGAR	n/a	Version 5.0 1990-2018	Version 6.0b 1970-2018
EIA	n/a	2005-2016	Version 220216 1993-2019
GCP	n/a	2005-2018	Version 2021v40 1750-2020
IEA	n/a	1990-2017	1990-2020
PRIMAP-hist	n/a	2005-2017	Version 2.3.1 1750-2019
Top-down fossil CO₂			
Emissions	n/a	IAP RAS fast-track inversion EU11+CHE	CIF-CHIMERE fast-track inversion EU27+UK 2005-2020
NGHGI land CO₂			
Emissions	CRF, submitted in 2018 LULUCF : 1990-2016 FL : 1995, 2000, 2005, 2010, 2015 GL : 1990, 2005, 2010, 2016 CL : 1990, 2005, 2010, 2016	CRF, submitted in 2019 LULUCF: 1990-2017 FL : 1990-2017 GL: 1990-2017 CL: 1990-2017	CRF, submitted in 2021 LULUCF: 1990- 2019 FL : 1990- 2019 GL: 1990- 2019 CL: 1990- 2019
Uncertainties	Uncertainty exists for 2016 (error propagation, 95 % confidence interval)	Uncertainty exists for 2016 (error propagation, 95 % confidence interval)	LULUCF: Uncertainty exists for 1990-2019 (error propagation, 95 % confidence interval, gap-filling) FL, GL, CL: Uncertainty exists for 2018 (error propagation, 95 % confidence interval)
Bottom-up terrestrial biosphere CO₂			
BLUE	Version GCP 1990-2017	Version GCP 1990-2018	Version GCP 1990- 2020 Version VERIFY 1990-2020

Commented [MOU2]: This entire table has been redone in response to a reviewer comment. A few changes have been tracked in response to a different reviewer comment.

Deleted: 2

Formatted: Caption - VERIFY, Left, Line spacing: single

Deleted: 2018

Formatted: Font: Bold

Deleted: land

CABLE-POP	n/a	n/a	1990-2020
CBM	2000, 2005, 2010, 2015	1990-2015	2000-2015 2017-2020 (estimate)
ECOSSE	n/a	1990-2018 (grassland) 1990-2018 (cropland)	1990-2018 (grassland) 1990-2020 (cropland)
EFISCEN	1995, 2000, 2010, 2015 Country totals EU27+UK	2005-2018 Country Totals EU27+UK	2005-2020 Spatially-explicit 15 countries
EPIC-IIASA	n/a	1990-2018 (cropland)	1990-2020 (cropland) 1990-2020 (grassland)
FAOSTAT	1990-2016	1990-2017	1990-2019
H&N	1990-2015	1990-2018	1990-2020
Lateral fluxes	n/a	(not accounted for in inversions) Emissions from inland waters	(accounted for in inversions) Emissions from inland waters Wood trade Crop trade 1990-2019
ORCHIDEE	n/a	version 2.2 1990-2018	version 3.0 1990-2020
TRENDY DVGMS	Version 6 1990-2017	Version 7 1990-2018	Version 10 1990-2020
Top-down terrestrial biosphere CO ₂ (global)			
Global Carbon Project	n/a	version 2019 2000-2018	version 2021 2010-2020
Top-down terrestrial biosphere CO ₂ (regional)			
CarboScopeRegional	n/a	2006-2018	2006-2020
CIF-CHIMERE	n/a	n/a	2005-2020
EUROCOM	n/a	Original version 2006-2015	Drought Version 2009-2018
LUMIA	n/a	n/a	2006-2020

Deleted: land

Deleted: land

Deleted: -----Section Break (Next Page)-----

Table A2: Methodological changes (in bold) of the current study with respect to Petrescu et al. (2020), Petrescu et al. (2021b) and an internal VERIFY update (v2020); n/a cells mean that there is no data available.

Formatted: Space After: 8 pt, Line spacing: Multiple 1,08 li

2558
2559

2560
2561

A2. UNFCCC NGHGI (2021)

2562
2563
2564
2565
2566
2567
2568
2569
2570
2571
2572
2573
2574

Annex I NGHGIs should follow principles of transparency, accuracy, consistency, completeness and comparability (TACCC) under the guidance of the UNFCCC (UNFCCC, 2014) and as mentioned above, shall be completed following the 2006 IPCC guidelines (IPCC, 2006). In addition, the IPCC 2019 Refinement (IPCC, 2019), which may be used to complement the 2006 IPCC guidelines, has updated sectors with additional emission sources and provides guidance on the use of atmospheric data for independent verification of GHG inventories.

Both approaches (BU and TD) provide useful insights on emissions from two different points of view. First, as outlined in Volume 1, Chapter 6 of the 2019 IPCC Refinement (IPCC, 2019), TD approaches act as an additional quality check for BU and NGHGI approaches, and facilitate a deeper understanding of the processes driving changes in different elements of GHG budgets. Second, while independent BU methods do not follow prescribed standards like the IPCC Guidelines, they do provide complementary information based on alternative input data at varying temporal, spatial, and sectoral resolution. This complementary information helps build trust in country GHG estimates, which form the basis of national climate mitigation policies. Additionally, BU estimates are needed as input for TD estimates. As there is no formal guideline to estimate uncertainties in TD or BU approaches, uncertainties are usually

2586 assessed from the spread of different estimates within the same approach, though some groups or institutions report
2587 uncertainties for their individual estimates using a variety of methods, for instance, by performing Monte Carlo
2588 sensitivity simulation by varying input data parameters. However, this can be logistically and computationally difficult
2589 when dealing with complex process-based models.

2590 Despite the important insights gained from complementary BU and TD emission estimates, it should be noted
2591 that comparisons with the NGHGI are not always straightforward. BU estimates often share common methodology
2592 and input data, and through harmonization, structural differences between BU estimates and NGHGIs can be
2593 interpreted. However, the use of common input data restricts the independence between the datasets and, from a
2594 verification perspective, may limit the conclusions drawn from the comparisons. On the other hand, TD estimates are
2595 constrained by independent atmospheric observations and can serve as an additional, potentially independent quality
2596 check for NGHGIs. Nonetheless, structural differences between NGHGIs (what sources and sinks are included, and
2597 where and when emissions/removals occur) and the actual fluxes of GHGs to the atmosphere must be taken into
2598 account during comparison of estimates. While NGHGIs go through a central QA/QC review process, the UNFCCC
2599 reporting requirements do not mandate large-scale observation-derived verification. Nevertheless, the individual
2600 countries may use atmospheric data and inverse modeling within their data quality control, quality assurance and
2601 verification processes, with expanded and updated guidance provided in chapter 6 of the 2019 Refinement of IPCC
2602 2006 Guidelines (IPCC, 2019). So far, only a few countries (e.g. Switzerland, UK, New Zealand and Australia) have
2603 used atmospheric observations to constrain national emissions and documented these verification activities in their
2604 national inventory reports (Bergamaschi et al., 2018), and none do so for CO₂.

2605 Under the UNFCCC convention and its Kyoto Protocol, national GHG inventories are the most important
2606 source of information to track progress and assess climate protection measures by countries. In order to build mutual
2607 trust in the reliability of GHG emission information provided, national GHG inventories are subject to standardized
2608 reporting requirements, which have been continuously developed by the Conference of the Parties (COP)²². The
2609 calculation methods for the estimation of greenhouse gases in the respective sectors is determined by the methods
2610 provided by the 2006 IPCC Guidelines for National Greenhouse Gas Inventories (IPCC, 2006). These Guidelines
2611 provide detailed methodological descriptions to estimate emissions and removals, as well as recommendations to
2612 collect the activity data needed. As a general overall requirement, the UNFCCC reporting guidelines stipulate that
2613 reporting under the Convention and the Kyoto Protocol must follow the five key principles of transparency, accuracy,
2614 completeness, consistency and comparability (TACCC).

2615 The reporting under UNFCCC shall meet the TACCC principles. The three main GHGs are reported in
2616 timeseries from 1990 up to two years before the due date of the reporting. The reporting is strictly source category
2617 based and is done under the Common Reporting Format tables (CRF), downloadable from the UNFCCC official
2618 submission portal: <https://unfccc.int/ghg-inventories-annex-i-parties/2021>.

2619

Formatted: Font: (Default) Times New Roman, 10 pt

²² The last revision has been made by COP 19 in 2013 (UNFCCC, 2013)

2620 NGHGI uncertainties

2621

2622 The presented uncertainties in the reported emissions of the individual countries and the EU27+UK bloc
2623 were calculated by using the methods and data used to compile the official GHG emission uncertainties that are
2624 reported by the EU under the UNFCCC (NIRs, 2022). The EU uncertainty analysis reported in the bloc's National
2625 Inventory Report (NIR) is based on country-level, Approach 1 uncertainty estimates (IPCC, 2006, Vol. 1, Chap. 3)
2626 that are reported by EU Member States, Iceland and United Kingdom under Article 7(1)(p) of EU (2013). These
2627 country-level uncertainty estimates are typically reported at beginning of a submission cycle and are not always
2628 revised with updated CRF submissions later in the submission cycle. Furthermore, the compiled uncertainties of some
2629 countries are incomplete (e.g., uncertainties not estimated for LULUCF and/or indirect CO₂ emissions, certain
2630 subsector emissions are confidential) and the sector and gas resolution at which uncertainties are provided varies
2631 between the countries. The EU inventory team therefore implements a procedure to harmonize and gap-fill these
2632 uncertainty estimates. A processing routine reads the individual country uncertainty files that are pre-formatted
2633 manually to assign consistent sector and gas labels to the respective estimates of emissions/removals and uncertainties.
2634 The uncertainty values are then aggregated to a common sector resolution, at which the emissions and removals
2635 reported in the uncertainty tables of the countries are then replaced with the respective values from the final CRF
2636 tables of the countries. Due to the issue of incompleteness mentioned above, the country-level data are then screened
2637 to identify residual GHG emissions and removals for which no uncertainty estimates have been provided. Where
2638 sectors are partially complete, the residual net emission is quantified in CO₂ equivalents and incorporated. An
2639 uncertainty is then estimated, by calculating the overall sector uncertainty of the sources and sinks that were included
2640 in that country's reported uncertainties estimates and assigning this percentage average to the residual net emission.
2641 In cases where for certain sectors no uncertainties have been provided at all (e.g., indirect CO₂ emissions, LULUCF),
2642 an average (median) sector uncertainty in percent is calculated from all the countries for which complete sectoral
2643 emissions and uncertainties were reported, and this average uncertainty is assigned to the country's sector GHG total
2644 reported in its final CRF tables.

2645 The country-level uncertainties presented in this paper, have been compiled using this same processing
2646 routine and using the uncertainties and CRF data reported by the countries in the 2021 submission. However, here the
2647 method has been expanded to gap-fill at the individual greenhouse gas level (CO₂ emissions and removals only) rather
2648 than at the aggregate GHG level. Furthermore, the expanded method here assigns the sub-sectoral uncertainties to the
2649 emissions and removals of the entire timeseries (1990-2019), rather than just the base year and latest year of the
2650 respective timeseries. This allows uncertainties to be sensitive to the sub-sectoral contributions to sectoral and national
2651 total emissions, which of course change over time. For each year of the timeseries, uncertainties in the total and
2652 sectoral CO₂ emissions are calculated using Gaussian error propagation, by summing the respective sub-sectoral
2653 uncertainties (expressed in kt CO₂) in quadrature and assuming no error correlation. In contrast, for the EU27+UK
2654 bloc, uncertainties in the total and sectoral CO₂ emissions were calculated to take into account error correlations
2655 between the respective country estimates at the subsector level. This was done by applying the same methods and
2656 assumptions described in the 2022 EU NIR (UNFCCC NIR, 2022). The subsector resolution applied for gap-filling

Moved (insertion) [1]

Formatted: Left, Line spacing: Multiple 1,08 li

2657 allows the routine to access respective data on emission factors from CRF Table Summary 3 and apply correlation
2658 coefficients (r) when aggregating the uncertainties. For a given subsector, it is assumed that the errors of countries
2659 using default factors are completely correlated (r = 1), while errors of countries using country-specific factors are
2660 assumed uncorrelated (r = 0). For countries using a mix of default and country-specific factors at the given subsector
2661 level, it is assumed that these errors are partially correlated (r = 0.5) with one another and with the errors of countries
2662 using the default factors only.

2663 Based on these correlation assumptions, the routine then aggregates CO₂ emissions/removals and
2664 uncertainties for the specified subsector resolution at the EU27+UK level. Uncertainties at sector total level are then
2665 aggregated from the subsector estimates assuming no correlation between subsectors. However, for countries reporting
2666 very coarse resolution estimates (e.g., total sector CO₂ emissions/removals) or where the sector has been partially or
2667 completely gap-filled, it is assumed that these uncertainties are partially correlated (r = 0.5) with one another and with
2668 the other reported subsector level estimates. Level uncertainties on the total EU27+UK CO₂ emissions and removals
2669 (with and without LULUCF) are then aggregated from the sector estimates assuming no error correlation between
2670 sectors.

2671 Note that the above procedure does not apply to LULUCF categories (FL, CL, and GL). Estimates for these
2672 values were taken directly from the EU NIR (2021) without gap-filling or consideration of correlations. An
2673 uncertainty greater than 100 % implies that either a sink or a source is possible. As the values are given for only one
2674 single year, this value is applied uniformly across the whole timeseries.

2676 **A3. Fossil CO₂ emissions**

2678 **A3.1. Bottom-up emission estimates**

2680 For further details of all datasets, see Andrew (2020).

2682 *UNFCCC NGHGI (2021)*

2684 The UNFCCC NGHGI CO₂ emissions/removals include estimates from five key sectors for the EU27+UK:
2685 1 Energy, 2 Industrial processes and product use (IPPU), 3 Agriculture, 4 LULUCF and 5 Waste. The tiers method a
2686 country applies depends on the national circumstances and the individual conditions of the land, which explains the
2687 variability of uncertainties among the sector itself as well as among EU countries. This annual published dataset
2688 includes all CO₂ emissions sources for those countries, and for most countries for the period 1990 to t-2. Some eastern
2689 European countries' submissions began in the 1980s.

2690 [Information on uncertainty calculation in the NGHGIs is found above in the general section on the NGHGI.](#)

2691

Formatted: Normal paragraph, Left, Indent: First line: 0 cm, Line spacing: single

Deleted: 1:

Formatted: Heading 2, Space After: 0 pt, Line spacing: single

Formatted: Heading 3, Space After: 0 pt, Line spacing: single

Formatted: Line spacing: Multiple 1,08 li, Don't keep with next, Don't keep lines together, Border: Top: (No border), Bottom: (No border), Left: (No border), Right: (No border), Between : (No border)

Deleted: Annex I NGHGIs should follow principles of transparency, accuracy, consistency, completeness and comparability (TACCC) under the guidance of the UNFCCC (UNFCCC, 2014) and as mentioned above, shall be completed following the 2006 IPCC guidelines (IPCC, 2006). In addition, the IPCC 2019 Refinement (IPCC, 2019), which may be used to complement the 2006 IPCC guidelines, has updated sectors with additional emission sources and provides guidance on the use of atmospheric data for independent verification of GHG inventories. ¶ Both approaches (BU and TD) provide useful insights on emissions from two different points of view. First, as outlined in Volume 1, Chapter 6 of the 2019 IPCC Refinement (IPCC, 2019), TD approaches act as an additional quality check for BU and NGHGI approaches, and facilitate a deeper understanding of the processes driving changes in different elements of GHG budgets. Second, while independent BU methods do not follow prescribed standards like the IPCC Guidelines, they do provide complementary information based on alternative input data at varying temporal, spatial, and sectoral resolution. This complementary information helps build trust in country GHG estimates, which form the basis of national climate mitigation policies. Additionally, BU estimates are needed as input for TD estimates. As there is no formal guideline to estimate uncertainties in TD or BU approaches, uncertainties are usually assessed from the spread of different estimates within the same approach, though some groups or institutions report uncertainties for their individual estimates using a variety of methods, for instance, by performing Monte Carlo sensitivity simulation by varying input data parameters. However, this can be logistically and computationally difficult when dealing with complex process-based models. ¶

Despite the important insights gained from complementary BU and TD emission estimates, it should be noted that comparisons with the NGHGI are not always straightforward. BU estimates often share common methodology and input data, and through harmonization, structural differences between BU estimates and NGHGIs can be interpreted. However, the use of common input data restricts the independence between the datasets and, from a verification perspective, may limit the conclusions drawn from the comparisons. On the other hand, TD estimates are constrained by independent atmospheric observations and can serve as an additional, nearly independent quality check for NGHGIs. Nonetheless, structural differences between NGHGIs (what sources and sinks are included, and where and when emissions/removals occur) and the actual fluxes of GHGs to the atmosphere must be taken into account during com[31]

2818 **EDGAR v6.0**

2819

2820 The first edition of the Emissions Database for Global Atmospheric Research was published in 1995. The
2821 dataset now includes almost all sources of fossil CO₂ emissions, is updated annually, and reports data for 1970 to year
2822 n-1. Estimates for v6.0 are provided by sector. Emissions are estimated fully based on statistical data from 1970 till
2823 2018 <https://data.jrc.ec.europa.eu/dataset/97a67d67-c62e-4826-b873-9d972c4f670b>.

2824 **Uncertainties:** EDGAR uses emission factors (EFs) and activity data (AD) to estimate emissions. Both EFs and AD
2825 are uncertain to some degree, and when combined, their uncertainties need to be combined too. To estimate EDGAR's
2826 uncertainties (stemming from lack of knowledge of the true value of the EF and AD), the methodology devised by
2827 IPCC (2006, Chapter 3) is adopted (Solazzo et al., 2021), including the use of default uncertainties. The overall
2828 relative uncertainty in emissions is thus given by simple error propagation for the product of two variables, where the
2829 overall relative uncertainty is the square root of the sum of squares of the relative uncertainties of the EF and AD. A
2830 log-normal probability distribution function is assumed in order to avoid negative values, and uncertainties are
2831 reported as the 95 % confidence interval according to IPCC (2006, chapter 3, equation 3.7). For emission uncertainty
2832 in the range 50 % to 230 % a correction factor is adopted as suggested by Frey et al. (2003) and IPCC (2006, chapter
2833 3, equation 3.4). Uncertainties are published in Solazzo et al. (2021).

2834

2835 **BP**

2836

2837 BP releases its Statistical Review of World Energy annually in June, the first report being published in 1952.
2838 Primarily an energy dataset, BP also includes estimates of fossil-fuel CO₂ emissions derived from its energy data (BP
2839 2011, 2017). The emissions estimates are totals for each country starting in 1965 to year n-1.

2840

2841 **CDIAC**

2842

2843 The original Carbon Dioxide Information Analysis Center included a fossil CO₂ emissions dataset that was
2844 long known as CDIAC. This dataset is now produced at Appalachian State University, and has been renamed CDIAC-
2845 FF (CDIAC, 2022). It includes emissions from fossil fuels (including gas flaring) and cement production from 1751
2846 to year n-3. Fossil-fuel emissions are derived from UN energy statistics, and cement emissions from USGS production
2847 data.

2848

2849 **EIA**

2850

2851 The US Energy Information Administration publishes international energy statistics and from these derives
2852 estimates of CO₂ emissions from energy combustion based on energy consumption. Data are currently available for
2853 the period 1980-2016.

Moved up [1]: NGHGI uncertainties

The presented uncertainties in the reported emissions of the individual countries and the EU27+UK bloc were calculated by using the methods and data used to compile the official GHG emission uncertainties that are reported by the EU under the UNFCCC (NIRs, 2022). The EU uncertainty analysis reported in the bloc's National Inventory Report (NIR) is based on country-level, Approach 1 uncertainty estimates (IPCC, 2006, Vol. 1, Chap. 3) that are reported by EU Member States, Iceland and United Kingdom under Article 7(1)(p) of EU (2013). These country-level uncertainty estimates are typically reported at beginning of a submission cycle and are not always revised with updated CRF submissions later in the submission cycle. Furthermore, the compiled uncertainties of some countries are incomplete (e.g., uncertainties not estimated for LULUCF and/or indirect CO₂ emissions, certain subsector emissions are confidential) and the sector and gas resolution at which uncertainties are provided varies between the countries. The EU inventory team therefore implements a procedure to harmonize and gap-fill these uncertainty estimates. A processing routine reads the individual country uncertainty files that are pre-formatted manually to assign consistent sector and gas labels to the respective estimates of emissions/removals and uncertainties. The uncertainty values are then aggregated to a common sector resolution, at which the emissions and removals reported in the uncertainty tables of the countries are then replaced with the respective values from the final CRF tables of the countries. Due to the issue of incompleteness mentioned above, the country-level data are then screened to identify residual GHG emissions and removals for which no uncertainty estimates have been provided. Where sectors are partially complete, the residual net emission is quantified in CO₂ equivalents and incorporated. An uncertainty is then estimated, by calculating the overall sector uncertainty of the sources and sinks that were included in that country's reported uncertainties estimates and assigning this percentage

Formatted: Line spacing: Multiple 1,08 li, Don't keep with next, Don't keep lines together, Border: Top: (No border), Bottom: (No border), Left: (No border), Right: (No border), Between : (No border)

Deleted: that is the overall

Deleted: y

Deleted: (uncertainty of the product of two variables)

Formatted: Font: Not Italic

Formatted: Space After: 8 pt, Line spacing: Multiple 1,08 li, Don't keep with next, Don't keep lines together, Border: Top: (No border), Bottom: (No border), Left: (No border), Right: (No border), Between : (No border)

Formatted: Font: Not Italic

Formatted: Left, Space After: 8 pt, Line spacing: Multiple 1,08 li

Formatted: Font: Not Italic

Formatted: Left, Space After: 8 pt, Line spacing: Multiple 1,08 li

Deleted: derives estimates of energy combustion CO₂ emissions...

2972

2973 *IEA*

2974

2975 The International Energy Agency publishes international energy statistics and from these derives estimates
2976 of CO₂ emissions from energy combustion. In addition, IEA also estimates emissions from the use of coal in the iron
2977 and steel industry, while not providing any other IPPU estimates. Emissions estimates start in 1960 for OECD
2978 members and 1971 for non-members, and run through n-1 for OECD members' totals, and year n-2 for members'
2979 details and non-members. Most subsector-level data from IEA are available for a fee, although some high-level
2980 emissions data can be accessed free-of-charge.

Formatted: Left, Space After: 8 pt, Line spacing: Multiple 1,08 li

Deleted: The International Energy Agency publishes international energy statistics and from these derives estimates of energy combustion CO₂ emissions including from the use of coal in the iron and steel industry

Deleted: Estimates are available by sector for a fee.

2981

2982 *GCP*

2983

2984 The Global Carbon Project includes estimates of fossil CO₂ emissions in its annual Global Carbon Budget
2985 publication. These include emissions from fossil fuels and cement production for the period 1750 to year n-1. GCP's
2986 fossil CO₂ dataset was once entirely derived solely from CDIAC's dataset, with some extension using BP data, but
2987 this has since changed as described in Andrew and Peters (2022).

Formatted: Left, Space After: 8 pt, Line spacing: Multiple 1,08 li

2988

2989 *CEDS*

2990

2991 The Community Emissions Data System has included estimates of fossil CO₂ emissions since 2018, with an
2992 irregular update cycle (CEDS, 2022). Energy data are directly from IEA, but emissions are scaled to higher-priority
2993 sources, including national inventories. Almost all emissions sources are included and estimates are published for the
2994 period 1750 to year n-1. Estimates are provided by subsector.

Formatted: Font: Not Italic

Formatted: Line spacing: Multiple 1,08 li, Don't keep with next, Don't keep lines together, Border: Top: (No border), Bottom: (No border), Left: (No border), Right: (No border), Between : (No border)

2995

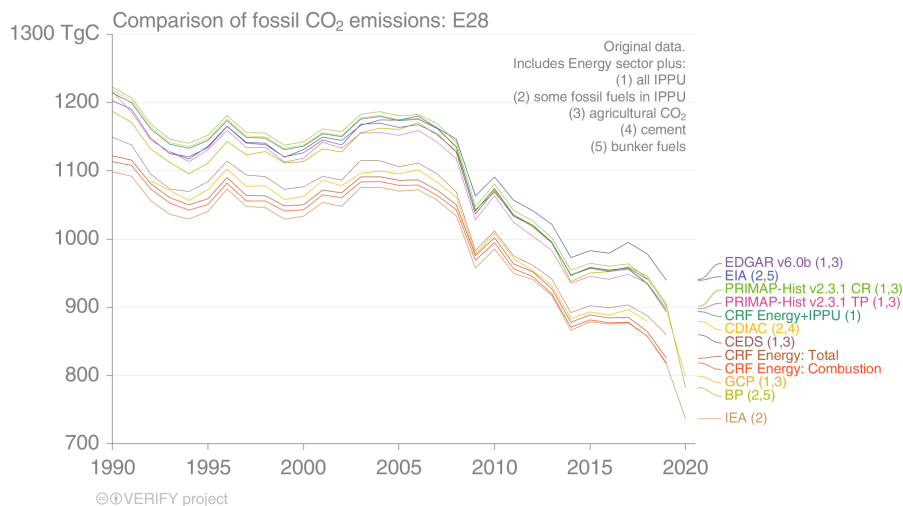
2996 *PRIMAPv2.2*

2997

2998 The PRIMAP-hist dataset combines several published datasets to create a comprehensive set of greenhouse
2999 gas emission pathways for every country and Kyoto gas, covering the years 1850 to 2018, and all UNFCCC (United
3000 Nations Framework Convention on Climate Change) member states as well as most non-UNFCCC territories. The
3001 data resolves the main IPCC (Intergovernmental Panel on Climate Change) 2006 categories. For CO₂, CH₄, and N₂O
3002 subsector data for Energy, Industrial Processes and Product Use (IPPU), and Agriculture is available. Due to data
3003 availability and methodological issues, version 2.2 of the PRIMAP-hist dataset does not include emissions from Land
3004 Use, Land-Use Change, and Forestry (LULUCF). More info at <https://zenodo.org/record/4479172#.YUsc6p0zbIU>.

Formatted: Font: Not Italic

Formatted: Left, Line spacing: Multiple 1,08 li



3010

3011 *Figure A1: Comparison of EU27+UK fossil CO₂ emissions from multiple inventory datasets. Identical to Fig. 2,*
 3012 *except that no system boundaries harmonization has been done. CDIAC does not report emissions prior to 1992 for*
 3013 *former-Soviet Union countries. CRF: UNFCCC NGHGI from the Common Reporting Format tables.*

Commented [MOU3]: Figure has been replaced.

Deleted: ;

Formatted: Caption - VERIFY, Line spacing: single

3014

3015

3016 **A3.2. Top-down CO₂ emission estimates**

3017

3018 *CIF-CHIMERE - fossil CO₂ emission inversion*

3019

3020 CIF-CHIMERE is used for both CO₂ land and CO₂ fossil emission estimates, and this section only describes
 3021 the CO₂ fossil estimates. The product is explained in more detail by Fortems-Cheiney and Broquet, 2021.

Formatted: Normal, Space After: 0 pt, Line spacing: single

Formatted: Font: Not Italic

Formatted: Line spacing: Multiple 1,08 li, Don't keep with next, Don't keep lines together, Border: Top: (No border), Bottom: (No border), Left: (No border), Right: (No border), Between : (No border)

3022 Results from previous atmospheric inversions of the European fossil CO₂ emissions indicated that there were
 3023 much larger uncertainties associated with the assimilation of CO data than with that of NO₂ data for such a purpose
 3024 (Konovalov et al, 2016; Konovalov and Llova, 2018). In this context, we have developed an atmospheric inversion
 3025 configuration quantifying monthly to annual budgets of the national emissions of fossil CO₂ in Europe based on the
 3026 assimilation of the long-term series of NO₂ spaceborne observations; the Community Inversion Framework (CIF); the
 3027 CHIMERE regional chemistry transport model (CTM); corrections to the TNO-GHGco-v3 inventory of NO_x
 3028 anthropogenic emissions at 0.5° horizontal resolution; and the conversion of NO_x anthropogenic emission estimates
 3029 into CO₂ fossil emission estimates. For the first time, to our knowledge, variational regional inversions have been
 3030 performed to estimate the European CO₂ fossil emissions using NO_x emissions from OMI satellite observations.
 3031 Particular attention is paid in the analysis assessing the consistency between the fossil CO₂ emissions estimates from

Formatted: Subscript

Formatted: Subscript

Formatted: Subscript

3033 our processing chain with the fossil CO₂ emission budgets provided by the TNO-GHGco-v3 inventory based on the
3034 emissions reported by countries to UNFCCC, which are assumed to be accurate in Europe. The algorithm first
3035 optimizes NO_x emissions and then assumes a fixed ratio of NO_x to fossil CO₂ emissions. However, long-term plans
3036 include the simultaneous inversion of all three gasses (CO₂, NO₂, and CO).

3037 The analysis is conducted over the period 2005 to 2020. CHIMERE is run over a 0.5°×0.5° regular grid and
3038 17 vertical layers, from the surface to 200hPa, with 8 layers within the first two kilometers. The domain includes 101
3039 (longitude) x 85 (latitude) grid-cells (15.25°W-35.75°E; 31.75°N-74.25°N) and covers Europe. CHIMERE is driven
3040 by the European Centre for Medium-Range Weather Forecasts (ECMWF) meteorological forecast (Owens and
3041 Hewson, 2018). The chemical scheme used in CHIMERE is MELCHIOR-2, with more than 100 reactions (Lattuati,
3042 1997; CHIMERE 2017), including 24 for inorganic chemistry. Climatological values from the LMDZ-INCA global
3043 model (Szopa et al., 2008) are used to prescribe mole fractions at the lateral and top boundaries and the initial
3044 atmospheric composition in the domain. Considering the short NO₂ lifetime, we do not consider its import from outside
3045 the domain: its boundary conditions are set to zero. Nevertheless, we take into account peroxyacetyl nitrate (PAN) for
3046 the large-scale transport of NO_x. Due to atmospheric chemistry, it represents an important and the associated NO_x
3047 reservoir and has a significant impact on the regional NO_x tropospheric columns observed by OMI.

3048 Several critical aspects of this workflow need to be highlighted: (i) Fortems-Cheiney and Broquet (2021)
3049 have not yet reported estimates of the uncertainty in the fossil CO₂ emissions (this requires the derivation of the
3050 uncertainties in the NO_x emission inversions and in the NO_x-to-FFCO₂ emission conversion), and (ii) the fossil CO₂
3051 emission budgets provided by the TNO-GHGco-v3 inventory are based on the emissions reported by countries to
3052 UNFCCC, which are assumed to be accurate in Europe, and therefore the NO_x inversion prior estimate is consistent
3053 with the inventory estimates (with respect to the NO_x-to-FFCO₂ emission conversion used to infer fossil CO₂
3054 emissions from the NO_x inversions).

3055 **Uncertainty:** There is no uncertainty estimate currently available for this product.

3056

3057 **A4. Land CO₂ emissions/removals**

3058

3059 **A4.1. Bottom-up CO₂ estimates**

3060

3061 UNFCCC NGHGI 2021 - LULUCF

3062

3063 For the biogenic CO₂ emissions from LULUCF (Sector 4 in the terminology of the NGHGs), methods for the
3064 estimation of CO₂ removals differ enormously among countries and land use categories. Each country uses its own
3065 country specific method which takes into account specific national circumstances (as long as they are in accordance
3066 with the 2006 IPCC guidelines), as well as IPCC default values, which are a "compromise between the level of detail
3067 that would be needed to create the most accurate estimates for each country, and the input data likely to be available

Formatted: Subscript

Formatted: Subscript

Deleted: concentration

Formatted: Subscript

Formatted: Subscript

Deleted: for the large-scale transport of NO_x

Formatted: Subscript

Formatted: Subscript

Formatted: Subscript

Formatted: Subscript

Deleted: 2:

Formatted: Font: Not Bold

Formatted: Normal, Space After: 0 pt, Line spacing: single

Formatted: Normal, Space After: 0 pt, Line spacing: single

Deleted: ¶

Formatted: Font: Not Italic

Formatted: Line spacing: Multiple 1,08 li, Don't keep with next, Don't keep lines together, Border: Top: (No border), Bottom: (No border), Left: (No border), Right: (No border), Between : (No border)

Deleted: *Under the convention and its Kyoto Protocol, national greenhouse gas (GHG) inventories are the most important source of information to track progress and assess climate protection measures by countries. In order to build mutual trust in the reliability of GHG emission information provided, national GHG inventories are subject to standardized reporting requirements, which have been continuously developed by the Conference of the Parties (COP)²⁴. The calculation methods for the estimation of greenhouse gases in the respective sectors is determined by the methods provided by the 2006 IPCC Guidelines for National Greenhouse Gas Inventories (IPCC, 2006). They provide detailed methodological descriptions to estimate emissions and removals, as well as recommendations to collect the activity data needed. As a general overall requirement, the UNFCCC reporting guidelines stipulate that reporting under the Convention and the Kyoto Protocol must follow the five key principles of transparency, accuracy, completeness, consistency and comparability (TACCC). ¶ The reporting under UNFCCC shall meet the TACCC principles. The three main GHGs are reported in timeseries from 1990 up to two years before the due date of the reporting. The reporting is strictly source category based and is done under the Common Reporting Format tables (CRF), downloadable from the UNFCCC official submission portal: <https://unfccc.int/ghg-inventories-annex-i-parties/2021>.*

Deleted: sector 4

3099 or readily obtainable in most countries" (Volume 1, Chapter 3 of IPCC, 2006). They may, therefore, result in higher
 3100 uncertainties. The EU GHG inventory underlies the assumption that the individual use of national country specific
 3101 methods leads to more accurate GHG estimates than the implementation of a single EU wide approach (UNFCCC,
 3102 2018b). Key categories for the EU27 are 4.A.1 Forest Land: Land Use CO₂, 4.A.2. Forest Land: Land Use CO₂, 4.B.1
 3103 Cropland Land Use CO₂, 4.B.2 Cropland Land Use CO₂, 4.C.1 Grassland Land Use CO₂, 4.C.2 Grassland Land Use
 3104 CO₂, 4.D.1 Wetlands Land Use CO₂, 4.E.2 Settlements Land Use CO₂, and 4.G Harvested Wood Production Wood
 3105 product CO₂. The tiered method a country applies depends on the national circumstances and the individual conditions
 3106 of the land, which explains the variability of uncertainties among the sector itself as well as among EU countries.

Deleted: which are usually more conservative and result in higher uncertainties.

3107 Table A4 shows the mean values of all LULUCF categories for the EU27+UK NGHGI (2021). The
 3108 contribution is calculated as the percentage of the sum of the absolute values of all the categories, in order to account
 3109 for differing signs.

Deleted: 3

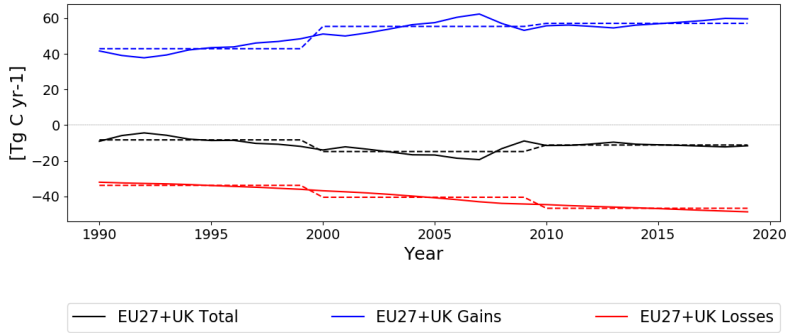
3110
 3111 *Table A4: LULUCF categories for the EU27+UK NGHGI (2021)*

Deleted: 3

Formatted: Caption - VERIFY, Left, Line spacing: single

Category	Mean value for 1990-2020 [Tg C]	Contribution to gross LULUCF flux [%]
Forest land remaining forest land	-107	56.0
Land converted to forest land	-13.0	6.80
Cropland remaining cropland	8.45	4.41
Land converted to cropland	14.0	7.33
Grassland remaining grassland	11.8	6.16
Land converted to grassland	-8.22	4.23
Wetlands remaining wetlands	2.89	1.51
Land converted to wetlands	1.09	0.567
Settlements remaining settlements	1.42	0.744
Land converted to settlements	11.8	6.15
Other land remaining other land	N/A	N/A
Land converted to other land	0.135	0.0706
Harvested wood products	-11.5	5.99

3112
 3113



3118

3119 *Figure A2: The gains, losses, and total HWP pools from the Common Reporting Format tables for the European*
 3120 *Union (Convention), which covers the EU27+UK. Dashed lines show the averages for 1990-1999, 2000-2009, and*
 3121 *2010-2019 for easy comparison with Fig. B4.*

Formatted: Caption - VERIFY, Left, Line spacing: single

Deleted: 3

3122

3123 **Uncertainty:** Methodology for the NGHGI UNFCCC submissions are based on Chapter 3 of 2006 IPCC Guidelines
 3124 for National Greenhouse Gas Inventories and is the same as described in Appendix A2.

Deleted: 1

3125

3126 *ORCHIDEE*

3127

3128 ORCHIDEE is a general ecosystem model designed to be coupled to an atmospheric model in the context of
 3129 modeling the entire Earth system. As such, ORCHIDEE calculates its prognostic variables (i.e., a multitude of **carbon,**
 3130 **water,** and energy fluxes) from the following environmental drivers: air temperature, wind speed, solar radiation, air
 3131 humidity, precipitation and atmospheric CO₂ **mole fraction.** As the run progresses, vegetation grows on each pixel,
 3132 divided into fifteen generic types (e.g., broadleaf temperate forests, C3 crops), which cycle carbon between the soil,
 3133 land surface, and atmosphere, through such processes such as photosynthesis, litter fall, and decay. Limited human
 3134 activities are included through the form of generic wood and crop harvests, which remove aboveground biomass on
 3135 an annual basis. The version reported here, ORCHIDEE-N v3, includes a dynamic nitrogen cycle coupled to the
 3136 vegetation carbon cycle which results in, among other things, limitations on photosynthesis in nitrogen-poor
 3137 environments (Vuichard et al., 2019)

Formatted: Font: Not Italic

Formatted: Line spacing: Multiple 1,08 li, Don't keep with next, Don't keep lines together, Border: Top: (No border), Bottom: (No border), Left: (No border), Right: (No border), Between : (No border)

Deleted: C

Deleted: , H₂O

Deleted: 2 concentration

Formatted: Subscript

3138

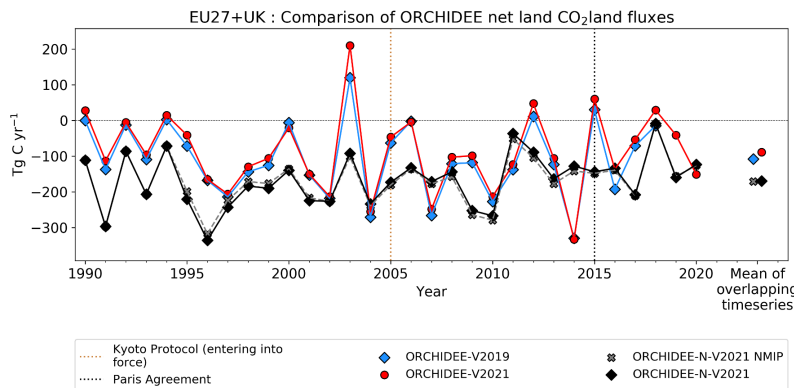
3139 Among other environmental indicators, ORCHIDEE simulates positive and negative CO₂ emissions from
 3140 plant uptake, soil decomposition, and harvests across forests, grasslands, and croplands. Activity data is based on land
 3141 use and land cover maps. For VERIFY, pixel land cover/land use fractions were based on a combination of the land
 use map LUH2v2h and the land cover project of the Climate Change Initiative (CCI) program of the European Space

Deleted: 2

Formatted: Subscript

3148 Agency (ESA). The latter is based on purely remotely sensed methods, while the former makes use of national harvest
 3149 data from the U.N. Food and Agricultural Organization.
 3150 **LUH2v2-ESACCI:** *quoted directly from Lurton et al. (2020):* “We describe here the input data and algorithms used
 3151 to create the land cover maps specific for our CMIP6 simulations using the historical/future reconstruction of land use
 3152 states provided as reference datasets for CMIP6 within the land use harmonization database LUH2v2h (Hurtt et al.,
 3153 2020). More details are provided on the devoted web page <https://orchidas.lscce.ipsl.fr/dev/lccci> which shows further
 3154 tabular, graphical and statistical data. The overall approach relies on the combination of the LUH2v2 data with present-
 3155 day land cover distribution derived from satellite observations for the past decades. The main task consists in allocating
 3156 the land-use types from LUH2v2 in the different PFTs for the historical period and the future scenarios. The **terrestrial**
 3157 **biospheric** vegetation in each grid cell is defined as the PFT distribution derived from the ESA-CCI land cover product
 3158 for the year 2010 to which pasture fraction and crop fraction from LUH2v2 (for the year 2010) have been subtracted
 3159 from grass and crop PFTs. This characterization of the **terrestrial biospheric** vegetation in terms of PFT distribution is
 3160 assumed invariant in time and is used for both the historical period and the different future scenarios”
 3161

- Formatted: French
- Formatted: English (US)
- Formatted: French
- Formatted: Font: (Default) Times New Roman, 10 pt
- Deleted: natural
- Deleted: natural
- Deleted: (Lurton et al., 2020)



3162
 3163 *Figure A3: A comparison of the version of ORCHIDEE used in previous synthesis of Petrescu et al. (2021b)*
 3164 *compared to the same version using the forcing prepared for this work (ORCHIDEE-V2021) and the version with*
 3165 *the coupled C-N cycle from this work (ORCHIDEE-N-V2021). For the current work, both the version shown with*
 3166 *the Europe-specific nitrogen forcing prepared under VERIFY for the years 1995-2018 (ORCHIDEE-N-V2021) and*
 3167 *that using the standard nitrogen forcing from the N₂O Model Intercomparison Project (NMIP; Tian et al., 2018) as*
 3168 *supplied to the TRENDY model intercomparison is shown (ORCHIDEE-N-V2021 NMIP).*

- Formatted: Caption - VERIFY, Left, Line spacing: single, Border: Top: (No border), Bottom: (No border), Left: (No border), Right: (No border), Between : (No border)

3169
 3170 **Uncertainty:** In the ORCHIDEE model, uncertainty arises from three primary sources: parameters, forcing data
 3171 (including spatial and temporal resolution), and model structure. Some researchers argue that the initial state of the
 3172 model (i.e., the values of the various carbon and water pools at the beginning of the production run, following model
 3173 spinup) represents a fourth area. However, the initial state of this version of ORCHIDEE is defined by its equilibrium

3177 state, and therefore a strong function of the parameters, forcing data, and model structure, with the only independent
3178 choice being the target year of the initial state. Out of the three primary areas of uncertainty, the climate forcing data
3179 is dictated by the VERIFY project itself, thus removing that source from explaining observed differences among the
3180 models, although it can still contribute to uncertainty between the ORCHIDEE results and the national inventories.
3181 The land use/land cover maps, another major source of uncertainty for ORCHIDEE carbon fluxes, have also been
3182 harmonized to a large extent between the bottom-up carbon budget models in the project. Parameter uncertainty and
3183 model structure thus represent the two largest sources of potential disagreement between ORCHIDEE and the other
3184 bottom-up carbon budget models. Computational cost prevents a full characterization of uncertainty due to parameter
3185 selection in ORCHIDEE (and dynamic global vegetation models in general), and uncertainties in model structure
3186 require the use of multiple models of the same type but including different physical processes. Such a comparison has
3187 not been done in the context of VERIFY, although the results from the TRENDY suite of models shown in Fig. 5 give
3188 a good indication of this. Figure A3 shows a small influence from the nitrogen forcing, likely because the European
3189 nitrogen forcing is only available from 1995-2018 and ORCHIDEE carries out almost 500 years of simulation prior
3190 to this point. Many major carbon pools (i.e., woody biomass, soil carbon) have built up a large amount of inertia over
3191 that time and are unlikely to undergo dramatic changes for any realistic forcing over the past. A similar conclusion
3192 can be reached from simulations ORCHIDEE-V2019 and ORCHIDEE-V2021 in Fig. A3, which only differ in
3193 meteorological forcing from 1981-2020.

3194

3195 *CABLE-POP*

3196

3197 CABLE-POP (Haverd et al., 2018) is a global terrestrial biosphere model developed around a
3198 core biogeophysics module (Wang & Leuning, 1998) and a biogeochemistry module including cycles of nitrogen and
3199 phosphorus (Wang et al., 2010). Only nitrogen cycling was turned on for the present simulations. The model also
3200 includes modules simulating woody demography (Haverd et al., 2013) as well as land use change and land
3201 management (Haverd et al., 2018). The model distinguishes seven plant functional types which can co-occur in a given
3202 grid cell. CABLE-POP does not simulate (natural) dynamic vegetation and the distribution and cover fraction of PFTs
3203 is only affected by land use change. Forest demography (establishment, age class distribution, mortality) is accounted
3204 for in the simulations, as are natural disturbances and forest management (wood harvest).

3205 For the simulations described here, a baseline land cover map was created from the HILDA+ dataset for the year 1901
3206 and vegetation classes in the dataset were reclassified to correspond to PFTs represented in CABLE-POP. Land use
3207 transitions as well as land management (harvest) were prescribed from the LUH2v2h dataset over the entire simulation
3208 period. Crops and pastures are treated as C3 grasses but are subject to agricultural harvest fluxes as given by LUH2v2h.
3209 The use of HILDA+ data for the land cover distribution and the LUH2v2h for the representation of land cover/land
3210 use change likely introduced additional uncertainties resulting from a potential mismatch between the two data sets.

3211

Deleted: 8

Formatted: Font: Not Italic

Formatted: Left, Space After: 8 pt, Line spacing: Multiple
1,08 li

Formatted: Font: Not Italic

Formatted: Font: Not Italic

Formatted: Font: Not Italic

Formatted: Font: Not Italic

Deleted: ¶

¶ *CO₂ Emissions from inland waters*¶

In this study we did not update these estimates and they are therefore identical to those in Petrescu et al. (2021b). These estimates represent a climatology of average annual CO₂ emissions from rivers, lakes and reservoirs at the spatial resolution of 0.1°. The approach combines CO₂ evasion fluxes from the global river network, as estimated by the empirical model of Lauerwald et al. (2015), with the lakes and reservoirs estimates by Hastie et al. (2019) for the boreal biome and by Raymond et al. (2013) for the lower latitudes. The Lauerwald et al. and Hastie et al. studies follow the same approach and rely on the development of a statistical prediction model for inland water pCO₂ at 0.5° using global, high-resolution geodata. The pCO₂ climatology was then combined with different estimates of the gas transfer velocity *k* to produce the resulting map of CO₂ evasion. The Raymond et al. study only provides mean flux densities at the much coarser spatial resolution of the so-called COSCAT regions. All estimates were then downscaled to 0.1° using the spatial distribution of European inland water bodies. Note that in contrast to Hastie et al. (2019), the areal distribution of lakes was extracted from the HYDROLAKES database (Messenger et al., 2016), to be consistent with the estimates of inland water N₂O and CH₄ presented by Petrescu et al. (2021b).¶
Uncertainty: Monte Carlo simulations were performed to constrain uncertainties resulting from both the pCO₂ prediction equation and the choice of the *k* formulation. ¶

3242 *CBM*

3243

3244 The Carbon Budget Model developed by the Canadian Forest Service (CBM-CFS3), can simulate the
3245 historical and future stand- and landscape-level C dynamics under different scenarios of harvest and natural
3246 disturbances (fires, storms), according to the standards described by the IPCC (Kurz et al., 2009). Since 2009, the
3247 CBM has been tested and validated by the Joint Research Centre of the European Commission (JRC), and adapted to
3248 the European forests. It is currently applied to 26 EU Member States, both at country and NUTS2 level (Pilli et al.,
3249 2016).

3250 Based on the model framework, each stand is described by area, age and land use classes and up to 10
3251 classifiers based on administrative and ecological information and on silvicultural parameters (such as forest
3252 composition and management strategy). A set of yield tables define the merchantable volume production for each
3253 species while species-specific allometric equations convert merchantable volume production into aboveground
3254 biomass at stand-level. At the end of each year the model provides data on the net primary production (NPP), carbon
3255 stocks and fluxes, as the annual C transfers between pools and to the forest product sector.

3256 The model can support policy anticipation, formulation and evaluation under the LULUCF sector, and it is
3257 used to estimate the current and future forest C dynamics, both as a verification tool (i.e., to compare the results with
3258 the estimates provided by other models) and to support the EU legislation on the LULUCF sector (Grassi et al., 2018a).
3259 In the biomass sector, the CBM can be used in combination with other models, to estimate the maximum wood
3260 potential and the forest C dynamic under different assumptions of harvest and land use change (Jonsson et al., 2018).
3261 **Uncertainty:** Quantifying the overall uncertainty of CBM estimates is challenging because of the complexity of each
3262 parameter. The uncertainty in CBM arises from three primary sources: parameters, forcing data (including spatial and
3263 temporal resolution) and model structure. It is linked to both activity data and emission factors (area, biomass volume
3264 implied by species specific equation to convert the merchantable volume to total aboveground biomass (used as a
3265 biomass expansion factor)) as well to the capacity of each model to represent the original values, in this case estimated
3266 through the mean percentage difference between the predicted and observed values. A detailed description of the
3267 uncertainty methodology is found in Pilli et al. (2017).

3268

3269 **Explanatory note on the extrapolation of Net Biome Productivity for the period 2017-2020** (Matteo Vizzarri,
3270 Roberto Pilli, Giacomo Grassi, EC-JRC)

3271 *Background*

3272 We performed a linear extrapolation of forest Net Biome Productivity (NBP) by country (EU 25 Member States and
3273 UK) in the period 2017-2020 based on the correlation between NBP and harvest from the period 2000-2015. Cyprus
3274 and Malta are excluded from the analysis because of missing historical data.

3275 *Input data*

3276 Table A.5 reports a summary of input data sources.

Formatted: Font: Not Italic

Formatted: Line spacing: Multiple 1,08 li, Don't keep with next, Don't keep lines together, Border: Top: (No border), Bottom: (No border), Left: (No border), Right: (No border), Between : (No border)

Deleted: 4

3278 Table A5: main input data used in the extrapolation of NBP for the period 2017-2020.

	Unit	Temporal resolution	Source
Wood removals (HWP pool)	t C	Annual (2000-2015)	CBM calibration run
Forest area	ha	Annual (2000-2020)	FAOSTAT ²⁵
Roundwood amount	m ³	Annual (2000-2020)	FAOSTAT ²⁶
NBP	t C	Annual (2000-2015)	CBM calibration run

Deleted: 4
 Formatted: Caption - VERIFY, Space Before: 0 pt, After: 0 pt, Don't keep with next, Border: Top: (No border), Bottom: (No border), Left: (No border), Right: (No border), Between : (No border)
 Formatted Table

3279
 3280 Assessment procedure

3281 The extrapolation of the NBP for the period 2017-2020 was obtained throughout the following steps:

- 3282 1. For each country (EU 25 Member States + UK), we first calculated the **average conversion factor** –
 3283 representing a correspondence between one ton of biomass carbon removed and one cubic meter of wood per
 3284 hectare – for the period 2000-2015 through equation [1]:

$$CF_{2000-2015} = \sum_{t=2000}^{2015} \frac{HWP_t}{RW_t} \cdot A_{2015} \quad \text{eq. (1)}$$

3285
 3286 where: $CF_{2000-2015}$ is the average conversion factor per hectare in the period 2000-2015 (t C m⁻³ ha⁻¹); HWP_t
 3287 is the carbon content per ha in harvested wood products in year t (t C year⁻¹), as derived from the CBM model run;
 3288 RW is the total roundwood removals in year t (m³ year⁻¹) (source: FAOSTAT²⁷); A_{2015} is the managed forest area in
 3289 year 2015 (ha; source: Forest Europe 2015).

- 3290 2. Using the average conversion factor estimated in eq. 1, we converted, for each country, the total roundwood
 3291 removals per ha derived from FAOSTAT for the period 2017-2020, to the corresponding amount of carbon
 3292 removals per ha, through equation [2]:
 3293

$$HWP_{conv} = CF_{2000-2015} \cdot \left(\frac{RW_t}{A_{2015}} \right) [\forall t = 2017 \div 2020] \quad \text{eq. (2)}$$

3295 where: HWP_{conv} is the amount of carbon removals per hectare in year t (t C ha⁻¹ year⁻¹); $CF_{2000-2015}$ is the
 3296 average conversion factor per hectare in the period 2000-2015 (t C m⁻³ ha⁻¹); RW_t is the total roundwood in year t
 3297 (m³ year⁻¹) (source: FAOSTAT²⁸); A_{2015} is the managed forest area in the year 2015 (ha).

- 3298 3. Then, for each country and the period 2000-2015, we performed a **linear regression** to search for significant
 3299 correlation between the harvest amount (i.e., HWP in t C ha⁻¹ yr⁻¹) and NBP, according to the generalized
 3300 equation:
 3301

$$NBP = a + b \cdot (HWP) \quad \text{eq. (3)}$$

Deleted: →
 Deleted: →
 Deleted: →
 Deleted: →
 Deleted: i.e.
 Formatted: Font colour: Auto
 Formatted: Font: (Default) Times New Roman, 8 pt, Font colour: Auto
 Formatted: Font: (Default) Times New Roman, 8 pt, No underline, Font colour: Auto
 Formatted: Font: (Default) Times New Roman, 8 pt, Font colour: Auto
 Formatted: Font colour: Auto
 Formatted: Font: (Default) Times New Roman, 8 pt, Font colour: Auto
 Formatted: Font: (Default) Times New Roman, 8 pt, No underline, Font colour: Auto
 Formatted: Font: (Default) Times New Roman, 8 pt, Font colour: Auto
 Formatted: Font colour: Auto
 Formatted: Font: 8 pt, Font colour: Auto
 Formatted: Font: 8 pt, No underline, Font colour: Auto
 Formatted: Font: 8 pt, Font colour: Auto
 Formatted: Font colour: Auto
 Formatted: Font: 8 pt, Font colour: Auto
 Formatted: Font: 8 pt, No underline, Font colour: Auto

²⁵ <https://www.fao.org/faostat/en/#data/RI>
²⁶ <https://www.fao.org/faostat/en/#data/FO>
²⁷ <https://www.fao.org/faostat/en/#data/FO>
²⁸ <https://www.fao.org/faostat/en/#data/FO>

3308 In this case, we assumed NBP as the dependent variable (t C ha⁻¹ year⁻¹), the amount of harvest (t C ha⁻¹ year⁻¹) as the main driver affecting the short term evolution of NBP, in absence of other exogenous natural
 3309 disturbances; *a* is the intercept of the linear trendline; *b* is the coefficient of the independent variable harvest
 3310 amount (i.e. HWP) (m³ ha⁻¹ year⁻¹). This approach is consistent with the methodological assumptions reported
 3311 in Jonsson et al. (2021).
 3312

3313 4. We finally calculated the **NBP in the period 2017-2020** for each country through equation [4]:

3314
$$NBP_{t,m} = (a + b \cdot HWP_{conv})_{t,m} \quad \text{eq. (4)}$$

3315 where: *NBP_{t,m}* is the Net Biome Productivity for year *t*, country *m* (t C ha⁻¹ year⁻¹); *a_{t,m}* is the intercept
 3316 of the linear trendline for year *t*, country *m*; *b_{t,m}* is the coefficient of the independent variable in the trendline;
 3317 *HWP_{conv(t,m)}* is the amount of carbon removal per ha for year *t*, country *m* (t C ha⁻¹ year⁻¹).

3318 Forest area and parameters used in equation [4] by country are reported in Table A6.

3319 Table A6: country-based forest area in 2015 and parameters used in equation [4]. *: significant (*p*<0.05); NS: not
 3320 significant (*p*>0.05).

EU 25 + UK	CF (2000-2015)	Intercept (a)	Coefficient (b)	<i>p</i> <0.05
Austria	0.28	2.60	-1.57	*
Belgium	0.18	2.97	-1.54	*
Bulgaria	0.22	1.17	-2.13	*
Croatia	0.28	1.42	-1.27	*
Czechia	0.22	2.55	-1.21	*
Denmark	0.16	1.92	-1.21	*
Estonia	0.20	1.16	-1.08	*
Finland	0.23	1.15	-1.20	*

Deleted: 5

Deleted: 5

Formatted: Caption - VERIFY, Space Before: 0 pt, After: 0 pt, Don't keep with next, Border: Top: (No border), Bottom: (No border), Left: (No border), Right: (No border), Between: (No border)

Formatted Table

EU 25 + UK	CF (2000-2015)	Intercept (a)	Coefficient (b)	p<0.05
France	0.19	1.63	-1.17	*
Germany	0.21	2.55	-1.23	*
Greece	0.20	1.17	-1.75	ns
Hungary	0.27	1.50	-1.54	*
Ireland	0.18	6.12	-5.45	*
Italy	0.23	0.69	0.39	ns
Latvia	0.19	2.00	-1.77	*
Lithuania	0.22	1.11	-0.89	*
Luxembourg	0.20	1.79	-1.40	*
Netherlands	0.22	2.44	-2.01	*
Poland	0.21	2.49	-2.16	*
Portugal	0.29	1.39	-1.01	*
Romania	0.32	1.54	-1.65	*
Slovakia	0.28	2.57	-1.42	*
Slovenia	0.24	2.07	-1.55	*
Spain	0.28	0.26	0.18	ns
Sweden	0.23	1.02	-1.20	*

Formatted Table

EU 25 + UK	CF (2000-2015)	Intercept (a)	Coefficient (b)	p<0.05
United Kingdom	0.19	2.27	-1.34	*

Formatted Table

3323

3324 *Additional notes*

3325 Because of biased estimates, values for the year 2016 were excluded from this analysis.

3326 Extrapolated NBP for Czech Republic, Ireland and Netherlands were negative (thus showing emissions) because of
 3327 an increase of harvest in the corresponding years (2017-2020) compared to the previous period 2000-2015. Estonia
 3328 shows negative extrapolated NBP only for the year 2018.

3329 *EFISCEN-Space*

3330

3331 The European Forest Information SCENario Model (EFISCEN) is a large-scale forest model that projects
 3332 forest resource development on a regional to European scale. The model uses aggregated national forest inventory
 3333 data as a main source of input to describe the current structure and composition of European forest resources. The
 3334 model projects the development of forest resources, based on scenarios for policy, management strategies and climate
 3335 change impacts. With the help of biomass expansion factors, stem wood volume is converted into whole-tree biomass
 3336 and subsequently to whole tree carbon stocks. Information on litter fall rates, felling residues and natural mortality is
 3337 used as input into the soil module YASSO (Liski et al., 2005), which is dynamically linked to EFISCEN and delivers
 3338 information on forest soil carbon stocks. The core of the EFISCEN model was developed by Prof. Ola Sallnäs at the
 3339 Swedish Agricultural University (Sallnäs, 1990). It has been applied to European countries in many studies since then,
 3340 dealing with a diversity of forest resource and policy aspects. A detailed model description is given by Verkerk et al.
 3341 (2016), with online information on availability and documentation of EFISCEN at <http://efiscen.efi.int>. The model
 3342 and its source code are freely available, distributed under the GNU General Public License conditions
 3343 (www.gnu.org/licenses/gpl-3.0.html).

Formatted: Font: Not Italic

Formatted: Line spacing: Multiple 1,08 li, Don't keep with next, Don't keep lines together, Border: Top: (No border), Bottom: (No border), Left: (No border), Right: (No border), Between : (No border)

Formatted: Font: (Default) Times New Roman, 10 pt

Formatted: Font: (Default) Times New Roman, 10 pt

Deleted: (Schelhaas et al., in prep)

3344 In this report the follow-up of the EFISCEN model was used, called EFISCEN-Space. EFISCEN-Space
 3345 simulates the development of the forest at the level of the plots as measured in the national forest inventories, thereby
 3346 providing a much higher spatial detail. The simulation is based on the distribution of trees over diameter classes rather
 3347 than age as in the old EFISCEN model. This allows the simulation of a wider variety of stand structures, species
 3348 mixtures and management options. Similar to the EFISCEN model, biomass expansion factors and the YASSO soil
 3349 carbon model are used to provide carbon balances for the forest. For use within VERIFY, individual plot results are
 3350 aggregated to a 0.125 degree grid. For the moment only 15 European member states are included, partly due to the
 3351 lack of an appropriate national forest inventory in the other member states, or because the data could not be shared.
 3352 No formal sensitivity and uncertainty analysis has been conducted yet.

3354 Figure 3 shows results which vary from year-to-year. In practice, the model was initialized with starting
3355 years depending on the country, assuming that all data applied to this year. The model then produced stock and flux
3356 changes for the subsequent five-year period, reporting a single mean value per pixel. To compute timeseries for the
3357 EU27+UK, it was further assumed that these values were valid across 2005-2020. As the fluxes were given per square
3358 meter of forest, they were scaled by the total area of the forest in each pixel found on the land use/land cover maps
3359 used by the ORCHIDEE DGVM. This explains why the numbers vary from year to year; the flux per square meter of
3360 forest does not change, but the total amount of forest area changes slightly. It should be noted that country-level values
3361 available on the VERIFY website are only available for the five-year period for which the model produces a mean
3362 result.

Deleted: 5

3364 **Uncertainties:** A sensitivity analysis of EFISCEN v3 is described in detail in Chapter 6 of the user manual (Schelhaas
3365 et al., 2007). Total sensitivity is caused by especially young forest growth, width of volume classes, age of felling and
3366 few other variables. Scenario uncertainty comes on top of this when projecting in future. Within VERIFY, a full
3367 uncertainty analysis has been completed, enabling the estimation of uncertainty ranges of the various output variables
3368 (Schelhaas et al., 2020).

Formatted: Font: Not Bold

3370 EPIC-IIASA

3371
3372 The Environmental Policy Integrated Climate (EPIC) model is a field-scale process-based model (Izaurrealde
3373 et al., 2006; Williams, 1990) which calculates, with a daily time step, crop growth and yield, hydrological, nutrient
3374 and carbon cycling, soil temperature and moisture, soil erosion, tillage, and plant environment control. Potential crop
3375 biomass is calculated from photosynthetically active radiation using the radiation-use-efficiency concept modified for
3376 vapor pressure deficit and atmospheric CO₂ mole fraction effect. Potential biomass is adjusted to actual biomass
3377 through daily stress caused by extreme temperatures, water and nutrient deficiency, or inadequate aeration. The
3378 coupled organic C and N module in EPIC (Izaurrealde et al., 2006) distributes organic C and N between three pools of
3379 soil organic matter (active, slow and passive) and two litter compartments (metabolic and structural). EPIC calculates
3380 potential transformations of the five compartments as regulated by soil moisture, temperature, oxygen, tillage and
3381 lignin content. Daily potential transformations are adjusted to actual transformations when the combined N demand
3382 in all receiving compartments exceeds the N supply from the soil. The transformed components are partitioned into
3383 CO₂ (heterotrophic respiration), dissolved C in leaching (DOC) and the receiving SOC pools. EPIC also calculates
3384 SOC loss with erosion.

Formatted: Font: Not Italic

Formatted: Line spacing: Multiple 1,08 li, Don't keep with next, Don't keep lines together, Border: Top: (No border), Bottom: (No border), Left: (No border), Right: (No border), Between : (No border)

3385 The EPIC-IIASA (version EU) modeling platform was built by coupling the field-scale EPIC version 0810
3386 with large-scale data on land cover (cropland and grasslands), soils, topography, field size, crop management practices
3387 and grassland cutting intensity aggregated at a 1x1 km grid covering European countries (Balkovič et al., 2018, 2013).
3388 In VERIFY, a total of 10 major European crops including winter wheat, winter rye, spring barley, grain maize, winter
3389 rapeseed, sunflower, sugar beet, potatoes, soybean and rice were used to represent agricultural production systems in
3390 European cropland. Crop fertilization and irrigation were estimated for NUTS2 statistical regions between 1995 and

Deleted: concentration

3393 2010 (Balkovič et al., 2013). For VERIFY, the simulations were carried out assuming conventional tillage, consisting
3394 of two cultivation operations and moldboard plowing prior to sowing and an offset disking after harvesting of cereals.
3395 Two row cultivations during the growing season were simulated for maize and one ridging operation for potatoes. It
3396 was assumed that 20 % of crop residues are removed in the case of cereals (excluding maize), while no residues are
3397 harvested for other crops.

3398 A total of five managed grassland types with distinct temperature requirements, biomass productivity, and
3399 phenology were used to represent the C-cycle in European grasslands. High-productive generic winter pasture and tall
3400 fescue-based grasslands were used for Atlantic Europe, low fescue grasslands for the cool climates of Nordic regions
3401 and high mountains, high-productive tall fescue-based grasslands and low-productive bluegrass types for continental
3402 Europe, and low-productive bromegrass and high-productive winter pastures in the Mediterranean regions. Annual
3403 nitrogen and carbon inputs, including inorganic and manure fertilization, and atmospheric N deposition, were obtained
3404 from ISIMIP3 (Jägermeyr et al., 2021). In this dataset, the annual manure production and the fraction of manure from
3405 livestock applied to cropland and rangeland were used from Zhang et al. (2017). The original manure data were re-
3406 gridded to half-degree spatial resolution in ISMIP3. In the model, manure is applied as an organic fertilizer with a
3407 C:N ration of 14.5:1. The organic carbon and nitrogen are added to the fresh organic litter pool where they decompose
3408 in a manner identical to the fresh litter from vegetation, while mineral N from manure is added to the soil nitrate and
3409 ammonium pools. The distribution of herbage biomass export intensity was constructed based on (Chang et al., 2016).

3410 **Uncertainty:** In EPIC, uncertainties arise from three primary sources which were described in detail by ORCHIDEE.
3411 A detailed sensitivity and uncertainty analysis of EPIC-IIASA regional carbon modeling is presented in (Balkovič et
3412 al., 2020).

3413

3414 *ECOSSE (grasslands)*

3415

3416 ECOSSE is a biogeochemical model that is based on the carbon model ROTH-C (Jenkinson and Rayner,
3417 1977; Jenkinson et al. 1987; Coleman and Jenkinson, 1996) and the nitrogen-model SUNDIAL (Bradbury et al., 1993;
3418 Smith et al., 1996). All major processes of the carbon and nitrogen dynamics are considered (Smith et al., 2010a,b).
3419 Additionally, in ECOSSE processes of minor relevance for mineral arable soils are implemented as well (e.g., methane
3420 emissions) to have a better representation of processes that are relevant for other soils (e.g., organic soils). ECOSSE
3421 can run in different modes and for different time steps. The two main modes are site specific and limited data. In the
3422 later version, basic assumptions/estimates for parameters can be provided by the model. This increases the uncertainty
3423 but makes ECOSSE a universal tool that can be applied for large scale simulations even if the data availability is
3424 limited. To increase the accuracy in the site-specific version of the model, detailed information about soil properties,
3425 plant input, nutrient application and management can be added as available.

3426 During the decomposition process, material is exchanged between the SOM pools according to first order
3427 rate equations, characterized by a specific rate constant for each pool, and modified according to rate modifiers
3428 dependent on the temperature, moisture, crop cover and pH of the soil. The model includes five pools with one of
3429 them being inert. The N content of the soil follows the decomposition of the SOM, with a stable C:N ratio defined for

Formatted: Font: Not Italic

Formatted: Space After: 8 pt, Line spacing: Multiple 1,08 li

3430 each pool at a given pH, and N being either mineralized or immobilized to maintain that ratio. Nitrogen released from
3431 decomposing SOM as ammonium (NH₄⁺) or added to the soil may be nitrified to nitrate (NO₃⁻).

3432 For spatial simulations the model is implemented in a spatial model platform. This allows to aggregate the
3433 input parameter for the desired resolution. ECOSSE is a one-dimensional model and the model platform provides the
3434 input data in a spatial distribution and aggregates the model outputs for further analysis. While climate data are
3435 interpolated, soil data are represented by the dominant soil type or by the proportional representation of the different
3436 soil types in the spatial simulation unit (this is in VERIFY a grid cell).

3437 **Uncertainty:** In ECOSSE, uncertainty arises from three primary sources: parameters, forcing data (including spatial
3438 and temporal resolution), and model structure. These uncertainties are not yet quantified.

3439

3440 *Bookkeeping models*

3441

3442 We make use of data from two bookkeeping models: **BLUE** (Hansis et al., 2015) and **H&N** (Houghton &
3443 Nassikas, 2017).

3444 The **BLUE** model provides a data-driven estimate of the net land use change fluxes. BLUE stands for
3445 “bookkeeping of land use emissions”. Bookkeeping models (Hansis, 2015; Houghton, 1983) calculate land-use change
3446 CO₂ emissions (sources and sinks) for transitions between various natural vegetation types and agricultural lands. The
3447 bookkeeping approaches keep track of the carbon stored in vegetation, soils, and products before and after the land-
3448 use change. In BLUE, land-use forcing is taken from the Land Use Harmonization, LUH2, for estimates within the
3449 annual global carbon budget. The model provides data at annual time steps and 0.25 degree resolution. Temporal
3450 evolution of carbon gain or loss, i.e., how fast carbon pools ~~respire~~ or regrow following a land-use change, is based
3451 on response curves derived from literature. The response curves describe ~~gradual respiration~~ of vegetation and soil
3452 carbon, including transfer to product pools of different lifetimes, as well as carbon uptake due to regrowth of
3453 vegetation and subsequent refilling of soil carbon pools. In this report we present two versions of BLUE:
3454 BLUEvVERIFY and BLUEvGCP. The BLUEvVERIFY version is a set of runs made for VERIFY, using the Hilda²⁹
3455 product (Ganzenmüller et al., 2022).

3456 The **H&N** model (Houghton et al., 1983) calculates land-use change CO₂ emissions and uptake fluxes for
3457 transitions between various natural vegetation types and agricultural lands (croplands and pastures). The original
3458 bookkeeping approach of Houghton (2003) keeps track of the carbon stored in vegetation and soils before and after
3459 the land-use change. Carbon gain or loss is based on response curves derived from literature. The response curves
3460 describe ~~gradual respiration~~ of vegetation and soil carbon, including transfer to product pools of different life-times,
3461 as well as carbon uptake due to regrowth of vegetation and consequent re-filling of soil carbon pools. Natural
3462 vegetation can generally be distinguished into primary and secondary land. For forests, a primary forest that is cleared
3463 can never return back to its original carbon density. Instead, long-term degradation of primary forest is assumed and
3464 represented by lowered standing vegetation and soil carbon stocks in the secondary forests. Apart from land use

Formatted: Font: Not Italic

Formatted: Line spacing: Multiple 1,08 li, Don't keep with next, Don't keep lines together, Border: Top: (No border), Bottom: (No border), Left: (No border), Right: (No border), Between : (No border)

Deleted: decay

Deleted: decay

Deleted: decay

²⁹<https://landchangestories.org/hildaplus/>

3468 transitions between different types of vegetation cover, forest management practices in the form of wood harvest
3469 volumes are included. Different from dynamic global vegetation models, bookkeeping models ignore changes in
3470 environmental conditions (climate, atmospheric CO₂, nitrogen deposition and other environmental factors). Carbon
3471 densities at a given point in time are only influenced by the land use history, but not by the preceding changes in the
3472 environmental state. Carbon densities are taken from observations in the literature and thus reflect environmental
3473 conditions of the last decades. In this study an updated H&N version submitted to the GCP2021 is used.

3474 **Uncertainty:** Uncertainties can be captured through simulations varying uncertain parameters, input data, or process
3475 representation. A large contribution of uncertainty can be expected from various input datasets. Apparent uncertainties
3476 arise from the land-use forcing data (Gasser et al., 2020; Hartung et al., 2021; Ganzenmüller et al., 2022), the
3477 equilibrium carbon densities of soil and vegetation and allocation of material upon a land-use transition (Bastos et al.,
3478 2021), and the response curves built to reflect carbon pool decay and regrowth after land-use transitions. Furthermore,
3479 studies have shown that different accounting schemes (Hansis et al., 2015) and initialization settings at the start of the
3480 simulations (Hartung et al., 2021) lead to different emission estimates even decades later.

3481

3482 *FAOSTAT*

3483

3484 FAOSTAT: Statistics Division of the Food and Agricultural Organization of the United Nations provides
3485 updates for the LULUCF CO₂ emissions for the period 1990-2019, available at:
3486 <https://www.fao.org/faostat/en/#data/GT> and its sub-domains. The FAOSTAT emissions land use database is
3487 computed following a Tier 1 approach of IPCC (2006). Geospatial data are the source of AD for the estimates of
3488 emissions from cultivation of organic soils, biomass and peat fires. GHG emissions are provided by countries, regions
3489 and special groups, with global coverage, relative to the period 1990-present (with annual updates). Land Use Total
3490 contains all GHG emissions and removals produced in the different Land Use sub-domains, representing four IPCC
3491 Land Use categories, of which three land use categories: forest land, cropland, grassland and biomass burning.
3492 LULUCF emissions consist of CO₂ associated with land use and change, including management activities. CO₂
3493 emissions/removals are computed at Tier 3 using carbon stock change. To this end, FAOSTAT uses Forest area and
3494 carbon stock data from FRA (2015), gap-filled and interpolated to generate annual time-series. As a result CO₂
3495 emissions/removals are computed for forest land and net forest conversion, representing respectively IPCC categories
3496 “Forest land” and “Forest land converted to other land uses”. CO₂ emissions are provided as by country, regions and
3497 special groups, with global coverage, relative to the period 1990-most recent available year (with annual updates),
3498 expressed as net emissions/removals as Gg CO₂, by underlying land use emission sub-domain and by aggregate (land
3499 use total).

3500 **Uncertainty:** FAOSTAT uncertainties are not available.

3501

3502 *TRENDY DGVMs*

3503

Formatted: Font: Not Italic

Formatted: Line spacing: Multiple 1,08 li, Don't keep with next, Don't keep lines together, Border: Top: (No border), Bottom: (No border), Left: (No border), Right: (No border), Between : (No border)

Formatted: Font: (Default) Times New Roman, 10 pt

Formatted: Font: Not Italic

Formatted: Line spacing: Multiple 1,08 li, Don't keep with next, Don't keep lines together, Border: Top: (No border), Bottom: (No border), Left: (No border), Right: (No border), Between : (No border)

3504 The TRENDY (Trends in net land-atmosphere carbon exchange over the period 1980-2010) project
3505 represents a consortium of dynamic global vegetation models (DGVMs) following identical simulation protocols to
3506 investigate spatial trends in carbon fluxes across the globe over the past century. As DGVMs, the models require
3507 climate, carbon dioxide, and land use change input data to produce results. In TRENDY, all three of these are
3508 harmonized to make the results across the whole suite of models more comparable. In the case of VERIFY, 15 of the
3509 16 models for TRENDY v10 (except for ISAM, *which after visual inspection showed several outlier years*) were used.
3510 While describing the details of all the models used here is clearly not possible, DGVMs calculate prognostic variables
3511 (i.e., a multitude of *carbon, water, and energy fluxes*) from the following environmental drivers: air temperature, wind
3512 speed, solar radiation, air humidity, precipitation and atmospheric CO₂ *mole fraction*. As the run progresses, vegetation
3513 grows on each pixel, divided into generic types which depend on the model (e.g., broadleaf temperate forests, C3
3514 crops), which cycle carbon between the soil, land surface, and atmosphere, through such processes such as
3515 photosynthesis, litter fall, and decay. Limited human activities are included depending on the model, typically
3516 removing aboveground biomass on an annual basis.

3517 Among other environmental indicators, DGVMs simulate positive and negative CO₂ emissions from plant
3518 uptake, soil decomposition, and harvests across forests, grasslands, and croplands. Activity data is based on land use
3519 and land cover maps and generally follows Approach 1 as described by the IPCC 2006 guidelines (enabling calculation
3520 of only net changes from year to year). For TRENDY, pixel land cover/land use fractions were based on the land use
3521 map LUH2 (Hurtt et al., 2020) and the HYDE land-use change data set (Klein Goldewijk et al., 2017a, b). Both of
3522 these maps rely on FAO statistics on agricultural land area and national harvest data.

3523 **Uncertainty:** In TRENDY v10 uncertainties are model specific and described by Friedlingstein et al. (2022). The
3524 spread of the 15 TRENDY models used by this study (Fig. 5) gives an idea of the uncertainty due to model structure
3525 in dynamic global vegetation models, as the forcing data was harmonized for all models.

3526

3527 *Net emissions from lateral transport of carbon (crops, wood, and inland waters)*

3528

3529 *Net carbon flux due to lateral transport includes both carbon imported into a country/pixel and respired and carbon*
3530 *assimilated in a country/pixel and then transported to a different country/pixel before respiration.*

3531

3532 Production and consumption of carbon do not always occur on the same grid points. This is particularly relevant for
3533 the land surface in the case of crops, wood products, and carbon transfers through the inland water network. The
3534 purpose of the work here is primarily to convert the flux changes of the top-down inversions into NGHGI-like stock
3535 changes. To convert the flux changes of the inversions (where a positive number represents a flux to the atmosphere,
3536 i.e., a source) into NGHGI-like stock changes, one needs to add the crop sink and remove the crop source. The crop
3537 sink comes from production numbers in the FAO food balance sheets, while the source is estimated by production
3538 plus import minus export (all from the FAO food balance sheets), and both terms make use of conversion factors for
3539 each commodity. We take the forestry balance sheets of FAO (production, import and export per commodity), and
3540 convert to C mass. For a given year, the fraction of this mass that is released later in the atmosphere in each country

Deleted: C

Deleted: H₂O

Deleted: concentration

Deleted: 8

Deleted: E

Formatted: Heading 4, Left, Line spacing: single

Formatted: Normal paragraph, Left, Line spacing: single

3546 is modeled with an e-folding decrease driven by experimental data per country (Mason Earles et al., 2012). Lateral
3547 transfers of carbon through inland waters also need to be removed from the inversion results as the terrestrial
3548 biospheric CO₂ uptake leached into the inland water network represents a carbon sink, while the fraction that is
3549 subsequently re-emitted as CO₂ before reaching the ocean is a carbon source. The inland water CO₂ outgassing
3550 originates from carbon imported with runoff as dissolved CO₂ or produced in-situ from the decomposition of terrestrial
3551 carbon inputs. Note further that a fraction of the net-uptake of atmospheric CO₂ over the continents does not
3552 accumulate on land, but is instead exported through the inland water network to the oceans; this fraction is included
3553 in the calculation. For regional carbon budgets, any river carbon export outside the boundaries of the region of interest
3554 (in this case, EU27+UK) needs to be known to separate net uptake of atmospheric C from the actual land C sink.

3555 Carbon fluxes to the atmosphere from rivers and lakes were obtained from maps described in Zscheischler
3556 et al. (2017). These methods are similar to those described previously in Petrescu et al. (2021b). The primary difference
3557 is that the updated estimates include smaller lakes and reservoirs not represented in the Global Lakes and Wetland
3558 Database through the use of a scaling law, in addition to the older results being created specifically for Europe, while
3559 the newer results are part of a global product. The emissions from the previous work totaled 25.5 Tg C yr⁻¹ for the
3560 EU27+UK, while those used here are 19.8 Tg C yr⁻¹ (with no variability from year-to-year). This difference is
3561 therefore small compared to the river C export, which is included this year for the first time and averages -73.8 Tg
3562 for the period 1990-2020.

3563 One important difference between the fluvial carbon exports reported here and those from a previous work
3564 (Ciais et al., 2021) are that those reported here are rescaled to reasonable global flux reflecting bias in inter-
3565 hemispheric exchange. Similar to Bastos et al. (2020), the dissolved organic carbon (DOC) and particulate organic
3566 carbon (POC) exports were rescaled per basin to match the estimates of Resplandy et al. (2018). The global total
3567 organic C was finally rescaled to 500 Tg C/yr, which is considered a reasonable global number based on different
3568 reviews and synthesis efforts (Regnier et al., 2013).

3569
3570

3571 A4.2. Top-down CO₂ emissions estimates

3572

3573 For the regional inversions, atmospheric observations of CO₂ were taken from multiple sources. For
3574 CarboScopeRegional, atmospheric observations were taken from the ICOS 2021.1 ATC (ICOS RI, 2021) and the
3575 GlobalViewPlus 6.1 product (Schuldt et al., 2021a). For the CIF-CHIMERE inversions, atmospheric observations of
3576 CO₂ for the period 2005-2020 were taken from the ICOS 2021.1 ATC (ICOS RI, 2021) and SNO SIFA L2 (SNO-
3577 IFA, 2023) releases, along with data distributed through the GlobalViewPlus 6.1 product (Schuldt et al., 2021a). For
3578 LUMIA inversions, atmospheric observations of CO₂ for the period 2006-2018 were taken from the dataset prepared
3579 for the 2018 drought task force initiative (Thompson et al., 2020). For the more recent years, data were used from the
3580 ICOS 2021.1 ATC release (ICOS RI, 2021), along with data distributed through the GlobalViewPlus 7.0 product
3581 (Schuldt et al., 2021b), and, for four sites, data distributed through the World Data Center for Greenhouse Gases.
3582

Formatted: Subscript

Formatted: Subscript

Formatted: Subscript

Formatted: Normal, Space After: 0 pt, Line spacing: single

Formatted: Font: (Default) Times New Roman

Formatted: Font: (Default) Times New Roman, Subscript

Formatted: Font: (Default) Times New Roman

Formatted: Normal paragraph

Formatted: Font: (Default) Times New Roman

Formatted: Font: (Default) Times New Roman, Subscript

Formatted: Font: (Default) Times New Roman

Formatted: Font: (Default) Times New Roman

Formatted: Font: (Default) Times New Roman

Formatted: Font: (Default) Times New Roman

Formatted: Subscript

Formatted: Font: (Default) Times New Roman

Formatted: Font: (Default) Calibri, Not Bold, Not Italic,
Font colour: Auto

Formatted: Normal, Space After: 0 pt, Line spacing: single

3583 *CarboScope-Regional*

3584

3585 CarboScopeRegional (CSR) (Munassar et al., 2022): CSR is a Bayesian Framework inversion system that employs a-
3586 priori knowledge of the surface-atmosphere carbon fluxes to regularize the solution of the ill-posed inverse problem
3587 arising from the sparseness of observations sampled over limited geographical locations throughout the domain of
3588 interest. Due to the heterogeneity of biogenic fluxes, the convention in CSR is to optimize Net Ecosystem Exchange
3589 (NEE) against measurements of CO₂ dry model fraction at 3-hourly temporal and 0.5° horizontal resolutions, while
3590 ocean fluxes and anthropogenic emissions are prescribed given their better knowledge available compared with NEE.
3591 The prior flux uncertainty is assumed to have a uniform shape in space and time and its spatial correlation is fitted to
3592 a hyperbolic decay function following the assumption of Kountouris et al. (2018a, b). Model-data mismatch
3593 uncertainty is defined weekly in the measurement covariance matrix varying over sites from 0.5 to 4 (ppm) according
3594 to the ability for atmospheric transport models to sample the true mole fraction at such locations (Rödenbeck, 2005).
3595 This uncertainty implicitly encompasses the combinations of atmospheric transport, representation, and measurement
3596 errors and is assumed to be independent at different locations. To separate the lateral influences originating from
3597 outside of the regional domain, the two-step scheme inversion (Rödenbeck et al., 2009) is applied to run a global
3598 inversion with the Eulerian model TM3 at coarse resolutions to provide the lateral boundary conditions to the regional
3599 inversion. In the regional inversion runs, the Lagrangian model STILT (Lin et al., 2003), forced by IFS data from
3600 ECMWF, is used to calculate the surface sensitivities “footprints” over the regional site network (receptors) at hourly
3601 temporal and 0.25° spatial resolutions. Typically, the prior fluxes of CO₂ are obtained from bottom-up model
3602 estimations. Thus, the diagnostic biosphere model VPRM calculates the biogenic fluxes at hourly temporal resolution
3603 preserving the diurnal cycle. Ocean fluxes are obtained from the CarboScope ocean-based fluxes developed in-house
3604 by Rödenbeck et al. (2014). Emissions of fossil fuel are taken from EDGAR_v4.3 inventories updated every year
3605 based on the British Petroleum statistics (BP), and are distributed in space and time using the COFFEE approach
3606 (Steinbach et al., 2011) according to fuel-type and sector.

3607 The v2021 CSR inversions underwent updates in comparison with the previous v2019:

- 3608 • v2019 from Petrescu et al. (2021b) excluded observations from two sites: La Muela (LMU) in Spain because
3609 of inconsistent datasets between releases, and Finokalia (FKL) in Greece due to errors in the dataset. These
3610 exclusions resulted in a larger C sink from 2013 onwards (Fig. 5, lower plot). FKL observations start at this
3611 time and are the dominant impact over south-east Europe, as it is the only site located there. In v2021
3612 inversions, we included corrected datasets from the FKL site.
- 3613 • Two new flask sites were included in the v2021 inversions: Shetland Islands in the UK and Centro
3614 Investigacion Baja in Spain. These sites are also used in the CarboScope global inversion that provides the
3615 far-field contributions to the EU domain.

3616

Formatted: Font: Not Italic

Formatted: Line spacing: Multiple 1,08 li, Don't keep with next, Don't keep lines together, Border: Top: (No border), Bottom: (No border), Left: (No border), Right: (No border), Between : (No border)

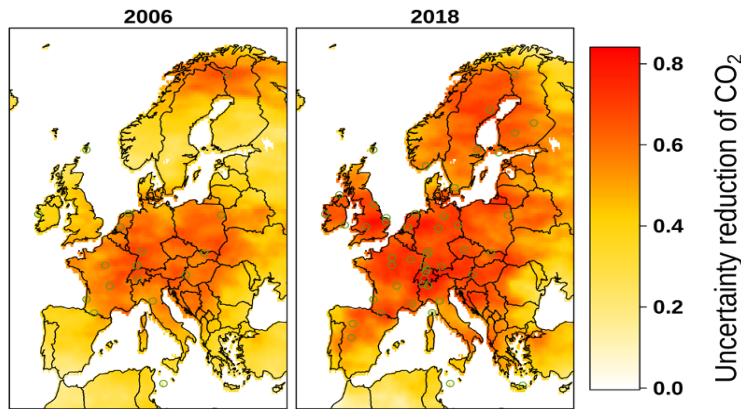
Formatted: Font: Not Bold

Deleted: concentration

Deleted: 9, upper plot

3619 **Uncertainty:** Uncertainties from top-down (TD) estimates can be reported as posterior Bayesian uncertainties.
3620 Following the methodology of Chevallier et al. (2007) the CSR inversion system computed maps of uncertainty
3621 reductions for 2006 and 2018 (Fig. A4). The reduction is carried out through an ensemble of 40 members of inversions
3622 using error realizations following a Monte Carlo (MC) approach. Circles on maps refer to locations of stations. In the
3623 inversion system, a MC method is used to generate N ensembles of realizations of prior errors and model-data
3624 mismatch errors. The inversion is repeated for each ensemble member starting from each set of prior and model-data
3625 mismatch errors to generate posterior fluxes. The posterior uncertainty is calculated as the spread over the optimized
3626 fluxes across the whole ensemble. The uncertainty reduction is then calculated as $1 - (\sigma_{\text{post}} / \sigma_{\text{prior}})$. It is clear that
3627 larger ensembles will lead to better convergence of the error reduction. However, due to computational limitations, 40
3628 ensemble members were selected as a good compromise.

3629



3630

3631 *Figure A4: CSR uncertainty reduction maps computed as $1 - (\sigma_{\text{post}} / \sigma_{\text{prior}})$ for 2006 and 2018 using a Monte Carlo*
3632 *approach focused on prior errors. The circles represent the observation stations network.*

Formatted: Caption - VERIFY, Line spacing: single

3633 Figure A4 represents a preliminary attempt at how the inclusion of additional observation stations (additional
3634 circles in the right-side figure for Germany, Switzerland, Finland compared to the left-side figure) might reduce the
3635 uncertainty. However, the two different simulation years (2006 and 2018) might also differ in terms of other factors
3636 which may lead to lower uncertainties in a given year (e.g., climatological conditions, such as the 2018 drought year).

3637 Several caveats remain. When comparing the uncertainty over pixels or subregions in the domain of interest,
3638 the maps of uncertainty reduction should be interpreted together with the maps of posterior uncertainty to give a better
3639 illustration of the magnitude of uncertainty. The maps of uncertainty reduction reflect only the random uncertainties.
3640 The systematic uncertainties are still poorly characterized, including uncertainties due to atmospheric transport
3641 modeling, dependence on the prior fluxes, and the weighting between the prior and observation uncertainties. To
3642 improve knowledge of the systematic uncertainties, dedicated studies with controlled comparisons between inversions
3643 using different atmospheric transport models (such as planned with the Community Inversion Framework, Berchet et

3644 al., 2021) are still needed. Furthermore, the posterior uncertainty and uncertainty reductions between inversions
3645 depend on internal parameterizations, e.g., the weighting of prior and observation uncertainties. Future efforts should
3646 focus on establishing best practices on how to set-up inversions and quantification of systematic uncertainties,
3647 including as well tests of the fidelity of models against data (Simmonds et al., 2021).

3648
3649

3650 *LUMIA*

3651 ▲

3652 The LUMIA inversion system (Monteil and Scholze, 2021) is a regional atmospheric inversion system, which
3653 was designed to produce estimates of the land-atmosphere carbon exchanges based on in-situ CO₂ observations from
3654 the ICOS network. It relies on the FLEXPART 10.4 Lagrangian transport model (Pisso et al., 2019) to compute the
3655 transport of CO₂ fluxes within a regional domain (15°W; 33°N to 35°E, 73°N) at a 0.5°, 3-hourly resolution. Boundary
3656 conditions are provided in the form of timeseries of far-field contributions at the observation sites, obtained from a
3657 global TM5-4DVAR inversion (using the 2-step inversion approach of Rödenbeck et al., 2009). Both transport models
3658 were driven by ECMWF ERA-Interim data, up to 2018, and by ECMWF ERA5 data afterwards.

3659 The inversions solve for weekly offsets to the prior NEE/NBP estimate, at a variable spatial resolution,
3660 highest where the observational coverage is better (up to 0.5° upwind of the observation sites). The optimal solution
3661 is searched for using a variational inversion approach (preconditioned conjugate gradient). The inversions were
3662 constrained by in-situ and flask observations from 66 European observation sites, although only a subset of these sites
3663 is usually available at a given time. The observation uncertainties were set to 1 ppm/week at all sites (the uncertainty
3664 of a single observation is therefore higher, on average 5.2 ppm, and given by \sqrt{n} , with n the number of assimilated
3665 observations at the same site in a ± 3.5 day window around the observation time). The prior NEE was produced using
3666 the LPJ-GUESS model (Smith et al., 2014), driven by ECMWF ERA5 meteorological data.

3667 The inversion also accounts for (prescribed) anthropogenic CO₂ fluxes from the EDGAR/TNO product
3668 (<https://doi.org/10.18160/Y9QV-S113>) and for atmosphere-ocean CO₂ exchanges from the Jena-CarboScope
3669 oc_v2021 product (https://www.bgc-jena.mpg.de/CarboScope/oc/oc_v2021.html). The uncertainties on the prior NEE
3670 were set proportional to the sum of the absolute value of the 3-hourly fluxes in each 7-day optimization interval (so
3671 the uncertainty is not zero even if the net flux is zero), and scaled to a total value of 0.45 PgC/year, accounting for
3672 covariances based on Gaussian (spatial) and exponential (temporal) correlation decay functions, with correlation
3673 lengths of respectively 500 km and 1 month (see Monteil and Scholze, 2021, for details) ▼

3674 The main differences from the LUMIA setup used in Thompson et al. (2014) are the specification of prior
3675 and observation uncertainties (here made, on purpose, more comparable to those used in the CSR inversions), and the
3676 implementation of flux optimization at a variable spatial resolution (which has negligible impact on the results but
3677 improves the model performance).

3678

3679 *CIF-CHIMERE - land CO₂*

3680 ▲

Formatted: Font: Not Italic

Formatted: Line spacing: Multiple 1,08 li, Don't keep with next, Don't keep lines together, Border: Top: (No border), Bottom: (No border), Left: (No border), Right: (No border), Between : (No border)

Formatted: No underline

Deleted: [https://www.bgc-jena.mpg.de/CarboScope/oc/oc_v2021.html...](https://www.bgc-jena.mpg.de/CarboScope/oc/oc_v2021.html)

Formatted: No underline

Deleted: ¶

Formatted: Space Before: 0 pt, After: 0 pt

Formatted: Font: Not Italic

Formatted: Line spacing: Multiple 1,08 li, Don't keep with next, Don't keep lines together

3684 CIF-CHIMERE is used for both CO₂ land and CO₂ fossil emission estimates, and this section only describes
3685 the CO₂ land estimates.

3686 The CIF-CHIMERE inversions have been generated with the variational mode of the Community Inversion
3687 Framework (CIF, Berchet et al., 2021) coupled to the regional Eulerian atmospheric chemistry-transport model
3688 CHIMERE (Menut et al., 2013; Mailler et al., 2017) and to its adjoint code. They are set-up in a manner that is close
3689 to that of the PYVAR-CHIMERE inversions of Broquet et al. (2013), of Thompson et al. (2020) and of Monteil et al.
3690 (2020).

3691 A European configuration of CHIMERE is used; this configuration covers latitudes 31.75-73.25 °N and
3692 longitudes 15.25 °W -34.75 °E with a 0.5 ° × 0.5 ° horizontal resolution and 17 vertical layers up to 200 hPa.
3693 Meteorological forcing for CHIMERE is generated using the European Center for Medium Range Weather
3694 Forecasting (ECMWF) operational forecasts. Initial, lateral and top boundary conditions for CO₂ mole fractions are
3695 generated from the new CAMS global CO₂ inversions v20r2 (Chevallier et al., 2010).

Deleted: concentration

3696 The inversion assimilates in situ CO₂ data from continuous measurements stations compiled in the VERIFY
3697 Deliverable D3.12 and in the Table A1 from the VERIFY CIF Inversion Protocol (Thompson et al., 2021). More
3698 specifically, the inversion assimilates 1-hour averages of the measured CO₂ mole fractions during the time window
3699 12:00-18:00 UTC for low altitude stations (below 1000 masl) and 0:00-6:00 UTC for high altitude stations (above
3700 1000 masl). The inversion optimizes 6-hourly mean NEE and ocean fluxes at the 0.5°×0.5° resolution of CHIMERE.
3701 The anthropogenic CO₂ emissions, considered as perfect and consequently not optimized in the inversions, are based
3702 on the spatial distribution of the EDGAR-v4.2 inventory, on national and annual budgets from the BP (British
3703 Petroleum) Statistics and on temporal profiles at hourly resolution derived with the COFFEE approach (Steinbach et
3704 al., 2011).

3705 The prior estimate of NEE and its uncertainty covariance matrix are specified using ORCHIDEE model
3706 simulations of NEE and respiration, respectively, following the general approach of Broquet et al. (2011). The
3707 temporal and spatial correlation scales for the prior uncertainty in NEE are set to ~1 month and 200 km (following the
3708 diagnostics of Kountouris et al., 2015), with no correlation between the four 6-hour windows of the same day. The
3709 ocean prior fluxes come from a hybrid product of the University of Bergen coastal ocean flux estimate and the
3710 Rödenbeck global ocean estimate (Rodenbeck et al., 2014). Fluxes from biomass burning are ignored. The observation
3711 error covariance matrix is set-up to be diagonal, ignoring the correlations between errors for different hourly averages
3712 of the CO₂ measurements (which has been justified by the analysis of Broquet et al., 2011). The variances for hourly
3713 data are based on the values from Broquet et al. (2013), which vary depending on the sites and season, and which are
3714 derived from Radon model-data comparisons.

3715 About 12 iterations are needed to reduce the norm of the gradient of J by 95 %, using the M1QN3 limited
3716 memory quasi-Newton minimisation algorithm (Gilbert et Lemaréchal, 1989). To cover the whole analysis period
3717 (2005-2020), a series of 7-month (including an overlapping of 15 days between consecutive periods) inversions is
3718 performed. Posterior estimates of NEE at 1-hourly and 0.5°×0.5° spatial resolution are generated for the full period of
3719 analysis.

3720

3722 **Uncertainty:** Estimates of the uncertainty of regional inversions over Europe can be found by comparing against the
3723 results of the other regional inversions in this work (the ensembles of EUROCOM, CarboScopeRegional, and
3724 LUMIA).

3726 *GCP 2021*

3727 ▲
3728 Top-down estimates of land biosphere fluxes are provided by a number of different inverse modeling systems
3729 that use atmospheric mole fraction data as input, as well as prior information on fossil emissions, ocean fluxes, and
3730 land biosphere fluxes. The land biosphere fluxes, and in some systems the ocean fluxes, are estimated using a statistical
3731 optimization involving atmospheric transport models. The inversion systems differ in the transport models used,
3732 optimization methods, spatiotemporal resolution, boundary conditions, and prior error structure (spatial and temporal
3733 correlation scales), thus using ensembles of such systems is expected to result in more robust top-down estimates.

3734 For this study, the global inversion results are taken from all six of the models reported in the GCP 2021:
3735 CTE (CarbonTracker Europe), CAMS (Copernicus Atmosphere Monitoring Service), CMS-Flux, JENA, NIES-
3736 NIWA, and UoE, with spatial resolutions ranging from 1°x1° for certain regions to 4°x5°. For details see Friedlingstein
3737 et al. (2022), in particular Table A4. Atmospheric observations for most model systems are taken from Cox et al.
3738 (2021) and Di Sarra et al. (2021). Note that one of the ensemble members (CMS-Flux) only covers the period 2010-
3739 2020, and therefore the ensemble results are only shown from 2010 until the last year common between all models
3740 (2018).

3742 *EUROCOM*

3743 ▲
3744 Top-down estimates at regional scales (up to 0.25°x0.25° resolution) for the period 2009 – 2018 are taken from
3745 three models used within EUROCOM (Monteil et al., 2020; Thompson et al., 2020): LUMIA, PYVAR, and CSR.
3746 The NAME model was excluded as visual inspection of monthly values identified it as a clear outlier. FLEXINVERT
3747 was excluded after visual inspection of annual values identified it as a clear outlier (Fig. A5). These inversions make
3748 use of more than 30 atmospheric observing stations within Europe, including flask data and continuous observations.
3749 The CarboScope-Regional (CSR) inversion system results were re-run for VERIFY using the extended period 2009-
3750 2020 using four different settings: three network configurations using 15, 40, or 46 sites, and one using all 46 sites but
3751 a factor two larger prior error correlation length scale (200 instead of 100 km). The CSR results reported to
3752 EUROCOM were not used, being instead replaced by the mean of the four updated CSR runs. The observational
3753 dataset used for the EUROCOM drought ensemble is accessible on the ICOS Carbon Portal (Drought 2018 Team and
3754 ICOS Atmosphere Thematic Centre, 2020).

Formatted: Font: Not Italic

Formatted: Left, Space After: 8 pt, Line spacing: Multiple
1,08 li

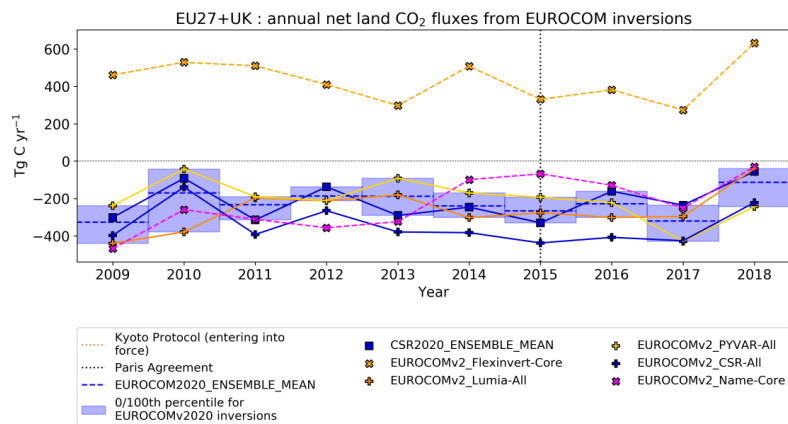
Deleted: concentration

Formatted: Font: 11 pt

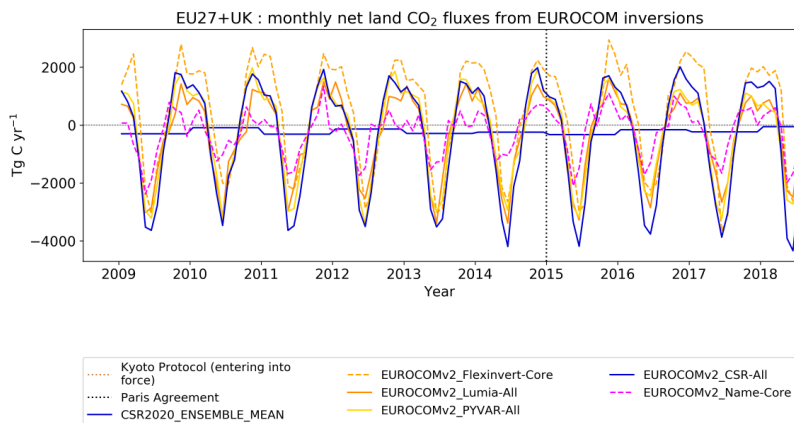
Formatted: Left, Space After: 8 pt, Line spacing: Multiple
1,08 li

Formatted: Normal paragraph, Left, Indent: First line: 0 cm,
Line spacing: single

Formatted: Font: Times New Roman, 10 pt



VERIFY Project



VERIFY Project

3756

3757 *Figure A5: Annual (top) and monthly (bottom) timeseries for inversions in EUROCOM (Monteil et al., 2020).*
 3758 *Inversions with solid lines were retained for the ensemble used in this work (shown in blue in the top figure for*
 3759 *clarity). Note that the CSR values from EUROCOM have been replaced by the mean of four CSR simulations*
 3760 *submitted under the VERIFY project (Appendix A1). Negative fluxes represent a sink into the land surface.*

3761

3762

3763

Formatted: Caption - VERIFY, Left, Line spacing: single

3764

3765 **A5. Input data**

3766

3767 **CRUERA**

3768

3769 The ERA5-Land (Muñoz-Sabater, 2019; 2021) dataset at 0.1-degree resolution over the global land surface
 3770 at hourly resolution was aggregated to three-hourly resolution and extracted for a 0.125 degree grid over Europe
 3771 (35N:73N, 25W:45E) to match the grid used in previous efforts within the VERIFY project. The variables extracted
 3772 are: air temperatures, wind components, surface pressure, downwelling longwave radiation, downwelling shortwave
 3773 radiation, snowfall, and total precipitation. From these, additional variables were calculated: total windspeed, specific
 3774 humidity, relative humidity, and rainfall. Of these, the air temperature, downwelling shortwave radiation, specific
 3775 humidity, and total precipitation were re-aligned with the CRU observation dataset (Harris et al., 2020) from 1901–
 3776 2020 so that monthly means at 0.5 degree pixels correspond exactly. Variation from observations is therefore present
 3777 only on sub-monthly temporal scales and sub-0.5 degree spatial scales. At the time of the model intercomparison,
 3778 ERA5-Land was only available from 1981-2020. Consequently, the years 1901-1980 were taken from the UERRA
 3779 HARMONIE-V1 dataset from ECMWF re-aligned with CRU observations under the VERIFY project and used in
 3780 Petrescu et al. (2021b). For both datasets, results were aggregated to daily and monthly temporal resolution for use
 3781 as needed in some models.

3782

3783 **HILDA+**

3784

3785 The full Hilda+ dataset is described in detail elsewhere (Winkler et al., 2020; Winkler et al., 2021). Hilda+
 3786 is available at 1x1km spatial and annual temporal resolution across the whole globe from 1960-2019 for six land use
 3787 classes (urban, cropland, pasture/rangeland, forest, unmanaged grass/shrubland, and sparse/no vegetation). The
 3788 algorithm uses earth observation data and land use statistics to generate annual land use/cover maps and transitions.
 3789 Probability maps for land use change categories are generated by using multiple earth-observation-based data
 3790 estimates of the extent of a given land cover category on a given pixel. The VERIFY project requires additional work
 3791 to satisfy the needs of the various modeling groups. For example, the maps were extended back to 1900 to meet the
 3792 needs of the DGVM groups. As observational data is lacking for the years pre-1960, the temporal trend of the
 3793 probability maps and the FAO land use database were used for extrapolation. In addition, forest areas were further
 3794 subdivided into six forest types (Evergreen, needle leaf; Evergreen, broad leaf; Deciduous, needle leaf; Deciduous,
 3795 broad leaf; Mixed; Unknown/Other) based on the ESA CCI land cover dataset (ESA 2017). Spatiotemporal forest type
 3796 dynamics within the forest category were included for 1992-2015. Before 1992 and after 2015, the static forest type
 3797 distribution as found in the years 1992 and 2015 in the ESA CCI land cover was assumed, respectively.

3798

Formatted: Font: Not Bold

Formatted: Normal, Space After: 0 pt, Line spacing: single

Formatted: Left, Space After: 8 pt, Line spacing: Multiple 1,08 li

Formatted: Left, Space After: 8 pt, Line spacing: Multiple 1,08 li

3799 NITROGEN DEPOSITION

3800

3801 Wet and dry deposition maps of ammonium and nitrate covering Europe from 1995-2018 were calculated at
3802 0.5 degree spatial and monthly temporal resolution by the EMEP MSC-W model (“EMEP model” hereafter). The
3803 EMEP model is a 3-D Eulerian chemistry transport model (CTM) developed at the EMEP Centre MSC-W under the
3804 Framework of the UN Convention on Long-Range Transboundary Air Pollution (CLRTAP). The EMEP model has
3805 traditionally been used to assess acidification, eutrophication and air quality over Europe, to underpin air quality policy
3806 decisions (e.g., the Gothenburg Protocol), and has been under continuous development reflecting new scientific
3807 knowledge and increasing computer power. The model was described in detail by Simpson et al. (2012) and later
3808 updated as described in the annual EMEP status reports (Simpson et al., 2022, and references therein). For the
3809 VERIFY project, output from the EMEP model version rv4.33 was used (Simpson et al., 2019), and averaged to annual
3810 temporal resolution. In these simulations, the model was driven by meteorological data from the ECWMF IFS
3811 (European Centre for Medium-Range Weather Forecasts – Integrated Forecast System) version cy40r1. Land-use data
3812 were taken from the CORINE land-cover maps (de Smet and Hettelingh, 2001), the Stockholm Environment Institute
3813 at York (SEIY), the Global Land Cover (GLC2000) database, and the Community Land Model (Oleson et al., 2010;
3814 Lawrence et al., 2011). For more details see Simpson et al. (2017).

3815

3816 COASTAL OCEAN FLUXES

3817

3818 Ocean CO₂ fluxes were prepared for use as prior estimates in the regional inversions by combining the Rödenbeck
3819 global ocean estimate (Rödenbeck et al., 2014) with coastal ocean fluxes for Europe prepared under the VERIFY
3820 project. The combined dataset was prepared by choosing the coastal flux map when available and otherwise the open
3821 ocean map. The coastal ocean fluxes were generated for an area extending from the western Mediterranean to the
3822 Barents Sea and cover shelf areas down to 500 m water depth or 100 km distance from shore. First, surface ocean
3823 fCO₂ observations are taken from the annually updated SOCAT database (Bakker et al., 2016; [Bakker et al., 2022](#))
3824 and gridded to a monthly 0.125°x0.125° grid. pCO₂ maps are created based on fitting a set of driver data (including
3825 sea surface temperature, mixed layer depth, chlorophyll concentration, and ice concentration) against the gridded fCO₂
3826 observations. Both random forest and multi-linear regressions were used. The general procedure is described
3827 elsewhere (Becker et al., 2021), but for the version reported here, random forest regressions were used instead of
3828 multi-linear regression and the region was extended to the south. The dataset was divided into seven subregions
3829 (Barents Sea, Norwegian Coast, North Sea, Baltic Sea, Northern Atlantic Coast/Celtic Sea, Southern Atlantic
3830 coast/Bay of Biscay, western Mediterranean) and each region was fitted separately (leaf size: 20, bag size: 500). The
3831 root mean square error (RMSE) of the random forest regressions was determined to be between 34 micro-atm (Baltic
3832 Sea) and 10 micro-atm (Barents Sea). Random forest regressions consist of many regression trees, each based on a
3833 random subset of data. Due to this internal structure, the overall RMSE can be seen as an out-of-box error estimate.
3834 The final fluxes are calculated from the pCO₂ maps with the atmospheric xCO₂ in the marine boundary layer and six-
3835 hourly wind speed data using the gas transfer coefficient and the Schmidt number after Wanninkhoff (2014), the

Formatted: Left, Space After: 8 pt, Line spacing: Multiple
1,08 li

Formatted: Left, Space After: 8 pt, Line spacing: Multiple
1,08 li

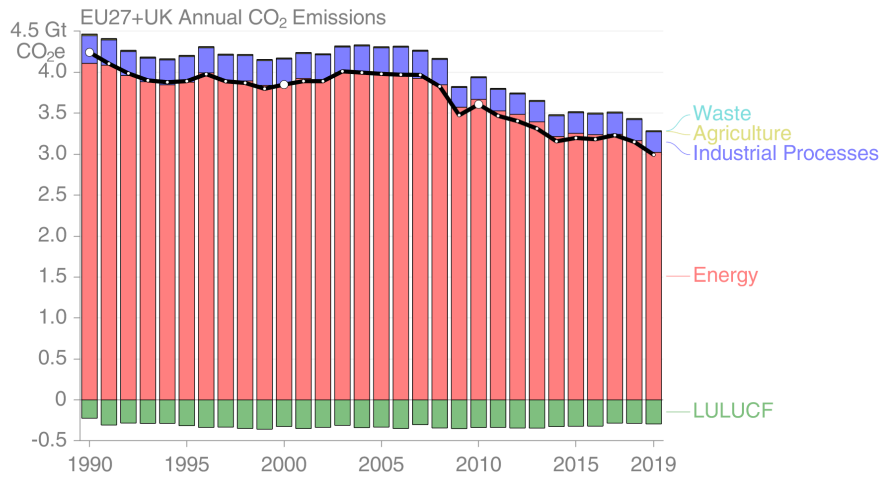
3836 coefficient a_0 of 0.2814 calculated after Naegler (2009) and 6-hourly winds from the NCEP-DOE Reanalysis 2 product
3837 (Kanamitsu et al., 2002).

3838
3839

3840 Appendix B. Additional figures

3841
3842

B1. Overview figures



3843
3844
3845

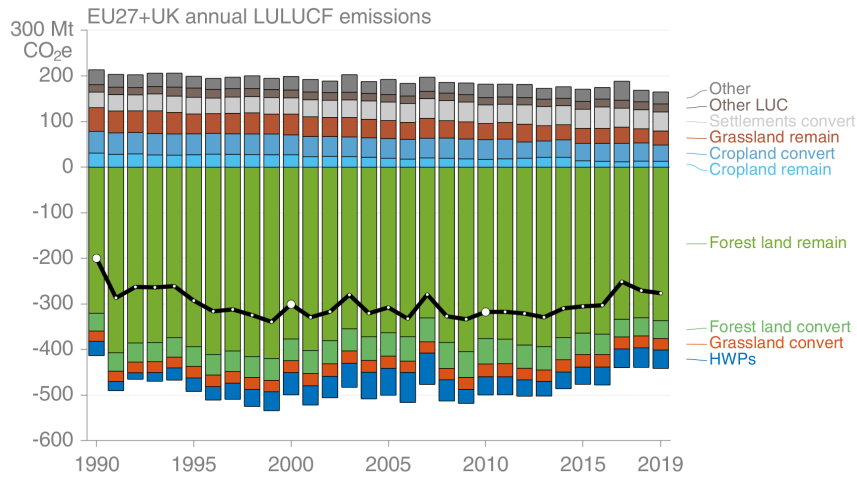
Figure B1: EU27+UK total annual GHG emissions from UNFCCC NGHGI (2021) submissions split per sector.

Formatted: Font: Not Bold

Formatted: Normal, Space After: 0 pt, Line spacing: single

Formatted: Heading 2

Formatted: Caption - VERIFY



3846

3847 *Figure B2: EU27+UK total annual GHG emissions from the LULUCF sector split in categories and sub-categories,*
 3848 *according to UNFCCC NGHGI (2021).*

Formatted: Caption - VERIFY

3849

3850 B2. CO₂ fossil

Deleted: CO2 fossil breakdown by fuel type

3851

Formatted: Subscript

3852 Figure B3 shows the CO₂ fossil emission estimates from EU27+UK split by major source categories for each
 3853 dataset for a single year. Sectors 1, 2, 3, and 5 are included for the UNFCCC NGHGI (2021) total, without indirect
 3854 emissions. A breakdown of the nine other fossil BU data sources corresponding to UNFCCC NGHGI sectors or
 3855 categories is not currently available.

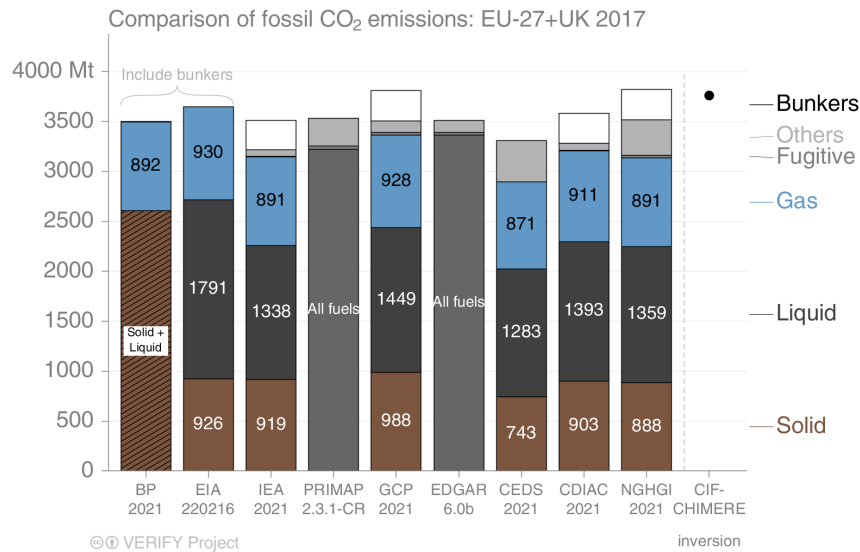
Formatted: Heading 2, Left, Line spacing: single

3856 As in Andrew (2020), we observe good agreement for the EU27+UK between all BU data sources and the
 3857 UNFCCC NGHGI (2021) data. The figure presents updated estimates for the year 2017, the most recent year when
 3858 all datasets reported estimates. Sectors 1, 2, 3, and 5 are included for the UNFCCC NGHGI (2021) total, without
 3859 indirect emissions.

Formatted: Font colour: Auto

3860 While most datasets agree well on total emissions, there are some differences. Both BP and the EIA include
 3861 bunker fuels and exclude most industrial process emissions. CEDS appears to be underestimating emissions from solid
 3862 fuels, for example lignite in Germany and oil shale in Estonia. IEA's emissions are lower because they exclude most
 3863 industrial processes. GCP's total matches the NGHGI exactly by design but remaps some of the fossil fuels used in
 3864 non-energy processes from "Others" to the fuel types used. CDIAC, PRIMAP, and EDGAR v6.0 all report total
 3865 emissions very similar to the UNFCCC NGHGI (2021). Larger differences are seen in the disaggregation of fuel types,
 3866 generally because of differing definitions.

Deleted: s



3869

3870

3871

3872

3873

3874

3875

3876

3877

3878

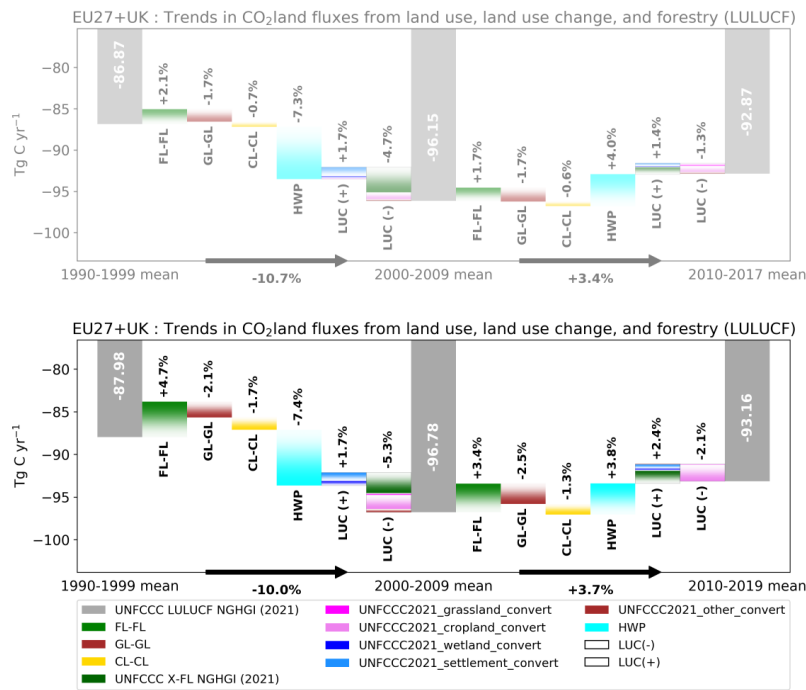
3879

3880

B3. CO₂ land

Formatted: Caption - VERIFY, Left, Line spacing: single

³⁰EDGAR v6.0 provides significant sectoral disaggregation of emissions, but not by fuel type due to license restrictions with the underlying energy data from the IEA.



Moved (insertion) [4]

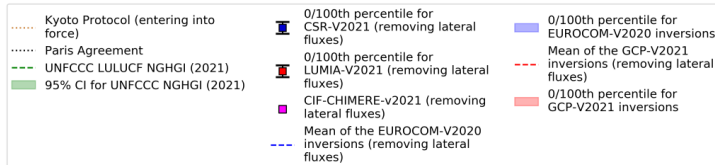
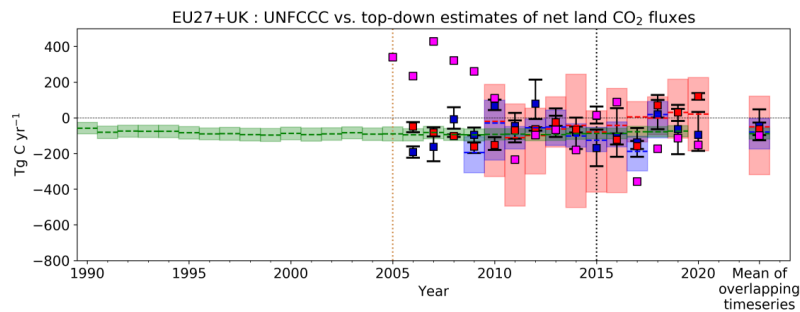
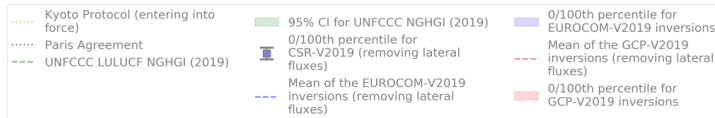
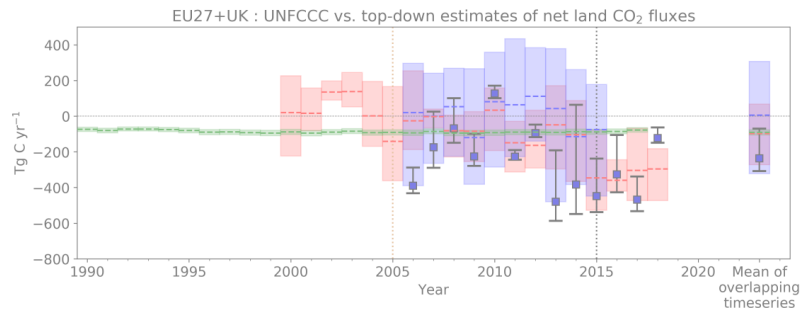
3881 VERIFY Project

3882 *Figure B4: The contribution of changes (%) in CO₂ land fluxes from various LULUCF categories to the overall*
 3883 *change in decadal mean for the EU27+UK as reported by Member States to the UNFCCC. The top plot shows the*
 3884 *previous NGHGI data from Petrescu et al. (2021b) and the bottom plot illustrates data from UNFCCC NGHGI*
 3885 *(2021). Changes in land categories converted to other land are grouped to show net gains and net losses in the*
 3886 *same column, with the bar color dictating which category each emission belongs to: note that the composition of the*
 3887 *“LUC(+)” and “LUC(-)” bars can change between time periods. Not shown are emissions from “Wetlands*
 3888 *remaining wetlands”, “Settlements remaining settlements”, and “Other land remaining other land” as none of the*
 3889 *BU models used distinguish these categories. The fluxes follow the atmospheric convention, where negative values*
 3890 *represent a sink while positive values represent a source. The color bars are shaded to guide the eye in the*
 3891 *direction of the change (white-to-color).*

Deleted: 3

Formatted: Caption - VERIFY, Left, Line spacing: single

3892



Moved (insertion) [3]

3894

3895 Figure B5: Comparison of inventories and atmospheric inversions for the total EU27+UK biogenic CO₂ fluxes from
 3896 Petrescu et al. (2021b) (top plot) and updated data from current study (bottom plot). Top-down inversion results
 3897 are: the global GCB2021 ensemble, the regional EUROCOM ensemble, the regional CarboScopeReg model with
 3898 multiple variants, the regional LUMIA model with multiple variants, and CIF-CHIMERE. The relative error in the
 3899 UNFCCC values represents the UNFCCC NGHGI (2021) Member states reported uncertainty computed with the

Deleted: 9

Formatted: Caption - VERIFY, Left, Line spacing: single

3901 error propagation method (95 % confidence interval) gap-filled and provided for every year of the timeseries. The
 3902 timeseries mean overlapping period is 2010-2018. The colored area represents the min/max of model ensemble
 3903 estimates. The same emissions due to lateral fluxes of carbon through rivers, crop trade, and wood trade are
 3904 removed from the top-down estimates in both the top and bottom graphs for consistency. The fluxes follow the
 3905 atmospheric convention, where negative values represent a sink while positive values represent a source. Note that
 3906 Petrescu et al. (2021b) presented the top plot including a suite of bottom-up models, which have been removed here
 3907 for clarity.

Deleted: clarity as they have already been presented in Fig. 8

3910 **Appendix C. Source specific methodologies: AD, EFs and** 3911 **uncertainties**

Formatted: Heading 1

3913 *Table C.1: Source specific activity data (AD), emission factors (EF) and uncertainty methodology for all current*
 3914 *VERIFY and non-VERIFY 2021 data products.*

Deleted: B

Formatted: Caption - VERIFY, Left

<i>Data sources CO₂ emission calculation</i>	<i>AD/Tier</i>	<i>EFs/Tier</i>	<i>Uncertainty assessment method</i>	<i>Emission data availability</i>
UNFCCC NGHGI (2021)	Country-specific information consistent with the IPCC Guidelines	IPCC guidelines / Country specific information for higher Tiers	IPCC guidelines (https://www.ipcc- nggip.iges.or.jp/public/2006g l/) for calculating the uncertainty of emissions based on the uncertainty of AD and EF, two different approaches: 1. Error propagation, 2. Monte Carlo Simulation <u>The EU GHG inventory team provided yearly harmonized and gap-filled uncertainties.</u>	NGHGI official data (CRFs) are found at https://unfccc.int/ghg- inventories-annex-i-parties/2021 (last access: June 2022).

Deleted: UBA Vienna provided yearly harmonized and gap-filled uncertainties

3915

Fossil CO₂

<p>BP CDIAC EIA IEA GCP CEDS PRIMAP-Hist</p>	<p>For further details, see Andrew (2020)</p>			
<p>EDGAR v6.0</p>	<p>International Energy Agency (IEA) for fuel combustion Food and Agricultural Organisation (FAO) for agriculture US Geological Survey (USGS) for industrial processes (e.g., cement, lime, ammonia and ferroalloys production) GGFR/NOAA for gas flaring World Steel Association for iron and steel production International Fertilisers Association (IFA) for urea consumption and production Complete description of the data sources can be found in Janssens-Maenhout et al. (2019) and in Crippa et al. (2019)</p>	<p>IPCC (2006): Tier 1 or Tier 2 depending on the sector</p>	<p>Tier 1 with error propagation by fuel type for CO₂ and accounting for covariances.</p>	<p>https://edgar.jrc.ec.europa.eu/datas_et_ghg60</p>
<p>CIF-CHIMERE</p>	<p>Tier 3 top-down 0.1° x 0.1° resolution maps of annual averages of fossil CO₂ anthropogenic emissions from EDGAR v4.3.2 Assimilation of satellite atmospheric mole fraction data: total column CO from IASI, and tropospheric column NO₂ from OMI</p>	<p>Tier 3 top-down regional inversions of CO and NO_x emissions using EMEP/CEIP as prior knowledge of the emissions and CO₂/CO and CO₂/NO_x emission ratios associated with the combustion of fossil fuel from EDGARv4.3.2.</p>	<p>Bayesian analysis in the CO and NO_x inversions along with propagation of uncertainties in fCO₂/CO and fCO₂/NO_x emission ratios</p>	<p>Detailed gridded data can be obtained by contacting the data providers: Gregoire Broquet gregoire.broquet@lsce.ipsl.fr https://verifydb.lsce.ipsl.fr/thredds/fileServer/verify/VERIFY_OUTP_UT/FCO2/CO2_Tier3TD_FossilFuel_CIF-CHIMERE_LSCE_ALL_EUR-85x101_1M_V2021_20210628_FORTEMSCHEINEY_2D.nc</p>
<p>CO₂ land: bottom-up</p>				

Formatted: Subscript

Formatted: Subscript

Formatted: Subscript

Deleted: concentration

Formatted: Subscript

3920

<p>BLUEvGCP</p> <p>BLUEvVERIFY</p>	<p>From LUH2: data on wood harvest, land cover types (primary, secondary, pasture, crop), and gross land use transitions (e.g. from secondary to pasture and back); Based on Pongratz et al. (2008) and Ramankutty and Foley (1999): Plant functional types (PFTs) of natural vegetation types</p> <p>Same as above with land cover from HILDA+ (Ganzenmüller et al., 2022)</p>	<p>Tier 3 (IPCC, 2006); PFT and land-cover type specific response curves describing the decay and regrowth of vegetation and soil carbon</p>	<p>N/A</p>	<p>Detailed gridded data can be obtained by contacting the data provider: Julia Pongratz: julia.pongratz@lmu.de https://verifydb.lscce.ipsl.fr/thredds/fileServer/verify/VERIFY_OUTP/UT/FCO2/CO2_Tier3BUPB_LandFlux_BLU-E-2021_bgc-jena_LAND_GLO-720x1440_1M_V2021_20211014_Pongratz_2D.nc https://verifydb.lscce.ipsl.fr/thredds/fileServer/verify/VERIFY_OUTP/UT/FCO2/CO2_Tier3BUPB_LandFlux_BLU-E-GCB-2021_bgc-jena_LAND_GLO-720x1440_1M_V2021_20211014_Pongratz_2D.nc</p>
<p>H&N</p>	<p>Simple assumptions about C-stock densities (per biome or per biome/country) based on literature</p>	<p>Transient change in C-stocks following a given transition (time dependent EF after an land use transition)</p>	<p>N/A</p>	<p>Detailed gridded data can be obtained by contacting the data provider: Richard A. Houghton rhoughton@woodwellclimate.org</p>
<p>ECOSSE</p>	<p>Tier 3 approach. The model is a point model, which provides spatial results by using spatial distributed input data (lateral fluxes are not considered). The model is a Tier 3 approach that is applied on grid map data, polygon organized input data or study sites.</p>	<p>IPCC (2006): Tier 3</p> <p>The simulation results will be allocated due to the available information (size of spatial unit, representation of considered land use, etc.).</p>	<p>N/A</p>	<p>Detailed gridded data can be obtained by contacting the data providers: Kuhnert, Matthias matthias.kuhnert@abdn.ac.uk Pete Smith: pete.smith@abdn.ac.uk https://verifydb.lscce.ipsl.fr/thredds/fileServer/verify/VERIFY_OUTP/UT/FCO2/CO2_Tier3BUPB_GrassFluxes_ECOSSE-lim-S1_UAbdn_CRP_EUR-304x560_1M_V2019_20200923_KUHNERT_2D.nc https://verifydb.lscce.ipsl.fr/thredds/fileServer/verify/VERIFY_OUTP/UT/FCO2/CO2_Tier3BUPB_CropFluxes_ECOSSE-SX_ABDN_CRP_EUR-142x179_1M_V2021_20220506_KUHNERT_2D.nc</p>

Formatted: Font: (Default) Times New Roman, 9 pt

Formatted: Font: (Default) Times New Roman, 9 pt

Formatted: Font: (Default) Times New Roman, 9 pt

Formatted: Font: (Default) Times New Roman, 9 pt

Field Code Changed

Formatted: Font: (Default) Times New Roman, 9 pt

Formatted: Font: (Default) Times New Roman, 9 pt

Formatted: Font: (Default) Times New Roman, 9 pt

Formatted: Font: (Default) Times New Roman, 9 pt

EPIC-IIASA Croplands	Tier 3 approach. Cropland: static 1×1 km cropland mask from CORINE-PELCOM. Initial SOC stock from the Map of organic carbon content in the topsoil (Lugato et al., 2014). “Static” crop management and input intensity by NUTS2 calibrated for 1995-2010 (Balković et al., 2013). Crop harvested areas by NUTS2 from EUROSTAT. Parameterization of soil carbon routine was updated based on Balković et al. (2020).	IPCC (2006): Tier 3 Land management and input factors for the cropland remaining cropland category as simulated by the EPIC-IIASA modeling platform, assuming the business-as-usual crop management calibrated for the 1995-2010 period. A 50-ha field is considered in each grid cell.	Sensitivity and uncertainty analysis of EPIC-IIASA regional soil carbon modeling (Balković et al, 2020).	Detailed gridded data can be obtained by contacting the data provider: Balković Juraj balkovic@iiasa.ac.at https://verifydb.lscce.ipsl.fr/thredds/fileServer/verify/VERIFY_OUTP/UT/FCO2/CO2_Tier3BUPB_CropFluxes_EPIC-S1_IIASA_CRP_EUR-304x560_1M_V2021_20211026_BALKOVIC_2D.nc
EPIC-IIASA grasslands	Tier 3 approach. Grassland: static 1x1 km mask from CORINE & PELCOM 2000, including pastures, herbaceous vegetation, heterogeneous agricultural areas, and permanent cropland. Initial SOC stock from the map of organic carbon content in the topsoil (Lugato et al., 2014) with a spin-up. Static grassland management and input intensity as adopted from (Chang et al., 2016) and ISIMIP (Jägermeyr et al., 2021).	IPCC (2006): Tier 3 Land management and input factors for the grassland remaining grassland category as simulated by the EPIC-IIASA modeling platform, calibrated for the 1995–2020 period.	N/A	Detailed gridded data can be obtained by contacting the data provider: Juraj Balković: balkovic@iiasa.ac.at https://verifydb.lscce.ipsl.fr/thredds/fileServer/verify/VERIFY_OUTP/UT/FCO2/CO2_Tier3BUPB_GrassFluxes_EPIC-S1_IIASA_GRS_EUR-304x560_1M_V2021_20220427_BALKOVIC_2D.nc
ORCHIDEE	For the land cover/land use input maps: data on wood harvest from the FAO	Tier 3 model, process based. Any emission factors enter in the form of generic parameters for a given ecosystem type fit against observational data (both site-level and remotely sensed).	None, though some information on uncertainty due to model structure is given by looking at the spread from the TRENDY suite of models, of which ORCHIDEE is a member.	Detailed gridded data can be obtained by contacting the data providers: Matthew McGrath matthew.mcgrath@lscce.ipsl.fr Philippe Peylin: peylin@lscce.ipsl.fr https://verifydb.lscce.ipsl.fr/thredds/fileServer/verify/VERIFY_OUTP/UT/FCO2/CO2_Tier3BUPB_CarbonCycle_ORCHIDEE-N-V32-VNDEP-S3_LSCE_LAND_EUR-304x560_1M_V2021_20211209_BASTRIKOV_2D.nc

Formatted: Font: (Default) Times New Roman, 9 pt

Formatted: French

Formatted: Font: (Default) Times New Roman, 9 pt, French

Formatted: Font: (Default) Times New Roman, 9 pt, French

Field Code Changed

Formatted: French

Formatted: Font: (Default) Times New Roman, 9 pt, French

CABLE-POP	For the land cover/land use input maps: data on wood harvest and agricultural land from the FAO	Tier 3 model, process based. Any emission factors enter in the form of generic parameters for a given ecosystem type fit against observational data (both site-level and remotely sensed).	None, though some information on uncertainty due to model structure is given by looking at the spread from the TRENDY suite of models, of which CABLE-POP is a member.	Model output (gridded data) can be obtained by contacting the data provider: Jürgen Knauer: J.Knauer@westernsydney.edu.au https://verifydb.lscce.ipsl.fr/thredds/fileServer/verify/VERIFY_OUTP/UT/FCO2/CO2_Tier3BUPB_Land-Flux_CABLE-POP_UWESTSYDNEY_LAND_GLO-304x560_1M_V2021_20220510_KNAUER_2D.nc
TRENDY v10	For the land cover/land use input maps: data on wood harvest and agricultural land from the FAO	Tier 3 models, process based. Any emission factors enter in the form of generic parameters for a given ecosystem type fit against observational data (both site-level and remotely sensed).	The spread of the 15 TRENDY models used gives an idea of the uncertainty due to model structure in dynamic global vegetation models, as the forcing data was harmonized for all models.	Detailed gridded data can be obtained by contacting the data provider: Sitch, Stephen S.A.Sitch@exeter.ac.uk
Statistical prediction model for CO₂ in inland waters	Hydrosheds 15s (Lehner et al., 2008) and Hydro1K (USGS, 2000) for river network, HYDROLAKES for lakes and reservoirs network and surface area (Messenger et al., 2016); river pCO ₂ data from GloRiCh (Hartmann et al., 2014), lake pCO ₂ database from Sobek et al. (2005); river channel slope and width calculated from GLOBE-DEM (GLOBE-Task-Team et al., 1999) and runoff data from Fekete et al. (2002). Geodata for predictors of pCO ₂ and gas transfer coefficient include air temperature, precipitation and wind speed (Hijmans et al., 2005), population density (CIESIN and CIAT), catchment slope	N/A	Monte Carlo runs (uncertainty on pCO ₂ and gas transfer velocity)	Detailed gridded data can be obtained by contacting the data providers: Ronny Lauerwald Ronny.Lauerwald@ulb.ac.be Pierre Regnier Pierre.Regnier@ulb.ac.be

Formatted: Font: (Default) Times New Roman, 9 pt

	gradient (Hydrosheds 15s), and terrestrial NPP (Zhao et al., 2005)			
CBM	National forest inventory data, Tier 2	EFs directly calculated by model, based on specific parameters (i.e., turnover and decay rates) defined by the user	N/A used from IPCC	Detailed gridded data can be obtained by contacting the data providers: Giacomo Grassi Giacomo.GRASSI@ec.europa.eu Matteo Vizzarri Matteo.VIZZARRI@ec.europa.eu Roberto Pilli roberto.pilli713@gmail.com
EFISCEN-Space	National forest inventory data, Tier 3	emission factor is calculated from net balance of growth minus harvest	Sensitivity analysis on EFISCEN V3 in the user manual (Schelhaas et al., 2007). Total sensitivity is caused by esp. young forest growth, width of volume classes, age of felling and few more. Scenario uncertainty comes on top of this when projecting in future.	Detailed gridded data can be obtained by contacting the data providers: Gert-Jan Nabuurs gert-jan.nabuurs@wur.nl Mart-Jan Schelhaas martjan.schelhaas@wur.nl
FAOSTAT	FAOSTAT Land Use Domain; Harmonized world soil; ESA CCI; MODIS 6 Burned area products	IPCC guidelines	IPCC (2006, Vol.4, p.10.33) - confidential Uncertainties in estimates of GHG emissions are due to uncertainties in emission factors and activity data. They may be related to, inter alia, natural variability, partitioning fractions, lack of spatial or temporal coverage, or spatial aggregation.	Agriculture total and subdomain specific GHG emissions are found for download at http://www.fao.org/faostat/en/#data/GT (last access: April 2022).
CO₂ land: Top-down				
CSR GCP ensemble (CTE, CAMS, CarboScope) EUROCOM (PYVAR-CHIMERE, LUMIA, FLEXINVERT, CSR, CTE-Europe) LUMIA CIF-CHIMERE	Tier 3 top-down approach, prior information from fossil emissions, ocean fluxes, and biosphere-atmosphere exchange Spatial resolutions ranging from 1°x1° for certain regions to 4°x5°. EUROCOM uses more than 30 atmospheric stations. CSR uses four different settings (as described in Appendix A4)	Tier 3 top-down Inversion systems based on atmospheric transport models	CSR - Gaussian probability distribution function, where the error covariance matrix includes errors in prior fluxes, observations and transport model representations. GCP : the different methodologies, the land-use and land-cover data set, and the different processes represented trigger the uncertainties between models, a semi-quantitative measure of uncertainty for annual and decadal emissions as best value judgment = at least a 68 % chance ($\pm 1\sigma$) EUROCOM : account for source of uncertainties via	Detailed gridded data can be obtained by contacting the data providers: CSR : Christoph Gerbig cgerbig@bgc-jena.mpg.de Saqr Munassar smunas@bgc-jena.mpg.de GCP : Pierre Friedlingstein P.Friedlingstein@exeter.ac.uk EUROCOM : Marko Scholze marko.scholze@nateko.lu.se Gregoire Broquet gregoire.broquet@isce.ipsl.fr

Deleted: 2

Field Code Changed

Field Code Changed

			<p>prior and model and observation error covariance matrices; assessment of the resulting uncertainties in fluxes based on spread</p> <p>LUMIA: The prior uncertainties are constructed using standard deviations proportional to the sum of the absolute value of the hourly NEE aggregated in each weekly optimization interval (so, in essence, uncertainties are large when the daily cycle of NEE is large), spatial correlation lengths of 500 km (Gaussian) and temporal correlation lengths of 1 month (Exponential).</p>	<p>LUMIA: Guillaume Monteil guillaume.monteil@nateko.lu.se</p> <p>CIF-CHIMERE: Gregoire Broquet gbroquet@lscce.ipsl.fr</p>
--	--	--	--	--

Field Code Changed

Formatted: English (US)

3925

3926

3927 Table C2: Comparison of the processes included in the inventories, bottom-up models and inversions.

Deleted: B2

Formatted: Caption - VERIFY, Left, Line spacing: single

Description	NGHGI	Global database	Process-based models				DGVMs			Bookkeeping Models				Inversions [#]
			E	E	C	E	C	T	O	B	B	H		
	U N F C C C ^a	F A O S T A T ^b	E C O S S E	E P I C - I I A S A	C B M	E F I S C E N - Space	C A B L E - P O P	T R E N D Y V I 0	O R C H I D E E	B L U E D G C P	B L U E V V E R I F Y	H & N		
Forest total	E	E	N	N	E	E	E	Acc. table A1 in GCB 2021 (Friedlingstein et al., 2022)	E	E ^b	E ^b	E ^b		
Split FL-FL / FL-X / X-FL	E	E	N	N	E	E/N/N	E		E	E ^b /E/E	E ^b /E/E	E ^b /E/E		
Cropland total	E	N	E	E	N	N	I		E	E ^b	E ^b	E ^b		
Split CL-CL / CL-X / X-CL	E	N	E	E/N/N	N	N	I		E	N/E/E	N/E/E	N/E/E		
Grassland total	E	N	E	N	N	N	E		E	E	E	E		
Split GL-GL /	E	N	E	N	N	N	E	E	N/E/E	N/E/E	N/E/E			

GL-X / X-GL														
Peatland accounting	E	E	N	N	N	N	N		N	N	N	N		
CO ₂ fertilization	I	I	N	E	N	N	E	Acc. table A1 in GCB 2021 (Friedling et al., 2022)	E	N ⁱ	N ⁱ	N ⁱ		
Climate induced impacts	I	I	N	E ^f	I ^b	I ^c	E		E	N ⁱ	N ⁱ	N ⁱ		
Natural disturbances (fires, insect, wind)	I	I	N	N	E	N	E		N	N ⁱ	N ⁱ	N ⁱ		
Soil Organic C dynamic	I		E	E	E	E	E		E	N	N	N		
Lateral C transport (river)	N	N	N	N	N	N	N		N	N	N	N		
Flux from Harvested Wood Products	E	N	N	N	I	N ^d	E		E	E	E	E		
Flux from Crop/Grass harvest	?	N	E	E ^e	N	N	E	E	I ⁱ	I ⁱ	I ⁱ			
Biomass burning	E	E	E	N ^g	E	N	N	N	N	E ^j	E ^j	E ^j		
N fertilization (with N dep)	I	N	E	N	N	N	E	N	N	N	N			
Flux from drained organic soils	I	E	E	N	I	N	N	I	E ^j	E ^j	E ^j			

Not included : N, Explicitly modeled : E, Implicitly modeled: I, Partly modeled : P

3929

3930

3931

3932

3933

3934

3935

3936

3937

^aUNFCCC and FAOSTAT are ensemble of country estimates calculated with specific methodology for each country, following some guidelines

^bThe climate effects can be estimated indirectly by CBM, using external additional input provided by other models

^cEFISCEN Space: Increment is sensitive to weather, but average weather

^dEFISCEN has only production in m³ but doesn't have a direct HWP module

^eCrop yield and residue harvest from cropland (20 % of residues harvested in case of cereals, no residue harvest for other crops)

^fEPIC-IIASA partly accounts for soil drought, i.e., plant growth limitation due to a lack of water in the soils. Heat stress and floods are not

accounted for, though

3938 ^aIn principle, burning of crop residues on cropland can be explicitly simulated by EPIC-IIASA. However, not done for VERIFY as it is not a
3939 relevant scenario for the business as usual cropland management in Europe
3940 ^bforest/cropland/grassland exist and have carbon stocks, but have carbon fluxes only through change to management. FL-FL includes all land-use
3941 induced effects (harvest slash and product decay, regrowth after [agricultural](#) abandonment and harvesting)
3942 ^cimplicit by using observation-based carbon densities that reflect harvest/climate/natural disturbances
3943 ^dpeat burning and peat drainage are not bookkeeping model output, but are added from various data sources during post processing
3944 ^eAccording to Table 2 in Monteil et al. (2020) and Table A3 in Friedlingstein et al. (2019)
3945 ^fThese categories are inputs to the inversions, not a result; the inversions adjust the total land-atmosphere C flux, regardless of what went into the
3946 prior, and the posterior flux cannot really be disaggregated into contributions from separate processes. In a sense, as long as a process is
3947 sufficiently significant to influence the CO₂ observations, it will have an impact on the inversion results
3948
3949

Deleted: agric

3950

3951 Author contributions

3952

3953 MJM processed original data, made Fig. [1, 3-6, A2, A3, A5, B4, and B5](#), edited the final manuscript, and coordinated
3954 [the response to reviewers](#); AMRP designed the initial research, led the discussions, wrote the initial draft of the paper
3955 and helped edit all the following versions; RMA made Fig. 2, A1, B3; BM provided the new UNFCCC gap-filled
3956 uncertainties and provided extensive support on questions related to NGHGs; PP, VB, and MJM processed the
3957 original data submitted to the VERIFY portal; PP, PB, and MJM designed and are managing the web portal; GP
3958 provided Figs. B1 and B2; GP, RMA, FD, BM, and GG made detailed reviews; SM made Fig. A4; PC, GB, PIP, MJ,
3959 RL, MK, JK, FC, OT, JP, RG, FNT, JB and GG gave detailed comments and advice on previous versions of the
3960 manuscript; all remaining co-authors provided data and commented on specific parts of the text related to their data
3961 sets.
3962

Deleted: 1,3-10

Deleted: and

Deleted: CQ made Fig. 11;

3963 Competing interests

3964 [Francesco N. Tubiello is a member of the editorial board of ESSD](#),
3965

Deleted: The

Deleted: authors declare that they have no conflict of interest.

3966 Acknowledgements

3967 We thank Aurélie Paquirissamy, Géraud Moulas and all ARTTIC team, for the great managerial support offered during
3968 the VERIFY project. FAOSTAT statistics are produced and disseminated with the support of its member countries
3969 to the FAO regular budget. The views expressed in this publication are those of the author(s) and do not necessarily
3970 reflect the views or policies of FAO. [Annual, gap-filled and harmonized NGHGI uncertainty estimates for the EU and
3971 its member states were provided by the EU GHG inventory team \(European Environment Agency and its European
3972 Topic Centre on Climate change mitigation\)](#). We acknowledge the work of other members of the EDGAR group
3973 (Edwin Schaaf, Jos Olivier). We acknowledge Stephen Sitch and the authors of the DGVMs TRENDY v10 ensemble
3974 models for providing us with the data. We thank all the national forest inventories that have made their data available:
3975 Ireland (John Redmond), Norway (Rasmus Astrup), Sweden (Jonas Fridman), Poland (Andrzej Talarczyk), Germany
3976 (BMEL), The Netherlands (WUR & Stichting Probos), Belgium (Flanders: Leen Govaere), Luxembourg (Thierry
3977 Palgen), France (IGN), Spain (MAPA), Switzerland (Esther Thürig), Italy (CREA), Czech Republic (Emil Cienciala),
3978 Slovak Republic (Vladimír Šebeň). We thank all the NFI field crews for their hard work. Timo Vesala thanks ICOS-
3979 Finland, University of Helsinki. Ingrid T. Luijckx and Wouter Peters thank the HPC cluster Aether at the University of

3986 Bremen, financed by DFG within the scope of the Excellence Initiative. MJM and VB were granted access to the
3987 HPC resources of GENCI-TGCC under the allocation A0130106328.

3988

3989

3990 **Financial support**

3991 This research has been supported by the European Commission, Horizon 2020 Framework Programme (VERIFY,
3992 grant no. 776810, for AB, AFC, AMRP, AP, CG, GB, GJM, GJN, GM, GP, HACDG, JB, LP, MJ, MJM, MK, MV,
3993 PP, PR, PS, RG, RMA, SD). MJM and GM also acknowledge funding from the European Union's Horizon 2020
3994 research and innovation programme under Grant Agreement No. 958927 (CoCO2). Philippe Ciais acknowledges
3995 the support of European Research Council Synergy project SyG-2013-610028 IMBALANCE-P and from the ANR
3996 CLand Convergence Institute. Ronny Lauerwald thanks the CLand Convergence Institute. Pierre Regnier
3997 acknowledges the ESM 2025. Gert-Jan Nabuurs thanks the Dutch National Forest Inventory funded by the Ministry
3998 Agriculture Nature Management and Food Quality. Guillaume Monteil's model computations were enabled by
3999 resources provided by the Swedish National Infrastructure for Computing (SNIC) at NSC partially funded by the
4000 Swedish Research Council through grant agreement no. 2018-05973.

4001

4002 **References**

4003 Andrew, R. M.: A comparison of estimates of global carbon dioxide emissions from fossil carbon sources, *Earth Syst.*
4004 *Sci. Data*, 12, 1437–1465, <https://doi.org/10.5194/essd-12-1437-2020>, 2020.

4005

4006 [Andrew, R. M., Peters, G.: The Global Carbon Project's fossil CO₂ emissions dataset. Global Carbon Project. Dataset.](https://doi.org/10.5281/zenodo.5569234)
4007 <https://doi.org/10.5281/zenodo.5569234>. Accessed 01 Oct 2021.

4008

4009 Armeth, A., Sitch, S., Pongratz, J., Stocker, B. D., Ciais, P., Poulter, B., Bayer, A. D., Bondeau, A., Calle, L., Chini,
4010 L. P., Gasser, T., Fader, M., Friedlingstein, P., Kato, E., Li, W., Lindeskog, M., Nabel, J. E. M. S., Pugh, T. A. M.,
4011 Robertson, E., Viovy, N., Yue, C., and Zaehle, S.: Historical carbon dioxide emissions caused by land-use changes
4012 are possibly larger than assumed. *Nature Geosci*, 10, 79–84, <https://doi.org/10.1038/ngeo2882>, 2017.

Deleted:

4014

4015 [Bakker, D. C. E., Alin, S. R., Becker, M., Bittig, H. C., Castaño-Primo, R., Feely, R. A., Gkritzalis, T., Kadono, K.,](#)
4016 [Kozyr, A., Lauvset, S. K., Metzl, N., Munro, D. R., Nakaoka, S., Nojiri, Y., O'Brien, K. M., Olsen, A., Pfeil, B.,](#)
4017 [Pierrot, D., Steinhoff, T., Sullivan, K. F., Sutton, A. J., Sweeney, C., Tilbrook, B., Wada, C., Wanninkhof, R.,](#)
4018 [Willstrand Wranne, A., Akl, J., Apelthun, L. B., Bates, N., Beatty, C. M., Burger, E. F., Cai, W.-J., Cosca, C. E.,](#)
4019 [Corredor, J. E., Cronin, M., Cross, J. N., De Carlo, E. H., DeGrandpre, M. D., Emerson, S., Enright, M. P., Enyo, K.,](#)
4020 [Evans, W., Frangoulis, C., Fransson, A., García-Ibáñez, M. I., Gehrung, M., Giannoudi, L., Glockzin, M., Hales, B.,](#)
4021 [Howden, S. D., Hunt, C. W., Ibáñez, J. S. P., Jones, S. D., Kamb, L., Körtzinger, A., Landa, C. S., Landschützer, P.,](#)
4022 [Lefèvre, N., Lo Monaco, C., Macovei, V. A., Maenner Jones, S., Meinig, C., Millero, F. J., Monacci, N. M., Mordy,](#)
4023 [C., Morell, J. M., Murata, A., Musielewicz, S., Neill, C., Newberger, T., Nomura, D., Ohman, M., Ono, T., Passmore,](#)
4024 [A., Petersen, W., Petihakis, G., Perivoliotis, L., Plueddemann, A. J., Rehder, G., Reynaud, T., Rodriguez, C., Ross,](#)
4025 [A. C., Rutgersson, A., Sabine, C. L., Salisbury, J. E., Schlitzer, R., Send, U., Skjelvan, I., Stamatakis, N., Sutherland,](#)
4026 [S. C., Sweeney, C., Tadokoro, K., Tanhua, T., Telszewski, M., Trull, T., Vandemark, D., van Ooijen, E., Voynova,](#)
4027 [Y. G., Wang, H., Weller, R. A., Whitehead, C., Wilson, D.: Surface Ocean CO₂ Atlas Database Version 2022](#)
4028 [\(SOCATv2022\) \(NCEI Accession 0253659\). Subset v2021. NOAA National Centers for Environmental Information.](#)
4029 [Dataset. <https://doi.org/10.25921/1h9f-nb73>. Accessed 01 July 2021.](#)

4030

4031 Balkovič, J., Madaras, M., Skalský, R., Folberth, C., Smatanová, M., Schmid, E., van der Velde, M., Kraxner, F.,
4032 Obersteiner, M.: Verifiable soil organic carbon modeling to facilitate regional reporting of cropland carbon change:
4033 A test case in the Czech Republic, *J. Environ. Manage.*, 274, 111206, <https://doi.org/10.1016/j.jenvman.2020.111206>,
4034 2020.

4035

4036 Balkovič, J., Skalský, R., Folberth, C., Khabarov, N., Schmid, E., Madaras, M., Obersteiner, M., van der Velde, M.:
4037 Impacts and Uncertainties of +2°C of Climate Change and Soil Degradation on European Crop Calorie Supply, *Earths*
4038 *Future*, 6, 373–395, <https://doi.org/10.1002/2017EF000629>, 2018.

4039

4040 Balkovič, J., van der Velde, M., Schmid, E., Skalský, R., Khabarov, N., Obersteiner, M., Stürmer, B., Xiong, W.: Pan-
4041 European crop modeling with EPIC: Implementation, up-scaling and regional crop yield validation, *Agric. Syst.*, 120,
4042 61–75, <https://doi.org/10.1016/j.agsy.2013.05.008>, 2013.

4043

4044 Bastos, A., Ciais, P., Friedlingstein, P., Sitch, S., Pongratz, J., Fan, L., Wigneron, J. P., Weber, U., Reichstein, M., Fu,
4045 Z., Anthoni, P., Arneth, A., Haverd, V., Jain, A. K., Joetzjer, E., Knauer, J., Lienert, S., Loughran, T., McGuire, P. C.,
4046 Tian, H., Viovy, N., and Zaehle, S.: Direct and seasonal legacy effects of the 2018 heat wave and drought on European
4047 ecosystem productivity, *Science Advances*, 6, eaba2724, DOI: 10.1126/sciadv.aba27, 2020a.

4048

4049 Bastos, A., O'Sullivan, M., Ciais, P., Makowski, D., Sitch, S., Friedlingstein, P., Chevallier, F., Rödenbeck, C.,
4050 Pongratz, J., Luijkx, I. T., Patra, P. K., Peylin, P., Canadell, J. G., Lauerwald, R., Li, W., Smith, N. E., Peters, W.,
4051 Goll, D. S., Jain, A. K., Kato, E., Lienert, S., Lombardozzi, D. L., Haverd, V., Nabel, J. E. M. S., Poulter, B., Tian,
4052 H., Walker, A. P., and Zaehle, S.: Sources of uncertainty in regional and global terrestrial CO₂ exchange estimates,
4053 *Global Biogeochemical Cycles*, 34, e2019GB006393, <https://doi.org/10.1029/2019GB006393>, 2020b.

4054

4055 [Basu, S., Lehman, S. J., Miller, J. B., Andrews, A. E., Sweeney, C., Gurney, K. R., Xu, X., Southon, J., and Tans, P.](#)
4056 [P.: Estimating US fossil fuel CO₂ emissions from measurements of ¹⁴C in atmospheric CO₂, *Proc. Nat. Acad. Sci.*,](#)
4057 [117, 13300-13307, <https://doi.org/10.1073/pnas.1919032117>, 2020.](#)

4058

4059 [Battin, T. J., Lauerwald, R., Bernhardt, E. S., Bertuzzo, E., Gener, L. G., Hall Jr, R. O., Hotchkiss, E. R., Maavara, T.,](#)
4060 [Pavelsky, T. M., Ran, L., Raymond, P., Rosentreter, J. A., and Regnier, P.: River ecosystem metabolism and carbon](#)
4061 [biogeochemistry in a changing world, *Nature*, 613, 449-459, <https://doi.org/10.1038/s41586-022-05500-8>, 2023.](#)

4062

4063 Becker, M., Olsen, A., Landschützer, P., Omar, A., Rehder, G., Rödenbeck, C., and Skjelvan, I.: The northern
4064 European shelf as an increasing net sink for CO₂, *Biogeosciences*, 18, 1127–1147, [https://doi.org/10.5194/bg-18-](https://doi.org/10.5194/bg-18-1127-2021)
4065 1127-2021, 2021.

Formatted: Normal paragraph

Formatted: Highlight

Formatted: Indent: First line: 0 cm

4066

4067 Berchet, A., Sollum, E., Thompson, R. L., Pison, I., Thanwerdas, J., Broquet, G., Chevallier, F., Aalto, T., Berchet,
4068 A., Bergamaschi, P., Brunner, D., Engelen, R., Fortems-Cheiney, A., Gerbig, C., Groot Zwaafink, C. D., Haussaire,
4069 J.-M., Henne, S., Houweling, S., Karstens, U., Kutsch, W. L., Lujikx, I. T., Monteil, G., Palmer, P. I., van Peet, J. C.
4070 A., Peters, W., Peylin, P., Potier, E., Rödenbeck, C., Saunois, M., Scholze, M., Tsuruta, A., and Zhao, Y.: The
4071 Community Inversion Framework v1.0: a unified system for atmospheric inversion studies, *Geosci. Model Dev.*, 14,
4072 5331–5354, <https://doi.org/10.5194/gmd-14-5331-2021>, 2021.

4073

4074 BP: 60 Years BP Statistical Review of World Energy: 1951–2011, available at:
4075 <https://www.bp.com/en/global/corporate/energy-economics/statistical-review-of-world-energy/downloads.html> (last
4076 access: 8 February 2019), 2011.

4077

4078 BP: BP Statistical Review of World Energy June 2018, available at: [https://www.bp.com/en/global/corporate/energy-](https://www.bp.com/en/global/corporate/energy-economics/statistical-review-of-world-energy/downloads.html)
4079 [economics/statistical-review-of-world-energy/downloads.html](https://www.bp.com/en/global/corporate/energy-economics/statistical-review-of-world-energy/downloads.html), (last access: 14 June 2018).

4080

4081 BP: Methodology for calculating CO₂ emissions from energy use, available at:
4082 <https://www.bp.com/en/global/corporate/energy-economics/statistical-review-of-world-energy/co2-emissions.html>
4083 (last access: 8 February 2019), 2017.

4084

4085 Bradbury, N. J., Whitmore, A. P., Hart, P. B. S., and Jenkinson, D. S.: Modelling the fate of nitrogen in crop and soil
4086 in the years following application of ¹⁵N-labelled fertilizer to winter wheat, *J. Agr. Sci.*, 121, 363-379,
4087 doi:10.1017/S0021859600085567, 1993.

4088

4089 Brophy, K., Graven, H., Manning, A. J., White, E., Arnold, T., Fischer, M. L., Jeong, S., Cui, X., and Rigby, M.:
4090 Characterizing uncertainties in atmospheric inversions of fossil fuel CO₂ emissions in California, *Atmos. Chem.*
4091 *Phys.*, 19, 2991–3006, <https://doi.org/10.5194/acp-19-2991-2019>, 2019.

4092

4093 Broquet, G., Chevallier, F., Rayner, P., Aulagnier, C., Pison, I., Ramonet, M., Schmidt, M., Vermeulen, A. T., and
4094 Ciais, P.: A European summertime CO₂ biogenic flux inversion at mesoscale from continuous in situ mixing ratio
4095 measurements,

4096 *J. Geophys. Res.*, 116, D23303, doi:10.1029/2011JD016202, 2011.

4097

4098 Broquet, G., Chevallier, F., Bréon, F.-M., Kadyrov, N., Alemanno, M., Apadula, F., Hammer, S., Haszpra, L.,
4099 Meinhardt, F., Morgui, J. A., Necki, J., Piacentino, S., Ramonet, M., Schmidt, M., Thompson, R. L., Vermeulen, A.
4100 T., Yver, C., and Ciais, P.: Regional inversion of CO₂ ecosystem fluxes from atmospheric measurements: reliability
4101 of the uncertainty estimates, *Atmos. Chem. Phys.*, 13, 9039–9056, <https://doi.org/10.5194/acp-13-9039-2013>, 2013.

4102

4103 CDIAC, <https://energy.appstate.edu/CDIAC> (last access: 10 November 2022).

4104

4105 Ceccherini, G., Duveiller, G., Grassi, G., Lemoine, G., Avitabile, V., Pilli, R., and Cescatti, A.: Abrupt increase in
4106 harvested forest area over Europe after 2015, *Nature*, 583, 72–77, <https://doi.org/10.1038/s41586-020-2438-y>, 2020.

4107

4108 CEDS v_2019_12_23, <https://www.pnnl.gov/projects/ceds> (last access: 10 November 2022).

4109

4110 Chang, J., Ciais, P., Herrero, M., Havlik, P., Campioli, M., Zhang, X., Bai, Y., Viovy, N., Joiner, J., Wang, X., Peng,
4111 S., Yue, C., Piao, S., Wang, T., Hauglustaine, D. A., Soussana, J.-F., Peregon, A., Kosykh, N., and Mironycheva-
4112 Tokareva, N.: Combining livestock production information in a process-based vegetation model to reconstruct the
4113 history of grassland management, *Biogeosciences*, 13, 3757–3776, <https://doi.org/10.5194/bg-13-3757-2016>, 2016.

4114

4115 [Chen, J., Wang, S., Kraxner, F., Balkovič, J., Xu, X., and Sun, L.: Spatial Analysis of the Soil Carbon Sequestration](#)
4116 [Potential of Crop-Residue Return in China Based on Model Simulation, *J. Resour. Ecol.*, 10, 184-195,
4117 <https://doi.org/10.5814/j.issn.1674-764x.2019.02.009>, 2019.](#)

4118

4119 Chevallier, F., Fisher, M., Peylin, P., Serrar, S., Bousquet, P., Bréon, F.-M., Chédin, A., and Ciais, P.: Inferring CO₂
4120 sources and sinks from satellite observations: Method and application to TOVS data, *J. Geophys. Res.*, 110, D24309,
4121 [doi:10.1029/2005JD006390](https://doi.org/10.1029/2005JD006390), 2005.

Formatted: Reference, Left, Line spacing: single, Don't keep with next, Don't keep lines together, Border: Top: (No border), Bottom: (No border), Left: (No border), Right: (No border), Between : (No border)

Formatted: Reference

Deleted: ¶

Formatted: Reference, Left, Line spacing: single, Don't keep with next, Don't keep lines together, Border: Top: (No border), Bottom: (No border), Left: (No border), Right: (No border), Between : (No border)

4123

4124 Chevallier, F., F.-M. Bréon, F.-M., and Rayner, P. J.: Contribution of the Orbiting Carbon Observatory to the
4125 estimation of CO₂ sources and sinks: Theoretical study in a variational data assimilation framework, *J. Geophys. Res.*,
4126 112, D09307, doi:10.1029/2006JD007375, 2007.

4127

4128 Chevallier, F., Ciais, P., Conway, T. J., Aalto, T., Anderson, B. E., Bousquet, P., Brunke, E. G., Ciattaglia, L., Esaki,
4129 Y., Fröhlich, M., Gomez, A. J., Gomez-Pelaez, A. J., Haszpra, L., Krummel, P., Langenfelds, R., Leuenberger, M.,
4130 Machida, T., Maignan, F., Matsueda, H., Morguí, J. A., Mukai, H., Nakazawa, T., Peylin, P., Ramonet, M., Rivier, L.,
4131 Sawa, Y., Schmidt, M., Steele, P., Vay, S. A., Vermeulen, A. T., Wofsy, S., and Worthy, D. : CO₂ surface fluxes at
4132 grid point scale estimated from a global 21-year reanalysis of atmospheric measurements. *J. Geophys. Res.*, 115,
4133 D21307, doi:10.1029/2010JD013887, 2010.

4134

4135 Ciais, P., Reichstein, M., Viovy, N., Granier, A., Ogée, J., Allard, V., Aubinet, M., Buchmann, N., Bernhofer Chr.,
4136 Carrara, A., Chevallier, F., De Noblet, N., Friend, A. D., Friedlingstein, P., Grünwald, T., Heinesch, B., Keronen, P.,
4137 Knohl, A., Krinner, G., Loustau, D., Manca, G., Matteucci, G., Miglietta, F., Ourcival, J. M., Papale, D., Pilegaard,
4138 K., Rambal, S., Seufert, G., Soussana, J. F., Sanz, M. J., Schulze, E. D., Vesala, T. and Valentini, R.: Europe-wide
4139 reduction in primary productivity caused by the heat and drought in 2003. *Nature*, 437, 529–533,
4140 <https://doi.org/10.1038/nature03972>, 2005.

4141

4142 Ciais, P., Crisp, D., Denier van der Gon, H., Engelen, R., Janssens-Maenhout, G., Heimann, M., Rayner, P., and
4143 Scholze, M.: Towards a European Operational Observing System to Monitor Fossil CO₂ emissions - Final Report
4144 from the expert group, https://www.copernicus.eu/sites/default/files/2019-09/CO2_Blue_report_2015.pdf, 2015.

4145

4146 Ciais, P., Yao, Y., Gasser, T., Baccini, A., Wang, Y., Lauerwald, R., Peng, S., Bastos, A., Li, W., Raymond, P.A. and
4147 Canadell, J.G., Peters, G. P., Andres, R. J., Chang, J., Yue, C., Dolman, A. J., Haverd, V., Hartmann, J., Laruelle, G.,
4148 Konings, A. G., King, A. W., Liu, Y., Luysaert, S., Maignan, F., Patra, P. K., Peregon, A., Regnier, P., Pongratz, J.,
4149 Poulter, B., Shvidenko, A., Valentini, R., Wang, R., Brouquet, G., Yin, Y., Zscheischler, J., Guenet, B., Goll, D. S.,
4150 Ballantyne, A.-P., Yang, H., Qiu, C., and Zhu, D.: Empirical estimates of regional carbon budgets imply reduced
4151 global soil heterotrophic respiration, *National Science Review*, 8, nwaal45, <https://doi.org/10.1093/nsr/nwaa145>,
4152 2021.

4153

4154 CoCO2: <https://coco2-project.eu/>, last access: 21 November 2022.

4155

4156 Coleman, K., Jenkinson, D. S.: RothC-26.3 - A model the turnover of carbon in soil. In: Powlson DS, Smith P, Smith

4157 JU (ed) Evaluation of soil organic matter models using existing long-term datasets, NATO ASI Series I, vol. 38.

4158 Springer, Berlin, pp 237–246, 1996.

4159

4160 [Conchedda, G. and Tubiello, F. N.: Drainage of organic soils and GHG emissions: validation with country data, Earth](#)

4161 [Syst. Sci. Data, 12, 3113–3137, https://doi.org/10.5194/essd-12-3113-2020, 2020.](#)

4162

Formatted: Reference, Left, Line spacing: single, Don't keep with next, Don't keep lines together, Border: Top: (No border), Bottom: (No border), Left: (No border), Right: (No border), Between : (No border)

Formatted: Not Highlight

Formatted: Reference, Left, Line spacing: single, Don't keep with next, Don't keep lines together, Border: Top: (No border), Bottom: (No border), Left: (No border), Right: (No border), Between : (No border)

4163 [Cox, A., Di Sarra, A. G., Vermeulen, A., Manning, A., Beyersdorf, A., Zahn, A., Manning, A., Watson, A., Karion,](#)
4164 [A., Hensen, A., Arlyn A., Frumau, A., Colomb, A., Scheeren, B., Law, B., Baier, B., Munger, B., Paplawsky, B.,](#)
4165 [Viner, B., Stephens, B., Daube, B., Labuschagne, C., Myhre, C. L., Hanson, C., Miller, C. E., Plass-Duelmer, C.,](#)
4166 [Gerbig, C., Sloop, C. D., Sweeney, C., Kubistin, D., Goto, D., Jaffe, D., Say, D., Van Dinter, D., Bowling, D., Lam,](#)
4167 [D. H. Y., Munro, D., Dickon Y., Worthy, D., Dlugokencky, E., Kozlova, E., Gloor, E., Cuevas, E., Reyes-Sanchez,](#)
4168 [E., Hints, E., Kort, E., Morgan, E., Obersteiner, F., Apadula, F., Gheusi, F., Meinhardt, F., Moore, F., Vitkova, G.,](#)
4169 [Chen, G., Bentz, G., Manca, G., Brailsford, G., Forster, G., Boenisch, H., Riris, H., Meijer, H., Timas, H., Matsueda,](#)
4170 [H., Huilin C., Levin, I., Lehner, I., Mammarella, I., Bartyzel, J., Abshire, J. B., Elkins, J. W., Levula, J., Necki, J.,](#)
4171 [Pichon, J. M., Peischl, J., Müller- Williams, J., Turnbull, J., Miller, J. B., Lee, J., Lin, J., Morgui, J.-A., DiGangi, J.](#)
4172 [P., Lavric, J., Hatakka, J., Coletta, J. D., Worsley, J., Holst, J., Kominkova, K., McKain, K., Saito, K., Aikin, K., Davis,](#)
4173 [K., Thoning, K., Tørseth, K., Haszpra, L., Mitchell, L., Gatti, L.V., Emmenegger, L., Chmura, M., Merchant, L., Sha,](#)
4174 [M. K., Delmotte, M., Fischer, Marc L., Schumacher, M., Torn, M., Leuenberger, M., Heimann, M., Steinbacher, M.,](#)
4175 [De Mazière, M., Sargent, M., Lindauer, M., Mölder, M., Martin, M. Y., Shook, M., Galkowski, M., Heliasz, M.,](#)
4176 [Marek, M. V., Ramonet, M., Miroslaw Z., Lopez, M., Sasakawa, M., Mihalopoulos, N., Miles, N., Lee, O. S.M.,](#)
4177 [Laurent, O., Peltola, O., Hermanssen, O., Trisolino, P., Cristofanelli, P., Kolari, P., Krummel, P., Shepson, P., Smith,](#)
4178 [P., Rivas, P. P., Bakwin, P., Bergamaschi, P., Keronen, P., Tans, P., Van Den Bulk, P., Keeling, R., Ramos, R.,](#)
4179 [Langenfelds, R., Leppert, R., Curcoll, R., Commane, R., Newman, S., Piacentino, S., Hammer, S., Richardson, S.,](#)
4180 [Biraud, S. C., Conil, S., Clark, S., Morimoto, S., Shuangxi F., Aoki, S., O'Doherty, S., Sites Climadat, Zaehle, S., De](#)
4181 [Wekker, S., Kawa, S. R., Montzka, S., Walker, S., Piper, S., Wofsy, S., Nichol, S., Schuck, T., Lauvaux, T., Ryerson,](#)
4182 [T., Seifert, T., Griffis, T., Biermann, T., Gehrlein, T., Machida, T., Laurila, T., Aalto, T., Gomez-Trueba, V., Kazan,](#)
4183 [V., Ivakhov, V., Joubert, W., Niwa, Y., and Loh, Z.: Multi-laboratory compilation of atmospheric carbon dioxide data](#)
4184 [for the period 1957–2019; obspack CO2 1 GLOBALVIEWplus v6.1 2021-03-01, NOAA Global Monitoring](#)
4185 [Laboratory \[data set\], <https://doi.org/10.25925/20201204>, 2021.](#)

4186
4187 Crippa, M., Oreggioni, G., Guizzardi, D., Muntean, M., Schaaf, E., Lo Vullo, E., Solazzo, E., Monforti-Ferrario, F.,
4188 Olivier, J.G.J., and Vignati, E.: Fossil CO2 and GHG emissions of all world countries - 2019 Report, EUR 29849 EN,
4189 Publications Office of the European Union, Luxembourg, 2019, ISBN 978-92-76-11100-9, doi:10.2760/687800,
4190 JRC117610, 2019.
4191

Formatted: Font colour: Text 1

Formatted: Font colour: Text 1

Formatted: Font colour: Text 1

4192 Deng, Z., Ciais, P., Tzompa-Sosa, Z. A., Saunio, M., Qiu, C., Tan, C., Sun, T., Ke, P., Cui, Y., Tanaka, K., Lin, X.,
4193 Thompson, R. L., Tian, H., Yao, Y., Huang, Y., Lauerwald, R., Jain, A. K., Xu, X., Bastos, A., Sitch, S., Palmer, P.
4194 I., Lauvaux, T., d'Aspremont, A., Giron, C., Benoit, A., Poulter, B., Chang, J., Petrescu, A. M. R., Davis, S. J., Liu,
4195 Z., Grassi, G., Albergel, C., Tubiello, F. N., Perugini, L., Peters, W., and Chevallier, F.: Comparing national
4196 greenhouse gas budgets reported in UNFCCC inventories against atmospheric inversions, *Earth Syst. Sci. Data*, 14,
4197 1639–1675, <https://doi.org/10.5194/essd-14-1639-2022>, 2022.

4198

4199 [Di Sarra, A. G., Karion, A., Arlyn Andrews, Colomb, A., Scheeren, B., Viner, B., Myhre, C. L., Miller, C. E., Plass-](#)
4200 [Duelmer, C., Plass-Duelmer, C., Sloop, C. D., Sweeney, C., Kubistin, D., Jaffe, D., Dlugokencky, E., Vitkova, G.,](#)
4201 [Manca, G., Huilin Chen, Lehner, I., Mammarella, I., Pichon, J. M., Müller-Williams, J., Miller, J. B., Lee, J., Hatakka,](#)
4202 [J., Holst, J., Kominkova, K., McKain, K., Thoning, K., Tørseth, K., Emmenegger, L., Sha, M. K., Delmotte, M.,](#)
4203 [Fischer, M. L., Schumacher, M., Leuenberger, M., Steinbacher, M., De Mazière, M., Lindauer, M., Mölder, M.,](#)
4204 [Heliasz, M., Marek, M. V., Ramonet, M., Lopez, M., Laurent, O., Hermanssen, O., Trisolino, P., Cristofanelli, P.,](#)
4205 [Smith, P., Bakwin, P., Bergamaschi, P., Keronen, P., Tans, P., Piacentino, S., Biraud, S. C., Conil, S., De Wekker, S.,](#)
4206 [Biermann, T., Laurila, T., Aalto, T., and Kazan, V.: Multi-laboratory compilation of atmospheric carbon dioxide data](#)
4207 [for the years 2020–2021; obspack CO2 1 NRT v6.1.1 2021-05-17, NOAA Global Monitoring Laboratory \[data](#)
4208 [set\], <https://doi.org/10.25925/20210517>, 2021.](#)

4209

4210 [Drought 2018 Team, ICOS Atmosphere Thematic Centre: Drought-2018 atmospheric CO₂ Mole Fraction product for](#)
4211 [48 stations \(96 sample heights\), Integrated Carbon Observation System \[data set\], \[https://doi.org/10.18160/ERE9-\]\(https://doi.org/10.18160/ERE9-9D85\)](#)
4212 [9D85](#), 2020.

Formatted: Reference, Left, Line spacing: single, Don't keep with next, Don't keep lines together, Border: Top: (No border), Bottom: (No border), Left: (No border), Right: (No border), Between : (No border)

Formatted: Font colour: Text 1

Formatted: Not Superscript/ Subscript

Formatted: Reference, Left, Line spacing: single, Don't keep with next, Don't keep lines together, Border: Top: (No border), Bottom: (No border), Left: (No border), Right: (No border), Between : (No border)

Formatted: Default Paragraph Font

4213
4214 Ducoudré, N. I., Laval, K., and Perrier, A.: SECHIBA, a new set of parameterizations of the hydrologic exchanges at
4215 the land-atmosphere interface within the LMD atmospheric general circulation model, *Journal of Climate*, 6, 248–
4216 273, <https://www.jstor.org/stable/26197219>, 1993.
4217
4218 ESA: Land Cover CCI Product User Guide Version 2. ESA. <http://maps.elie.ucl.ac.be/CCI/viewer/index.php>, (last
4219 access: 10 November 2022), 2017.
4220
4221 EU: REGULATION (EU) No 525/2013 OF THE EUROPEAN PARLIAMENT AND OF THE COUNCIL of 21 May
4222 2013 on a mechanism for monitoring and reporting greenhouse gas emissions and for reporting other information at
4223 national and Union level relevant to climate change and repealing Decision No 280/2004/EC, [https://eur-](https://eur-lex.europa.eu/legal-content/EN/TXT/PDF/?uri=CELEX:32013R0525&from=EN)
4224 [lex.europa.eu/legal-content/EN/TXT/PDF/?uri=CELEX:32013R0525&from=EN](https://eur-lex.europa.eu/legal-content/EN/TXT/PDF/?uri=CELEX:32013R0525&from=EN), 2013.
4225
4226 EU: Regulation (EU) 2018/841 of the European Parliament and of the Council of 30 May 2018 on the inclusion of
4227 greenhouse gas emissions and removals from land use, land use change and forestry in the 2030 climate and energy
4228 framework, and amending Regulation (EU) No 525/2013 and Decision No 529/2013/EU, [https://eur-](https://eur-lex.europa.eu/legal-content/EN/TXT/?uri=uriserv:OJ.L_.2018.156.01.0001.01.ENG)
4229 [lex.europa.eu/legal-content/EN/TXT/?uri=uriserv:OJ.L_.2018.156.01.0001.01.ENG](https://eur-lex.europa.eu/legal-content/EN/TXT/?uri=uriserv:OJ.L_.2018.156.01.0001.01.ENG), 2018a.
4230
4231 EU: Regulation (EU) 2018/842 of the European Parliament and of the Council of 30 May 2018 on binding annual
4232 greenhouse gas emission reductions by Member States from 2021 to 2030 contributing to climate action to meet
4233 commitments under the Paris Agreement and amending Regulation (EU) No 525/2013, [https://eur-](https://eur-lex.europa.eu/legal-content/EN/TXT/?uri=CELEX:32018R0842)
4234 [lex.europa.eu/legal-content/EN/TXT/?uri=CELEX:32018R0842](https://eur-lex.europa.eu/legal-content/EN/TXT/?uri=CELEX:32018R0842), 2018b.
4235
4236 EU: Communication COM/2020/562: Stepping up Europe’s 2030 climate ambition Investing in a climate-neutral
4237 future for the benefit of our people, [https://knowledge4policy.ec.europa.eu/publication/communication-com2020562-](https://knowledge4policy.ec.europa.eu/publication/communication-com2020562-stepping-europe%E2%80%99s-2030-climate-ambition-investing-climate_en)
4238 [stepping-europe%E2%80%99s-2030-climate-ambition-investing-climate_en](https://knowledge4policy.ec.europa.eu/publication/communication-com2020562-stepping-europe%E2%80%99s-2030-climate-ambition-investing-climate_en), (last access: 10 November 2022), 2020.

4239

4240 EU: Procedure 2021/0201/COD, COM (2021) 554: Proposal for a REGULATION OF THE EUROPEAN
4241 PARLIAMENT AND OF THE COUNCIL amending Regulations (EU) 2018/841 as regards the scope, simplifying
4242 the compliance rules, setting out the targets of the Member States for 2030 and committing to the collective
4243 achievement of climate neutrality by 2035 in the land use, forestry and agriculture sector, and (EU) 2018/1999 as
4244 regards improvement in monitoring, reporting, tracking of progress and review, [https://eur-](https://eur-lex.europa.eu/procedure/EN/2021_201)
4245 [lex.europa.eu/procedure/EN/2021_201](https://eur-lex.europa.eu/procedure/EN/2021_201), 2021a.

4246

4247 EU: Regulation (EU) 2021/1119 of the European Parliament and of the Council of 30 June 2021 establishing the
4248 framework for achieving climate neutrality and amending Regulations (EC) No 401/2009 and (EU) 2018/1999
4249 ('European Climate Law'), <https://eur-lex.europa.eu/legal-content/EN/TXT/?uri=CELEX:32021R1119>, 2021b.

4250

4251 EU NIR: Annual European Union greenhouse gas inventory 1990–2019 and inventory report 2021, Submission to the
4252 UNFCCC Secretariat, EEA/PUBL/2021/066, 2021.

4253

4254 EU NIR: Annual European Union greenhouse gas inventory 1990–2020 and inventory report 2022, Submission to the
4255 UNFCCC Secretariat, EEA/PUBL/2022/023, 2022.

4256

4257 Federici, S., Tubiello, F. N., Salvatore, M., Jacobs, H., and Schmidhuber, J.: New estimates of CO₂ forest emissions
4258 and removals: 1990–2015, *Forest Ecol. Manage.*, 352, 89–98, <https://doi.org/10.1016/j.foreco.2015.04.022>, 2015.

4259

4260 Feng, L., Palmer, P. I., Parker, R. J., Deutscher, N. M., Feist, D. G., Kivi, R., Morino, I., and Sussmann, R.: Estimates
4261 of European uptake of CO₂ inferred from GOSAT XCO₂ retrievals: sensitivity to measurement bias inside and outside
4262 Europe, *Atmos. Chem. Phys.*, 16, 1289–1302, <https://doi.org/10.5194/acp-16-1289-2016>, 2016.

4263

4264 Fortems-Cheiney, A., Pison, I., Broquet, G., Dufour, G., Berchet, A., Potier, E., Coman, A., Siour, G., and Costantino,
4265 L.: Variational regional inverse modeling of reactive species emissions with PYVAR-CHIMERE-v2019, *Geosci.*
4266 *Model Dev.*, 14, 2939–2957, <https://doi.org/10.5194/gmd-14-2939-2021>, 2021.

4267

4268 Fortems-Cheiney, A and Broquet, G.: D2.12: Final re-analysis of the national scale CO₂ anthropogenic emissions
4269 over 2005-2015, https://projectworkspace.eu/sites/VERIFY/Deliverables/WP2/VERIFY_D2.12_Final%20re-

4270 analysis%20of%20the%20national%20scale%20CO2%20anthropogenic%20emissions%20over%202005-
4271 2015_v1.pdf, 2021.
4272
4273 FRA: Global Forest Resources Assessment 2015: How are the world's forest changing?, 2015, Rome, Italy, available
4274 at: <http://www.fao.org/3/a-i4793e.pdf> (last access: 10 December 2019), 2015.
4275
4276 Frey, H.C.: Evaluation of an Approximate Analytical Procedure for Calculating Uncertainty in the Greenhouse Gas
4277 Version of the Multi-Scale Motor Vehicle and Equipment Emissions System, Prepared for Office of Transportation
4278 and Air Quality, U.S. Environmental Protection Agency, Ann Arbor, MI, May 30, 2003.
4279
4280 Friedlingstein, P., O'Sullivan, M., Jones, M. W., Andrew, R. M., Hauck, J., Olsen, A., Peters, G. P., Peters, W.,
4281 Pongratz, J., Sitch, S., Le Quéré, C., Canadell, J. G., Ciais, P., Jackson, R. B., Alin, S., Aragão, L. E. O. C., Armeth,
4282 A., Arora, V., Bates, N. R., Becker, M., Benoit-Cattin, A., Bittig, H. C., Bopp, L., Bultan, S., Chandra, N., Chevallier,
4283 F., Chini, L. P., Evans, W., Florentie, L., Forster, P. M., Gasser, T., Gehlen, M., Gilfillan, D., Gkritzalis, T., Gregor,
4284 L., Gruber, N., Harris, I., Hartung, K., Haverd, V., Houghton, R. A., Ilyina, T., Jain, A. K., Joetzjer, E., Kadono, K.,
4285 Kato, E., Kitidis, V., Korsbakken, J. I., Landschützer, P., Lefèvre, N., Lenton, A., Lienert, S., Liu, Z., Lombardozzi,
4286 D., Marland, G., Metz, N., Munro, D. R., Nabel, J. E. M. S., Nakaoka, S.-I., Niwa, Y., O'Brien, K., Ono, T., Palmer,
4287 P. I., Pierrot, D., Poulter, B., Resplandy, L., Robertson, E., Rödenbeck, C., Schwinger, J., Séférian, R., Skjelvan, I.,
4288 Smith, A. J. P., Sutton, A. J., Tanhua, T., Tans, P. P., Tian, H., Tilbrook, B., van der Werf, G., Vuichard, N., Walker,
4289 A. P., Wanninkhof, R., Watson, A. J., Willis, D., Wiltshire, A. J., Yuan, W., Yue, X., and Zaehe, S.: Global Carbon
4290 Budget 2020, *Earth Syst. Sci. Data*, 12, 3269–3340, <https://doi.org/10.5194/essd-12-3269-2020>, 2020.
4291
4292 Friedlingstein, P., Jones, M. W., O'Sullivan, M., Andrew, R. M., Bakker, D. C. E., Hauck, J., Le Quéré, C., Peters, G.
4293 P., Peters, W., Pongratz, J., Sitch, S., Canadell, J. G., Ciais, P., Jackson, R. B., Alin, S. R., Anthoni, P., Bates, N. R.,
4294 Becker, M., Bellouin, N., Bopp, L., Chau, T. T. T., Chevallier, F., Chini, L. P., Cronin, M., Currie, K. I., Decharme,
4295 B., Djeutchouang, L. M., Dou, X., Evans, W., Feely, R. A., Feng, L., Gasser, T., Gilfillan, D., Gkritzalis, T., Grassi,
4296 G., Gregor, L., Gruber, N., Gürses, Ö., Harris, I., Houghton, R. A., Hurtt, G. C., Iida, Y., Ilyina, T., Luijkx, I. T., Jain,
4297 A., Jones, S. D., Kato, E., Kennedy, D., Klein Goldewijk, K., Knauer, J., Korsbakken, J. I., Körtzinger, A.,
4298 Landschützer, P., Lauvset, S. K., Lefèvre, N., Lienert, S., Liu, J., Marland, G., McGuire, P. C., Melton, J. R., Munro,
4299 D. R., Nabel, J. E. M. S., Nakaoka, S.-I., Niwa, Y., Ono, T., Pierrot, D., Poulter, B., Rehder, G., Resplandy, L.,
4300 Robertson, E., Rödenbeck, C., Rosan, T. M., Schwinger, J., Schwingshackl, C., Séférian, R., Sutton, A. J., Sweeney,

4301 C., Tanhua, T., Tans, P. P., Tian, H., Tilbrook, B., Tubiello, F., van der Werf, G. R., Vuichard, N., Wada, C.,
4302 Wanninkhof, R., Watson, A. J., Willis, D., Wiltshire, A. J., Yuan, W., Yue, C., Yue, X., Zaehle, S., and Zeng, J.:
4303 Global Carbon Budget 2021, *Earth Syst. Sci. Data*, 14, 1917–2005, <https://doi.org/10.5194/essd-14-1917-2022>, 2022.
4304
4305 Ganzenmüller, R., Bultan, S., Winkler, K., Fuchs, R., Zabel, F., and Pongratz, J.: Land-use change emissions based
4306 on high-resolution activity data substantially lower than previously estimated: *Environmental Research Letters*, 17,
4307 64050, DOI 10.1088/1748-9326/ac70d8, 2022.
4308
4309 [Gasser, T. and Ciais, P.: A theoretical framework for the net land-to-atmosphere CO₂ flux and its implications in the](#)
4310 [definition of "emissions from land-use change". *Earth Syst. Dynam.*, 4, 171–186. \[https://doi.org/10.5194/esd-4-171-\]\(https://doi.org/10.5194/esd-4-171-2013\)](#)
4311 [2013, 2013.](#)
4312
4313 Gasser, T., Crepin, L., Quilcaille, Y., Houghton, R. A., Ciais, P., and Obersteiner, M.: Historical CO₂ emissions from
4314 land use and land cover change and their uncertainty, *Biogeosciences*, 17, 4075–4101, [https://doi.org/10.5194/bg-17-](https://doi.org/10.5194/bg-17-4075-2020)
4315 [4075-2020](#), 2020.
4316
4317 Grassi, G., House, J., Kurz, W. A., Cescatti, A., Houghton, R. A., Peters, G. P., Sanz, M. J., Vi nas, R. A., Alkama, .,
4318 Armeth, A., Bondeau, A., Dentener, F., Fader, M., Federici, S., Friedlingstein, P., Jain, A. K., Kato, E., Koven, C. D.,
4319 Lee, D., Nabel, J. E. M. S., Nassikas, A. A., Perugini, L., Rossi, S., Sitch, S., Viovy, N., Wiltshire, A., and Zaehle, S.:
4320 Reconciling global-model estimates and country reporting of anthropogenic forest CO₂ sinks, *Nat. Clim. Chang.*, 8,
4321 914–920, <https://doi.org/10.1038/s41558-018-0283-x>, 2018a.
4322
4323 Grassi, G., Pilli, R., House, J., Federici, S., and Kurz, W. A.: Science-based approach for credible accounting of
4324 mitigation in managed forests, *Carbon balance Manag.*, 13, 8, <https://doi.org/10.1186/s13021-018-0096-2>, 2018b.
4325
4326 Grassi, G., Cescatti, A., Matthews, R., Duveiller, G., Amia, A., Federici, S., House, J., de Noblet-Ducoudré, N., Pilli,
4327 R., and Vizzarri, M.: On the realistic contribution of European forests to reach climate objectives, *Carbon balance*
4328 *Manag.*, 14, 8, <https://doi.org/10.1186/s13021-019-0123-y>, 2019.
4329

Formatted: Reference

4330 Grassi, G., Conchedda, G., Federici, S., Abad Viñas, R., Korosuo, A., Melo, J., Rossi, S., Sandker, M., Somogyi, Z.,
4331 Vizzarri, M., and Tubiello, F. N.: Carbon fluxes from land 2000–2020: bringing clarity to countries' reporting, *Earth*
4332 *Syst. Sci. Data*, 14, 4643–4666, <https://doi.org/10.5194/essd-14-4643-2022>, 2022a.

Deleted: ¶

4334 [Grassi, G., Schwingshackl, C., Gasser, T., Houghton, R. A., Sitch, S., Canadell, J. G., Cescatti, A., Ciais, P., Federici,](#)
4335 [S., Friedlingstein, P., Kurz, W. A., Sanz Sanchez, M. J., Abad Viñas, R., Alkama, R., Bultan, S., Ceccherini, G., Falk,](#)
4336 [S., Kato, E., Kennedy, D., Knauer, J., Korosuo, A., Melo, J., McGrath, M. J., Nabel, J. E. M. S., Poulter, B.,](#)
4337 [Romanovskaya, A. A., Rossi, S., Tian, H., Walker, A. P., Yuan, W., Yue, X., and Pongratz, J.: Harmonising the land-](#)
4338 [use flux estimates of global models and national inventories for 2000–2020, *Earth Syst. Sci. Data*, 15, 1093–1114,](#)
4339 <https://doi.org/10.5194/essd-15-1093-2023>, 2023.

Deleted: ¶

4340
4341 [Gray, A. N., Whittier, T. R., and Harmon, M. E.: Carbon stocks and accumulation rates in Pacific Northwest forests:](#)
4342 [role of stand age, plant community, and productivity, *Ecosphere*, 7, e01224, <https://doi.org/10.1002/ecs2.1224>, 2016.](#)

Deleted: Grassi, G., Schwingshackl, C., Gasser, T., Houghton, R. A., Sitch, S., Canadell, J. G., Cescatti, A., Ciais, P., Federici, S., Friedlingstein, P., Kurz, W. A., Sanz Sanchez, M. J., Abad Viñas, R., Alkama, R., Ceccherini, G., Kato, E., Kennedy, D., Knauer, J., Korosuo, A., McGrath, M. J., Nabel, J., Poulter, B., Rossi, S., Walker, A. P., Yuan, W., Yue, X., and Pongratz, J.: Mapping land-use fluxes for 2001–2020 from global models to national inventories, *Earth Syst. Sci. Data Discuss.* [preprint], <https://doi.org/10.5194/essd-2022-245>, in review, 2022b. ¶

Formatted: Reference

4344 Hansis, E., Davis, S. J., and Pongratz, J.: Relevance of methodological choices for accounting of land use change
4345 carbon fluxes, *Glob. Biogeochem. Cy.*, 29, 1230–1246, <https://doi.org/10.1002/2014GB004997>, 2015.

4347 Hartung, K., Bastos, A., Chini, L., Ganzenmüller, R., Havermann, F., Hurtt, G. C., Loughran, T., Nabel, J. E. M. S.,
4348 Nützel, T., Obermeier, W. A., and Pongratz, J.: Bookkeeping estimates of the net land-use change flux – a sensitivity
4349 study with the CMIP6 land-use dataset, *Earth Syst. Dynam.*, 12, 763–782, <https://doi.org/10.5194/esd-12-763-2021>,
4350 2021.

4352 Harris, I., Osborn, T.J., Jones, P., and Lister, D.: Version 4 of the CRU TS monthly high-resolution gridded
4353 multivariate climate dataset, *Sci Data* 7, 109, <https://doi.org/10.1038/s41597-020-0453-3>, 2020.

4355 Hastie, A., Lauerwald, R., Ciais, P., and Regnier, P. : Aquatic carbon fluxes dampen the overall variation of net
4356 ecosystem productivity in the Amazon basin: An analysis of the interannual variability in the boundless carbon cycle,
4357 *Global Change Biology*, 25 (6), pp. 2094–2111, DOI: 10.1111/gcb.14620, 2019.

4358

4371 Haverd, V., Smith, B., Cook, G. D., Briggs, P. R., Nieradzki, L., Roxburgh, S. H., Liedloff, A., Meyer, C. P., and
4372 Canadell, J. G.: A stand-alone tree demography and landscape structure module for Earth system models, *Geophysical*
4373 *Research Letters*, 40, 5234–5239, <https://doi.org/10.1002/grl.50972>, 2013.

4374

4375 Haverd, V., Smith, B., Nieradzki, L., Briggs, P. R., Woodgate, W., Trudinger, C. M., Canadell, J. G., and Cuntz, M.:
4376 A new version of the CABLE land surface model (Subversion revision r4601) incorporating land use and land cover
4377 change, woody vegetation demography, and a novel optimisation-based approach to plant coordination of
4378 photosynthesis, *Geosci. Model Dev.*, 11, 2995–3026, <https://doi.org/10.5194/gmd-11-2995-2018>, 2018.

4379

4380 Houghton, R., Hobbie, J., Melillo, J., Moore, B., Peterson, B., Shaver, G., and Woodwell, G.: Changes in the carbon
4381 content of terrestrial biota and soils between 1860 and 1980: A net release of CO₂ to the atmosphere, *Ecol. Monogr.*,
4382 53, 235–262, <https://doi.org/10.2307/1942531>, 1983.

4383

4384 Houghton, R. A.: Revised estimates of the annual net flux of carbon to the atmosphere from changes in land use and
4385 land management 1850–2000, *Tellus B*, 55, 378–390, <https://doi.org/10.3402/tellusb.v55i2.16764>, 2003.

4386

4387 Houghton, R. A., House, J. I., Pongratz, J., van der Werf, G. R., DeFries, R. S., Hansen, M. C., Le Quéré, C., and
4388 Ramankutty, N.: Carbon emissions from land use and land-cover change, *Biogeosciences*, 9, 5125–5142,
4389 <https://doi.org/10.5194/bg-9-5125-2012>, 2012.

4390

4391 Houghton, R. A. and Nassikas, A. A.: Global and regional fluxes of carbon from land use and land cover change
4392 1850–2015, *Glob. Biogeochem. Cy.*, 31, 456–472, <https://doi.org/10.1002/2016GB005546>, 2017.

4393

4394 Hurtt, G. C., Chini, L., Sahajpal, R., Frolking, S., Bodirsky, B. L., Calvin, K., Doelman, J. C., Fisk, J., Fujimori, S.,
4395 Klein Goldewijk, K., Hasegawa, T., Havlik, P., Heinemann, A., Humpenöder, F., Jungclaus, J., Kaplan, J. O., Kennedy,
4396 J., Krisztin, T., Lawrence, D., Lawrence, P., Ma, L., Mertz, O., Pongratz, J., Popp, A., Poulter, B., Riahi, K.,
4397 Shevliakova, E., Stehfest, E., Thornton, P., Tubiello, F. N., van Vuuren, D. P., and Zhang, X.: Harmonization of global
4398 land use change and management for the period 850–2100 (LUH2) for CMIP6, *Geosci. Model Dev.*, 13, 5425–5464,
4399 <https://doi.org/10.5194/gmd-13-5425-2020>, 2020.

4400

4401 [ICOS RI: ICOS Atmosphere Release 2021-1 of Level 2 Greenhouse Gas Mole Fractions of CO₂, CH₄, N₂O, CO₂,
4402 meteorology and 14CO₂ \[data set\], <https://doi.org/10.18160/WJY7-5D06>, 2021.](#)
4403
4404 IPCC: Good Practice Guidance for Land use, Land use Change and Forestry, Chapter 3, 3.3, [https://www.ipcc-
4406 ggip.iges.or.jp/public/gpplulucf/gpplulucf_files/GPG_LULUCF_FULL.pdf](https://www.ipcc-
4405 ggip.iges.or.jp/public/gpplulucf/gpplulucf_files/GPG_LULUCF_FULL.pdf), (last access: 10 January 2022), 2003.
4407 IPCC: Guidelines for National Greenhouse Gas Inventories, Prepared by the National Greenhouse Gas Inventories
4408 Programme. IGES, Japan, <https://www.ipcc-nggip.iges.or.jp/public/2006gl/>, 2006, (last access: 10 January 2022),
4409 2006.
4410
4411 IPCC: Refinement to the 2006 IPCC Guidelines for National Greenhouse Gas Inventories, available at:
4412 <https://www.ipcc.ch/report/2019-refinement-to-the-2006-ipcc-guidelines-for-national-greenhouse-gas-inventories>,
4413 (last access: 10 January 2022), 2019.
4414
4415 IPCC: Supplement to the 2006 IPCC Guidelines for National Greenhouse Gas Inventories: Wetlands, edited by:
4416 Hiraishi, T., Krug, T., Tanabe, K., Srivastava, N., Baasansuren, J., Fukuda, M., and Troxler, T. G., IPCC, Switzerland,
4417 2014.
4418
4419 IPCC: Summary for Policymakers. In: Climate Change 2021: The Physical Science Basis. Contribution of Working
4420 Group I to the Sixth Assessment Report of the Intergovernmental Panel on Climate Change [Masson-Delmotte, V., P.
4421 Zhai, A. Pirani, S.L. Connors, C. Péan, S. Berger, N. Caud, Y. Chen, L. Goldfarb, M.I. Gomis, M. Huang, K. Leitzell,
4422 E. Lonnoy, J.B.R. Matthews, T.K. Maycock, T. Waterfield, O. Yelekçi, R. Yu, and B. Zhou (eds.)].Cambridge
4423 University Press, Cambridge, United Kingdom and New York, NY, USA, pp. 3–32, doi:10.1017/9781009157896.001,
4424 2021.
4425
4426 Izaurrealde, R. C., Williams, J. R., McGill, W. B., Rosenberg, N.J., and Jakas, M. C. Q.: Simulating soil C dynamics
4427 with EPIC: Model description and testing against long-term data, *Ecol. Model.* 192, 362–384,
4428 <https://doi.org/10.1016/j.ecolmodel.2005.07.010>, 2006.
4429
4430 Janssens-Maenhout, G., Crippa, M., Guizzardi, D., Muntean, M., Schaaf, E., Dentener, F., Bergamaschi, P., Pagliari,
4431 V., Olivier, J. G. J., Peters, J. A. H. W., van Aardenne, J. A., Monni, S., Doering, U., Petrescu, A. M. R., Solazzo, E.,

Formatted: Font colour: Text 1

Formatted: Font colour: Text 1

Formatted: Font colour: Text 1

Deleted: ¶

4433 and Oreggioni, G. D.: EDGAR v4.3.2 Global Atlas of the three major greenhouse gas emissions for the period 1970–
4434 2012, *Earth Syst. Sci. Data*, 11, 959–1002, <https://doi.org/10.5194/essd-11-959-2019>, 2019.

4435

4436 Jägermeyr, J., Müller, C., Ruane, A.C., Elliott, J., Balkovic, J., Castillo, O., Faye, B., Foster, I., Folberth, C., Franke,
4437 J.A., Fuchs, K., Guarin, J.R., Heinke, J., Hoogenboom, G., Iizumi, T., Jain, A.K., Kelly, D., Khabarov, N., Lange, S.,
4438 Lin, T.-S., Liu, W., Mialyk, O., Minoli, S., Moyer, E.J., Okada, M., Phillips, M., Porter, C., Rabin, S.S., Scheer, C.,
4439 Schneider, J.M., Schyns, J.F., Skalsky, R., Smerald, A., Stella, T., Stephens, H., Webber, H., Zabel, F., and
4440 Rosenzweig, C.: Climate impacts on global agriculture emerge earlier in new generation of climate and crop models.
4441 *Nat. Food*, 2, 873–885, <https://doi.org/10.1038/s43016-021-00400-y>, 2021.

4442

4443 Jenkinson, D. S., Hart, P. B. S., Rayner, J. H., and Parry, L. C.: Modelling the turnover of organic matter in long-term
4444 experiments at Rothamsted, *INTECOL Bulletin*, 15, 1987.

4445

4446 Jenkinson, D. S., and Rayner, J. H.: The turnover of organic matter in some of the Rothamsted classical experiments,
4447 *Soil. Sci.*, 123, 298–305, <https://doi.org/10.1097/00010694-197705000-00005>, 1977.

4448

4449 Jonsson, R., Blujdea, V. N., Fiorese, G., Pilli, R., Rinaldi, F., Baranzelli, C., and Camia, A.: Outlook of the European
4450 forest-based sector: forest growth, harvest demand, wood-product markets, and forest carbon dynamics implications,
4451 *iForest*, 11, 315–328, <https://doi.org/10.3832/ifor2636-011>, 2018.

4452

4453 Jonsson, R., Rinaldi, F., Pilli, R., Fiorese, G., Hurmekoski, E., Cazzaniga, N., Robert, N., and Camia, A.: Boosting the
4454 EU forest-based bioeconomy: Market, climate, and employment impacts, *Technological Forecasting and Social
4455 Change*, 163, 120478, <https://doi.org/10.1016/j.techfore.2020.120478>, 2021.

4456

4457 Kanamitsu, M., Ebisuzaki, W., Woollen, J., Yang, S., Hnilo, J. J., Fiorino, M., and Potter, G. L.: NCEP–DOE AMIP-
4458 II Reanalysis (R-2). *Bulletin of the American Meteorological Society*, 83, 1631–1644, [https://doi.org/10.1175/BAMS-
4459 83-11-1631](https://doi.org/10.1175/BAMS-
4459 83-11-1631), 2002.

4460

4461 Klein Goldewijk, K., Beusen, A., Doelman, J., and Stehfest, E.: Anthropogenic land-use estimates for the Holocene;
4462 HYDE 3.2, *Earth Syst. Sci. Data*, 9, 927–953, <https://doi.org/10.5194/essd9-927-2017>, 2017a.

4463

4464 Klein Goldewijk, K., Dekker, S. C., and van Zanden, J. L.: Per capita estimations of long-term historical land use and
4465 the consequences for global change research, *J. Land Use Sci.*, 12, 313– 337,
4466 <https://doi.org/10.1080/1747423X.2017.1354938>, 2017b.

4467

4468 Koehl, M., Hildebrandt, R., Olschofsky, K., Koehler, R., Roetzer, T., Mette, T., Pretzsch, H., Koethke, M., Dieter,
4469 M., Abiy, M., Makeschin, F., and Kenter, B.: Combating the effects of climatic change on forests by mitigation
4470 strategies, *Carbon Balance and Management*, 5, 8, <https://doi.org/10.1186/1750-0680-5-8>, 2010.

4471

4472 Konovalov, I. B., Berezin, E. V., Ciais, P., Broquet, G., Zhuravlev, R. V., and Janssens-Maenhout, G.: Estimation of
4473 fossil-fuel CO₂ emissions using satellite measurements of "proxy" species, *Atmos. Chem. Phys.*, 16, 13509–13540,
4474 <https://doi.org/10.5194/acp-16-13509-2016>, 2016.

4475

4476 Konovalov, I. B., and Lvova, D. A. : First, fast-track, Re-analysis of the national scale CO₂ anthropogenic emissions
4477 over 2005-2015, internal VERIFY report:
4478 [https://projectworkspace.eu/sites/VERIFY/Deliverables/WP2/VERIFY_D2.10_First,%20fast-track,%20Re-](https://projectworkspace.eu/sites/VERIFY/Deliverables/WP2/VERIFY_D2.10_First,%20fast-track,%20Re-analysis%20of%20the%20national%20scale%20CO2%20anthropogenic%20emissions%20over%202005-2015.pdf)
4479 [analysis%20of%20the%20national%20scale%20CO₂%20anthropogenic%20emissions%20over%202005-2015.pdf](https://projectworkspace.eu/sites/VERIFY/Deliverables/WP2/VERIFY_D2.10_First,%20fast-track,%20Re-analysis%20of%20the%20national%20scale%20CO2%20anthropogenic%20emissions%20over%202005-2015.pdf),
4480 (last access: 15 September 2020), 2018.

4481

4482 Kountouris, P., Gerbig, C., Rödenbeck, C., Karstens, U., Koch, T. F., and Heimann, M.: Technical Note: Atmospheric
4483 CO₂ inversions on the mesoscale using data-driven prior uncertainties: methodology and system evaluation, *Atmos.*
4484 *Chem. Phys.*, 18, 3027–3045, <https://doi.org/10.5194/acp-18-3027-2018>, 2018a.

4485

4486 Kountouris, P., Gerbig, C., Rödenbeck, C., Karstens, U., Koch, T. F., and Heimann, M.: Atmospheric CO₂ inversions
4487 on the mesoscale using data-driven prior uncertainties: quantification of the European terrestrial CO₂ fluxes, *Atmos.*
4488 *Chem. Phys.*, 18, 3047–3064, <https://doi.org/10.5194/acp-18-3047-2018>, 2018b.

4489

4490 Krinner, G., Viovy, N., de Noblet-Ducoudré N., Ogée, J., Polcher, J., Friedlingstein, P., Ciais, P., Sitch, S., and
4491 Prentice, I. C.: A dynamic global vegetation model for studies of the coupled atmosphere-biosphere system, *Global*
4492 *Biogeochemical Cycles*, 19, GB1015, doi:10.1029/2003GB002199, 2005.

4493

4494 Kumarathunge, D. P., Medlyn, B. E., Drake, J. E., Tjoelker, M. G., Aspinwall, M. J., Battaglia, M., Cano, F. J., Carter,
4495 K. R., Cavaleri, M. A., Cernusak, L. A., Chambers, J. Q., Crous, K. Y., De Kauwe, M. G., Dillaway, D. N., Dreyer,
4496 E., Ellsworth, D. S., Ghannoum, O., Han, Q., Hikosaka, K., Jensen, A. M., Kelly, J. W. G., Kruger, E. L., Mercado,
4497 L. M., Onoda, Y., Reich, P. B., Rogers, A., Slot, M., Smith, N. G., Tarvainen, L., Tissue, D. T., Togashi, H. F.,
4498 Tribuzy, E. S., Uddling, J., Vårhammar, A., Wallin, G., Warren, J. M. and Way, D. A.: Acclimation and adaptation
4499 components of the temperature dependence of plant photosynthesis at the global scale, *New Phytologist*, 222, 768-
4500 784, <https://doi.org/10.1111/nph.15668>, 2019.

4501

4502 Kurz, W. A., Dymond, C. C., White, T. M., Stinson, G., Shaw, C. H., Rampley, G. J., Smyth, C., Simpson, B. N.,
4503 Neilson, E. T., Trofymow, J. A., Metsaranta, J., and Apps, M. J.: CBMCF3: a model of carbon dynamics in forestry
4504 and land use change implementing IPCC standards, *Ecol. Model.*, 220, 480–504,
4505 <https://doi.org/10.1016/j.ecolmodel.2008.10.018>, 2009.

4506

4507 Lauerwald, R., Laruelle, G. G., Hartmann, J., Ciais, P., and Regnier, P. A. G.: Spatial patterns in CO₂ evasion from
4508 the global river network, *Global Biogeochemical Cycles*, 29, 534–554. <https://doi.org/10.1002/2014GB004941015>,
4509 2015.

4510

4511 Lawrence, D. M., Oleson, K. W., Flanner, M. G., Thornton, P. E., Swenson, S. C., Lawrence, P. J., Zeng, X., Yang,
4512 Z.-L., Levis, S., Sakaguchi, K., Bonan, G. B., and Slater, A. G.: Parameterization Improvements and Functional and
4513 Structural Advances in Version 4 of the Community Land Model, *Journal of Advances in Modeling Earth Systems*,
4514 3, M03001, DOI 10.1029/2011MS000045, 2011.

4515

4516 Le Quéré, C., Raupach, M. R., Canadell, J. G., Marland, G., Bopp, L., Ciais, P., Conway, T. J., Doney, S. C., Feely,
4517 R. A., Foster, P., Friedlingstein, P., Gurney, K., Houghton, R. A., House, J. I., Huntingford, C., Levy, P. E., Lomas,
4518 M. R., Majkut, J., Metz, N., Ometto, J. P., Peters, G. P., Prentice, I. C., Randerson, J. T., Running, S. W., Sarmiento,
4519 J. L., Schuster, U., Sitch, S., Takahashi, T., Viovy, N., van der Werf, G. R., and Woodward, F. I.: Trends in the sources
4520 and sinks of carbon dioxide, *Nat. Geosci.*, 2, 831–836, <https://doi.org/10.1038/ngeo689>, 2009.

4521

4522 Liski, J., Palosuo, T., Peltoniemi, M., and Sievänen, R.: Carbon and decomposition model Yasso for forest soils, *Ecol.*
4523 *Model.*, 189, 168–182, <https://doi.org/10.1016/J.ECOLMODEL.2005.03.005>, 2005.

4524

4525 Liu, J., Baskaran, L., Bowman, K., Schimel, D., Bloom, A. A., Parazoo, N. C., Oda, T., Carroll, D., Menemenlis, D.,
4526 Joiner, J., Commancin, R., Daube, B., Gatti, L. V., McKain, K., Miller, J., Stephens, B. B., Sweeney, C., and Wofsy,
4527 S.: Carbon Monitoring System Flux Net Biosphere Exchange 2020 (CMS-Flux NBE 2020), *Earth Syst. Sci. Data*, 13,
4528 299–330, <https://doi.org/10.5194/essd-13-299-2021>, 2021.

4529

4530 Lugato, E., Panagos, P., Bampa, F., Jones, A., Montanarella, L.: A new baseline of organic carbon stock in European
4531 agricultural soils using a modeling approach, *Glob. Change Biol.*, 20, 313–326, <https://doi.org/10.1111/gcb.12292>,
4532 2014.

4533

4534 Lurton, T., Balkanski, Y., Bastrikov, V., Bekki, S., Bopp, L., Braconnot, P., Brockmann, P., Cadule, P., Contoux, C.,
4535 Cozic, A., Cugnet, D., Dufresne, J.-L., Éthé, C., Foujols, M.-A., Ghattas, J., Hauglustaine, D., Hu, R.-M., Kageyama,
4536 M., Khodri, M., Lebas, N., Levvasseur, G., Marchand, M., Ottlé, C., Peylin, P., Sima, A., Szopa, S., Thiéblemont,
4537 R., Vuichard, N., and Boucher, O.: Implementation of the CMIP6 Forcing Data in the IPSL-CM6A-LR Model. *Journal*
4538 *of Advances in Modeling Earth Systems*, 12(4), e2019MS001940, <https://doi.org/10.1029/2019MS001940>, 2020.

4539

4540 Luyssaert, S., Abril, G., Andres, R., Bastviken, D., Bellassen, V., Bergamaschi, P., Bousquet, P., Chevallier, F., Ciais,
4541 P., Corazza, M., Dechow, R., Erb, K.-H., Etiope, G., Fortems-Cheiney, A., Grassi, G., Hartmann, J., Jung, M.,
4542 Lathière, J., Lohila, A., Mayorga, E., Moosdorf, N., Njakou, D. S., Otto, J., Papale, D., Peters, W., Peylin, P.,
4543 Raymond, P., Rödenbeck, C., Saarnio, S., Schulze, E.-D., Szopa, S., Thompson, R., Verkerk, P. J., Vuichard, N.,
4544 Wang, R., Wattenbach, M., and Zaehle, S.: The European land and inland water CO₂, CO, CH₄ and N₂O balance
4545 between 2001 and 2005, *Biogeosciences*, 9, 3357–3380, <https://doi.org/10.5194/bg-9-3357-2012>, 2012.

4546

4547 Luyssaert, S., Marie, G., Valade, A., Chen, Y. Y., Njakou Djomo, S., Ryder, J., Otto, J., Naudts, K., Lansø, A. S.,
4548 Ghattas, J., and McGrath, M. J.: Trade-offs in using European forests to meet climate objectives, *Nature*, 562, 259–
4549 262, <https://doi.org/10.1038/s41586-018-0577-1>, 2018.

4550

4551 Mason Earles, J., Yeh, S. and Skog, K.: Timing of carbon emissions from global forest clearance, *Nature Clim Change*,
4552 2, 682–685, <https://doi.org/10.1038/nclimate1535>, 2012.

4553

4554 McGrath, M. J., Petrescu, A. M. R., Peylin, P., Andrew, R. M., Matthews, B., Dentener, F., Balkovič, J., Bastrikov,
4555 V., Becker, M., Broquet, G., Ciais, P., Fortems, A., Ganzenmüller, R., Grassi, G., Harris, I., Jones, M., Knauer, J.,

Deleted:

4557 Kuhnert, M., Monteil, G., Munassar, S., Palmer, P. I., Peters, G. P., Qiu, C., Schelhaas, M.-J., Tarasova, O., Vizzarri,
4558 M., Winkler, K., Balsamo, G., Berchet, A., Briggs, P., Brockmann, P., Chevallier, F., Conchedda, G., Crippa, M.,
4559 Dellaert, S., Denier van der Gon, H. A. C., Filipek, S., Friedlingstein, P., Fuchs, R., Gauss, M., Gerbig, C., Guizzardi,
4560 D., Günther, D., Houghton, R. A., Janssens-Maenhout, G., Lauerwald, R., Lerink, B., Lujikx, I. T., Moulas, G.,
4561 Muntean, M., Nabuurs, G.-J., Paquirissamy, A., Perugini, L., Peters, W., Pilli, R., Pongratz, J., Regnier, P., Scholze,
4562 M., Serengil, Y., Smith, P., Solazzo, E., Thompson, R. L., Tubiello, F. N., Vesala, T. and Walther, S.: Data for the
4563 consolidated European synthesis of CO₂ emissions and removals for EU27 and UK: 1990-2020,
4564 <https://doi.org/10.5281/zenodo.8148461>, 2023,
4565
4566 Menut, L., Bessagnet, B., Khvorostyanov, D., Beekmann, M., Blond, N., Colette, A., Coll, I., Curci, G., Foret, G.,
4567 Hodzic, A., Mailler, S., Meleux, F., Monge, J.-L., Pison, I., Siour, G., Turquety, S., Valari, M., Vautard, R., and
4568 Vivanco, M. G.: CHIMERE 2013: a model for regional atmospheric composition modeling, *Geosci. Model Dev.*, 6,
4569 981–1028, <https://doi.org/10.5194/gmd-6-981-2013>, 2013.
4570
4571 Messenger, M. L., Lehner, B., Grill, G., Nedeva, I. and Schmitt, O.: Estimating the volume and age of water stored in
4572 global lakes using a geo-statistical approach, *Nat. Commun.*, 7, 13603, doi:10.1038/ncomms13603, 2016.
4573
4574 Monteil, G., Broquet, G., Scholze, M., Lang, M., Karstens, U., Gerbig, C., Koch, F.-T., Smith, N. E., Thompson, R.
4575 L., Lujikx, I. T., White, E., Meesters, A., Ciais, P., Ganesan, A. L., Manning, A., Mischurow, M., Peters, W., Peylin,
4576 P., Tarniewicz, J., Rigby, M., Rödenbeck, C., Vermeulen, A., and Walton, E. M.: The regional European atmospheric
4577 transport inversion comparison, EUROCOM: first results on European-wide terrestrial carbon fluxes for the period
4578 2006–2015, *Atmos. Chem. Phys.*, 20, 12063–12091, <https://doi.org/10.5194/acp-20-12063-2020>, 2020.
4579
4580 Monteil, G., and Scholze, M.: Regional CO₂ inversions with LUMIA, the Lund University Modular Inversion
4581 Algorithm, v1.0, *Geoscientific Model Development*, 14, 3383–3406, <https://doi.org/10.5194/gmd-14-3383-2021>,
4582 2021.
4583
4584 Mueller, N., Gerber, J., Johnston, M., Ray, D. K., Ramankutty, N., and Foley, J. A.: Closing yield gaps through nutrient
4585 and water management, *Nature*, 490, 254–257, <https://doi.org/10.1038/nature11420>, 2012.
4586

Deleted: <https://doi.org/10.5281/zenodo.7365863>

Deleted: 2

Formatted: Font: (Default) Times New Roman, 10 pt

4589 Muñoz-Sabater, J.: ERA5-Land hourly data from 1981 to present, Copernicus Climate Change Service (C3S) Climate
4590 Data Store (CDS), DOI 10.24381/cds.e2161bac, (last access: 1 May 2021), 2019.
4591

4592 Muñoz-Sabater, J., Dutra, E., Agustí-Panareda, A., Albergel, C., Arduini, G., Balsamo, G., Boussetta, S., Choulga,
4593 M., Harrigan, S., Hersbach, H., Martens, B., Miralles, D. G., Piles, M., Rodríguez-Fernández, N. J., Zsoter, E.,
4594 Buontempo, C., and Thépaut, J.-N.: ERA5-Land: A state-of-the-art global reanalysis dataset for land applications,
4595 Earth Syst. Sci. Data, 13, 4349–4383, <https://doi.org/10.5194/essd-13-4349-2021>, 2021.
4596

4597 Nabuurs, G, Lindner, M, Verkerk, H, Gunia, K, Deda, P, Michalak, R, and Grassi, G.: First signs of carbon sink
4598 saturation in European forest biomass, Nature Climate Change 3, 792-796, <https://doi.org/10.1038/nclimate1853>,
4599 2013.
4600

4601 Nabuurs, G. J., Delacote, P., Ellison, D., Hanewinkel, M., Hetemäki, L., Lindner, M., and Ollikainen, M.: By 2050
4602 the mitigation effects of EU forests could nearly double through climate smart forestry, Forests, 8, 484,
4603 <https://doi.org/10.3390/f8120484>, 2017.
4604

4605 Nabuurs, G. J., Arets, E. J. M. M., and Schelhaas, M. J.: Understanding the implications of the EU-LULUCF regulation
4606 for the wood supply from EU forests to the EU, Carbon Balance Manag., 13, 18, [https://doi.org/10.1186/s13021-018-](https://doi.org/10.1186/s13021-018-0107-3)
4607 0107-3, 2018.
4608

4609 Naegler, T.: Reconciliation of excess 14C-constrained global CO2 piston velocity estimates, Tellus B, 61, 372–384,
4610 <https://doi.org/10.1111/j.1600-0889.2008.00408.x>, 2009.
4611

4612 Naudts, K., Chen, Y., McGrath, M., Ryder, J., Valade, A., Otto, J., and Luysaert, S.: Europe’s forest management
4613 did not mitigate climate warming, Science, 351, 597–600, <https://doi.org/10.1126/science.aad7270>, 2016.
4614

4615 Niwa, Y., Fujii, Y., Sawa, Y., Iida, Y., Ito, A., Satoh, M., Imasu, R., Tsuboi, K., Matsueda, H., and Saigusa, N.: A
4616 4D-Var inversion system based on the icosahedral grid model (NICAM-TM 4D-Var v1.0) – Part 2: Optimization
4617 scheme and identical twin experiment of atmospheric CO2 inversion, Geosci. Model Dev., 10, 2201–2219,
4618 <https://doi.org/10.5194/gmd-10-2201-2017>, 2017.
4619

4620 Oleson, K.: Technical Description of the Community Land Model (CLM). NCAR Technical Note. TN-478+STR.
4621 10.5065/D6RR1W7M, 2010.
4622
4623 Petrescu, A. M. R., Peters, G. P., Janssens-Maenhout, G., Ciais, P., Tubiello, F. N., Grassi, G., Nabuurs, G.-J., Leip,
4624 A., Carmona-Garcia, G., Winiwarter, W., Höglund-Isaksson, L., Günther, D., Solazzo, E., Kiesow, A., Bastos, A.,
4625 Pongratz, J., Nabel, J. E. M. S., Conchedda, G., Pilli, R., Andrew, R. M., Schelhaas, M.-J., and Dolman, A. J.:
4626 European anthropogenic AFOLU greenhouse gas emissions: a review and benchmark data, *Earth Syst. Sci. Data*, 12,
4627 961–1001, <https://doi.org/10.5194/essd-12-961-2020>, 2020.
4628
4629 Petrescu, A. M. R., McGrath, M. J., Andrew, R. M., Peylin, P., Peters, G. P., Ciais, P., Broquet, G., Tubiello, F. N.,
4630 Gerbig, C., Pongratz, J., Janssens-Maenhout, G., Grassi, G., Nabuurs, G.-J., Regnier, P., Lauerwald, R., Kuhnert, M.,
4631 Balkovič, J., Schelhaas, M.-J., Denier van der Gon, H. A. C., Solazzo, E., Qiu, C., Pilli, R., Kononov, I. B.,
4632 Houghton, R. A., Günther, D., Perugini, L., Crippa, M., Ganzenmüller, R., Lujikx, I. T., Smith, P., Munassar, S.,
4633 Thompson, R. L., Conchedda, G., Monteil, G., Scholze, M., Karstens, U., Brockmann, P., and Dolman, A. J.: The
4634 consolidated European synthesis of CO₂ emissions and removals for the European Union and United Kingdom: 1990–
4635 2018, *Earth Syst. Sci. Data*, 13, 2363–2406, <https://doi.org/10.5194/essd-13-2363-2021>, 2021b.
4636
4637 Pilli, R., Grassi, G., Kurz, W. A., Moris, J. V., and Viñas, R. A.: Modelling forest carbon stock changes as affected
4638 by harvest and natural disturbances – II. EU-level analysis including land use changes, *Carbon Balance and*
4639 *Management*, 11, 20, <https://doi.org/10.1186/s13021-016-0059-4>, 2016.
4640
4641 Pilli, R., Grassi, G., Kurz, W. A., Fiorese, G., and Cescatti, A.: The European forest sector: past and future carbon
4642 budget and fluxes under different management scenarios, *Biogeosciences*, 14, 2387–2405, [https://doi.org/10.5194/bg-](https://doi.org/10.5194/bg-14-2387-2017)
4643 [14-2387-2017](https://doi.org/10.5194/bg-14-2387-2017), 2017.
4644
4645 Pilli, R., Alkama, R., Cescatti, A., Kurz, W. A., and Grassi, G.: The European forest carbon budget under future
4646 climate conditions and current management practices, *Biogeosciences*, 19, 3263–3284, [https://doi.org/10.5194/bg-19-](https://doi.org/10.5194/bg-19-3263-2022)
4647 [3263-2022](https://doi.org/10.5194/bg-19-3263-2022), 2022.
4648
4649 Pinty B., Janssens-Maenhout, G., Dowell, M., Zunker, H., Brunhes, T., Ciais, P., Dec, D., Denier van der Gon, H.,
4650 Dolman, H., Drinkwater, M., Engelen, R., Heimann, M., Holmlund, K., Husband, R., Kentarchos, A., Meijer, Y.,

4651 Palmer, P., and Scholze, M.: An Operational Anthropogenic CO₂ Emissions Monitoring & Verification Support
4652 capacity - Baseline Requirements, Model Components and Functional Architecture, European Commission Joint
4653 Research Centre, EUR 28736 EN, doi: 10.2760/39384, 2017.
4654
4655 Pisso, I., Sollum, E., Grythe, H., Kristiansen, N. I., Cassiani, M., Eckhardt, S., Arnold, D., Morton, D., Thompson, R.
4656 L., Groot Zwaafink, C. D., Evangeliou, N., Sodemann, H., Haimberger, L., Henne, S., Brunner, D., Burkhart, J. F.,
4657 Fouilloux, A., Brioude, J., Philipp, A., Seibert, P., and Stohl, A.: The Lagrangian particle dispersion model
4658 FLEXPART version 10.4, *Geosci. Model Dev.*, 12, 4955–4997, <https://doi.org/10.5194/gmd-12-4955-2019>, 2019.
4659
4660 Polcher, J., McAvaney, B., Viterbo, P., Gaertner, M.-A., Hahmann, A., Mahfouf, J.-F., Noilhan, J., Phillips, T.,
4661 Pitman, A.J., Schlosser, C.A., Schulz, J.-P., Timbal, B., Verseghy D., and Xue, Y.: A proposal for a general interface
4662 between land-surface schemes and general circulation models, *Global and Planetary Change*, 19, 263-278,
4663 [https://doi.org/10.1016/S0921-8181\(98\)00052-6](https://doi.org/10.1016/S0921-8181(98)00052-6), 1998.
4664
4665 Pongratz, J., Reick, C. H., Houghton, R. A., and House, J. I.: Terminology as a key uncertainty in net land use and
4666 land cover change carbon flux estimates, *Earth Syst. Dynam.*, 5, 177–195, <https://doi.org/10.5194/esd-5-177-2014>,
4667 2014.
4668
4669 Pongratz, J., Schwingshackl, C., Bultan, S., Obermeier, W., Havermann, F., and Guo, S.: Land Use Effects on Climate:
4670 Current State, Recent Progress, and Emerging Topics. *Curr Clim Change Rep*, 7, 99–120,
4671 <https://doi.org/10.1007/s40641-021-00178-y>, 2021.
4672
4673 Pongratz, J., Reick, C., Raddatz, T., and Claussen, M.: A reconstruction of global agricultural areas and land cover
4674 for the last millennium, *Global Biogeochemical Cycles*, 22, <https://doi.org/10.1029/2007GB003153>, 2008.
4675
4676 [Prentice, I. C., Liang, X., Medlyn, B. E., and Wang, Y.-P.: Reliable, robust and realistic: the three R's of next-](#)
4677 [generation land-surface modelling, *Atmos. Chem. Phys.*, 15, 5987–6005, <https://doi.org/10.5194/acp-15-5987-2015>,](#)
4678 [2015.](#)
4679
4680 Ramankutty, N., and Foley, J. A.: Estimating historical changes in global land cover: Croplands from 1700 to 1992,
4681 *Global biogeochemical cycles*, 13, 997-1027, <https://doi.org/10.1029/1999GB900046>, 1999.
4682

Formatted: Reference, Left, Line spacing: single, Border:
Top: (No border), Bottom: (No border), Left: (No border),
Right: (No border), Between : (No border)

Formatted: Reference

4683 Raymond, P. A., Hartmann, J., Lauerwald, R., Sobek, S., McDonald, C., Hoover, M., and Guth, P. : Global carbon
4684 dioxide emissions from inland waters, *Nature*, 503, 355–359, <https://doi.org/10.1038/nature12760>, 2013.
4685
4686 RECAPP2: <https://www.globalcarbonproject.org/Reccap/index.htm>, last access: 22 November 2022.
4687
4688 Regnier, P., Friedlingstein, P., Ciais, P., Mackenzie, F. T., Gruber, N., Janssens, I. A., Laruelle, G. G., Lauerwald, R.,
4689 Luysaert, S., Andersson, A. J., Arndt, S., Arnosti, C., Borges, A. V., Dale, A. W., Gallego-Sala, A., Godd ris, Y.,
4690 Goossens, N., Hartmann, J., Heinze, C., Ilyina, T., Joos, F., LaRowe, D. E., Leifeld, J., Meysman, F. J. R., Munhoven,
4691 G., Raymond, P. A., Spahni, R., Suntharalingam, P., and Thullner, M.: Anthropogenic perturbation of the carbon
4692 fluxes from land to ocean, *Nature Geosci*, 6, 597–607, <https://doi.org/10.1038/ngeo1830>, 2013.
4693
4694 Reichstein, M., Bahn, M., Ciais, P., Frank, D., Mahecha, M. D., Seneviratne, S. I., Zscheischler, J., Beer, C.,
4695 Buchmann, N., Frank, D. C., Papale, D., Rammig, A., Smith, P., Thonicke, K., van der Velde, M., Vicca, S., Walz,
4696 A., and Wattenbach, M.: Climate extremes and the carbon cycle, *Nature*, 500, 287-95, doi: 10.1038/nature12350,
4697 2013.
4698
4699 Resplandy, L., Keeling, R.F., R denbeck, C. Stephens, B. B., Khatiwala, S., Rodgers, K. B., Long, M. C., Bopp, L.,
4700 and Tans, P. P.: Revision of global carbon fluxes based on a reassessment of oceanic and riverine carbon transport,
4701 *Nature Geosci*, 11, 504–509, <https://doi.org/10.1038/s41561-018-0151-3>, 2018.
4702
4703 R denbeck, C.: Estimating CO2 sources and sinks from atmospheric mixing ratio measurements using a global
4704 inversion of atmospheric transport, Tech. Rep. 6, Max Planck Institute for Biogeochemistry, Jena, Germany, 2005.
4705
4706 R denbeck, C., Gerbig, C., Trusilova, K., and Heimann, M.: A two-step scheme for high-resolution regional
4707 atmospheric trace gas inversions based on independent models, *Atmos. Chem. Phys.*, 9, 5331–5342,
4708 <https://doi.org/10.5194/acp-9-5331-2009>, 2009.
4709
4710 R denbeck, C., Bakker, D. C., Metzl, N., Olsen, A., Sabine, C., Cassar, N., Reum, F., Keeling, R. F. and Heimann,
4711 M.: Interannual sea–air CO2 flux variability from an observation-driven ocean mixed-layer scheme, *Biogeosciences*,
4712 11, 4599-4613, <https://doi.org/10.5194/bg-11-4599-2014>, 2014.
4713
4714 Salln s, O.: A matrix model of the Swedish forest, *Studia Forestalia Suecica*, 183, 1-23,
4715 <https://pub.epsilon.slu.se/4514/>, 1990.
4716
4717 Scarlet, N, Martinov, M, and Dallemand, J.F.: Assessment of the availability of agricultural crop residues in the
4718 European Union: potential and limitations for bioenergy use, *Waste Manag*, 10, 1889-97, doi:
4719 10.1016/j.wasman.2010.04.016, 2010.

Formatted: Font: (Default) Times New Roman, 10 pt

4720

4721 Scharnweber, T., Smiljanic, M., Cruz-Garcia, R., Manthey, M., and Wilmking, M.: Tree growth at the end of the 21st
4722 century - the extreme years 2018/19 as template for future growth conditions, *Environ. Res. Lett.*, 15, 074022,
4723 <https://doi.org/10.1088/1748-9326/ab865d>, 2020.

4724

4725 Schelhaas, M.-J., Nabuurs, G.-J., Verkerk, P.J., Hengeveld, G., Packalen, T., Sallnäs, O., Pilli, R., Grassi, G., Forsell,
4726 N., Frank, S., Gusti, M., and Havlik, P.: Forest Resource Projection Tools at the European Level. In: Barreiro, S.,
4727 Schelhaas, M.-J., McRoberts, R.E., Kändler, G. (Eds.), *Forest Inventory-based Projection Systems for Wood and*
4728 *Biomass Availability*, Springer International Publishing, Cham, pp. 49-68, 2017.

4729

4730 [Schuldt, K. N., Jacobson, A. R., Aalto, T., Andrews, A., Bakwin, P., Bergamaschi, P., Biermann, T., Biraud, S. C.,](#)
4731 [Chen, H., Colomb, A., Conil, S., Cristofanelli, P., De Mazière, M., De Wekker, S., Delmotte, M., Dlugokencky, E.,](#)
4732 [Emmenegger, L., Fischer, M. L., Hatakka, J., Heliasz, M., Hermanssen, O., Holst, J., Jaffe, D., Karion, A., Kazan, V.,](#)
4733 [Keronen, P., Kominkova, K., Kubistin, D., Laurent, O., Laurila, T., Lee, J., Lehner, I., Leuenberger, M., Lindauer,](#)
4734 [M., Lopez, M., Mammarella, I., Manca, G., Marek, M. V., McKain, K., Miller, J. B., Miller, C. E., Myhre, C. L.,](#)
4735 [Mölder, M., Müller-Williams, J., Piacentino, S., Pichon, J. M., Plass-Duelmer, C., Ramonet, M., Scheeren, B.,](#)
4736 [Schumacher, M., Sha, M. K., Sloop, C. D., Smith, P., Steinbacher, M., Sweeney, C., Tans, P., Thoning, K., Trisolino,](#)
4737 [P., Tørseth, K., Viner, B., Vitkova, G., di Sarra, A. G.: Multi-laboratory compilation of atmospheric carbon dioxide](#)
4738 [data for the period 2020-2021; obspack_co2_1_NRT_v6.1_2021-02-02; NOAA Earth System Research Laboratory,](#)
4739 [Global Monitoring Laboratory \[data set\], \[http://doi.org/10.25925/20210108_2021a\]\(http://doi.org/10.25925/20210108_2021a\).](#)

4740

4741 [Schuldt, K. N., Mund, J., Luijckx, I. T., Aalto, T., Abshire, J. B., Aikin, K., Andrews, A., Aoki, S., Apadula, F., Baier,](#)
4742 [B., Bakwin, P., Bartyzel, J., Bentz, G., Bergamaschi, P., Beyersdorf, A., Biermann, T., Biraud, S. C., Boenisch, H.,](#)
4743 [Bowling, D., Brailsford, G., Chen, G., Chen, H., Chmura, L., Clark, S., Climadat, S., Colomb, A., Commane, R.,](#)
4744 [Conil, S., Cox, A., Cristofanelli, P., Cuevas, E., Curcoll, R., Daube, B., Davis, K., De Mazière, M., De Wekker, S.,](#)
4745 [Coletta, J. D., Delmotte, M., DiGangi, J. P., Dlugokencky, E., Elkins, J. W., Emmenegger, L., Fang, S., Fischer, M.,](#)
4746 [Forster, G., Frumau, A., Galkowski, M., Gatti, L. V., Gehrlein, T., Gerbig, C., Gheusi, F., Gloor, E., Gomez-](#)
4747 [Trueba, V., Goto, D., Griffis, T., Hammer, S., Hanson, C., Haszpra, L., Hatakka, J., Heimann, M., Heliasz, M., Hensen,](#)
4748 [A., Hermanssen, O., Hints, E., Holst, J., Ivakhov, V., Jaffe, D., Joubert, W., Karion, A., Kawa, S. R., Kazan, V.,](#)
4749 [Keeling, R., Keronen, P., Kolari, P., Kominkova, K., Kort, E., Kozlova, E., Krummel, P., Kubistin, D., Labuschagne,](#)
4750 [C., Lam, D. H., Langenfelds, R., Laurent, O., Laurila, T., Lauvaux, T., Lavric, J., Law, B., Lee, O. S., Lee, J., Lehner,](#)
4751 [I., Leppert, R., Leuenberger, M., Levin, I., Levula, J., Lin, J., Lindauer, M., Loh, Z., Lopez, M., Machida, T.,](#)
4752 [Mammarella, I., Manca, G., Manning, A., Manning, A., Marek, M. V., Martin, M. Y., Matsueda, H., McKain, K.,](#)
4753 [Meijer, H., Meinhardt, F., Merchant, L., Mihalopoulos, N., Miles, N., Miller, C. E., Miller, J. B., Mitchell, L.,](#)
4754 [Montzka, S., Moore, F., Morgan, E., Morgui, J.-A., Morimoto, S., Munger, B., Munro, D., Myhre, C. L., Mölder, M.,](#)
4755 [Müller-Williams, J., Necki, J., Newman, S., Nichol, S., Niwa, Y., O'Doherty, S., Obersteiner, F., Paplawsky, B.,](#)
4756 [Peischl, J., Peltola, O., Piacentino, S., Pichon, J. M., Piper, S., Plass-Duelmer, C., Ramonet, M., Ramos, R., Reyes-](#)

Formatted: Font: (Default) Times New Roman, 10 pt

Formatted: Justified, Line spacing: 1,5 lines

Formatted: Font: (Default) Times New Roman, 10 pt, Font colour: Text 1

Formatted: Font: (Default) Times New Roman, 10 pt, Font colour: Text 1

Formatted: Font: (Default) Times New Roman, 10 pt, Font colour: Text 1

Formatted: Font colour: Text 1

Formatted: Font: (Default) Times New Roman, 10 pt

4757 [Sanchez, E., Richardson, S., Riris, H., Rivas, P. P., Ryerson, T., Saito, K., Sargent, M., Sasakawa, M., Say, D.,](#)
4758 [Scheeren, B., Schuck, T., Schumacher, M., Seifert, T., Sha, M. K., Shepson, P., Shook, M., Sloop, C. D., Smith, P.,](#)
4759 [Steinbacher, M., Stephens, B., Sweeney, C., Tans, P., Thoning, K., Timas, H., Torn, M., Trisolino, P., Turnbull, J.,](#)
4760 [Torseth, K., Vermeulen, A., Viner, B., Vitkova, G., Walker, S., Watson, A., Wofsy, S., Worsley, J., Worthy, D., Young,](#)
4761 [D., Zaehe, S., Zahn, A., Zimnoch, M., di Sarra, A. G., van Dinter, D., van den Bulk, P.: \(2021\): Multi-laboratory](#)
4762 [compilation of atmospheric carbon dioxide data for the period 1957-2020;](#)
4763 [obspack_co2_1 GLOBALVIEWplus v7.0 2021-08-18; NOAA Earth System Research Laboratory, Global](#)
4764 [Monitoring Laboratory \[data set\], \[http://doi.org/10.25925/20210801_2021b\]\(http://doi.org/10.25925/20210801_2021b\).](#)
4765
4766 Seidl, R., Schelhaas, M. J., Rammer, W. and Verkerk, P. J.: Increasing forest disturbances in Europe and their impact
4767 on carbon storage, *Nature Clim Change*, 4, 806–810, <https://doi.org/10.1038/nclimate2318>, 2014.
4768
4769 Silva, J. P., Toland, J., Jones, W., Eldrige, J., Thorpe, E., O'Hara, E.: LIFE and Europe's grasslands: Restoring a
4770 forgotten habitat, report by the European Commission,
4771 <https://ec.europa.eu/environment/archives/life/publications/lifepublications/lifefocus/documents/grassland.pdf>, (last
4772 access: 10 November 2022), 2008.
4773
4774 Simmonds, P., Palmer, P. I., Rigby, M., McCulloch, A., O'Doherty, S. G., and Manning, A. J.: Tracers for evaluating
4775 computational models of atmospheric transport and dispersion at regional to global scales, *Atm. Env.*, 246, 118074,
4776 [doi:10.1016/j.atmosenv.2020.118074](https://doi.org/10.1016/j.atmosenv.2020.118074), 2021.
4777
4778 Simpson, D., Benedictow, A., Berge, H., Bergström, R., Emberson, L. D., Fagerli, H., Flechard, C. R., Hayman, G.
4779 D., Gauss, M., Jonson, J. E., Jenkin, M. E., Nyíri, A., Richter, C., Semeena, V. S., Tsyro, S., Tuovinen, J.-P.,
4780 Valdebenito, Á., and Wind, P.: The EMEP MSC-W chemical transport model – technical description, *Atmos. Chem.*
4781 *Phys.*, 12, 7825-7865, [doi:10.5194/acp-12-7825-2012](https://doi.org/10.5194/acp-12-7825-2012), 2012.
4782
4783 Simpson, D., Bergström, R., Imhof, H., and Wind, P.: Updates to the emep/msc-w model, 2016-2017. In
4784 *Transboundary particulate matter, photo-oxidants, acidifying and eutrophying components. EMEP Status Report*
4785 *1/2017. The Norwegian Meteorological Institute, Oslo, Norway, 2017.*
4786
4787 Simpson, D., Bergström, R., Tsyro, S., and Wind, P.: Updates to the EMEP MSC-W model, 2018- 2019. In
4788 *Transboundary particulate matter, photo-oxidants, acidifying and eutrophying components. EMEP Status Report*
4789 *1/2019. The Norwegian Meteorological Institute, Oslo, Norway, 2019.*
4790
4791 Simpson, D., Gonzalez Fernandez, I. A., Segers, A., Tsyro, S., Valdebenito, A., and Wind, P.: Updates to the EMEP
4792 MSC-W model, 2021-2022. In *Transboundary particulate matter, photo-oxidants, acidifying and eutrophying*
4793 *components. EMEP Status Report 1/2022. The Norwegian Meteorological Institute, Oslo, Norway, 2022.*

Deleted: ¶
Schelhaas, M. J., Hengeveld, G. M., Filipek, S., König, L.,
Lerink, B., Staritsky, I., de Jong, A., Sikkema, R., and
Nabuurs, G. J.: Documentation of the EFISCEN Space
model, in prep. ¶

4799

4800 De Smet, P. A. M., and Hettelingh, J.-P.: Intercomparison of Current European Land Use/Land Cover Databases,
4801 Status Report 2001 Coordination Center for Effects, RIVM Report 259101010, Bilthoven, Netherlands, pp. 41-52,
4802 2001.

4803

4804 Smith, J. U., Bradbury, N. J., and Addiscott, T.M.: SUNDIAL: A PC-based system for simulating nitrogen dynamics
4805 in arable land, *Agron J*, 88, 38-43, <https://doi.org/10.2134/agronj1996.00021962008800010008x>, 1996.

4806

4807 Smith, J. U., Gottschalk, P., Bellarby, J., Chapman, S., Lilly, A., Towers, W., Bell, J., Coleman, K., Nayak, D. R.,
4808 Richards, M. I., Hillier, J., Flynn, H. C., Wattenbach, M., Aitkenhead, M., Yeluripurti, J. B., Farmer, J., Milne, R.,
4809 Thomson, A., Evans, C., Whitmore, A. P., Falloon, P. and Smith, P.: Estimating changes in national soil carbon stocks
4810 using ECOSSE – a new model that includes upland organic soils. Part I. Model description and uncertainty in national
4811 scale simulations of Scotland, *Climate Research*, 45, 179-192, doi: 10.3354/cr00899, 2010a.

4812

4813 Smith, J. U., Gottschalk, P., Bellarby, J., Chapman, S., Lilly, A., Towers, W., Bell, J., Coleman, K., Nayak, D. R.,
4814 Richards, M. I., Hillier, J., Flynn, H. C., Wattenbach, M., Aitkenhead, M., Yeluripurti, J. B., Farmer, J., Milne, R.,
4815 Thomson, A., Evans, C., Whitmore, A.P., Falloon, P. and Smith, P.: Estimating changes in national soil carbon stocks
4816 using ECOSSE – a new model that includes upland organic soils. Part II Application in Scotland, *Climate Research*,
4817 45, 193-205, doi: 10.3354/cr00902, 2010b.

4818

4819 Smith, B., Wärlind, D., Arneth, A., Hickler, T., Leadley, P., Siltberg, J., and Zachle, S.: Implications of incorporating
4820 N cycling and N limitations on primary production in an individual-based dynamic vegetation model, *Biogeosciences*,
4821 11, 2027–2054, <https://doi.org/10.5194/bg-11-2027-2014>, 2014.

4822

4823 [SNO-IFA, ICOS-CAL-FCL: SNO-IFA ATC Atmosphere Release SNO-IFA-L2-2022.1 of L2 Greenhouse Gas Mole](https://doi.org/10.25326/410_2023)
4824 [Fractions of CO₂, CH₄. \[Dataset\]. Aeris. \[https://doi.org/10.25326/410_2023\]\(https://doi.org/10.25326/410_2023\).](https://doi.org/10.25326/410_2023)

4825

4826 Solazzo, E., Crippa, M., Guizzardi, D., Muntean, M., Choulga, M., and Janssens-Maenhout, G.: Uncertainties in the
4827 Emissions Database for Global Atmospheric Research (EDGAR) emission inventory of greenhouse gases, *Atmos.*
4828 *Chem. Phys.*, 21, 5655–5683, <https://doi.org/10.5194/acp-21-5655-2021>, 2021.

4829

4830 Thompson, R. L., Broquet, G., Gerbig, C., Koch, T., Lang, M., Monteil, G., Munassar, S., Nickless, A., Scholze, M.,
4831 Ramonet, M., Karstens, U., van Schaik, E., Wu, Z. and Rödenbeck, C.: Changes in net ecosystem exchange over
4832 Europe during the 2018 drought based on atmospheric observations, *Phil. Trans. R. Soc. B*, 375, 20190512,
4833 <http://dx.doi.org/10.1098/rstb.2019.0512>, 2020.

4834

Formatted: Font colour: Text 1

Formatted: Font colour: Text 1

Formatted: Font colour: Text 1

4835 Toreti, A., Belward, A., Perez-Dominguez, I., Naumann, G., Luterbacher, J., Cronie, O., Lorenzo Seguini, L.,
4836 Manfron, G., Lopez-Lozano, R., Baruth, B., van den Berg, M., Dentener, F., Ceglar, A., Chatzopoulos, T., and
4837 Zampieri, M.: The exceptional 2018 European water seesaw calls for action on adaptation, *Earth's Future*, 7, 652–663,
4838 <https://doi.org/10.1029/2019EF001170>, 2019.

4840 [Tubiello, F. N., Conchedda, G., Wanner, N., Federici, S., Rossi, S., and Grassi, G.: Carbon emissions and removals](#)
4841 [from forests: new estimates, 1990–2020, *Earth Syst. Sci. Data*, 13, 1681–1691, \[https://doi.org/10.5194/essd-13-1681-\]\(https://doi.org/10.5194/essd-13-1681-2021\)](#)
4842 [2021, 2021.](#)

Formatted: Reference, Left, Line spacing: single

Formatted: Font: (Default) Calibri, 11 pt, Not Highlight

4844 UK NIR: UK Greenhouse Gas Inventory, 1990 to 2020, Annual Report for Submission under the Framework
4845 Convention on Climate Change, 978-0-9933975-8-5, 2022.

4846 UNFCCC: Kyoto Climate Change Decision, available at: [https://unfccc.int/process-and-meetings/conferences/past-](https://unfccc.int/process-and-meetings/conferences/past-conferences/kyoto-climate-change-conference-december-1997/decisions-kyoto-climate-change-conference-december-1997)
4848 [conferences/kyoto-climate-change-conference-december-1997/decisions-kyoto-climate-change-conference-](https://unfccc.int/process-and-meetings/conferences/past-conferences/kyoto-climate-change-conference-december-1997/decisions-kyoto-climate-change-conference-december-1997)
4849 [december-1997](https://unfccc.int/process-and-meetings/conferences/past-conferences/kyoto-climate-change-conference-december-1997/decisions-kyoto-climate-change-conference-december-1997), (last access: 5 October 2020), 1997.

4850 UNFCCC: Decision 24/CP.19 Revision of the UNFCCC reporting guidelines on annual inventories for Parties
4851 included in Annex I to the Convention, FCCC/CP/2013/10/Add.3, 2014.

4852 UNFCCC: NGHGI 2021 NIR reports: National Inventory Submissions 2021, available at: [https://unfccc.int/ghg-](https://unfccc.int/ghg-inventories-annex-i-parties/2021)
4855 [inventories-annex-i-parties/2021](https://unfccc.int/ghg-inventories-annex-i-parties/2021), (last access: 01 January 2022), 2022a.

4856 UNFCCC: NGHGI 2021 CRFs, available at: <https://unfccc.int/ghg-inventories-annex-i-parties/2021>, (last access 01
4858 March 2022), 2022b.

4860 VERIFY: <http://verify.lsce.ipsl.fr/>, last access: 21 November 2022.

Formatted: Font: (Default) Times New Roman, 10 pt

4861 VERIFY Synthesis Plots: <http://webportals.ipsl.jussieu.fr/VERIFY/FactSheets/>, last access: 21 November 2022.

Formatted: Font: (Default) Times New Roman, 10 pt

4864 van der Laan-Luijkx, I. T., van der Velde, I. R., van der Veen, E., Tsuruta, A., Stanislawska, K., Babenhauserheide,
4865 A., Zhang, H. F., Liu, Y., He, W., Chen, H., Masarie, K. A., Krol, M. C., and Peters, W.: The CarbonTracker Data
4866 Assimilation Shell (CTDAS) v1.0: implementation and global carbon balance 2001–2015, *Geosci. Model Dev.*, 10,
4867 2785–2800, <https://doi.org/10.5194/gmd-10-2785-2017>, 2017.

4868 Verkerk, P. J., Schelhaas, M.-J., Immonen, V., Hengeveld, G., Kiljunen, J., Lindner, M., Nabuurs, G.-J., Suominen,
4870 T., and Zudin, S.: Manual for the European Forest Information Scenario model (EFISCEN 4.1), EFI Technical Report
4871 99, European Forest Institute, 49 pp., 2016.

4872

4873 Viovy, N.: Interannuality and CO₂ sensitivity of the SECHIBA-BGC coupled SVAT-BGC model, *Physics and*
4874 *Chemistry of The Earth*, 21, 489–497, [https://doi.org/10.1016/S0079-1946\(97\)81147-0](https://doi.org/10.1016/S0079-1946(97)81147-0), 1996.

4875

4876 Vizzarri, M., Pilli, R., Korosuo, A., Blujdea, V. N. B., Rossi, S., Fiorese, G., Abad-Vinas, R., Colditz, R. R., and
4877 Grassi, G.: Setting the forest reference levels in the European Union: overview and challenges, *Carbon Balance*
4878 *Manage*, 16, 23, <https://doi.org/10.1186/s13021-021-00185-4>, 2021.

4879

4880 Wang, Y.-P., and Leuning, R.: A two-leaf model for canopy conductance, photosynthesis and partitioning of available
4881 energy I: Model description and comparison with a multi-layered model, *Agricultural and Forest Meteorology*, 91,
4882 89–111, [https://doi.org/10.1016/S0168-1923\(98\)00061-6](https://doi.org/10.1016/S0168-1923(98)00061-6), 1998.

4883

4884 Wang, Y. P., Law, R. M., and Pak, B.: A global model of carbon, nitrogen and phosphorus cycles for the terrestrial
4885 biosphere, *Biogeosciences*, 7, 2261–2282, <https://doi.org/10.5194/bg-7-2261-2010>, 2010.

4886

4887 Wanninkhof, R.: Relationship between wind speed and gas exchange over the ocean revisited: Gas exchange and wind
4888 speed over the ocean, *Limnol. Oceanogr.-Meth.*, 12, 351–362, <https://doi.org/10.4319/lom.2014.12.351>, 2014.

4889

4890 Williams, J. R.: The Erosion-Productivity Impact Calculator (EPIC) Model: A Case History, *Philos. Trans. R. Soc. B*
4891 *Biol. Sci.* 329, 421–428, <https://doi.org/10.1098/rstb.1990.0184>, 1990.

4892

4893 Winkler, K., Fuchs, R., Rounsevell, M. D. A., and Herold, M.: HILDA+ Global Land Use Change between 1960 and
4894 2019. PANGAEA, <https://doi.org/10.1594/PANGAEA.921846>, 2020.

4895

4896 Winkler, K., Fuchs, R., Rounsevell, M. and Herold, M.: Global land use changes are four times greater than previously
4897 estimated, *Nat Commun*, 12, 2501, <https://doi.org/10.1038/s41467-021-22702-2>, 2021.

4898

4899 WMO: United in Science Report, available at: <https://public.wmo.int/en/our-mandate/climate/wmo-statement-state-of-global-climate>, (last access: January 2022), 2021.

4900

4901

4902 Yvon-Durocher, G., Caffrey, J., Cescatti, A., Dossena, M., del Giorgio, P., Gasol, J. M., Montoya, J. M., Pumpanen,
4903 J., Staehr, P. A., Trimmer, M., Woodward, G., and Allen, A. P.: Reconciling the temperature dependence of respiration
4904 across timescales and ecosystem types, *Nature*, 487, 472–476, <https://doi.org/10.1038/nature11205>, 2012.

4905

4906 [Zhang, J., Balkovič, J., Azevedo, L.B., Skalský, R., Bouwman, A.F., Xu, G., Wang, J., Xu, M., and Yu, C.: Analyzing](#)
4907 [and modelling the effect of long-term fertilizer management on crop yield and soil organic carbon in China. *Sci, Total*](#)
4908 [Environ. 627, 361-372. <https://doi.org/10.1016/j.scitotenv.2018.01.090>, 2018.](#)

4909

Formatted: Reference, Left, Line spacing: single

Formatted: Reference

4910 Zhang, B., Tian, H., Lu, C., Dangal, S. R. S., Yang, J., and Pan, S.: Global manure nitrogen production and application
4911 in cropland during 1860–2014: a 5 arcmin gridded global dataset for Earth system modeling, *Earth Syst. Sci. Data*, 9,
4912 667–678, <https://doi.org/10.5194/essd-9-667-2017>, 2017.

4913

4914 Zscheischler, J., Mahecha, M. D., Avitabile, V., Calle, L., Carvalhais, N., Ciais, P., Gans, F., Gruber, N., Hartmann,
4915 J., Herold, M., Ichii, K., Jung, M., Landschützer, P., Laruelle, G. G., Lauerwald, R., Papale, D., Peylin, P., Poulter,
4916 B., Ray, D., Regnier, P., Rödenbeck, C., Roman-Cuesta, R. M., Schwalm, C., Tramontana, G., Tyukavina, A.,
4917 Valentini, R., van der Werf, G., West, T. O., Wolf, J. E., and Reichstein, M.: Reviews and syntheses: An empirical
4918 spatiotemporal description of the global surface–atmosphere carbon fluxes: opportunities and data limitations,
4919 *Biogeosciences*, 14, 3685–3703, <https://doi.org/10.5194/bg-14-3685-2017>, 2017.

4920

Page 1: [1] Deleted Microsoft Office User 15/06/2023 18:52:00

Page 1: [1] Deleted Microsoft Office User 15/06/2023 18:52:00

Page 1: [1] Deleted Microsoft Office User 15/06/2023 18:52:00

Page 1: [1] Deleted Microsoft Office User 15/06/2023 18:52:00

Page 1: [1] Deleted Microsoft Office User 15/06/2023 18:52:00

Page 1: [1] Deleted Microsoft Office User 15/06/2023 18:52:00

Page 1: [1] Deleted Microsoft Office User 15/06/2023 18:52:00

Page 1: [1] Deleted Microsoft Office User 15/06/2023 18:52:00

Page 1: [1] Deleted Microsoft Office User 15/06/2023 18:52:00

Page 1: [1] Deleted Microsoft Office User 15/06/2023 18:52:00

Page 1: [1] Deleted Microsoft Office User 15/06/2023 18:52:00

Page 1: [1] Deleted Microsoft Office User 15/06/2023 18:52:00

Page 1: [1] Deleted Microsoft Office User 15/06/2023 18:52:00

Page 1: [1] Deleted Microsoft Office User 15/06/2023 18:52:00

Page 1: [1] Deleted Microsoft Office User 15/06/2023 18:52:00

▲
Page 1: [1] Deleted **Microsoft Office User** **15/06/2023 18:52:00**

▼
▲
Page 1: [1] Deleted **Microsoft Office User** **15/06/2023 18:52:00**

▼
▲
Page 1: [1] Deleted **Microsoft Office User** **15/06/2023 18:52:00**

▼
▲
Page 1: [2] Formatted **Microsoft Office User** **28/03/2023 19:06:00**

French

▲
Page 1: [2] Formatted **Microsoft Office User** **28/03/2023 19:06:00**

French

▲
Page 1: [3] Formatted **Microsoft Office User** **15/07/2023 14:51:00**

Font colour: Text 1, Superscript

▲
Page 1: [3] Formatted **Microsoft Office User** **15/07/2023 14:51:00**

Font colour: Text 1, Superscript

▲
Page 1: [3] Formatted **Microsoft Office User** **15/07/2023 14:51:00**

Font colour: Text 1, Superscript

▲
Page 1: [4] Deleted **Microsoft Office User** **15/06/2023 18:51:00**

✘
▲
Page 1: [4] Deleted **Microsoft Office User** **15/06/2023 18:51:00**

✘
▲
Page 1: [5] Deleted **Microsoft Office User** **28/03/2023 17:36:00**

✘
▲
Page 1: [5] Deleted **Microsoft Office User** **28/03/2023 17:36:00**

✘
▲
Page 1: [6] Deleted **Microsoft Office User** **28/03/2023 17:36:00**

✘
▲
Page 1: [6] Deleted **Microsoft Office User** **28/03/2023 17:36:00**

✘
▲

Page 11: [7] Formatted Microsoft Office User 15/07/2023 13:32:00

Footer Char, Font: (Default) Calibri, 11 pt, Font colour: Auto

Page 11: [8] Formatted Microsoft Office User 15/07/2023 13:32:00

Footer Char, Font: (Default) Calibri, 11 pt, Font colour: Auto

Page 11: [9] Formatted Microsoft Office User 15/07/2023 13:32:00

Footer Char, Font: (Default) Calibri, 11 pt, Font colour: Auto

Page 11: [10] Formatted Microsoft Office User 15/07/2023 13:32:00

Footer Char, Font: (Default) Calibri, 11 pt, Font colour: Auto

Page 11: [11] Formatted Microsoft Office User 15/07/2023 13:32:00

Footer Char, Font: (Default) Calibri, 11 pt, Font colour: Auto

Page 11: [12] Formatted Microsoft Office User 15/07/2023 13:32:00

Footer Char, Font: (Default) Calibri, 11 pt, Font colour: Auto

Page 22: [13] Deleted Microsoft Office User 11/07/2023 13:29:00

Page 22: [13] Deleted Microsoft Office User 11/07/2023 13:29:00

Page 22: [13] Deleted Microsoft Office User 11/07/2023 13:29:00

Page 22: [13] Deleted Microsoft Office User 11/07/2023 13:29:00

Page 22: [13] Deleted Microsoft Office User 11/07/2023 13:29:00

Page 22: [14] Deleted Microsoft Office User 13/07/2023 07:22:00

Page 22: [15] Deleted Microsoft Office User 01/07/2023 07:20:00

Page 22: [15] Deleted **Microsoft Office User** **01/07/2023 07:20:00**

Page 22: [15] Deleted **Microsoft Office User** **01/07/2023 07:20:00**

Page 22: [15] Deleted **Microsoft Office User** **01/07/2023 07:20:00**

Page 22: [15] Deleted **Microsoft Office User** **01/07/2023 07:20:00**

Page 22: [15] Deleted **Microsoft Office User** **01/07/2023 07:20:00**

Page 22: [15] Deleted **Microsoft Office User** **01/07/2023 07:20:00**

Page 25: [16] Deleted **Microsoft Office User** **14/07/2023 16:12:00**

Page 25: [17] Deleted **Microsoft Office User** **13/07/2023 18:05:00**

Page 25: [18] Deleted **Microsoft Office User** **06/07/2023 19:51:00**

Page 25: [19] Deleted **Microsoft Office User** **13/07/2023 18:23:00**

Page 28: [20] Formatted **Microsoft Office User** **11/07/2023 18:16:00**

Normal paragraph, Left, Line spacing: single, Widow/Orphan control, Border: Top: (No border), Bottom: (No border), Left: (No border), Right: (No border), Between : (No border)

Page 28: [21] Deleted **Microsoft Office User** **13/07/2023 18:28:00**

Page 28: [22] Deleted **Microsoft Office User** **13/07/2023 18:29:00**

Page 28: [23] Deleted **Microsoft Office User** **11/07/2023 18:16:00**

Page 29: [24] Deleted **Microsoft Office User** **17/04/2023 20:06:00**

Page 33: [25] Deleted **Microsoft Office User** **13/07/2023 19:09:00**

Page 33: [26] Formatted **Microsoft Office User** **14/07/2023 17:37:00**

Font: (Default) Times New Roman, 10 pt

Page 33: [26] Formatted **Microsoft Office User** **14/07/2023 17:37:00**

Font: (Default) Times New Roman, 10 pt

Page 33: [26] Formatted **Microsoft Office User** **14/07/2023 17:37:00**

Font: (Default) Times New Roman, 10 pt

Page 33: [26] Formatted **Microsoft Office User** **14/07/2023 17:37:00**

Font: (Default) Times New Roman, 10 pt

Page 33: [26] Formatted **Microsoft Office User** **14/07/2023 17:37:00**

Font: (Default) Times New Roman, 10 pt

Page 33: [26] Formatted **Microsoft Office User** **14/07/2023 17:37:00**

Font: (Default) Times New Roman, 10 pt

Page 33: [26] Formatted **Microsoft Office User** **14/07/2023 17:37:00**

Font: (Default) Times New Roman, 10 pt

Page 33: [26] Formatted **Microsoft Office User** **14/07/2023 17:37:00**

Font: (Default) Times New Roman, 10 pt

Page 33: [26] Formatted **Microsoft Office User** **14/07/2023 17:37:00**

Font: (Default) Times New Roman, 10 pt

Page 33: [27] Deleted **Microsoft Office User** **14/07/2023 17:22:00**

Page 33: [27] Deleted **Microsoft Office User** **14/07/2023 17:22:00**

Page 33: [28] Formatted Microsoft Office User 07/07/2023 18:36:00

Superscript

Page 33: [28] Formatted Microsoft Office User 07/07/2023 18:36:00

Superscript

Page 37: [29] Deleted Microsoft Office User 07/07/2023 18:42:00

✖

Page 43: [30] Deleted Microsoft Office User 12/07/2023 17:44:00

▼

Page 52: [31] Deleted Microsoft Office User 30/06/2023 18:18:00

✖